Bulk Compositional Analysis of Quartz–hosted Fluid Inclusions from the South Mountain Batholith, Nova Scotia

By

Fergus Michael Tweedale

A Thesis Submitted to
Saint Mary's University, Halifax, Nova Scotia
in Partial Fulfillment of the Requirements for
the Degree of Masters of Science in Applied Science.

March 2018, Halifax, Nova Scotia

Approved:	Dr. Jacob Hanley Supervisor Department of Geology Saint Mary's University
Approved:	Dr. Dan Kontak Supervisory Committee Harquail School of Earth Sciences Laurentian University
Approved:	Dr. Joel Gagnon Supervisory Committee Department Earth and Environmental Studies University of Windsor
Approved:	Dr. Robert Singer Supervisory Committee Department of Chemistry Saint Mary's University
Date:	March 13, 2019

ABSTRACT

Bulk Compositional Analysis of Quartz-hosted Fluid Inclusions from the South Mountain Batholith, Nova Scotia

by Fergus Michael Tweedale

The objective of this research is to further develop and assess the evaporate mound analysis protocol as an exploration tool, and apply the methodology to a batholith–wide survey of secondary quartz–hosted fluid inclusions in the mineralised South Mountain Batholith (SMB) of Nova Scotia. Results indicate a multi–element (Cl, Na, Ca, K, F, S, Mn, Fe, Zn, Cu, Pb) diversity in hydrothermal fluids hosted in felsic intrusive bodies sampled at a regional scale. Significant was the detection of F (avg. 23 wt. % of the total mound) as an anion in many evaporate mounds, and novel is its widespread occurrence in barren areas. Contact–style, or fault–related, mineralisation associated with externally–derived fluids is recognizable in regional–scale (i.e., 1 sample per 100 km^2) application of evaporate mound analysis, but an equivalent hydrothermal/magmatic signature in the bulk composition of fluid inclusions, at the regional–scale of observation, eludes detection despite an exhaustive analytical protocol and sampling density throughout various phases of the SMB.

March 13, 2019.

DEDICATION

This thesis is dedicated to my Mom, Ann Tweedale, who passed away July, 2018. Her boys miss her constantly.

ACKNOWLEDGEMENTS

Firstly, D.B. Clarke is thanked for introducing me to the South Mountain Batholith during my undergraduate studies and for directing me towards further studies in Nova Scotia with Jake. During the research for and writing of this graduate thesis, I received much support and assistance from the Saint Mary's Department of Geology: Pierre Jutras and Victor Owen are thanked for inviting me to participate in their local field trips, and for sharing their views of Nova Scotia geology; Randy Corney is thanked for helping me develop skills with cutting rocks and with preparing fluid inclusion wafers and thin sections; Xiang Yang is thanked for a lot of help with SEM work; Erin Adlakha is thanked for help with the interpretation of SED–EDS data; and I must express sincere gratefulness to my graduate student cohort for sharing the ups and downs of this experience.

Big thanks to Dan Kontak, for recognizing my interest in geology, for suggesting that we formalize a methodology for evaporate mound analysis and for giving me some space in his research universe. Greg Baker, way over there in the Department of Geography, is thanked for his expert assistance with developing a computer–based map of the study area. Neil Rogers, our contact at the Geological Survey of Canada, is thanked for taking me into the field and exploring rocks in Yarmouth County.

Most importantly, and to the person who made everything possible for me and my family, a massive thank you to Jacob for his supervision and support of this thesis, for his patience with letting me do things my way, for unrestricted access to his fluid inclusion lab and for catching my attention in igneous petrology classes all those years ago. The rest is history!

Table of Contents

Table of Figures

Table of Tables

Table of Tables for Appendix A

Table of Tables for Appendix B

CHAPTER 1: INTRODUCTION

1.0 Magmatic–hydrothermal mineralization and fluid inclusions

Locating mineralised centres hosted within granitoid intrusions is challenging, and there is a general paucity of exploration tools specifically designed for such environments. Given the magmatic–hydrothermal origin of granite–related mineral deposits (*e.g.*, Candela, 1990, O'Reilly *et al.* 1982), samples of the paleo–fluids that circulated through the host rocks may, in some instances, preserve chemical information pertaining to the distribution of mineralised centres. Fluid inclusions represent microscopic (typically 10 μm) samples of fluids trapped either on former faces of growing crystals or along healed fluid–coated fracture planes. Fluid inclusions are fossilized paleofluid samples (Fig. 1.1).

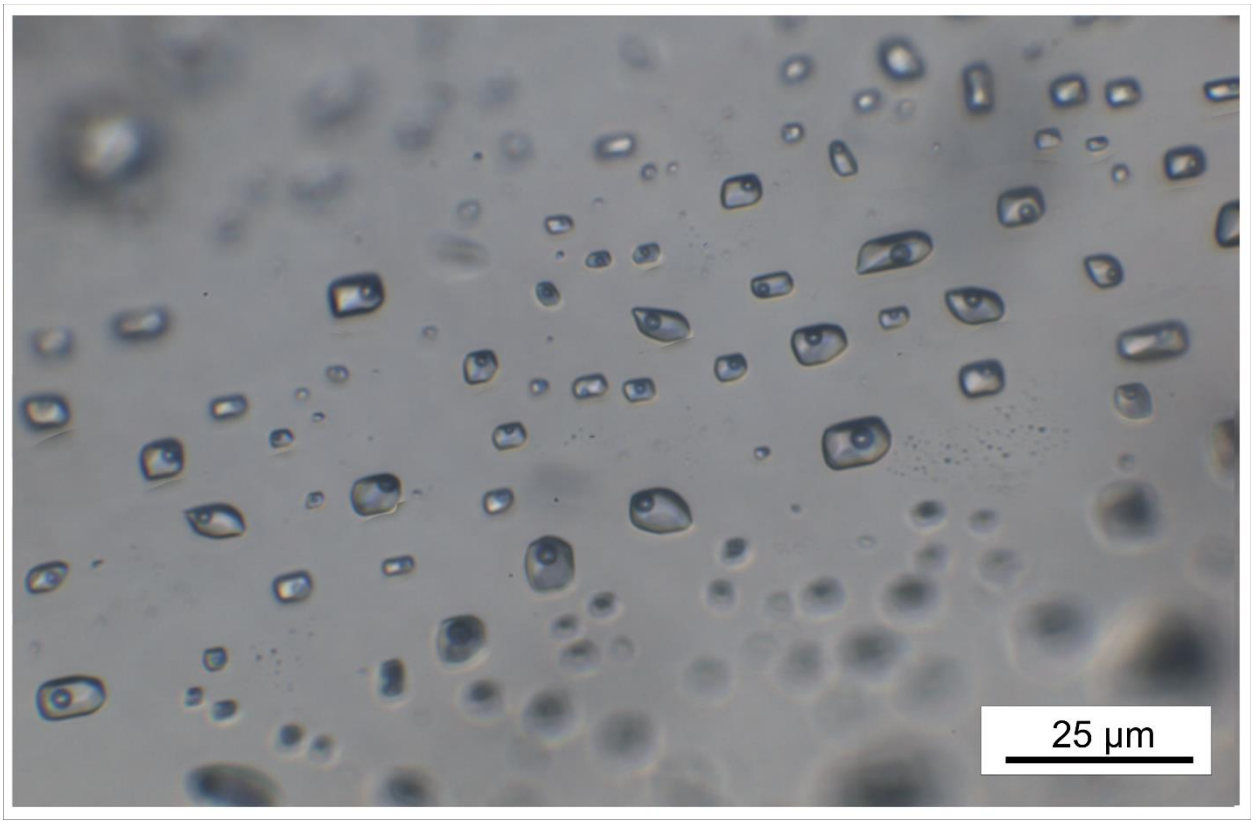

Figure 1.1: Fluid inclusions hosted by quartz in a granitoid rock from the South Mountain Batholith (SMB). Here the 1 – 10 µm size inclusions, which are easily resolvable by standard microscopy, are two phase aqueous liquid–vapour type.

1.1 Sampling area

1.1.1 Geological setting of South Mountain Batholith

The SMB (Fig. 1.2), is the largest granitoid intrusion in the Northern Appalachians, mainly intrudes the conformable succession of folded late Neoproterozoic– to early Paleozoic Meguma Supergroup sedimentary rocks which were regionally metamorphosed to mainly lower greenschist facies, but locally to lower amphibolite facies, prior to intrusion (White *et al.* 2012, Hicks *et al.* 1998). Along its western contact, some portions (< 10 % of the SMB perimeter) of the batholith intruded Ordovician to early Devonian metasedimentary and metavolcanic rocks of the Rockville Notch Group (White *et al.* 2012). Horton Group sedimentary rocks that host Carboniferous (Famennian and Tournaisian) aged fossils non–conformably overlie the northeast corner of the batholith (Martel *et al.* 1993). Radiometric ages for the batholith constrain its emplacement to 372 – 361 Ma by Rb–Sr whole–rock isochron analysis (Clarke & Halliday 1980), 367 Ma (mean age from 22 samples) by $^{40}Ar/^{39}Ar$ and K–Ar analyses of muscovite and biotite (Reynolds *et al.* 1981) and 381–373 Ma by U–Pb zircon dating (Bickerton *et al.* 2018, Keppie *et al.* 1993). Gravity–based modelling suggests an average basal depth of 7 km (Benn *et al.* 1999). The provincial gravity map (Fisher 2006) indicates two areas with relatively greater thickness, one centred on the municipality of New Ross, and the other on the Davis Lake pluton.

The batholith is a composite intrusion, broadly subdivided into two phases of temporally and lithologically distinct plutons (Fig. 3). Early Stage 1 plutons are dominantly monzogranites and granodiorites, and later Stage 2 plutons are dominantly monzogranites and leucomonzogranites (MacDonald *et al.* 1992). Contacts between plutons are either intrusive, fault–bounded or gradational. The mineralogy, geochemistry and petrogenesis of the SMB are extensively described (*e.g.*, McKenzie & Clarke 1975, Muecke & Clarke 1981, Clarke *et al.* 1997,

MacDonald 2001, Clarke *et al.* 2004). There is a spatial association between the New Ross and Davis Lake plutons and intrusion–related magmatic–hydrothermal styles of mineralization (Sn–Zn–Cu–Ag, Mn–Fe–P, U–Cu, Au–W), and the entire batholith is an area of considerable interest in terms of potential exploration (O'Reilly *et al.* 1982, Chatterjee *et al.* 1985, Carruzzo *et al.* 2000, MacDonald 2001, Baldwin 2017).

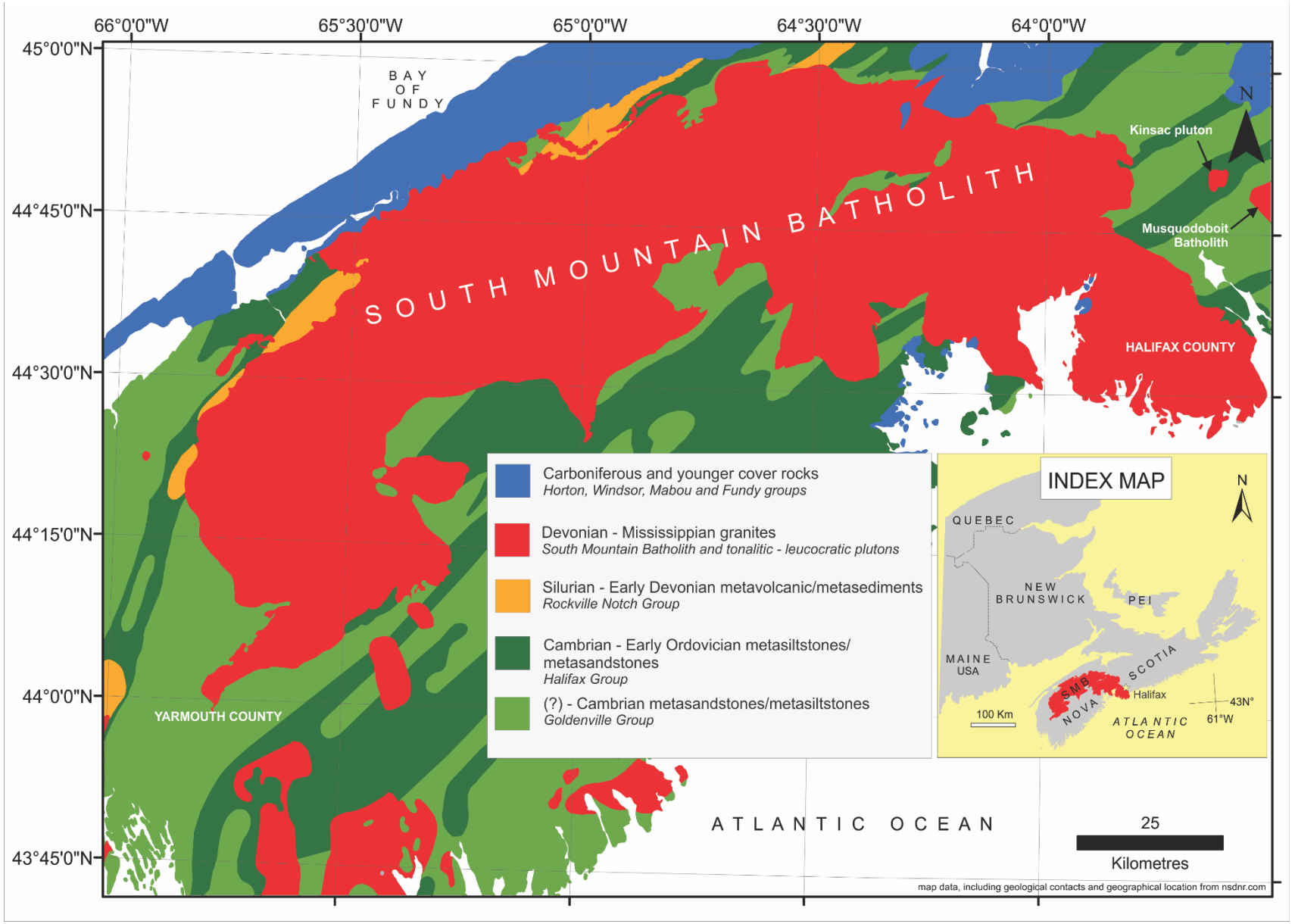
66°0'0"W
65°30'0"W
65°0'0"W
64°30'0"W
64°0'0"W
45°0'0"N
44°45'0"N
44°30'0"N
44°15'0"N
44°0'0"N
43°45'0"N
BAY OF FUNDY
SOUTH MOUNTAIN BATHOLITH
Kinsac pluton
Musquodoboit Batholith
HALIFAX COUNTY
YARMOUTH COUNTY
ATLANTIC OCEAN
N
Carboniferous and younger cover rocks
Horton, Windsor, Mabou and Fundy groups
Devonian - Mississippian granites
South Mountain Batholith and tonalitic - leucocratic plutons
Silurian - Early Devonian metavolcanic/metasediments
Rockville Notch Group
Cambrian - Early Ordovician metasiltstones/ metasandstones
Halifax Group
(?) - Cambrian metasandstones/metasiltstones
Goldenville Group
INDEX MAP
QUEBEC
NEW BRUNSWICK
PEI
MAINE USA
NOVA SCOTIA
SMB
Halifax
100 Km
43N°
61°W
ATLANTIC OCEAN
25
Kilometres
map data, including geological contacts and geographical location from nsdnr.com

Figure 1.2 (previous page): Geological setting of the South Mountain Batholith (SMB), Nova Scotia, Canada.

1.1.2 Areas of known mineralization

The distribution of known mineral deposits in the SMB is batholith–wide and includes mineral occurrences, mineral prospects and past–producing mines (Fig. 1.3). Mineralised centres display local–scale variations in mineralogy and styles with four styles recognized that includes vein, breccia, pegmatite and greisen (MacDonald 2001). Commodities associated with each type of deposit are shown in Figure 1.3.

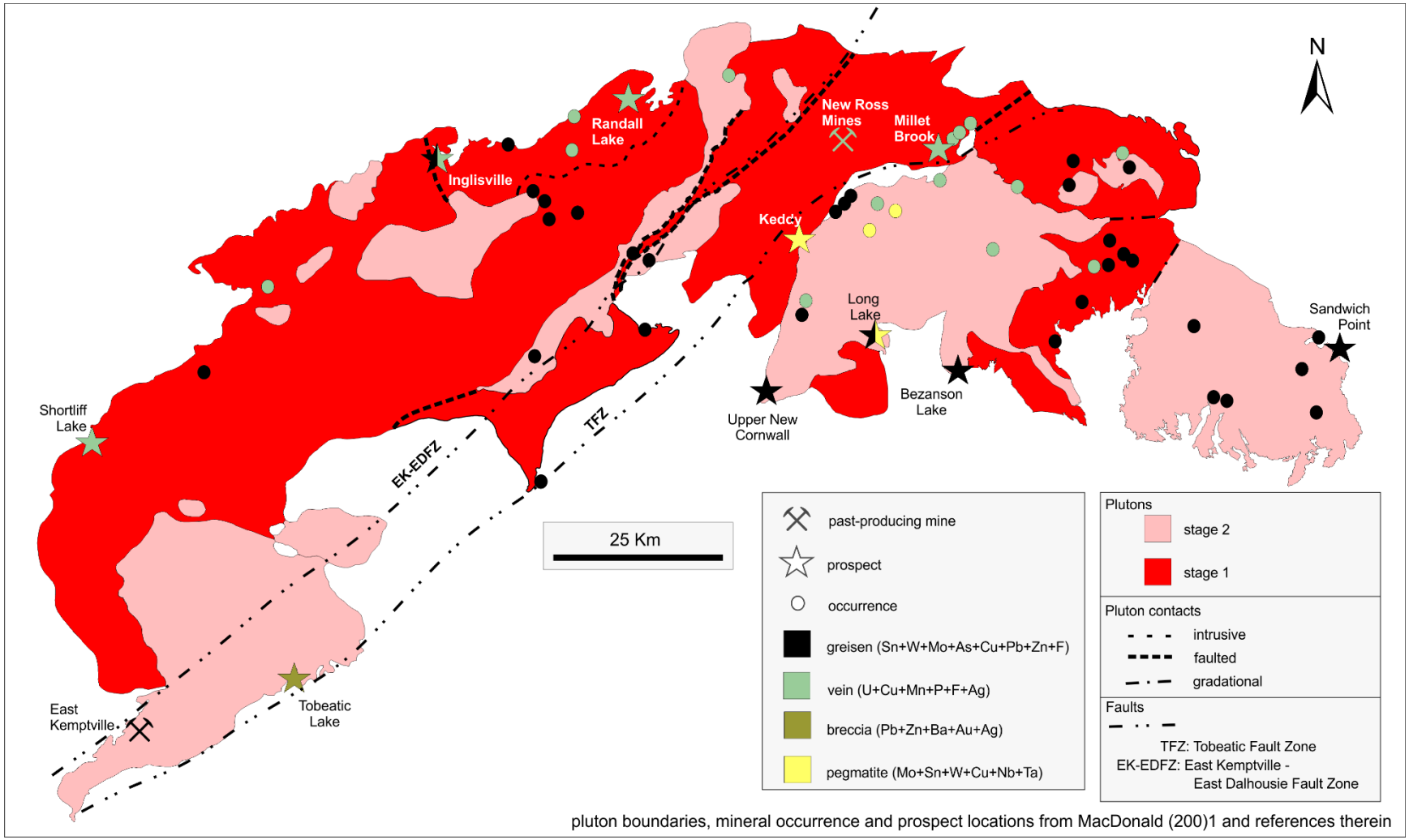

pluton boundaries, mineral occurrence and prospect locations from MacDonald (200)1 and references therein

Figure 1.3 (previous page): Map showing mineral occurrences in the SMB which in general have a local distribution. Large greisen deposits are proximal to SMB–Meguma contact zones. Known vein deposits occur along NE–trending faulting zones located in the interior of the batholith. Occurrence of breccia deposits is restricted to Tobeatic Fault zone. Known pegmatite deposits are hosted uniquely by the New Ross pluton.

1.2 Structure of thesis

This thesis comprises four chapters. Chapter 1 first provides an introduction to the thesis and a clear statement of its objective which is then followed by a geological description of the study area, the South Mountain Batholith of Nova Scotia. Chapter 2 provides a step–by–step methodology for evaporate mound analysis (EMA) which is used to quantify the chemical composition of aqueous fluid inclusions. The EMA methodology is formalized and fully described in this chapter. In Chapter 3, the EMA methodology is integrated with conventional petrographic analysis of alteration mineral systematics in granitoid rocks of the SMB and collectively developed into an exploration tool. The limitations of the method and recommendations for future work are outlined in Chapter 4. All data collected for this research are tabulated the appendices that appear at the end of the document.

1.3 References

BALDWIN, G. 2017. A New Look at Mineral Occurrences Associated with the South Mountain Batholith, Southwestern Nova Scotia, *In* Geoscience and Mines Branch, Report of Activities 2016–17. Nova Scotia Department of Natural Resources, Report ME 2017–001, 3–4.

BENN, K., HORNE, R.J., KONTAK, D.J., PIGNOTTA, G.S., & EVANS, N.G. 1999. Syn–Acadian emplacement model for the South Mountain Batholith, Meguma Terrane, Nova Scotia: Magnetic fabric and structural analyses. Geological Society of America Bulletin, 109, 1279–1293

BICKERTON, L., KONTAK, D.J., SAMSON, I.M., MURPHY, J.B., & KELLETT, D.A. 2018. U–Pb geochronology of the South Mountain Batholith, Nova Scotia. *In* Targeted Geoscience Initiative – 2017 Report of Activities (N. Rogers, ed.). Geological Survey of Canada, Open File 8358, Ottawa, Canada (61–65) doi:10.4095/306391

BODNAR R.J. (2003). Introduction to fluid inclusions. *In* Fluid Inclusions: Analysis and Interpretation (I. Samson, A. Anderson, & D. Marshall, eds.). Mineralogical Association of Canada, Short Course 32, Ottawa, Canada (1–8).

CANDELA, P.A. 1990. Theoretical constraints on the chemistry of the magmatic aqueous phase, *In* Ore–bearing granite systems; Petrogenesis and mineralizing processes (H.J. Stein & J.L. Hannah, eds.). Geological Society of America Special Paper 246, Boulder, United States (11–20).

CARRUZZO, S., KONTAK, D.J., & CLARKE, D.B. 2000. Granite–hosted mineral deposits of the New Ross area, South Mountain Batholith, Nova Scotia, Canada: P, T and X constraints of fluids using fluid inclusion thermometry and evaporate analysis. Transactions of the Royal Society of Edinburgh: Earth Sciences 91, 303–319.

CHATTERJEE, A. K., STRONG, D.F., CLARKE, D.B., ROBERTSON, J., POLLOCK, D., & MUECKE, G.K. 1985. Geochemistry of the Granodiorite hosting Uranium Mineralisation at Millet Brook. *In* Guide to the granites and mineral deposits of southwestern Nova Scotia (A.K. Chatterjee & D.B. Clarke, eds.). Nova Scotia Department of Energy and Mines, Paper 85–3, Halifax, Canada (63 – 114).

CLARKE, D. B., MACDONALD, M. A., & ERDMANN, S. 2004. Chemical variation in Al_2O_3–CaO–Na_2O–K_2O space: controls on the peraluminosity of the South Mountain Batholith. Canadian Journal of Earth Sciences 41, 785–798.

CLARKE, D.B., MACDONALD, M.A., & TATE, M.C. 1997. Late Devonian mafic–felsic magmatism in the Meguma Zone, Nova Scotia. *In* The nature of magmatism in the Appalachian Orogen. (A.K. Sinha, J.B. Whalen, & J.P. Hogan, eds.). Geological Society of America Memoir 191, Boulder, United States (107–127).

CLARKE, D.B. & HALLIDAY, A.N. 1980. Strontium isotope geology of the South Mountain Batholith, Nova Scotia. Geochimica et Cosmochimica Acta 44(8), 1045–1058.

FISHER, B.E. (compiler) 2006. Digital Version of Nova Scotia Department of Natural Resources Map ME 1979–3, Bouguer Gravity Anomaly Map of Nova Scotia, scale 1:500 000, Compiled by J. D. Keppie, 1979.

HICKS, R.J., JAMIESON, R.J., & REYNOLDS, P.H. 1998. Detrital and metamorphic $^{40}Ar/^{39}Ar$ ages from muscovite and whole–rock samples, Meguma Supergroup, southern Nova Scotia. Canadian Journal of Earth Sciences 36 22–32.

KEPPIE, J.D. 2000. Geological Map of the Province of Nova Scotia. Department of Natural Resources, Mines and Energy Branch, Map Map ME 2000–1, scale 1: 500 000.

KEPPIE, J.D., DALLMEYER, R.D., KROGH, T.E., & AFTALION, M. 1993. Dating mineralization using several isotopic methods: An example from the South Mountain Batholith, Nova Scotia, Canada. Chemical Geology 103, 251–270.

KONTAK, D.J., & COREY, M. 1988. Metasomatic origin of spessartine–rich garnet in the South Mountain Batholith, Nova Scotia. Canadian Mineralogist 26, 315–334.

MACDONALD, M.A. 2001. Geology of the South Mountain Batholith, Southwestern Nova Scotia. Nova Scotia Department of Natural Resources, Open File Report ME 2001–2.

MACDONALD, M.A., HORNE, R.J., COREY, M.C., & HAM, L.J. 1992. An overview of recent bedrock mapping and follow–up petrological studies of South Mountain Batholith, southwestern Nova Scotia, Canada. Atlantic Geology 28, 7–28.

MACKENZIE, C.B., & CLARKE, D.B., 1975. Petrology of the South Mountain Batholith, Nova Scotia. Canadian Journal of Earth Sciences 12, 1209–1218

MARTEL, T.A., MCGREGOR, C.D., & UTTING, J. 1993. Stratigraphic significance of upper Devonian and Lower Carboniferous miospores from the type area of the Horton Group, Nova Scotia. Canadian Journal of Earth Sciences 30, 1091–1098.

MUECKE, G.K. & CLARKE, D.B. (1981) Geochemical Evolution of the South Mountain Batholith, Nova Scotia: Rare–Earth Element Evidence. Canadian Mineralogist 19, 133–145.

O'REILLY, G.A., FARLEY, E.J., & CHAREST, M.H 1982. Metasomatic–Hydrothermal Mineral Deposits of the New Ross–Mahone Bay Area, Nova Scotia. Nova Scotia Department of Mines and Energy, Paper 82–2, p. 15–21.

REYNOLDS, P.H., ZENTILLI, M., & MUECKE, G.K. 1981. K–Ar and $^{40}Ar/^{39}Ar$ geochronology of granitoid rocks from southern Nova Scotia: Its bearing on the geological evolution of the Meguma Zone of the Appalachians. Canadian Journal of Earth Sciences 18, 386–394.

WHITE, C.E., PALACIOS, T., JENSEN, S. & BARR, S.M. 2012. Cambrian–Ordovician acritarchs in the Meguma terrane, Nova Scotia, Canada: Resolution of early Paleozoic stratigraphy and implications for paleogeography. Geological Society of America Bulletin 124 (11/12) 1773–1792.

CHAPTER 2: EVAPORATE MOUND ANALYSIS BY SCANNING ELECTRON MICROSCOPY–ENERGY–DISPERSIVE X–RAY SPECTROMETRY (SEM–EDS): A METHOD FOR OBTAINING MULTI–ELEMENT COMPOSITIONAL CONSTRAINT ON HYDROTHERMAL FLUIDS

F. Tweedale[1], J. Hanley[1], and D. Kontak[2]*

1. Department of Geology, Saint Mary's University, Halifax, NS, Canada B3H 3C3

2. Department of Earth Sciences, Laurentian University, Sudbury, Ontario P3E 2C6

Corresponding author: fergus.tweedale@smu.ca

Number of pages: 89

Number of figures: 23

Number of tables: 7

For submission to *Canadian Mineralogist*

Abstract

Evaporate mounds are discrete salt piles that precipitate from the volatilised aqueous fluid released when fluid inclusions rupture during controlled thermal decrepitation of the host mineral. These mounds represent, at least partially, the bulk solute composition of their precursor fluids. As part of a batholith–wide survey of quartz–hosted fluid inclusions from the mineralised (Sn, W, U, base metals) ca. 380 Ma South Mountain Batholith (SMB) of Nova Scotia, we further developed the previously utilised SEM–EDS methodology for evaporate mound analysis (EMA), which is fully described here. For EMA application to the SMB, the recommended protocol is: (i) rapid (i.e., 50°C/min), stage heating to 500°C to avoid volatilisation of F and Cl; (ii) collection of EDS spectra from 16 mounds/chip to ensure a representative data; (iii) a minimum of two chips per sample to

evaluate wafer–scale variation in fluid inclusion abundance and chemistry; (iv) a minimum 60–second acquisition time for detection of all solute elements typically encountered; and (v) charge–balance assessment of mounds to assess quality of data. From the analysis of discrete evaporate mounds attributable to single fluid inclusions, the range of non–volatile fluid inclusion solute elements (listed in order of abundance) included: Cl^{-}, F^{-}, S^{2-}, Na^{+}, Ca^{2+}, K^{+}, Mn^{2+}, Fe^{2+} and Zn^{2+}. This diversity of elements cannot be quantified by more tedious and time–consuming methods, including microthermometry and LA–ICP–MS analyses. That F is detected as a major element in the evaporate mounds throughout the study area reveals that F is a significant anion in non–mineralising hydrothermal fluids. The rigorous assessment of the EMA method presented shows it is a time– and cost–effective means to determine the major solute chemistry of fluids in hydrothermal settings and as such should become universally applied as part of such studies.

2.0 Introduction

Previous studies (*e.g.*, Chryssoulis & Wilkinson 1983, Haynes & Kesler 1987a, Kontak 2004) demonstrate the considerable potential evaporate mound analysis (EMA) has as both a research and exploration tool. The reliability of the method for obtaining multicomponent compositional data of individual aqueous saline fluid inclusions was quantitatively demonstrated by results obtained from the analysis of synthetic fluid inclusions (Haynes *et al.* 1988). Although the EMA method has seen some application to a variety of hydrothermal deposit settings (*e.g.*, Savard & Chi 1998, Kontak *et al.* 2002, Kontak & Clark 2002, Carruzzo *et al.* 2000, Palmer & Williams–Jones 1996, Kontak & Kyser 2011), a rigorous evaluation of the conventional methodology for EMA does not appear in the available literature. We have developed and refined an EMA methodology that is now in regular use in both the Mineral Exploration and Ore Fluids Laboratory (MEOFL) at Saint Mary's University, Halifax, Nova Scotia, Canada (*e.g.*, Neyedley *et al.* 2017,

Kerr et al. 2018) and as a complement to fluid:chemical studies at Laurentian University, Sudbury Ontario (Mathieu *et al.* 2013, Pandur *et al.* 2015, Kontak & Tuba 2017, McDivitt *et al.* 2018, Hahn *et al.* 2018). Evaporate mound analysis provides a cost–effective straightforward methodology that produces results in rapid manner. In addition, laboratory facilitation of EMA work only requires some dedicated technical support of the SEM, favouring application to exploration research. This paper details the step–by–step EMA methodology proposed for use as part of the research protocol in ore deposit studies, and also presents the preliminary results of its application to a regional–scale study of quartz–hosted fluid inclusions in granitoid samples from the mineralised 380 Ma South Mountain Batholith (SMB) of Nova Scotia (Fig. 2.1). In a complementary paper (Tweedale *et al.* in prep., 2019), a more detailed and exhaustive application of the approach is applied to the mineralised SMB which integrates EMA with petrographic analysis of the hydrothermal alteration of the host granitoids.

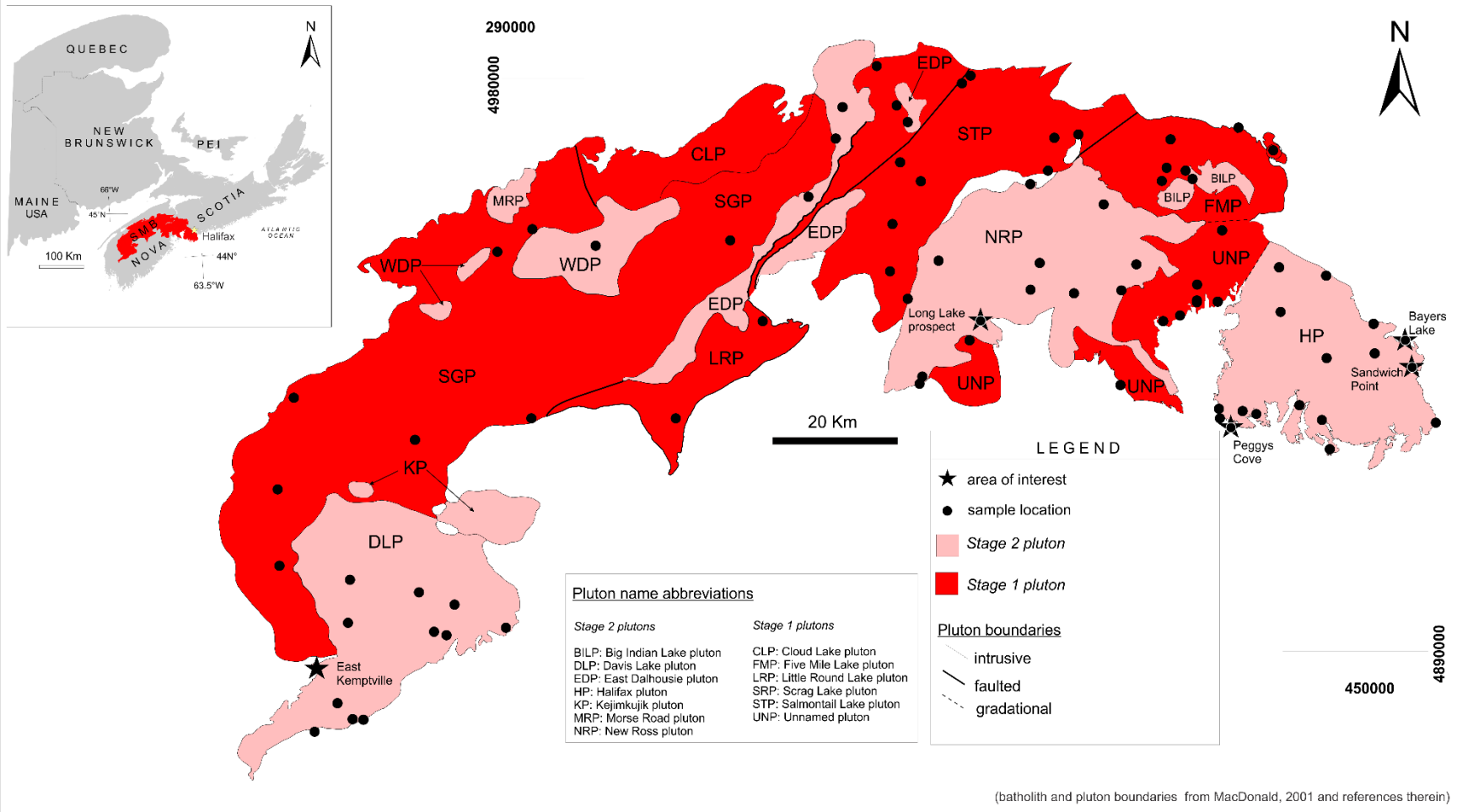

Figure 2.1: Geological map of the South Mountain Batholith. Sample locations are part of batholith–wide EMA survey, which is subject of a future publication

2.0.1 Background

Physical and chemical evidence that constrains the nature of hydrothermal fluids implicated in crustal mineralization comes from the direct analysis of fluid inclusions (*e.g.*, Roedder 1984, Yardley & Bodnar 2014 and references therein). Analytical methods developed for fluid–inclusion studies are numerous, which attests both to the usefulness of the chemistry preserved in fluid inclusions and to the difficulty in its quantification. With few exceptions (Samson *et al.* 1995, Kontak 2004), sample material used in fluid inclusion research is collected from mine sites or areas of known mineralization (Table 2.1) since this is the intent of such studies. Therefore, the data obtained from such research is generally only used to interpret the evolution of a mineralizing fluid from a known deposit or occurrence. It is possible however, that the chemical fingerprinting of a mineralising fluid extends beyond an unidentified ore–body and may in fact extend into an apparently barren peripheral area. This approach has in fact been explored in recent years to define the chemical footprint of, for example, porphyry deposit settings (*e.g.*, Mount Polley, British Columbia; Pisiak *et al.* 2017) and some large gold deposits (*e.g.*, Malartic deposit, Quebec; De Souza *et al.* 2015) using mineral chemistry. Herein we provide a means of testing this hypothesis by first establishing the protocol necessary in such a study using a simple and cost–effective method of analyzing the major solute chemistry of fluid inclusions with the EMA method.

2.0.2 Determining the presence of fluid inclusion solutes

Bulk chemical properties of saline aqueous fluid inclusions are typically obtained by destructive or non–destructive techniques. Microthermometry, the conventional method for fluid inclusion research, is non–destructive. In contrast, bulk leach analysis, LA–ICP–MS and EMA are destructive techniques.

In the case of microthermometry, the freezing point depression of aqueous inclusions, as indicated by the temperature of ice melting in previously frozen inclusions, is combined with the binary H_2O–NaCl system (Bodnar & Vityk 1994) to infer salinity of the fluid and is expressed in terms of weight percent NaCl equivalent (wt. % $NaCl_{equiv}$). The presence of other solutes, (i.e., Ca^{2+}, K^{+}, Mn^{2+}) is inferred by the observed depressing of the ideal H_2O–NaCl binary eutectic temperature (i.e., T_e = –21.2ºC). Metastability is also an unavoidable problem associated with temperature–induced phase behaviour (Samson & Walker 2000, Bakker & Baumgartner 2012) and has consequences for the meaningful interpretation of microthermometric data.

TABLE 2.1. SUMMARIZED DATA FROM OTHER RESEARCH REPORTING ANALYSIS OF EVAPORATE MOUNDS USING THE SEM-EDS TECHNIQUE

Location and setting	Size of study area	Host mineral	Number of samples	Number of analyses	Major solute cations	Major solute anions	Minor solutes	*Other analytical techniques used	Conclusion relevant to this study	Reference
Guadalcazar granite, Mexico	6 Km^2	Qtz	18	354	Na, K, Ca, Mn, Fe, Zn, Ag, Ba	Cl	Ag	Bt geothermometry, decrepitation-ICP	Ag occurs in 1/18 samples. Mineralized sample proximal to known Ag-deposit	Chryssoulis & Wilkinson (1983)
quartz vein cutting metasediments/metavolcanics, Pamour Mine, Abitibi Greenstone Belt, Ontario	metre-scale quartz vein stockwork	Qtz	3	43	Na, K, Ca, Mg, Zn, Fe, P, Ti	Cl, S	Au, Zn	gas chromotography leachate analysis	detectable S in mounds	Walsh *et al.* (1988)
hypogene quartz kaolinite from strongly deformed area of the South Mountain Batholith, Nova Scotia	2.5 Km^2	Qtz	1	15	Na, K, Ba	Cl	Si, Kln	stable isotopes (O), SEM-EDS analysis of evacuated cavities	abundance of evacuated cavities without any precipitates interpretated as V-rich inclusions	Kontak & Kyser (2001)
altered pegmatitic syenite, Tamazeght complex, High Atlas Mountains, Morrocco	68 Km^2	Ne	10	not specified	Na, Ca, Mn, Fe, K	Cl		SEM-EDS analysis of evacuated cavities	EDS system employed not sensitive to F	Salvi *et al.* (2000)
breccia pipes in Pinatosa; fault-hosted breccia in Red Cloud, Gallinas Mountains, New Mexico	24 Km^2	Qtz, Fl		not specified	Na, K, Ca	Cl, S		raman analysis of solid phases hosted by L-V-S inclusions	identification of two distinct inclusion populations: Na-K-Cl-S (early) and Na-Cl (late)	Williams-Jones *et al.* (2000)
Dunbrack deposit: vein hosted in Musquodoboit Batholith, Nova Scotia	metre-scale quartz veins	Qtz	1	20	Na,K, Ca	Cl	Pb, Cu, Zn, Ag	$^{40}Ar^{39}Ar$ dating, stable isotopes (S, O, D), whole-rock geochemisstry	two distinct mound populations: Na-Cl type and Na-K-Ca-Cl type	Kontak *et al.* (1999)
Oka carbonitite complex, Québec	18 Km^2	Ap, Cal	3	27	Na, K, Ca, Mg	Cl, S		leachate analysis	charge imbalances between 18 - 53%	Samson *et al. (1995)*
Jubilee (J) and Gays River (GR) MVT-type deposits, Nova Scotia	not determined	Dol, Sp, Cal	5	31 (GR) 34 (J)	Na, Ca, K, Mg	Cl	Zn, Pb		analyzed standards to determine appropriate beam SEM voltage for EDS mound analysis	Savard & Chi (1998)
Gays River carbonate-hosted Zn-Pb deposit, Nova Scotia	not determined	Spl, Cal, Brt, Qtz, Fl	1	10	Na, Ca, Mg, Fe	not given	Zn, Pb	gas chromatography	Major solutes: Na, Ca, Mg; Minor solute: Mn; no mound production in Cal or Brt	Kontak (1998)
Pine Point (PP) / East Tennessese (ET) MVT deposits	10 km^2 (ET); 250 km^2 (PP)	Spl, Dol (ET); Spl, Dol, Ga (PP)	not specified	179 (ET); 78 (PP)	Na, Ca, K, Mg, Fe	Cl, S	Zn, Pb		correlation between depressed final melt temperatures and increased Ca: Na ratio	Haynes & Kesler (1987)
Pegmatite, greisen and vein deposits, South Mountain Batholith, Nova Scotia	500 km^2	Qtz	not specified	236	Na, Ca, K, Fe, Ba, Cu, Zn, Ni	Cl, S	Sn, W, U, Mo, Cu and Mn		major solute species: Na, Cl, K, Ca, minor solute species: S, Fe, Ba, Cu, Zn	Carruzzo *et al.* (2000)
Pegmatite-hosted REE deposit in alkaline granite and syenite, T-zone deposit, Thor Lake, NWT	25 km^2	growth zones in Qtz	3	13	Na, Ce	Cl, S	Mg, Al, P, K, Ca, Pr	LA-ICP-MS, raman spectroscopy	REEs in mounds, charge imbalances 5 - 45%	Feng (2014)
East Kemptville tin deposit, Nova Scotia	< 1 km^2	Qtz, Cst	4	c. 200	Na, Fe, Mn, K, Ca	Cl, S	Sr, Ba, Zn, P	gas chromotography	Elevated content of Fe (23 wt. %) and Mn (37 wt. %) in mounds	Kontak *et al.* (2001)

Mineral abbreviations after Kretz (1983).

* All studies, excluding Savard & Chi (1998) and Samson et al., (1995) include microthermometric analysis of fluid inclusions

Destructive analytical techniques are comparable in broad terms, but important differences exist. Crush–leach analysis of bulk samples (Alderton *et al.* 1982) provides an average measurement of the composition of all inclusions hosted in the sample, but the composition of individual inclusions is not obtainable. Laser micro–beam techniques (i.e., LA–ICP–MS) target individual fluid inclusions and permit measurement of a large spectrum of analyzed elements, but analytical challenges can be significant. For example, the estimation of the internal standard concentration for data quantification becomes increasingly problematic with increasing fluid salinity and chemical complexity of the fluid (Allen *et al.* 2005). Additionally, high ionization energies associated with halogens, notably F and Cl, precludes routine quantification by LA–ICP–MS (Pettke *et al.* 2012, Guillong *et al.* 2003).

An alternative, relatively simple and cost–effective method of assessing the major solute chemistry of fluids is to overheat inclusions and induce decrepitation (Roedder 1984, p. 212), and if a fracture, either natural or induced, connects ruptured inclusions to the surface, evaporate mounds may precipitate on the sample surface. Locating and analysing evaporate mounds requires only a scanning electron microscope (SEM) equipped with an energy dispersive X–ray (EDS) spectrometer (Haynes *et al.* 1988, Kontak 2004). Results of EMA done by EMPA (Carruzzo *et al.* 2000) show a compositional diversity of SMB quartz–hosted fluid inclusions (Fig. 2.2). We emphasize that EDS analysis of evaporate mounds is distinguished from the analysis of fluid–inclusion daughter minerals (Metzger *et al.* 1977, Kamenetsky *et al.* 1999, Salvi *et al.* 2000, Elmi Assadzadeh *et al.* 2016), the analysis of evaporate mounds by EMPA (Zaw *et al.* 2003) and cyrogenic SEM–EDS techniques (Shepherd *et al.* 1998).

This paper describes a step–by–step EMA methodology that includes guidelines for (1) sample preparation, (2) petrographic characterization of inclusions, (3) decrepitation techniques,

(4) decrepitation temperature (5) considerations for customized calibration of EDS data, (6) optimization of EDS acquisition conditions, and (7) data screening.

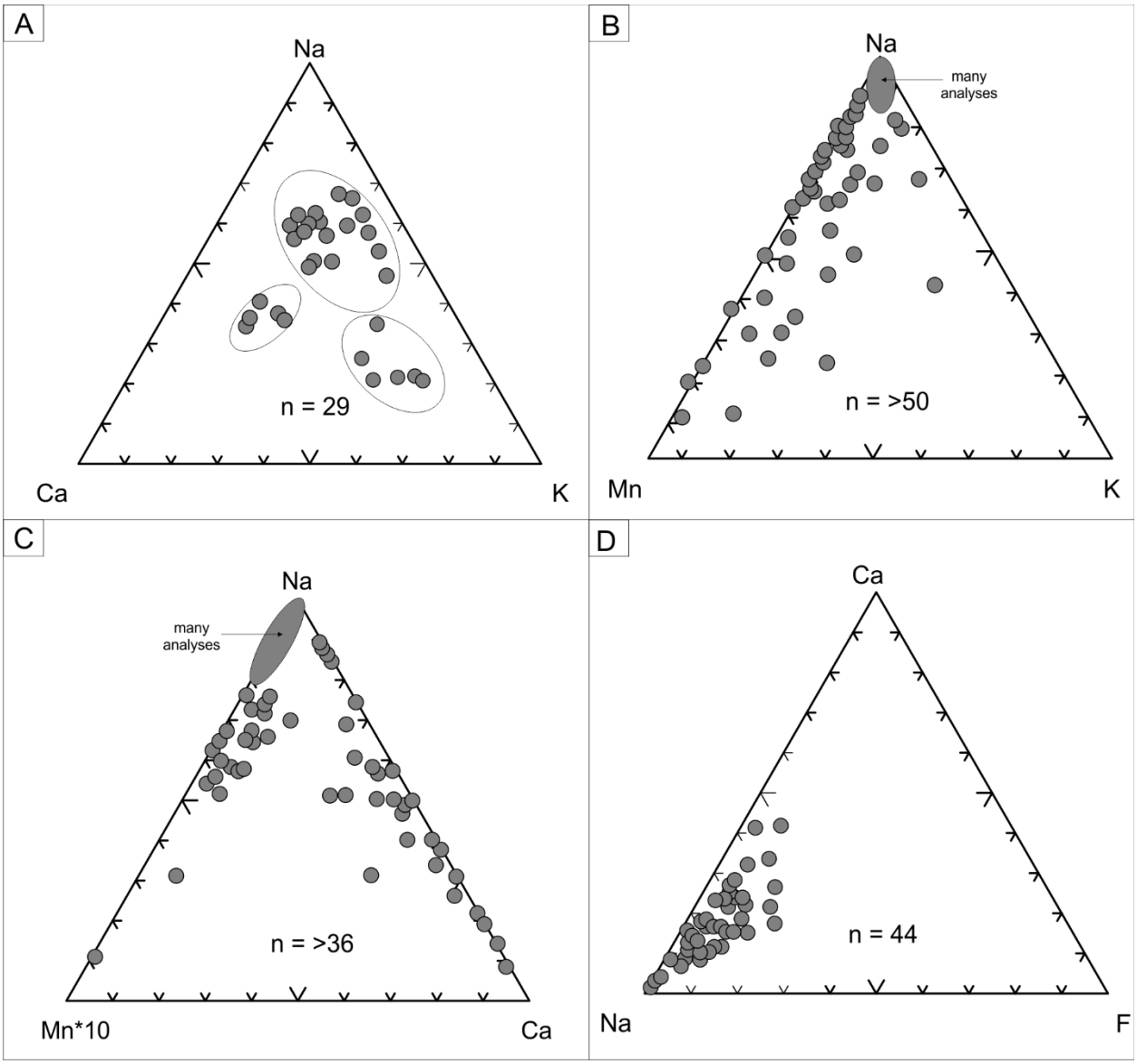

Figure 2.2: Ternary plots from past EMA research displaying relative abundance of selected major solute elements in SMB quartz–hosted fluid inclusions. (A) Aplite–pegmatite rock, Long Lake prospect (modified from Carruzzo *et al.* 2000). (B) Mineralised granite and pegmatite rock samples, East Kemptville tin mine, Nova Scotia (modified from Kontak 2004). (C) Barren aplite–pegmatite sheets, Peggys Cove (modified from Kontak 2004). (D) Mineralised vein quartz, Sandwich Point (modified from Kontak & Kyser 2011). Note the F–enriched fluids from Sandwich Point.

2.1 Methodology

2.1.1 Sample preparation

One centimetre–thick, rectangular (20 x 40 mm) blocks cut from rock slabs were polished and then mounted onto standard petrographic glass slides using Crystalbond™ wash–away adhesive. Using a standard trim saw, the blocks were then cut to 250–300 µm thick wafers, which was reduced to 150–200 µm thickness using a standard cup grinder, followed by machine polishing. After machine polishing with silicon carbide disks (500 – 4000 grit), a polyester diamond cloth impregnated with 9 µm diamond paste was used for final polishing. Selection of quartz chips for decrepitation was based on light microscope observation of near–surface fluid inclusions. In this study, quartz 'chips' are an aggregate of individual quartz grains, as it is not usually possible to extract single quartz grains. A benchtop rotary tool equipped with a high–precision ultra–thin circular blade was used to remove selected chips from the polished wafer. Soaking in an acetone bath for a minimum of 12 hours released quartz chip from the glass slide. Floated chips were either immediately loaded into an oven or Linkham heating/freezing stage or stored in a desiccation chamber until analysed. Following heating, decrepitated chips were removed from the oven or heating /freezing stage and mounted on a SEM–compatible sample holder with double–sided carbon tape or appropriate epoxy and taken immediately to SEM–EDS for analysis or stored in desiccation chamber for future analysis. Figure 2.3 summarizes the above process.

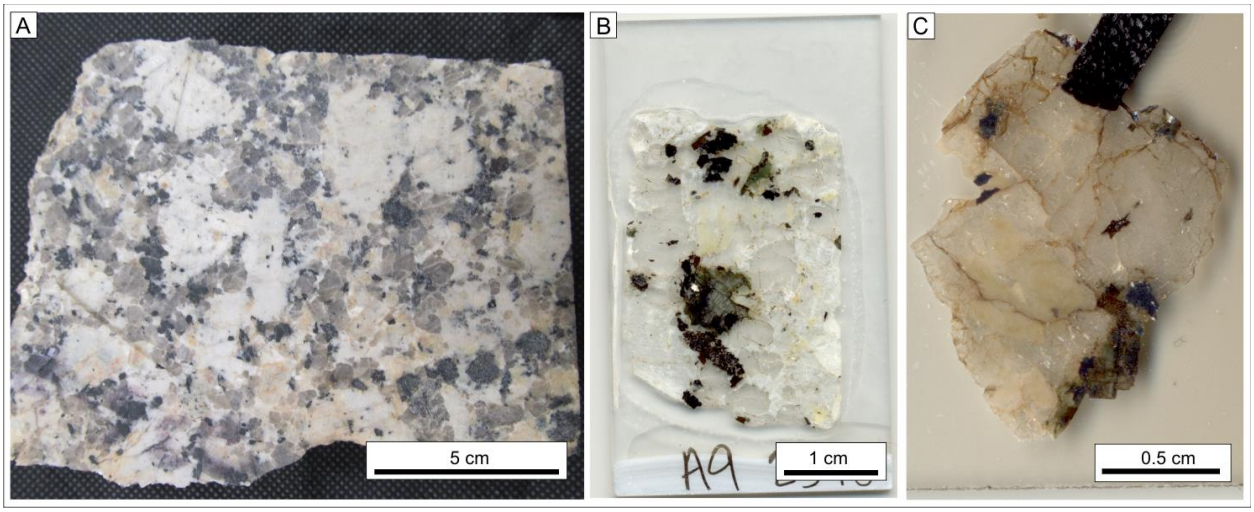

Figure 2.3: Preparation of fluid inclusion chips from slab sample A09–2378. (A) Decimetre–scale slab samples provide material for preparation of doubly polished fluid inclusion wafers. (B) Fluid–inclusion wafer, approximately 150 µm thick, affixed to glass slide with acetone–soluble Crystal Bond™. (C) A roughly 1 cm^2 quartz chip was cut and, after decrepitation, mounted on glass slide, which was then carbon–coated and stored in desiccation chamber until SEM–EDS analysis.

2.1.2 Petrographic work

Fluid inclusions wafers were assessed using standard transmitted light microscopic observations in order to detect if the quartz chips hosted a relative abundance of fluid inclusions. Characterization of the size, abundance and types of fluid inclusions is recommended, but the main objective of microscope work is to identify quartz chips that host a relatively high abundance of inclusions occurring near the upper surface of the wafer. The latter was thus the critical step of selecting material for subsequent preparation of material for EMA. Representative images of suitable material used in this study will be shown in a published report (Tweedale *et al.* in prep, 2019) where they are arranged from low to high potential for generating sufficient mounds suitable for EMA.

2.1.3 Synthesis of standard materials and charge imbalance

During preliminary analysis of evaporate mounds from the SMB, it became apparent that charge imbalance between Σanions and Σcations was an issue and required attention. We also note the importance of this issue as it was not highlighted in all other related studies (*cf.* Haynes *et al.* 1988, Kontak 2004). The largest negative charge imbalances occurred in mounds with significant F (i.e., up to 40 wt. % of the total mound), such as shown in the crystallised mound with fluoride and halide salts of Figure 2.4. Potential sources of charge imbalance include: (1) element volatilisation during decrepitation; (2) volatilisation of mound elements during electron bombardment, as noted for analysis of alkalis for example in feldspars and glasses; (3) secondary fluorescence during electron bombardment; and (4) inability to directly detect certain mound elements (*e.g.*, OH^-, O^-, H^+). To assess potential volatilisation and/or secondary fluorescence of mound elements during SEM work, a series of mixed NaCl–CaF_2 powders were synthesized by mixing portions of laboratory–grade NaCl and CaF_2 and pulverizing with an agate mortar–and–pestle in a clean

controlled laboratory setting. Once mixed, these standard powders were carefully placed onto aluminum holders, carbon–coated and loaded into the SEM for analysis.

To reduce errors associated with the topography and potential inhomogeneity of the hand–ground powered samples prepared for the above standard, a second set of standards were prepared by solvation of homogenized NaCl–CaF_2 powders in boiling water using the same starting materials. The hot solution was then pipetted and evaporated onto clean thin section plates, and a thin–film salt residue precipitated. These thin–film samples were subsequently analysed using the same procedure used to analyze the powdered samples.

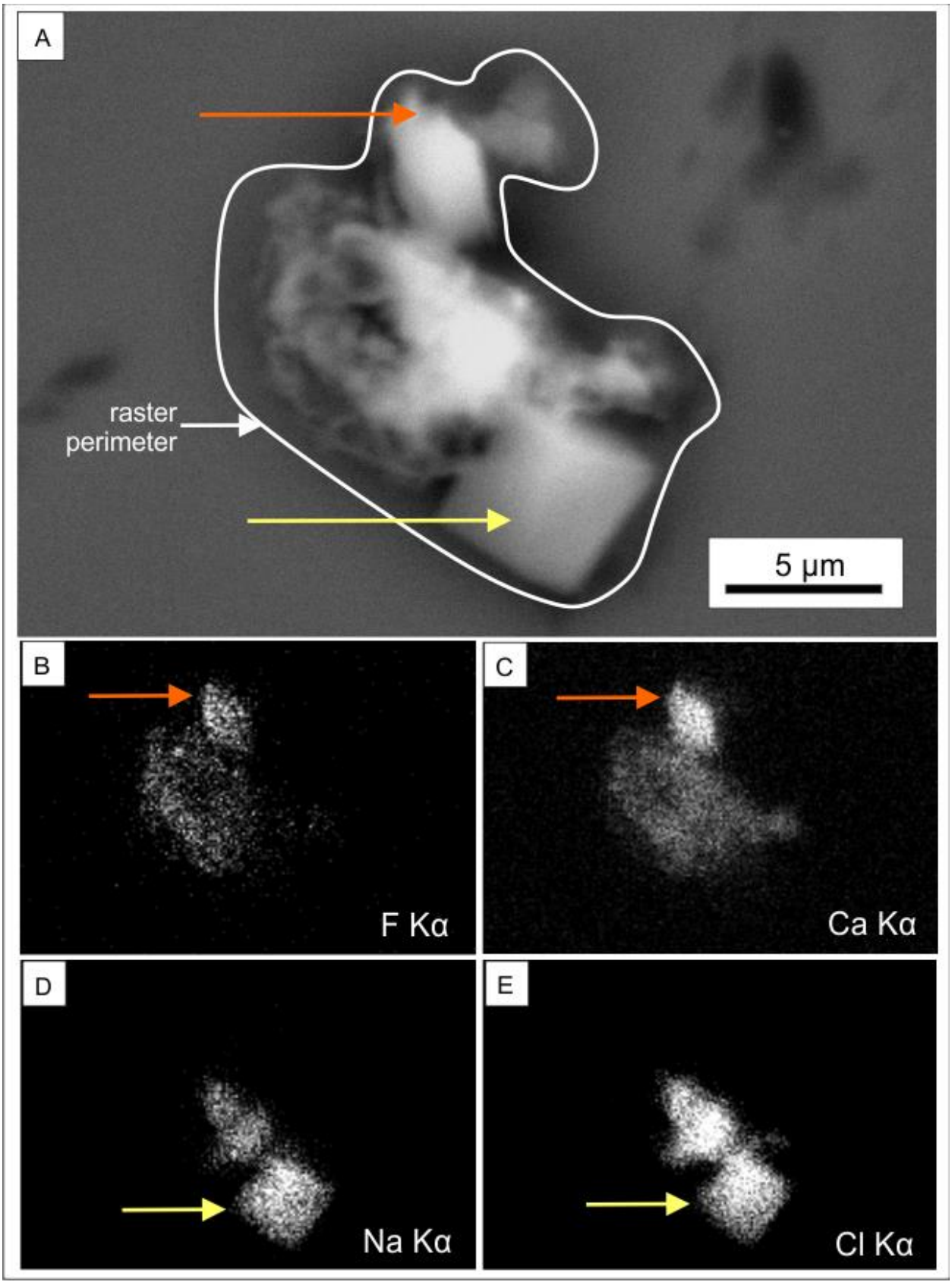
A
raster
perimeter
5 µm
B
F Kα
C
Ca Kα
D
Na Kα
E
Cl Kα

Figure 2.4 (previous page): SEM back scattered electron image (A) and EDS X–ray maps (B to E) of a quartz–hosted evaporate mound. The arrows highlight the presence of NaCl salt (yellow arrows) and Ca–fluoride salt (orange arrows). The X–ray maps shown follow: (B) F, (C) Ca, (D) Na and (E) Cl. Identification of a Ca–fluoride salt demanded that we address analytical issues associated with fluorine.

2.1.4 SEM–EDS instrumentation

During the course of this study, the evaporate mounds and synthetic powders were imaged and analyzed using two instruments housed in the Department of Geology, Saint Mary's University, Halifax, Nova Scotia, Canada: (1) a thermal emission LEO® 1450 SEM equipped with an Oxford Instrument® X–max 80 mm^2 silicon–drift detector (SDD) EDS, and (2) a field emission Tescan® MIRA 3 LMU SEM coupled with the same EDS system. During imaging and X–ray analysis of the mounds, the SEM was operated at an accelerating voltage of 20 – 30 keV for instrument 1 and 20 keV for instrument 2. The EDS detector is equipped with a thin polymer window that allows routine detection of light ($Z < 12$) and heavy ($13 < Z < 82$) elements in evaporate mounds at concentrations as low 1000 ppm (0.1 wt. %). The accompanying INCA data reduction software included a Phi–Rho–Z matrix correction scheme and signal counts were calibrated at fixed wavelengths through the analysis of stoichiometric synthetic and natural oxides, metals, alloys and mineral standards. Notably, Na, F, K, Cl and Ca were calibrated with standards of $NaAlSi_3O_8$, MgF_2, KCl and $CaSi_2O_6$, respectively, which are stored in an automated software database. The minimum detection limit is estimated at 0.1 wt. % based on repeated analyses of standards.

2.1.5 Optimizing analytical procedures

Efficient application of EMA to exploration research requires optimization of analytical parameters specific to the study area in question. To this end, a small subset of samples were chosen for preliminary analysis. Preliminary results are compared in order to determine: (1) the optimal decrepitation temperature; (2) the minimum number of analyses required to generate representative data; (3) the optimal EDS acquisition time; (4) appropriate mode of EDS analysis, and (5) decrepitation technique. Given that an exploration project may require analysis of 1000s

of samples, these preliminary considerations are important for ensuring collection of meaningful data in a cost–effective manner.

2.1.5.1 Decrepitation temperature

Decrepitation temperature of fluid inclusions is a function of a variety of parameters which include size, fluid density (i.e., isochoric projection in PT space), shape, volatiles present (*e.g.*, CO_2), and the strength of the host phase (Bodnar *et al.* 1989). An optimal decrepitation temperature for EMA work can be determined indirectly by evaluating the relationship between the homogenization temperature (T_h) and inclusion size for a single–inclusion origin (see Fig. 1 in Haynes *et al.* 1988), or a fluid inclusion assemblage (FIA). Following a review of other EMA research conducted on quartz–hosted fluid inclusions (Table 2.2), aliquots of quartz chips from a single sample of mineralised (Mo) quartz–feldspar pegmatite were individually heated to 300°, 400° and 500°C.

2.1.5.2 Minimum number of analysis required

In order to assess the minimum number of mounds needed to obtain reliable and chemically representative data for an assemblage of aqueous inclusions, we compared results collected from variably sized data sets for a single sample. Specifically, analyses were obtained from four independent data sets with n = 8, 16, 32 and 64 mound analyses from a single centimetre–scale quartz chip.

2.1.5.3 Acquisition time

The optimal EDS acquisition time is the minimum count time that the EDS ‘counts’ generated X–rays from the target material, in this case the evaporate mound, in order to ensure that all major and minor solute elements are identified. To determine the optimal (i.e., practical) acquisition time,

we evaluate results generated from the repeat analysis of mounds using acquisition times of 5, 10, 20, 40, 60 and 100 seconds.

Table 2.2. DECREPITATION TEMPERATURES USED IN OTHER SEM-EDS FLUID-INCLUSION RESEARCH

Host rock	Host mineral	Dominant fluid inclusion type	Decrepitaion temp. range (°C)	Reference
n/a	synthetic quartz	$L_{aq}V$	360 - 420	Haynes *et al. (*1988)
altered granite, pegmatite, greisen, veins	quartz	$L_{aq}V$, $L_{aq}V$-Halite (H), L_{aq}-V-H-Sylvite (S)	350 - 500	Kontak (2004)
granitoid	quartz	L_{aq}, V, $L_{aq}V$, $L_{aq}V$±solid, $L_{aq}V$-H	400 - 420	Carruzzo *et al*. (2000)
carbonitite	apatite, calcite	$L_{aq}V$, $L_{aq}V$-H	400 - 500	Samson *et al*. (1995)
carbonate	calcite, dolomite, sphalerite	not specified	420	Savard & Chi (1998)
intrusive breccia associated with quartz syenite	fluorite, quartz, bastnaesite, barite	$L_{aq}V$-solid, L_{aq}-V,	400	William-Jones *et al*. (2000)
quartz-kaolinite breccia	quartz	$L_{aq}V$	450 - 600	Kontak & Kyser (2001)
granite-hosted veins	quartz	V, L_{aq}, L_{aq}-solid, V-solid	up to 570	Chryssoulis & Wilkinson (1983)
brecciated carbonate	sphalerite and dolomite	not specified	325 - 350	Haynes & Kesler (1987)
rhyolite/sedimentary	quartz	$L_{aq}V$	350-400	Zaw et al. (2003)
vein infill	quartz, sphalerite	L_{aq}-CO_2-CH_4-solid	500	Walsh *et al*. (1988)
metasedimentary	quartz	$L_{aq}V$	300 - 350	Heinrich & Cousens (1989)

2.1.5.4 Mode of analysis: point versus raster

Mound dimensions largely determine if point–mode or raster–mode analysis is appropriate. Point–mode provides representative data for mounds with diameters of 5 μm and smaller which reflects the size of the excitation volume of the SEM beam in a light element matrix (i.e., alkali–rich mound and silica host). Point–mode analysis is also appropriate for targeted domains within a evaporate mound or within the decrepitation cavity (Salvi *et al.* 2000). In contrast, raster–mode provides compositional data for the entire mound and precludes problems such as variable mound chemistry related to elemental fractionation (Haynes & Kesler 1987b, Walker 1998, Tweedale *et al.* 2013, Pandur *et al.* 2015).

2.1.5.5 Decrepitation techniques

Mound generation requires oven–heating or stage–heating of mineral chips. To assess potential variation in mound size and abundance between the two techniques, two quartz chips from two samples were selected (4 chips total). For oven–heating, a Thermacraft® clamshell furnace operated at a heating rate of 10°C/minute was used. In contrast, the Linkham® heating/freezing stage was operated at a heating rate of 50°C/minute. The oven method requires the selected quartz chips be carefully arranged face–up on a heat–resistant sample tray. Whereas ovens can accommodate many chips in a single run, standard heating/freezing stages mounted on a petrographic microscope can only accommodate a single *ca*. 1 cm^2 or smaller grain but can be set to run at 0.1 and 150ºC/minute. In addition, stage heating affords real–time viewing of decrepitation.

2.1.6 Data screening

The objective of data screening is to eliminate mound analyses that may misrepresent the solute chemistry of the decrepitated inclusion. For this evaluation, both the size (i.e., in context of salinity and decrepitate cavity size; see discussion below) and morphology of individual mounds must be assessed, charge balance calculated and compositional homogeneity evaluated (Haynes *et al.* 1988). Size is determined by the measuring the long–axis diameter of the mound, whereas the morphologies of individual mounds describes their habits (*e.g.*, granular, massive, equant, dendritic, *etc*.). For the charge balance, the respective charges for the Σcations and Σanions are calculated based on the atomic abundances and charge (*e.g.*, Na^{+}, Ca^{2+}, Cl^{-}, F^{-}) and ideally the magnitude of the $\sum+ = \sum-$, Deviations indicated by imbalance suggest error.

2.1.7 Data evaluation and processing

Additional general guidelines for EMA studies (Kontak 2004) require three basic steps for data reduction. Firstly, the substrate (host) chemical signal (*e.g.*, quartz) may or may not be removed from the signal (Fig. 2.5) and is discussed in more detail below in terms of how it may influence the final data. Secondly, removal of mound analyses in which Al detection is > 5 wt. %, as these reflects contamination by solid mineral fragments (*e.g.*, mica or feldspar) of unknown origin and thus, may not accurately represent fluid inclusion solute load (Kontak *et al.* 2014). Thirdly, the EDS data set is scanned for internal consistency such that single populations of fluids can be determined, and anomalous results are identified.

In regard to step 1 above, there are three ways that the contribution of the substrate, in this case quartz which is the most common phase, can be managed and these are evaluated below. In Figure 2.5 is presented a comparative summary of the results from analysis of three evaporate mounds using the following three data reduction methods:

1) *Subtraction method*: an EDS signal of the substrate is subtracted from that of the mound and the residual is used as the final analysis for the solutes.

2) *Normalization without background subtraction*: the signal is processed without modification and the solute data detected are normalized to 100 wt. % after removing Si and O from the analysis.

3) *Normalization after correcting for quartz substrate*: the EDS signal is processed after removal of Si and O from the spectra which provides a residual analysis with 100% solute data.

The most important aspect of which procedure is used relates to elements that fall between Cl and Si on the EDS spectra because of the elevated Si background. The latter will for example affect the counts for Mo and S and may lead to false positive anomalies where not present (Fig. 2.5), or where present will actually decrease their true abundances. For this reason, method 2 is considered the default method for data processing, but where mounds are large and little quartz is detected in the analysis method 3 can be used.

2.1.8 Sample–scale heterogeneity

To evaluate wafer–scale variation in evaporate mound abundance, morphology and chemistry, a greisen sample collected from the Long Lake molybdenum prospect (Fig. 2.1; O'Reilly *et al.* 1982) was selected for multi–grain analysis. Three quartz grains selected from same fluid–inclusion wafer were heated in an identical manner.

2.1.9 Comparing EMA and microthermometric results

To compare microthermometric and EMA data, a sample hosting abundant fluid inclusions that were large enough to be easily located by microscopy was selected. The sample chosen was a ca 10 cm euhedral quartz sample collected from a pegmatite in a granodiorite phase of the SMB proximal its contact with Meguma metasedimentary rocks in the Bayers Lake area of Halifax (Fig.

2.1). The selected quartz crystal is inundated with 2–phase, liquid–rich inclusions of < 1 μm to > 100 μm size and thus very amenable to routine microthermometric analysis.

2.1.10 Microthermometry

Microthermometric measurements were performed at SMU using a calibrated Linkham® FTIR 600 heating–freezing stage mounted on an Olympus® BX51 polarizing light microscope. Analyses of synthetic fluid inclusion standards (melting point and critical point of pure water) were used for stage calibration. Total uncertainties with thermometric measurements range from ±2 to 3ºC for temperatures near the extremes of working conditions (–180º to 560ºC), to < ± 0.2ºC for temperatures recorded near 0ºC (i.e., ice melting).

2.2 Results

2.2.1 Petrographic characterization of fluid inclusions

Petrographic study of several hundred archived thin sections of the SMB reveals the pervasive presence (i.e., batholith–wide) of secondary aqueous fluid inclusions hosted by magmatic quartz. Most commonly, the inclusions form linear arrays along annealed fractures oriented obliquely to the plane of observation (Fig. 2.6A, B). Lack of visible growth zones in the quartz using either plane polarized light or in crossed nicols precludes an absolute assessment of all the inclusions, hence some may in fact be of primary origin. Thus, the nature of the inclusions is most consistent with a secondary origin. The vast majority of the observed fluid inclusions are 5 – 20 μm size, but rarely to 40 μm, and are 2–phase liquid–rich (L_{aq}–V) aqueous types. They, have oval, equant or irregular shapes and have consistent 90/10 L:V phase volume ratios (Fig 2.6C). Subordinate populations include monophase liquid (L_{aq}) and monophase vapour (V) types of 5 – 15 μm size (Fig 2.6D, E), in addition to rare three–phase L_{aq}–V–S (halite or sylvite) inclusions that are present in pegmatite and greisen samples (Fig. 2.6F, G).

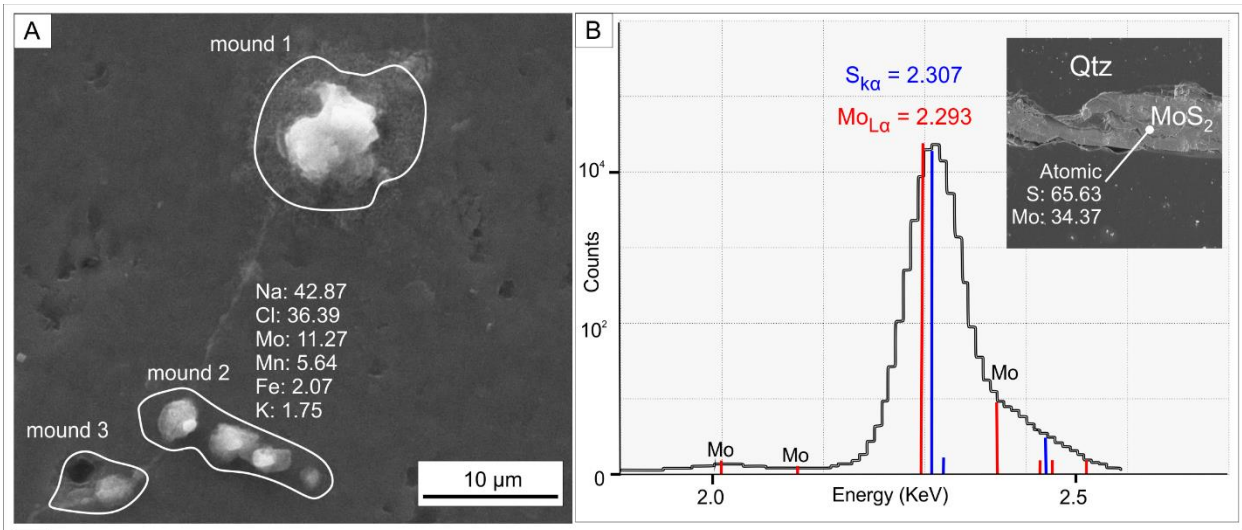

C Tabulated EDS results generated using three data reduction methods.

Sample	Data reduction method	O	Na	Si	S	Cl	K	Mn	Fe	Mo	Total	Σ+	Σ-	Σdiff	Σdiff%
		weight percent										atomic weight			
background		57.96		42.04							100.00	5.99	7.25	-1.26	-9.51
mound 1	1		31.93		2.39	43.73	9.89	9.94	2.12		100.00	2.08	1.38	0.70	20.14
mound 1	2		33.23		2.70	42.65	9.57	9.74	2.11		100.00	2.12	1.37	0.75	21.45
mound 1	3		32.35		2.66	45.04	8.63	9.29	2.03		100.00	2.04	1.44	0.60	17.35
mound 2	1		42.13		4.50	43.02	1.72	6.45	2.18		100.00	2.19	1.49	0.70	18.87
mound 2	2		45.49		5.03	38.83	1.93	6.37	2.35		100.00	2.34	1.41	0.94	24.91
mound 2	3		45.28		4.50	40.35	1.67	5.95	2.25		100.00	2.31	1.42	0.89	23.89
mound 3	1		42.87		4.94	43.21	2.41	4.56	2.01		100.00	2.17	1.53	0.64	17.27
mound 3	2		46.35		5.57	38.29	2.60	4.86	2.33		100.00	2.34	1.43	0.92	24.28
mound 3	3		46.32		4.93	39.75	2.22	4.55	2.22		100.00	2.32	1.43	0.89	23.71

Figure 2.5: Data reduction methods.(A) SEM-SE image showing three mounds hosted by a cassiterite quartz sample from the East Kemptville tin mine. Note the uncorrected (i.e., default) composition of mound 2, which includes a false-positive detection of Mo. (B) Energy-dispersive spectrum for the analysis of stoichiometric molybdenum hosted by the Long lake quartz pegmatite. Note the asymmetry in the large peak which suggests an overlap of Mo and S signals, which explains the susceptibility of false positive signals for Mo. (C) Tabulated EDS results generated using three different data reduction methods (see text for details).

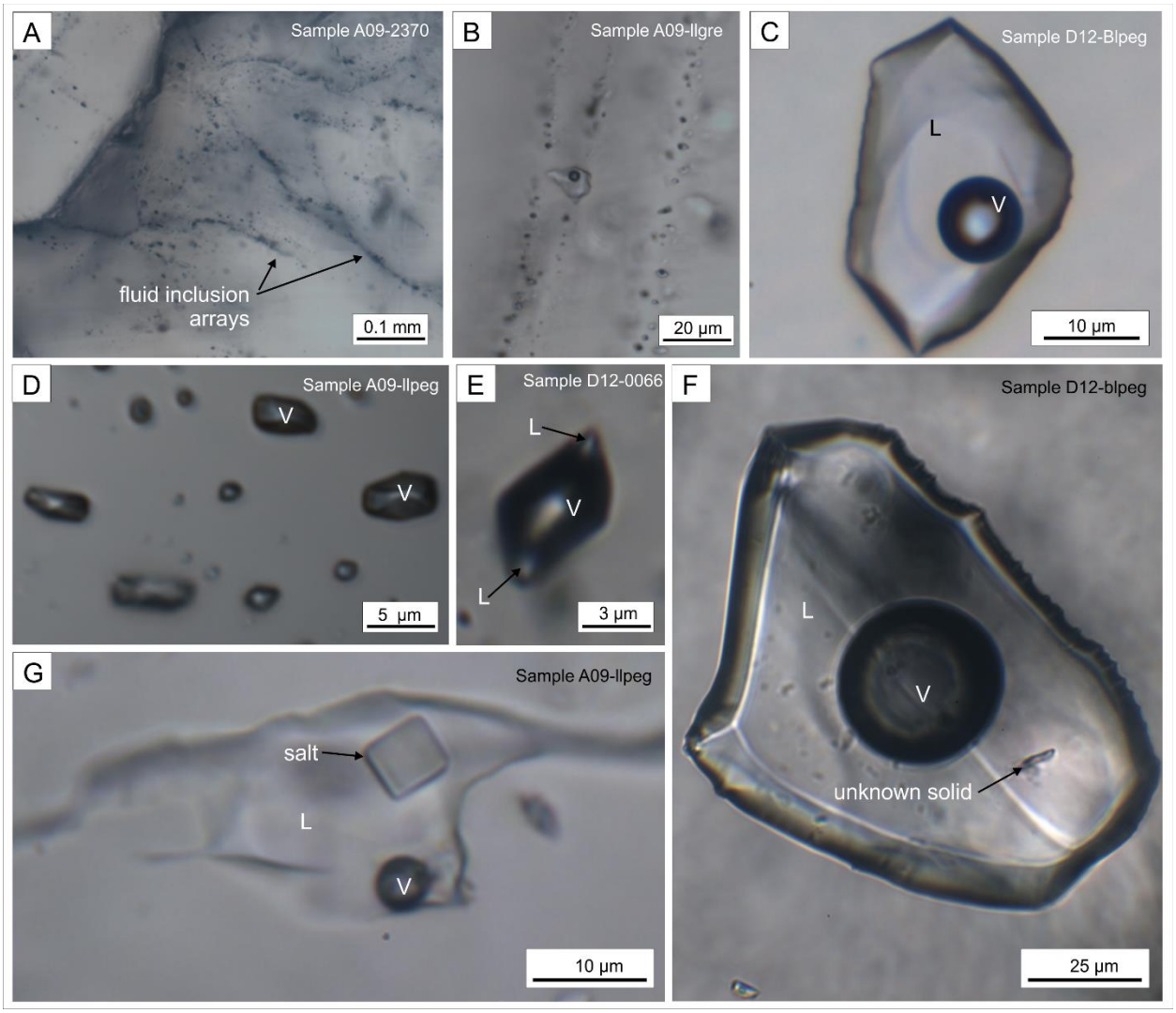

Figure 2.6 (previous page): Transmitted–light photomicrographs of quartz–hosted fluid inclusions in samples from the SMB. (A) Low–magnification view of a linear array of fluid inclusions linear defining annealed fractures. (B) High–magnification view of linear arrays of fluid inclusions. (C) Two–phase (L–V) aqueous fluid inclusion displaying the typical 90:10 L:V ratio that characterizes the quartz–hosted inclusions in the SMB. Relatively uncommon types of fluid inclusions observed in the SMB include single–phase L–rich (D), two–phase V–rich (E), three phase L–V–halite (F) two–phase L–V with unknown solid (G).

2.2.2 EDS Accuracy

The analysis of mixed NaCl–CaF_2 powders of known composition provides data to estimate the accuracy of EDS analysis of evaporate mounds (Table 2.3). Charge imbalances associated with all the analyses of these standard powders are negative, suggesting that volatilisation of F and Cl by the electron beam does not occur, or that volatilisation effects are offset by a process that artificially increases F and Cl detection concentrations (*e.g.*, secondary fluorescence). When compared to actual values, the quantified errors for the powdered halite are 2 and 3% relative for Na and Cl (Table 2.3), respectively. Results for the mixed powder standards show that the magnitude of error for Na and Cl is positively related with CaF_2 content, progressively increasing to 32% and 15 % relative for Na and Cl, respectively. In contrast, error associated with F and Ca detection is not related to the amount of CaF_2 in the powder. The largest error in F detection (41% relative) occurs in the powder with the least amount of CaF_2. The largest error in Ca detection (43% relative) occurs in the powder with 60% CaF_2. Overall, the percent error in the quantification of F, Na, Cl and Ca in the NaCl–CaF_2 powders results in the overestimation of F by up to 40% (relative), up to 32% (relative) for Na, and underestimates of up to 40% (relative) for Ca and up to 15% (relative) for Cl.

2.2.3 EDS Precision

Spectrometer precision was assessed by repeated analysis (n = 16) of a single multi–component evaporate mound using consistent beam conditions (20 kV and 2nA) and acquisition time (60 seconds). Relative standard deviations (RSD) for elements comprising > 5 wt. % (F, Na, Cl, Ca) of the total mound composition vary from 0.63 to 1.09%, whereas the RSD for minor solutes, in this case K, is > 10% (Table 2.4).

TABLE 2.3. ACTUAL COMPOSITIONS AND SEM-EDS RESULTS FROM THE ANALYSIS OF MIXED NACL-CAF_2 POWDERS. MEASURED VALUES ARE AVERAGED FROM 4 ANALYSES OF EACH POWDER

NaCl/CaF2 ratio	composition (wt. %)					average measured value (wt. %)					charge imbalance Σdiff% (atomic)	percent error			
	%F	%Na	%Cl	%Ca	Total	%F	%Na	%Cl	%Ca	Total		F	Na	Cl	Ca
100/0		39.24	60.76		100.00		38.21	61.79		100.00	-2.37		2.69	1.66	
90/10	4.87	35.32	54.68	5.13	100.00	8.38	34.64	51.79	5.20	100.00	-3.69	41.89	1.95	5.59	1.23
80/20	9.73	31.39	48.61	10.27	100.00	13.17	33.62	45.27	7.95	100.00	-2.89	26.07	6.62	7.38	29.18
70/30	14.60	27.47	42.53	15.40	100.00	20.45	31.30	36.88	11.37	100.00	-4.64	28.62	12.25	15.32	35.47
60/40	19.47	23.55	36.45	20.53	100.00	23.90	28.32	33.37	14.41	100.00	-5.98	18.56	16.87	9.25	42.52
50/50	24.09	19.82	30.68	25.41	100.00	30.69	24.37	26.50	18.44	100.00	-8.80	21.48	18.69	15.76	37.79
40/60	29.20	15.70	24.30	30.80	100.00	36.30	20.67	21.03	22.01	100.00	-11.26	19.56	24.04	15.58	39.95
25/75	36.50	9.81	15.19	38.50	100.00	44.11	14.52	13.80	27.57	100.00	-14.92	17.26	32.41	10.07	39.64
0/100	48.67			51.33	100.00	61.95			38.05	100.00	-26.40	21.44			34.91

TABLE 2.4. STATISTICAL DATA FOR REPEAT ANALYSIS (N = 16) OF SINGLE EVAPORATE MOUND (INSET) USED TO ASSESS EDS SPECTROMETER PRECISION. DATA IN WEIGHT PERCENT OF THE TOTAL MOUND

	min	max	ave.	δ	RSD*
F	35.80	37.03	36.41	0.28	0.78
Na	19.15	19.52	19.34	0.12	0.61
Cl	30.73	31.93	31.51	0.34	1.09
K	0.43	0.64	0.53	0.06	11.90
Ca	12.23	12.60	12.37	0.11	0.86

RSD: relative standard deviation

RSD = δ x 100)/μ, where δ = standard deviation and μ = mean.

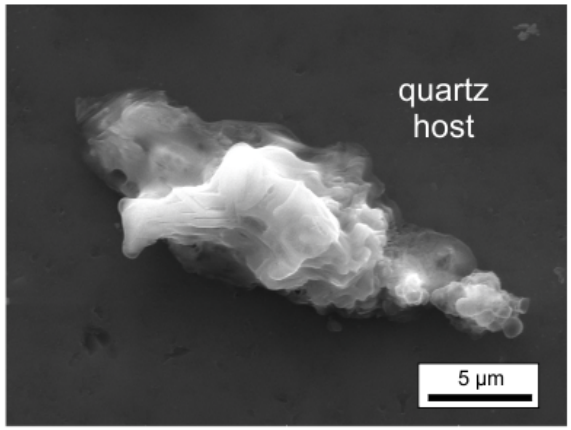

2.2.4 Reducing error associated with detection of F

In order to address the charge imbalance noted in some mounds, generally the ones enriched in both Ca and F, synthetic mixtures of NaCl–CaF_2 powders in different proportions were generated and analysed (Table 2.3). The results indicate that the magnitude of this imbalance is positively related to the amount of CaF_2 present; we note that the reason for this may be related to fluorescence and is further addressed below In order to address the imbalance issue we applied linear calibration equations derived from binary plots of actual or known contents of the synthetic samples versus their measured compositions derived from the analysis of synthetic mounds (not shown here). This had the effect therefore of not only correcting elemental concentrations and thus the apparent accuracy of the analyses, but also the magnitude of negative charge imbalances. This is illustrated by the results obtained from analysing the same synthetic mixtures and applying correction equations to the results. Plots displaying wt. % of the four elements versus expected results are shown in Fig. 2.7.

The effect of applying the calibration equations to naturally occurring mounds varies depending on the amount of F present. For evaporate mounds with < ~20 wt. % F, charge imbalance is usually positive and thus the calibration equations shift the charge imbalance further from charge neutrality (Fig 2.8). In the case of mounds with > ~20 wt. % F, where negative charge imbalances occur, the calibration causes the charge imbalances to shift closer to neutrality (Fig. 2.9). Regardless of F content, the Ca/Na wt. % ratio of mound data increases when the equations are applied. Given the importance of the Ca/Na ratio in mound analysis for interpretation of processes, the decision to 'improve' the apparent accuracy of results by developing and analyzing standards is discretionary and influenced by fluid composition, and therefore setting dependent (i.e., F–rich versus F–poor).

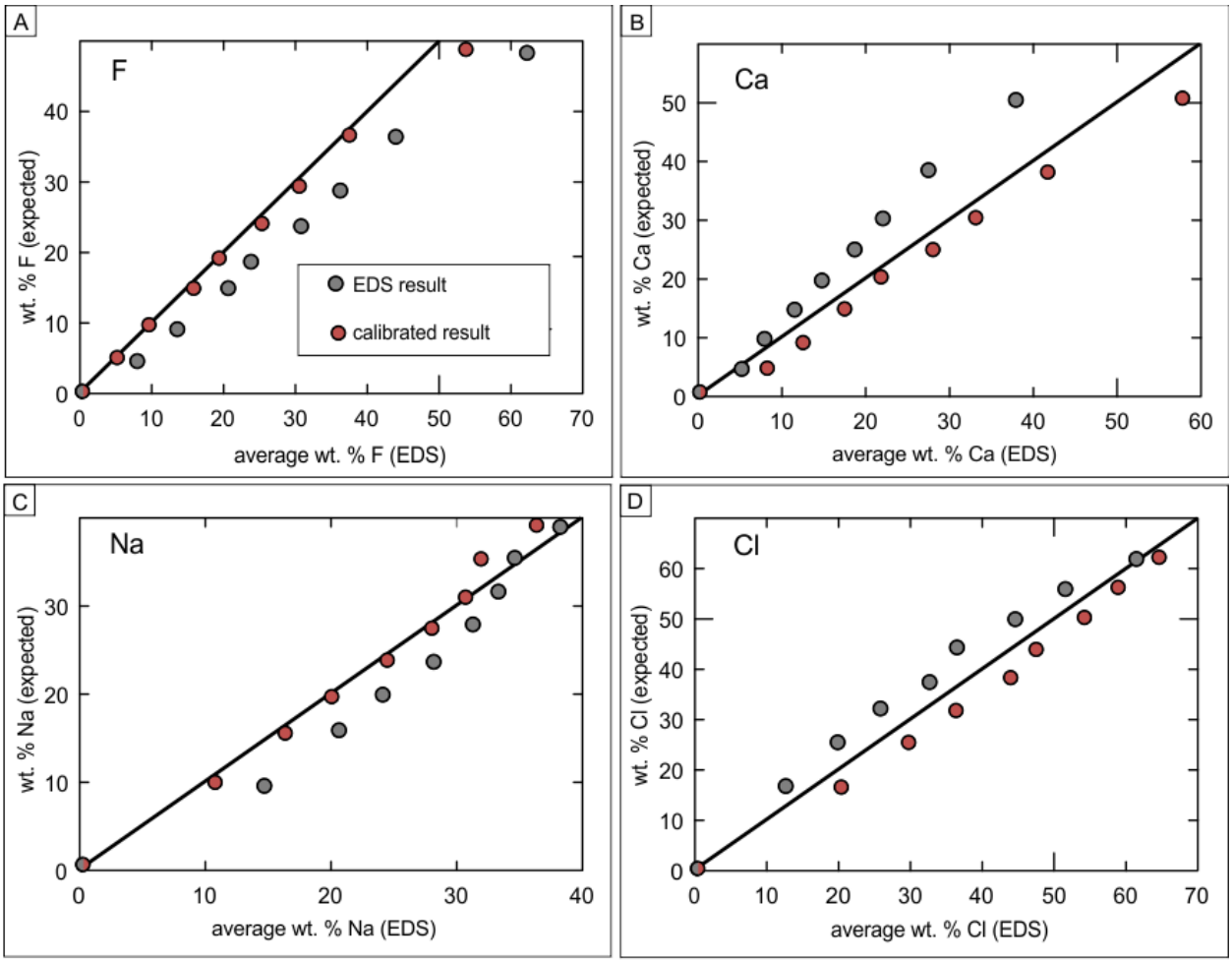

Figure 2.7: Biplots of expected versus EDS analysis results for F, Ca, Na, and Cl.These plots compare SEM–EDS analyses of synthetic NaCl–CaF2 powders before (grey dots) and after (red dots) correction was applied based on calibration equations derived from the analysis of synthetic mixtures of NaCl–CaF2 materials as discussed in the text Note that when all the four elements analysed are corrected (red dots) they plot closer to the one–to–one line than the uncorrected raw EDS data (grey circles).

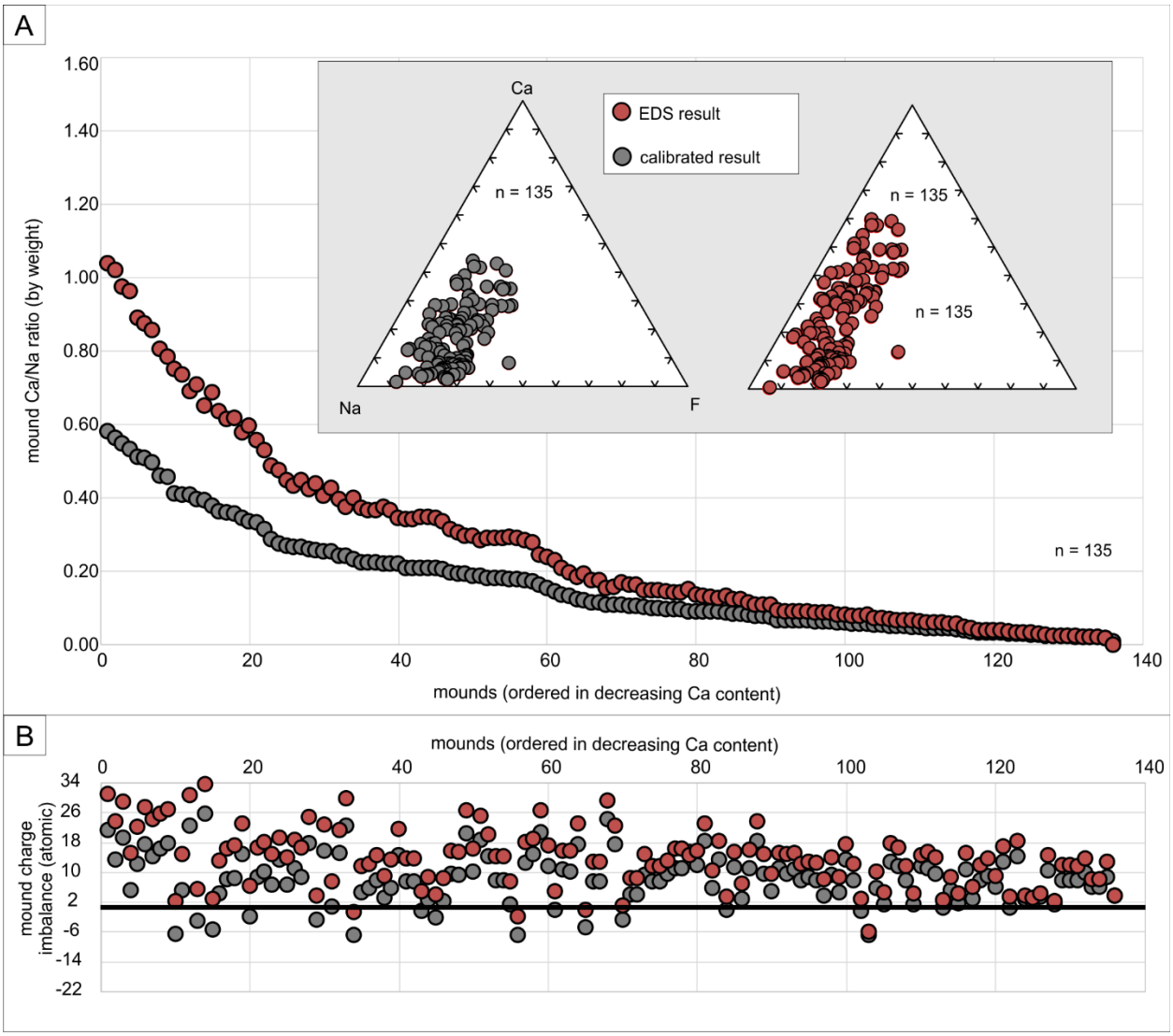

Figure 2.8: Comparison of original (grey circles) and corrected (red circles) EDS results for mounds with 1 – 20 wt. % detectable F. (A) Ca–Na–F plots of the original and corrected EDS data (in wt. %). (B) Binary plot of Ca/Na wt. % ratios with mounds ordered by decreasing Ca content and ternary (Na–Ca–F) wt. % plots. The difference in Ca/Na ratios between calibrated and EDS–quantified data is positively related to detection of Ca in the EDS signal. (C) Binary plot of charge imbalance with mounds ordered as above. The general effect of calibrating the EDS data is to slightly decrease the magnitude of the charge imbalance.

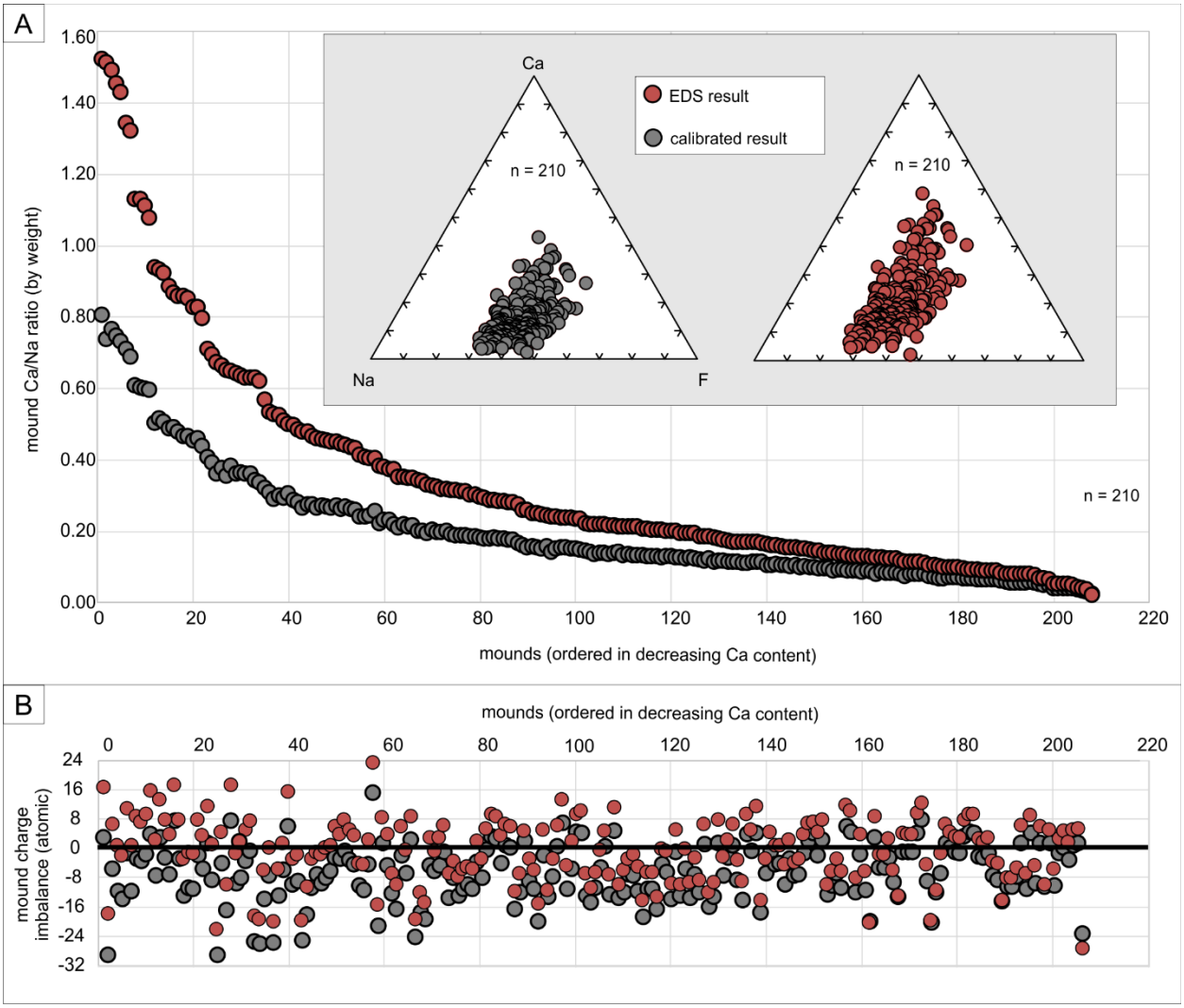

Figure 2.9: Comparison of externally calibrated (red circles) and EDS–quantified (grey circles) results for mounds with 21 – 40 wt. % detectable F. (A) Binary plot of Ca/Na wt. % ratios with mounds ordered by decreasing Ca content and ternary (Na–Ca–F) wt. % plots. The difference in Ca/Na ratios between calibrated and EDS–quantified data is the same as above, and therefore independent of F.

2.2.5 Evaporate mounds

2.2.5.1 Morphological characteristics

In addition to discrete generally sub–spherical evaporate mounds and linear mound arrays reported in other EMA studies (*e.g.*, Haynes & Kesler 1987b, Haynes *et al.* 1988, Kontak 2004), other evaporative residues, including non–linear arrays, evaporative salt flats (i.e., dispersed evaporate residue without discrete mounds) and evaporate channel infill within polishing scratches also precipitate (Fig. 2.10). Real–time viewing during stage–heating experiments showed fluid leaking out of fractures and across the sample surface. Presumably, these events produced some of these other residue morphologies. To avoid the ambiguity of analyzing decrepitate residues that may represent a mixture of escaped fluids from more than one inclusion, we analyzed only evaporate mounds characterized as sub–spherical and isolated salt piles displaying an obvious perimeter measuring between 3 – 40 μm in diameter that encloses a central mass of salt crystals with equant to massive habits. The volumes of evaporate residue within this size range theoretically originate from single fluid inclusions with diameters < 25 μm and salinities of < 23 wt. % total salinity (Haynes *et al.* 1988). The common occurrence of such mounds immediately adjacent to decrepitation pits support this claim (Fig. 2.11). Solid and/or daughter phases observed in decrepitation pits suggests that in some cases physical segregation of inclusion phases (solids from liquid) occurs during decrepitation (Fig. 2.12).

2.2.5.2 Evaporative residues

Evaporate residues with chemically distinct domains that lack an obvious relationship to a single decrepitation pit are herein not considered to be representative of singularly evacuated inclusions and thus have to be carefully evaluated in terms of providing useful chemical data in the same way

as mounds. Thus, an absence of well–defined, non–overlapping perimeters (Fig. 2.13) precludes using such mounds without scrutiny. The likely origin of these evaporative residues is fluid flow on the quartz surface, followed by fluid fractionation prior to complete evaporation of the fluid's aqueous component. However, owing to the possibility of contamination from adjacent inclusions with a different origin and composition, such evaporative residues are not considered for analysis because their origin cannot be reliably linked to single fluid inclusions.

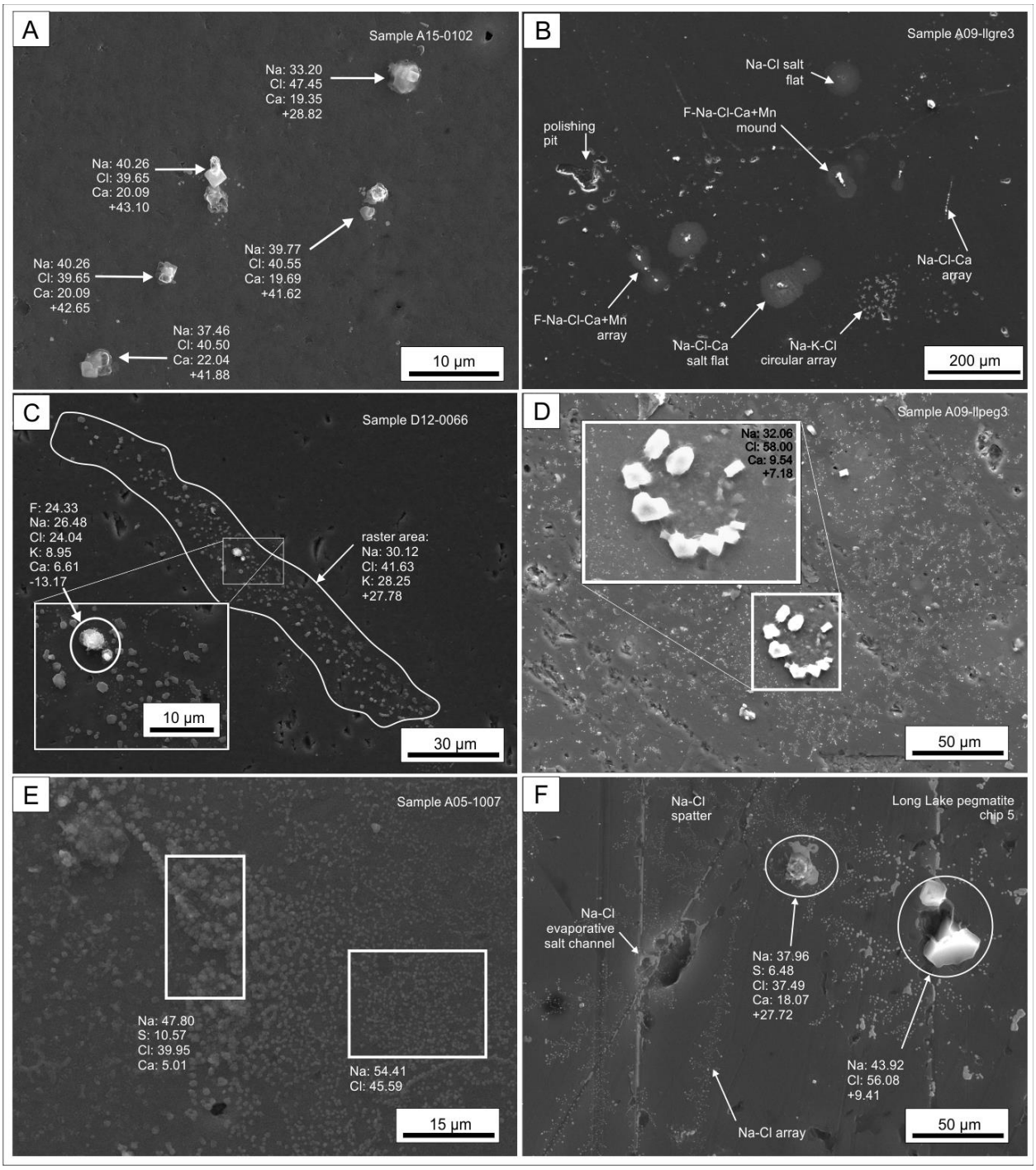
A
Sample A15-0102
Na: 33.20
Cl: 47.45
Ca: 19.35
+28.82
Na: 40.26
Cl: 39.65
Ca: 20.09
+43.10
Na: 39.77
Cl: 40.55
Ca: 19.69
+41.62
Na: 40.26
Cl: 39.65
Ca: 20.09
+42.65
Na: 37.46
Cl: 40.50
Ca: 22.04
+41.88
10 µm
B
Sample A09-llgre3
Na-Cl salt flat
polishing pit
F-Na-Cl-Ca+Mn mound
Na-Cl-Ca array
F-Na-Cl-Ca+Mn array
Na-Cl-Ca salt flat
Na-K-Cl circular array
200 µm
C
Sample D12-0066
F: 24.33
Na: 26.48
Cl: 24.04
K: 8.95
Ca: 6.61
-13.17
raster area:
Na: 30.12
Cl: 41.63
K: 28.25
+27.78
10 µm
30 µm
D
Sample A09-llpeg3
Na: 32.06
Cl: 58.00
Ca: 9.54
+7.18
50 µm
E
Sample A05-1007
Na: 47.80
S: 10.57
Cl: 39.95
Ca: 5.01
Na: 54.41
Cl: 45.59
15 µm
F
Na-Cl spatter
Long Lake pegmatite chip 5
Na-Cl evaporative salt channel
Na: 37.96
S: 6.48
Cl: 37.49
Ca: 18.07
+27.72
Na: 43.92
Cl: 56.08
+9.41
Na-Cl array
50 µm

Figure 2.10 (previous page): SEM–SE images of evaporate mounds and evaporative residues.(A) Discrete, roughly spherical evaporative mounds. (B) Population of giant (i.e., > 50 µm long–axis diameters) evaporate mounds. (C) Linear array of evaporate mounds. (D) Sodium-Ca-Cl mound situated within an extensive area of evaporative debris. (E) Evaporative salt flat composed of two compositionally distinct areas. EDS results correspond to adjacent raster areas (white boxes) (F) Evaporative residue infilling a polishing scratch and creating an evaporative residue channel and collage of diverse evaporative mound morphologies, which likely reflect fluid flow across surface of host mineral grain prior to evaporation of the aqueous component.

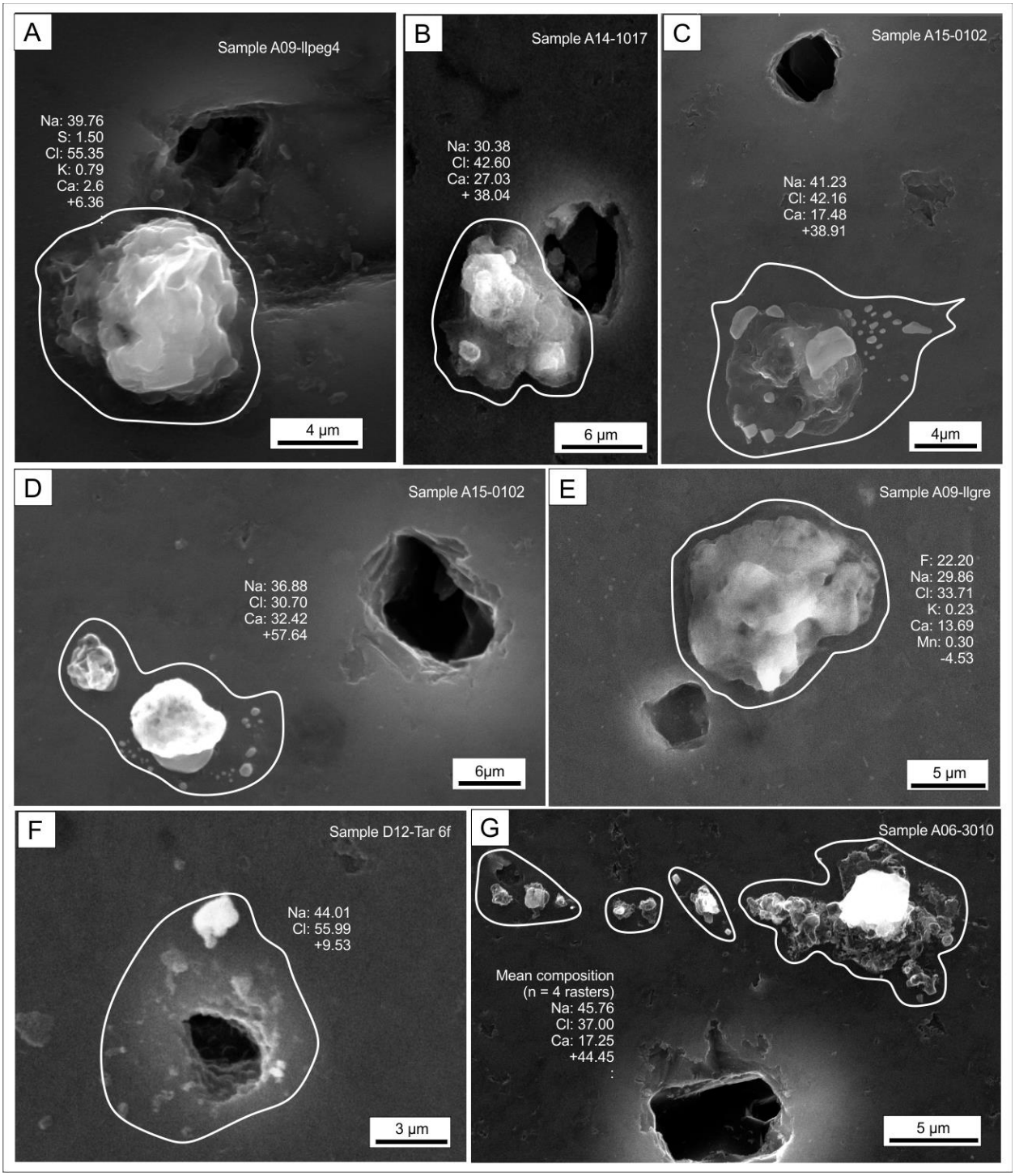
A
Sample A09-llpeg4
Na: 39.76
S: 1.50
Cl: 55.35
K: 0.79
Ca: 2.6
+6.36
4 µm
B
Sample A14-1017
Na: 30.38
Cl: 42.60
Ca: 27.03
+ 38.04
6 µm
C
Sample A15-0102
Na: 41.23
Cl: 42.16
Ca: 17.48
+38.91
4µm
D
Sample A15-0102
Na: 36.88
Cl: 30.70
Ca: 32.42
+57.64
6µm
E
Sample A09-llgre
F: 22.20
Na: 29.86
Cl: 33.71
K: 0.23
Ca: 13.69
Mn: 0.30
-4.53
5 µm
F
Sample D12-Tar 6f
Na: 44.01
Cl: 55.99
+9.53
3 µm
G
Sample A06-3010
Mean composition
(n = 4 rasters)
Na: 45.76
Cl: 37.00
Ca: 17.25
+44.45
5 µm

Figure 2.11 (previous page): SEM–SE images of evaporate mounds proximal to evacuated fluid inclusions (i.e., pits). White lines outline raster perimeters. (A) Mound of NaCl with minor S and Ca and trace K perched on pit rim. (B) Mound of Na–Ca–Cl perched on decrepitate pit. (C, D) Mounds of Na–Ca–Cl proximal to decrepitation pit. (E) Mound of Na–Ca–F–with trace K and Mn proximal to decrepitation pit. Note the large size of the mound relative to the pit. (F) Halo of NaCl evaporate mound circling a decrepitation pit. (G) Array of discrete Na–Ca–Cl mounds proximal to a large decrepitation pit which suggests they all originated from this single fluid inclusion.

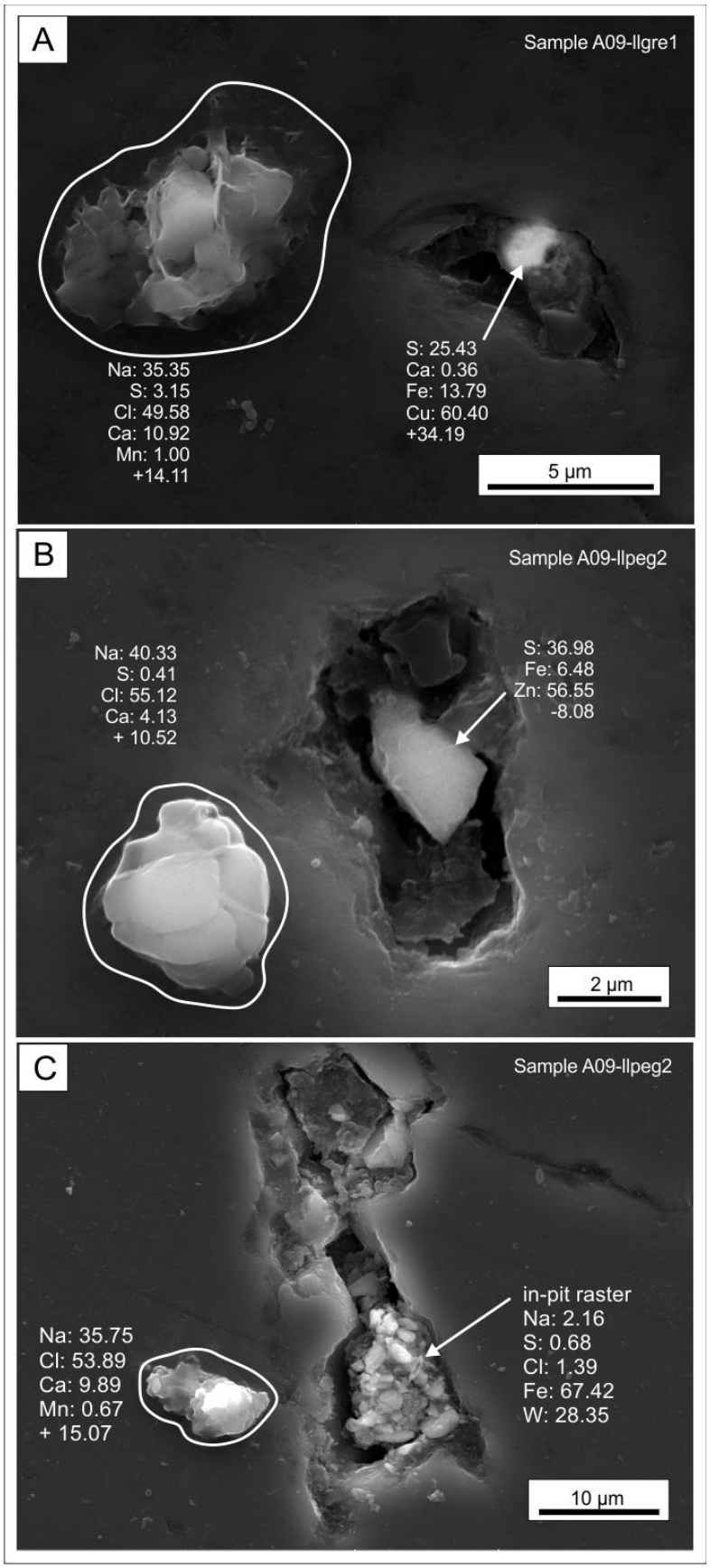
A
Sample A09-llgre1
Na: 35.35
S: 3.15
Cl: 49.58
Ca: 10.92
Mn: 1.00
+14.11
S: 25.43
Ca: 0.36
Fe: 13.79
Cu: 60.40
+34.19
5 µm
B
Sample A09-llpeg2
Na: 40.33
S: 0.41
Cl: 55.12
Ca: 4.13
+ 10.52
S: 36.98
Fe: 6.48
Zn: 56.55
-8.08
2 µm
C
Sample A09-llpeg2
Na: 35.75
Cl: 53.89
Ca: 9.89
Mn: 0.67
+ 15.07
in-pit raster
Na: 2.16
S: 0.68
Cl: 1.39
Fe: 67.42
W: 28.35
10 µm

Figure 2.12 (previous page): SEM–SE images of evaporate mounds proximal to decrepitation pits containing solid phases. Closed white–lines mark the perimeter of rastered areas. (A) Mound proximal to decrepitate pit in which a Cu–Fe sulphide phase occurs. (B) NaCl mound with trace S and minor Ca proximal to pit that is partially infilled by Fe sphalerite. (C) Sodium–Ca–Cl mound with minor Mn adjacent to large decrepitation pit partially infilled with solids of Fe–W composition (atomic proportions: Na = 6.10%, S = 1.40%, Cl = 2.59%, Fe = 79.65%, W = 10.17%).

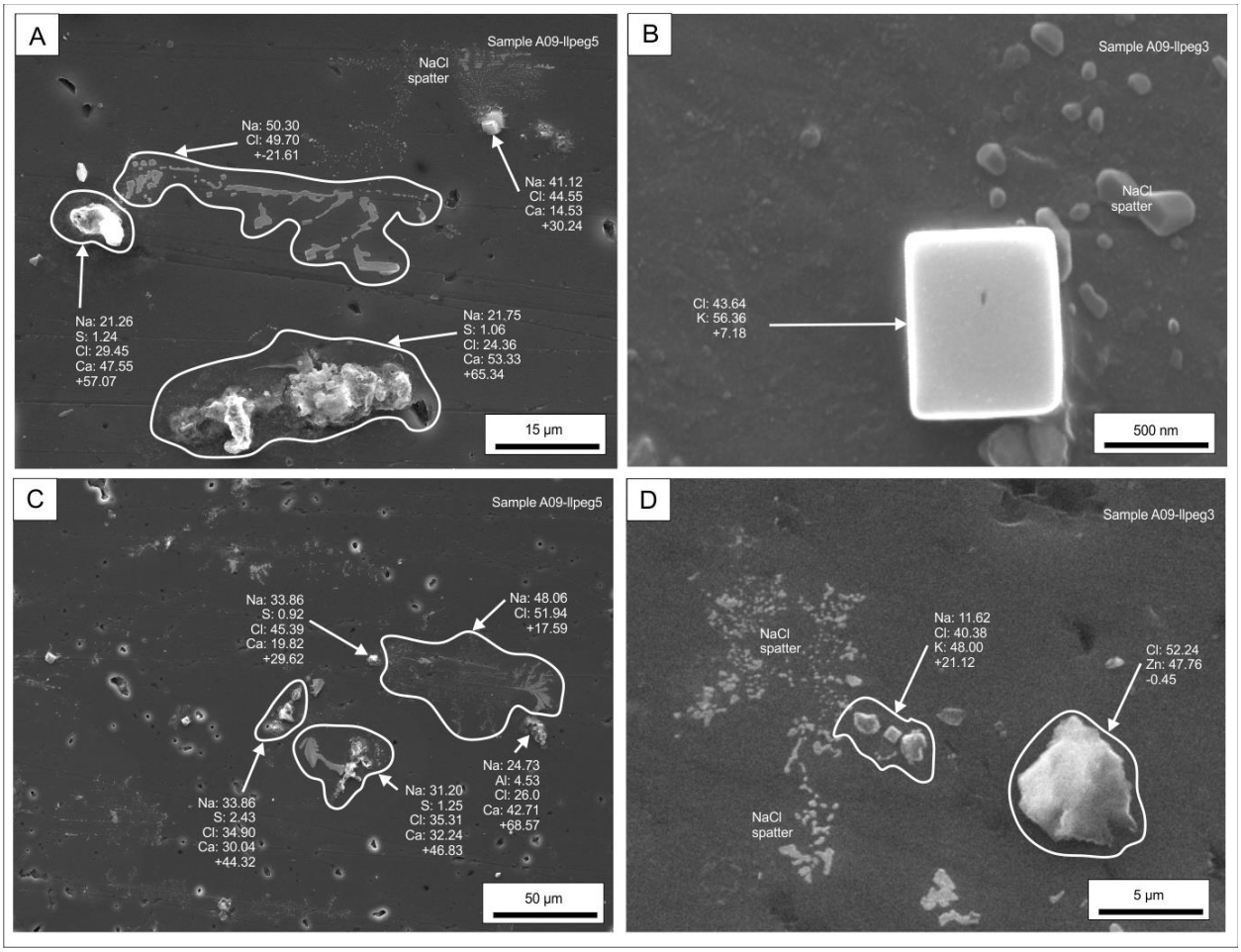

Figure 2.13: SEM–SE images of evaporate residue that are not distinguishable as evaporate mounds. White perimeter outlines indicate areas of raster analyses whereas black arrows are point analyses. (A) Black hash line divides area of evaporate mound (below) from areas evaporative residue (above). Note compositional similarities between residues and mound. (B) Cubic KCl evaporative residue proximal to smaller NaCl blebs. (C) Areas of evaporative residues in which evaporate mounds are not reliably identified. (D) Areas of evaporative residues proximal to a sphalerite micro–grain of unknown origin.

2.2.5.3 Composition

Based on the over 1300 EMA done on quartz–hosted fluid inclusions of the SMB, collectively at least 14 elements (Fig. 2.14) have been recognized above the minimum detection limit of 0.1 wt. %. Chlorine and Na detection occurs in all mounds, albeit in variable proportions, whereas Ca is detected in 75% and K and F are each detected in approximately 30%. Mounds comprised of > 10 wt. % K are devoid of Ca and F. Based on chemical composition, six mound types are recognized (Fig. 2.15). Major solutes are cation and anion species present in concentrations > 5 wt. % of the total mound, are recognized. The presence of > 2 wt. % of transition (i.e., Mn, Fe, Cu, Zn) and other metals (Sn, Pb) defines a metal element–bearing mound.

2.2.5.4 Relationship between mound composition and salt–crystal habit

Evaporate mounds formed by the precipitation of salt crystals displaying a cubic habit are common to NaCl type mounds. However, K–salt crystals also display cubic habits. More commonly, K–enriched mounds display a dendritic morphology. These generalisations aside, the morphology of salt crystals within an evaporate mound is not diagnostic of its chemical composition (Fig. 2.15).

2.2.5.5 Substantiating mound heterogeneity

A comparison of EDS point–mode and raster–mode analyses of a single NaCl mound substantiates chemical fractionation within single evaporate mounds (Fig. 2.16). In some point analyses, an observed deviation from the average and raster values suggests that, as described earlier, a single point–mode analysis does not necessarily provide a representative chemistry of the fractionated mound and instead raster–mode must be used.

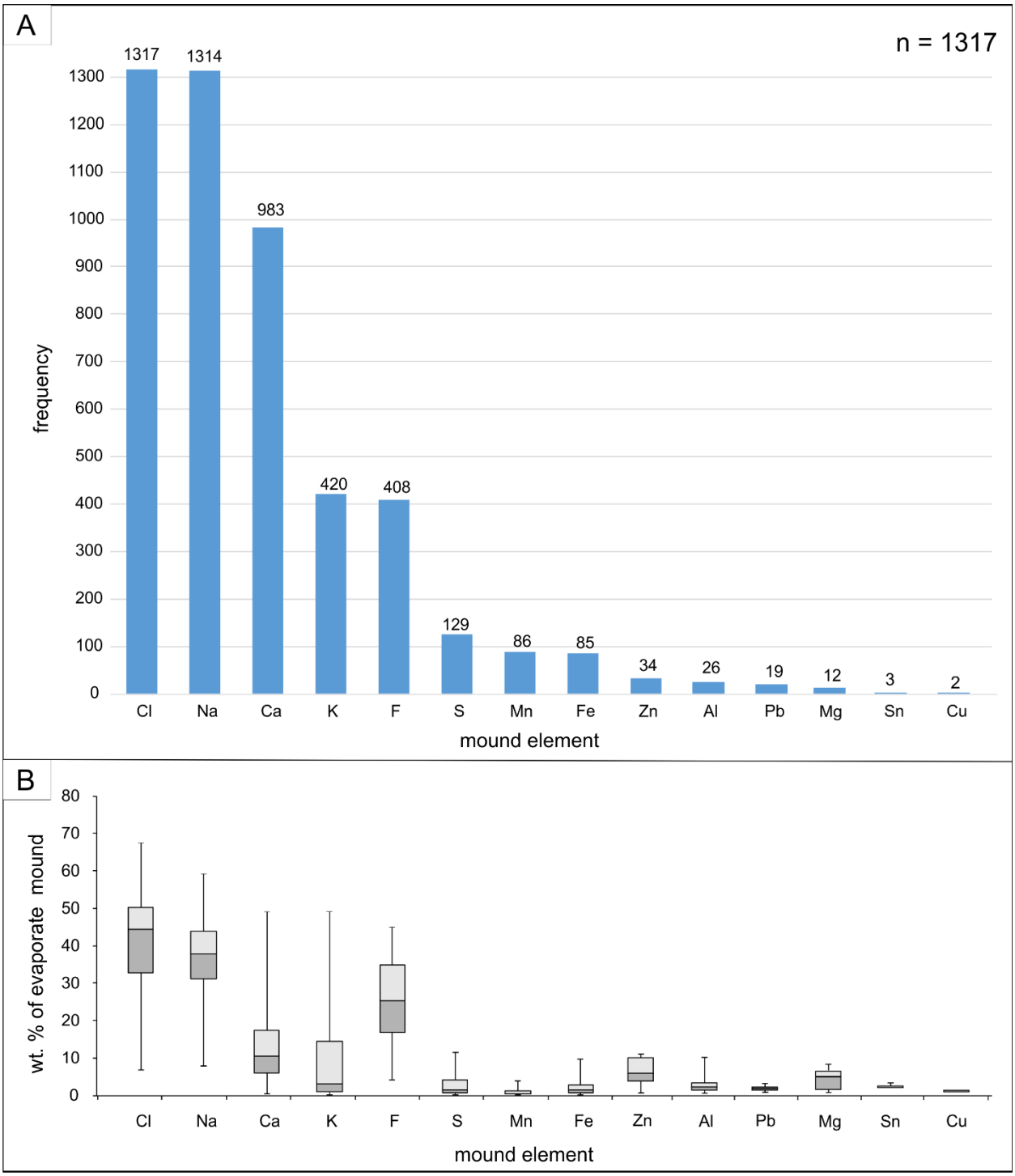

Figure 2.14: Summary of EMA for the SMB showing the multi–element diversity of the quartz–hosted fluid inclusions. (A) Histogram plot displaying mound elements in order of decreasing abundance of detection. (B) Box–and–whisker plots displaying the detection ranges of each element.

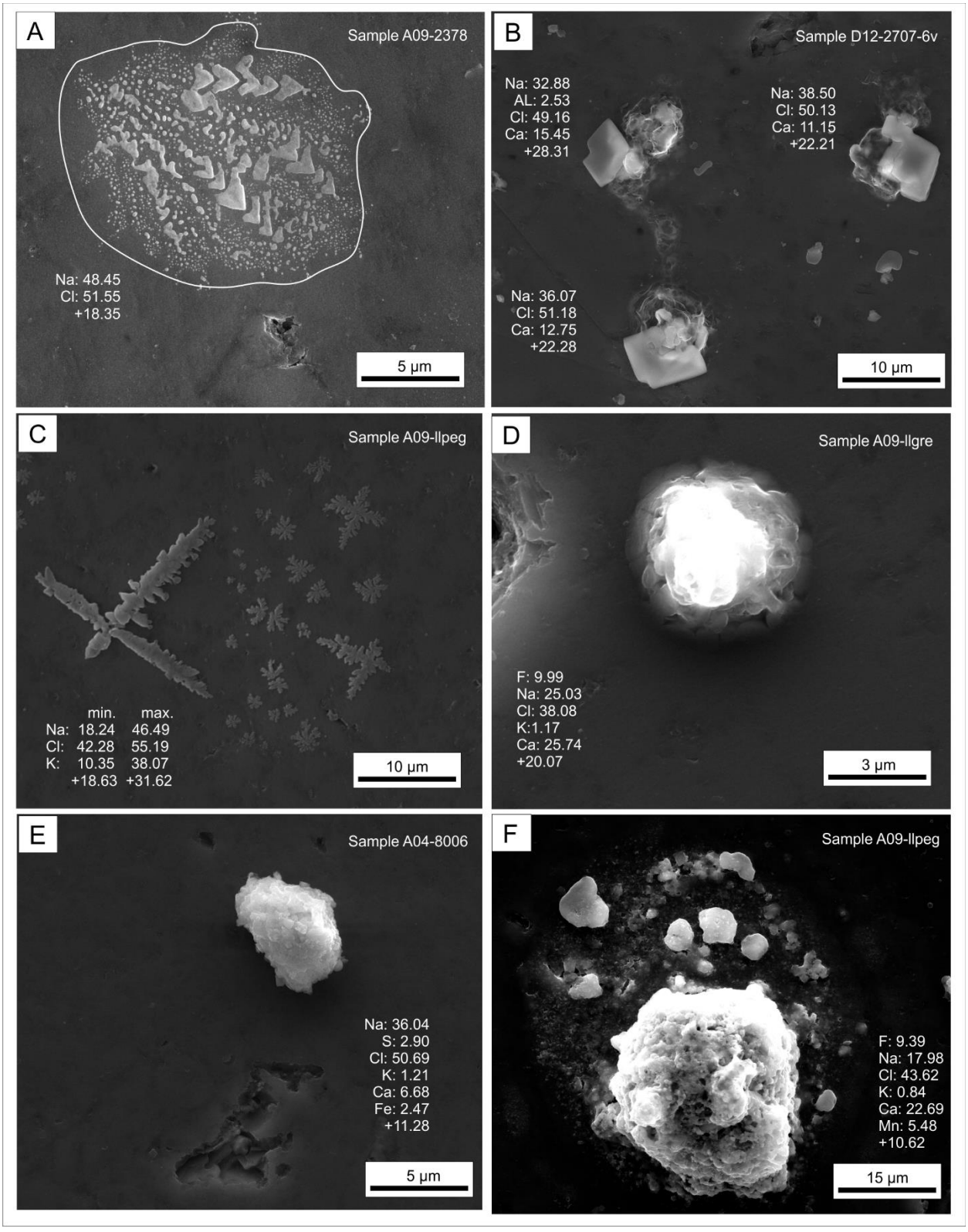
A
Sample A09-2378
Na: 48.45
Cl: 51.55
+18.35
5 µm
B
Sample D12-2707-6v
Na: 32.88
AL: 2.53
Cl: 49.16
Ca: 15.45
+28.31
Na: 38.50
Cl: 50.13
Ca: 11.15
+22.21
Na: 36.07
Cl: 51.18
Ca: 12.75
+22.28
10 µm
C
Sample A09-llpeg
min. max.
Na: 18.24 46.49
Cl: 42.28 55.19
K: 10.35 38.07
+18.63 +31.62
10 µm
D
Sample A09-llgre
F: 9.99
Na: 25.03
Cl: 38.08
K:1.17
Ca: 25.74
+20.07
3 µm
E
Sample A04-8006
Na: 36.04
S: 2.90
Cl: 50.69
K: 1.21
Ca: 6.68
Fe: 2.47
+11.28
5 µm
F
Sample A09-llpeg
F: 9.39
Na: 17.98
Cl: 43.62
K: 0.84
Ca: 22.69
Mn: 5.48
+10.62
15 µm

Figure 2.15 (previous page): SEM–SE photomicrographs of evaporate mound compositional types. (A) NaCl mounds are the only two component (i.e., NaCl) type of mound. (B) Na–Ca chloride mounds with roughly uniform compositions. (C) Sodium–Cl mound devoid of Ca. (D) Na–Ca–Cl–F mounds commonly have a negative charge imbalance. (E) NaCl mound with minor S–K–Ca–Fe. (F) Ca-Na-Cl-F mound with minor Mn and trace K.

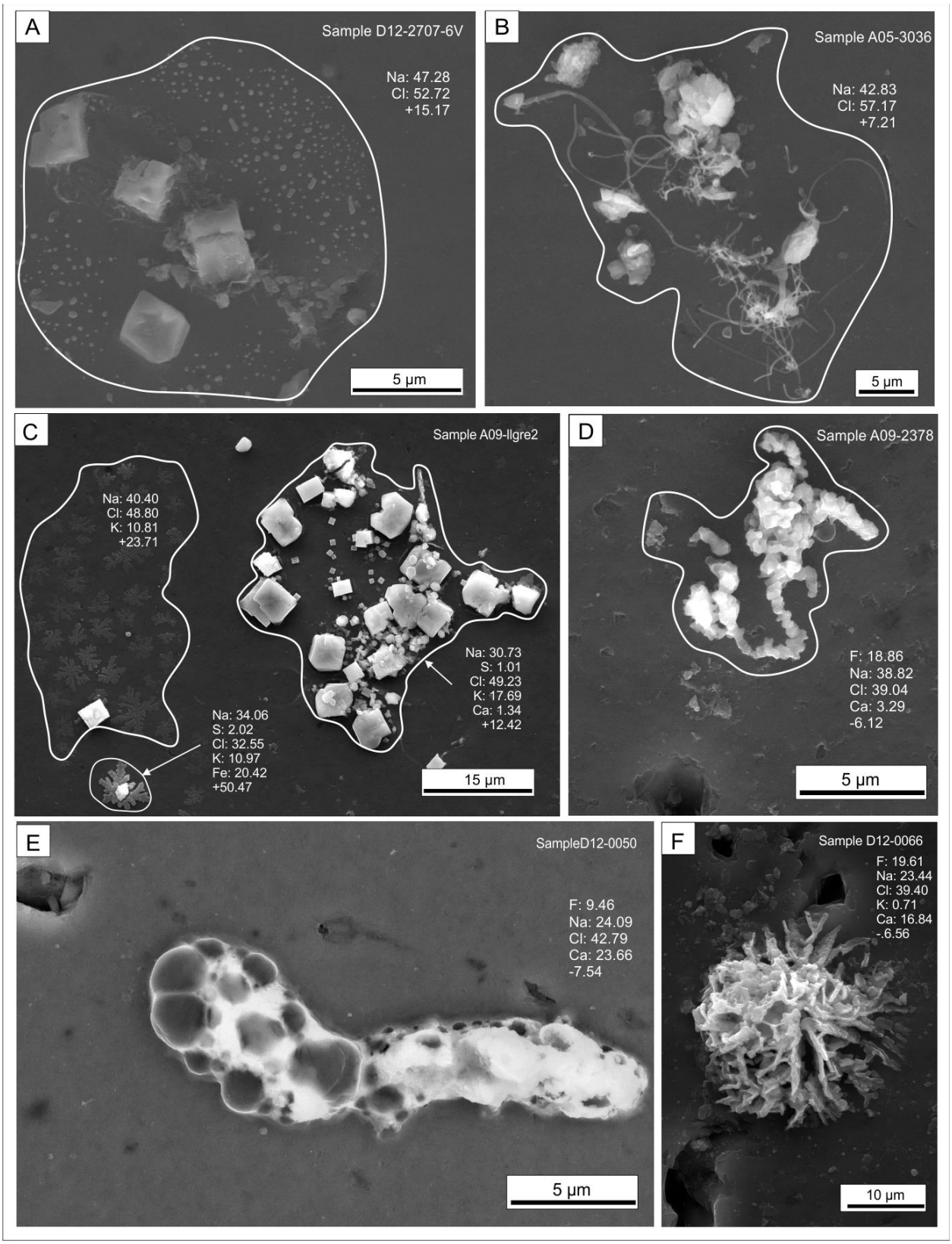
A
Sample D12-2707-6V
Na: 47.28
Cl: 52.72
+15.17
5 µm
B
Sample A05-3036
Na: 42.83
Cl: 57.17
+7.21
5 µm
C
Sample A09-Ilgre2
Na: 40.40
Cl: 48.80
K: 10.81
+23.71
Na: 30.73
S: 1.01
Cl: 49.23
K: 17.69
Ca: 1.34
+12.42
Na: 34.06
S: 2.02
Cl: 32.55
K: 10.97
Fe: 20.42
+50.47
15 µm
D
Sample A09-2378
F: 18.86
Na: 38.82
Cl: 39.04
Ca: 3.29
-6.12
5 µm
E
SampleD12-0050
F: 9.46
Na: 24.09
Cl: 42.79
Ca: 23.66
-7.54
5 µm
F
Sample D12-0066
F: 19.61
Na: 23.44
Cl: 39.40
K: 0.71
Ca: 16.84
-.6.56
10 µm

Figure 2.16 (previous page): SEM–SE images displaying diversity of evaporate mound morphologies. NaCl mounds composed of (A) salt grains with cubic habit within a blebby halo of spatter and (B) amorphous salt grains connected by stringy salt precipitate. Potassium–enriched mounds displaying (C) two contrasting mound textures including rounded dendritic salt piles (left) and collection of cubic salt grains (right). Fluorine–enriched mounds displaying (D) amorphous shape, (E) apparently porous elongated shape and (F) cone–shaped corrugate–textured shape.

A

EDS data for 15 point analyses and 1 raster analysis of single decrepitate mound. Raster area outlined by white hash line. All data in weight percent.

Point	Na	Cl	K	Ca	TOTAL
1	67.70	28.74	3.56		100.00
2	53.51	37.08	9.41		100.00
3	61.97	36.78	1.25		100.00
4	64.40	35.60			100.00
5	49.19	39.13	11.67		100.00
6	58.10	39.14	2.76		100.00
7	62.23	34.52	2.44	0.81	100.00
8	66.30	33.70			100.00
9	62.21	36.11	1.68		100.00
10	62.02	35.57	2.41		100.00
11	59.67	38.60	1.73		100.00
12	61.93	35.25	2.12	0.71	100.00
13	64.95	35.05			100.00
14	64.04	34.63	1.33		100.00
15	61.81	36.48	1.71		100.00
point analysis (mean)	61.33	35.76	2.80	0.10	100.00
raster analysis	64.45	33.46	2.08		100.00

B

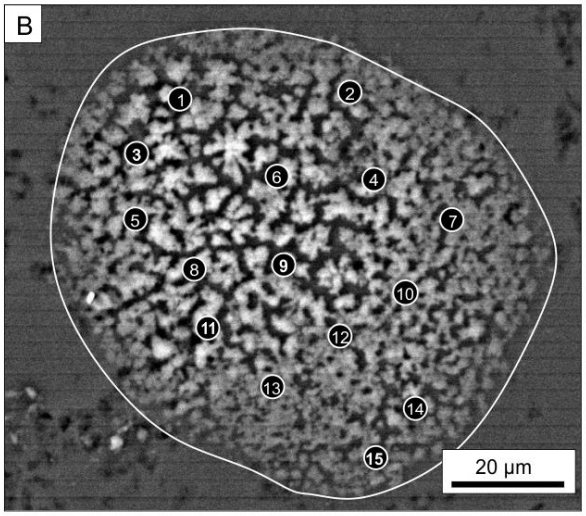

C

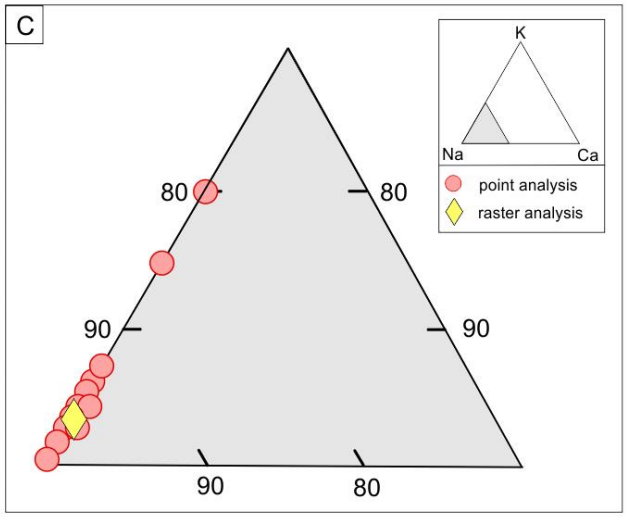

Figure 2.17 (previous page): A SEM–BSE image of a Na–K–Cl evaporate salt mound with tabulate data for point and raster type analyses.(A) Summary of the tabulated EDS data collected from point analyses (n = 15) and a single raster analysis. (B) The SEM–BSE image of the large evaporate mound showing the locations of point analyses (numbered circles) and raster area (white line). (C) Ternary plot (in wt. %) of the tabulated data comparing the raster analysis with the point data.

2.2.5.6 Chip–scale variation in mound compositions

The abundance and composition of evaporate mounds within a single quartz wafer was assessed by analysing three quartz chips (Fig. 2.18) from the sample. In terms of mound production, the abundance of mounds produced in chip 1 was approximately 2x that for chips 2 and 3, but the mound sizes were generally similar (12.7 μm ±8.1, 1σ; 15.8 μm ±7.0, 1σ; 10.2 μm ±5.8 1σ for chips 1, 2 and 3 respectively). As for mound compositions, two distinct populations were noted, one with Na–Ca–K–Cl–F and the other with Na–Ca–Cl–F (Fig. 2.18). In terms of the F content, which varied, it was detected in ~50% of mounds hosted by chip 1, in ~75% of mounds hosted by chip 2, and in all but one mound in chip 3 whereas its abundance was highest in chip 3 (21.2 wt. %) which was 2x that in chip 2 mounds (11.8 wt. %) and approximately 3x that in chip 1 mounds (7.5 wt. %). The average Ca/Na ratios was generally consistent in all three chips (1.01 ±0.72, 1σ; 1.05 ±0.53, 1σ; 0.85 ±0.56, 1σ for chips 1, 2 and 3 respectively). The inconsistencies noted for mound abundance and composition among the chips may be explained by wafer–scale variability in inclusion types.

2.2.6 Analytical parameters

2.2.6.1 Decrepitation temperature

Mounds generated by oven–heating three quartz pegmatite chips to 300°, 400° and 500°C, respectively, suggests that decrepitation temperature does not influence mound size. The mean size of mounds hosted by each chip is comparable (avg. ± 1σ): 16.0 μm ± 13.6, 9.6 μm ± 8.6, and 15.2 μm ± 10.1 for chips heated to 300°, 400° and 500°C respectively. Mound compositional variation with temperature is explained by chance occurrence of individual chips cut from the same wafer hosting non–identical fluid inclusion populations (Fig. 2.19). In other words, the absence of

Na–K–Cl mounds in the high temperature chip is not an effect of heating to 500°C. The increase in mean charge imbalance with increasing temperature may be the effect of heating, since elevated temperature is a reasonable mechanism by which chlorine volatilises.

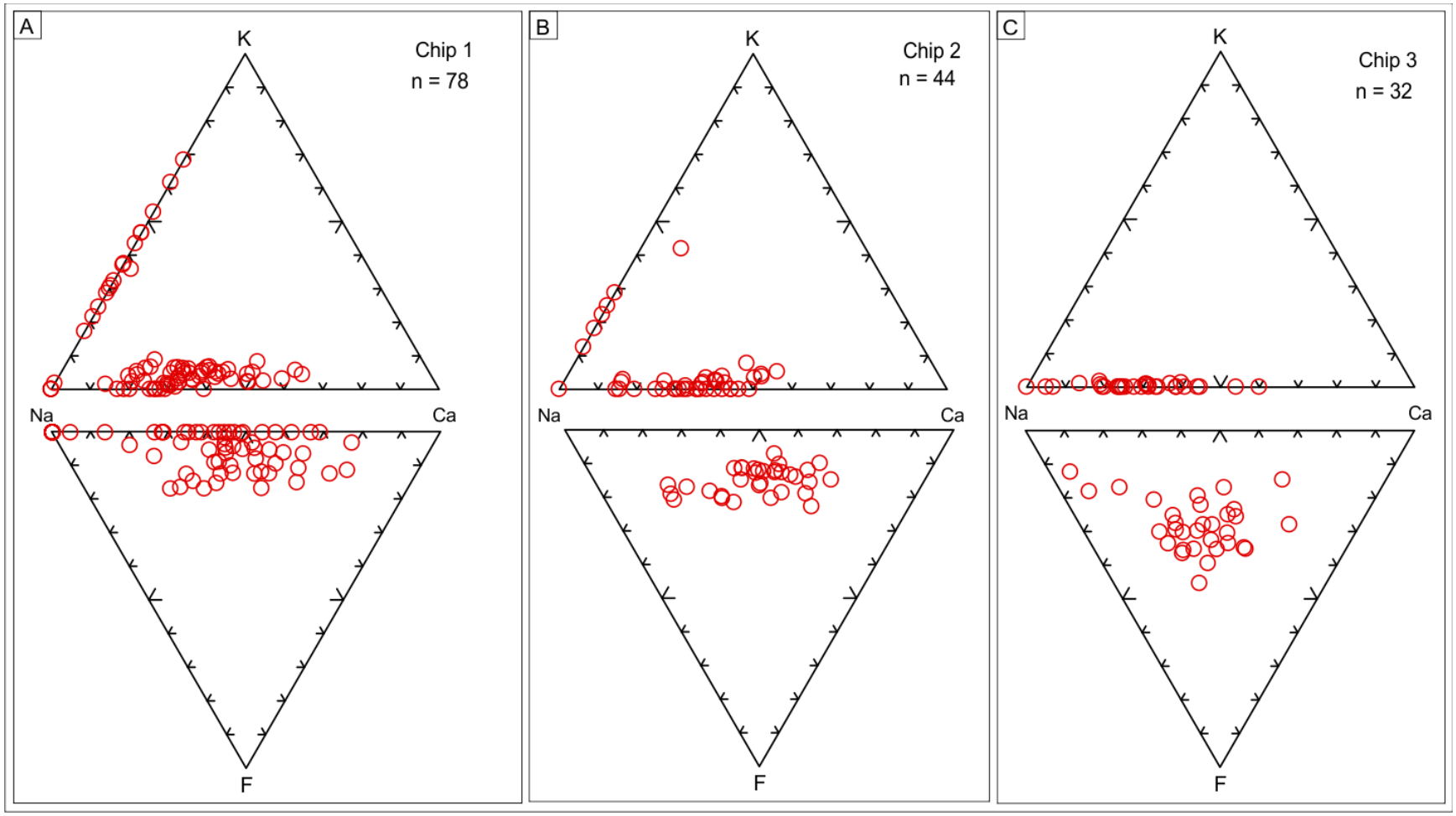
A
K
Chip 1
n = 78
Na
Ca
F
B
K
Chip 2
n = 44
Na
Ca
F
C
K
Chip 3
n = 32
Na
Ca
F

Figure 2.18 (previous page): Ternary plots of select evaporate–mound elements (Na–K–Ca and Ca–F–Na) for three chips cut from a single fluid–inclusion quartz wafer from a greisen sample. (A) Mounds hosted by chip 1 have detectable F–Na–K–Ca and define two groupings. (B) Chip 2 mounds contain detectable levels of all 4 elements, but fewer K–bearing mounds than chip 1. (C) Chip 3 mounds have detectable F, Na and Ca, but are devoid of K. Note that Cl is present but note included in the plots.

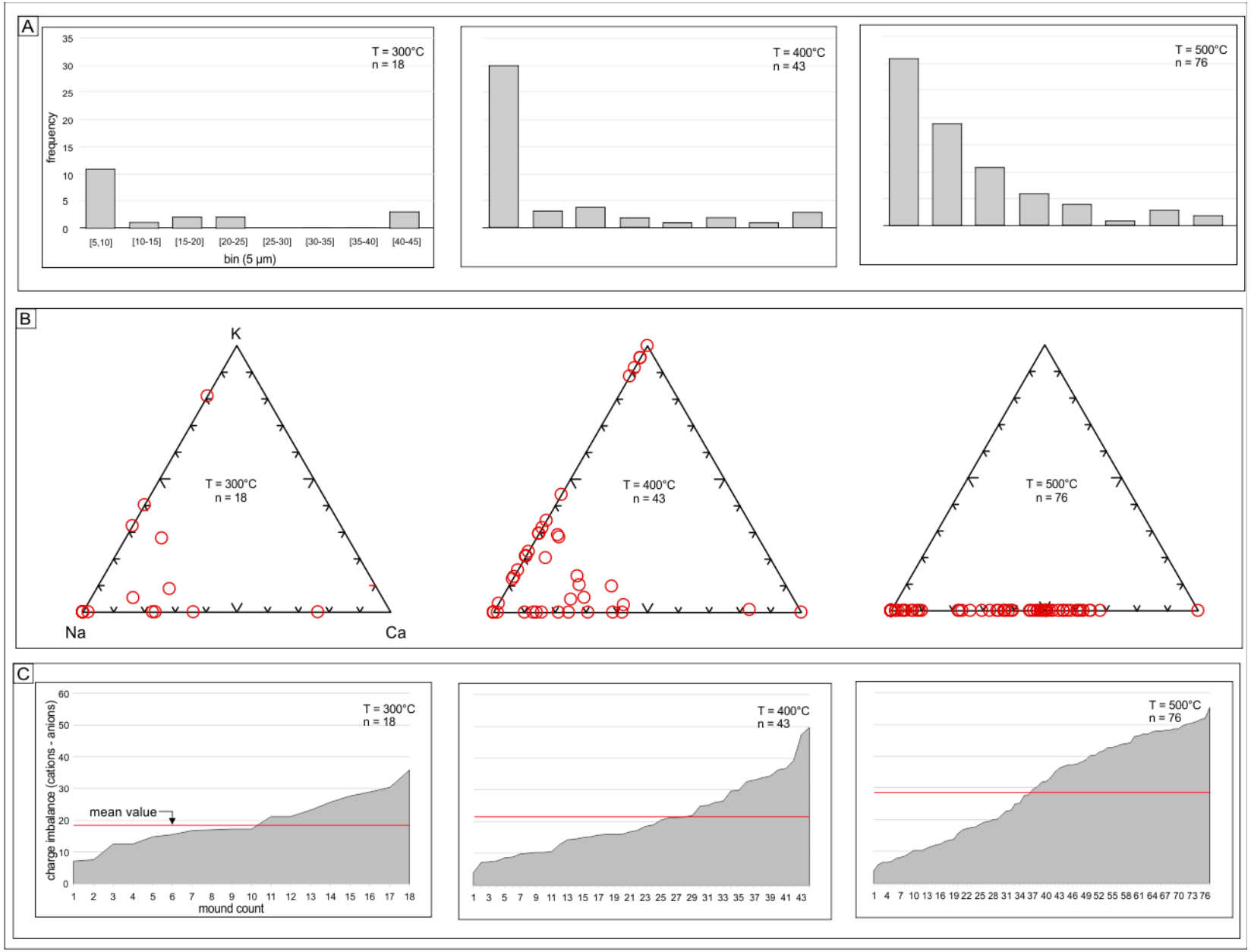
A
T = 300°C
n = 18
frequency
bin (5 µm)
[5,10]
[10-15]
[15-20]
[20-25]
[25-30]
[30-35]
[35-40]
[40-45]
T = 400°C
n = 43
T = 500°C
n = 76
B
K
Na
Ca
T = 300°C
n = 18
T = 400°C
n = 43
T = 500°C
n = 76
C
charge imbalance (cations - anions)
mean value
mound count
T = 300°C
n = 18
T = 400°C
n = 43
T = 500°C
n = 76

Figure 2.19 (previous page): Assessment of relationship between decrepitation temperatures (at 300°, 400° and 500°C) and evaporate mound characteristics. (A) Binary charts showing frequency of mound sizes. The increase in the number of mounds generated with T reflects decrepitation of more small inclusions which is expected since there is a critical internal pressure needed to overcome the confining pressure of the quartz. This data suggests that evaporate mound abundance appears to increase with decrepitation temperature. (B) Ternary plots (Na–K–Ca) of EMA. Note that NaCl and Na–Ca–Cl types are observed in all three chips, but that the Na–K–Cl type mounds observed at the two lower temperature chips are not detected in the high temperature chip. (C) Area charts displaying charge imbalances associated with the EMA which highlights that the mean charge imbalance increases with decrepitation temperature.

2.2.6.2 Number of mounds analysed per chip

To determine the minimum number of mound analyses required to obtain a representative data set, we analysed four discrete mound populations (n = 8, 16, 32, 62) occurring in a single ~3 cm^2 quartz chip; the results are summarized in Figure 2.20. The smallest data set (n = 8) appears to be an outlier for the following reasons: (i) NaCl–type mounds were not detected, (ii) Mn was not detected, and (iii) the average Ca/Na ratio was low relative to the three larger data sets. Four mound types (Na–Cl, Na–Ca–Cl–F, Na–Ca–Mn–Cl–F and Na–K–Cl) were identified consistently in the three larger data sets. In other words, the three data sets (n = 16, 32 and 62) detect the same number of evaporate mound types, thus revealing the same chemical constraint on the hydrothermal fluids that circulated through this sample.

2.2.6.3 EDS acquisition time

Two multi–component mounds (Na–Ca–K–Cl–F and Na–Ca–K–Mn–Cl–F)) were selected for repeated EDS analysis using 5–, 20–, 40–, 60– and 100–second EDS acquisition times (Fig. 2.21). Results for the analysis of the Na–Ca–K–Cl–F mound were consistent throughout the experimental range, which suggests minimal interference from the quartz substrate. However, for the mound the abundances varied with low abundance elements not detected until longer count times accumulated which suggest quartz interferences diluted the signal intensity. In this latter mound, 60 seconds is the optimal run time for acquiring a representative result, whereas in the former, results from a 5–second analysis are identical to a 100–second analysis. The magnitude of the Si signal is a good indicator of degree of background interference. To make the best use of this indicator, a raster trace made on the inner side of the mound perimeter will minimize the unwanted SiO_2 background, and in cases when the signal for the quartz substrate is relatively low, shorter run times will provide a representative result. Charge deficiencies associated with the two mounds are consistent

throughout the experimental range. However, raw EDS data for the Na–Cl±S±K±Ca demonstrate the potential for false positive signals for elements with characteristic X-rays that overlap with the spectrum generated by a major solute element. For example, As (Lα = 1.282) overlaps a strong Na spectral signal (i.e., peak) for Na (Kα = 1.041), and unspecified characteristic X-rays for Pb overlap Cl and Si peaks generated during longer ES acquisition times (Table 2.5). Generating anomalous S signals due to the removal SiO_2 during data reduction is not influenced by acquisition time (Table 2.5), which reconfirms the inconsequence on results of removing SiO_2 in from EDS spectrum, and thus permitting more time-efficient data processing without compromising data quality

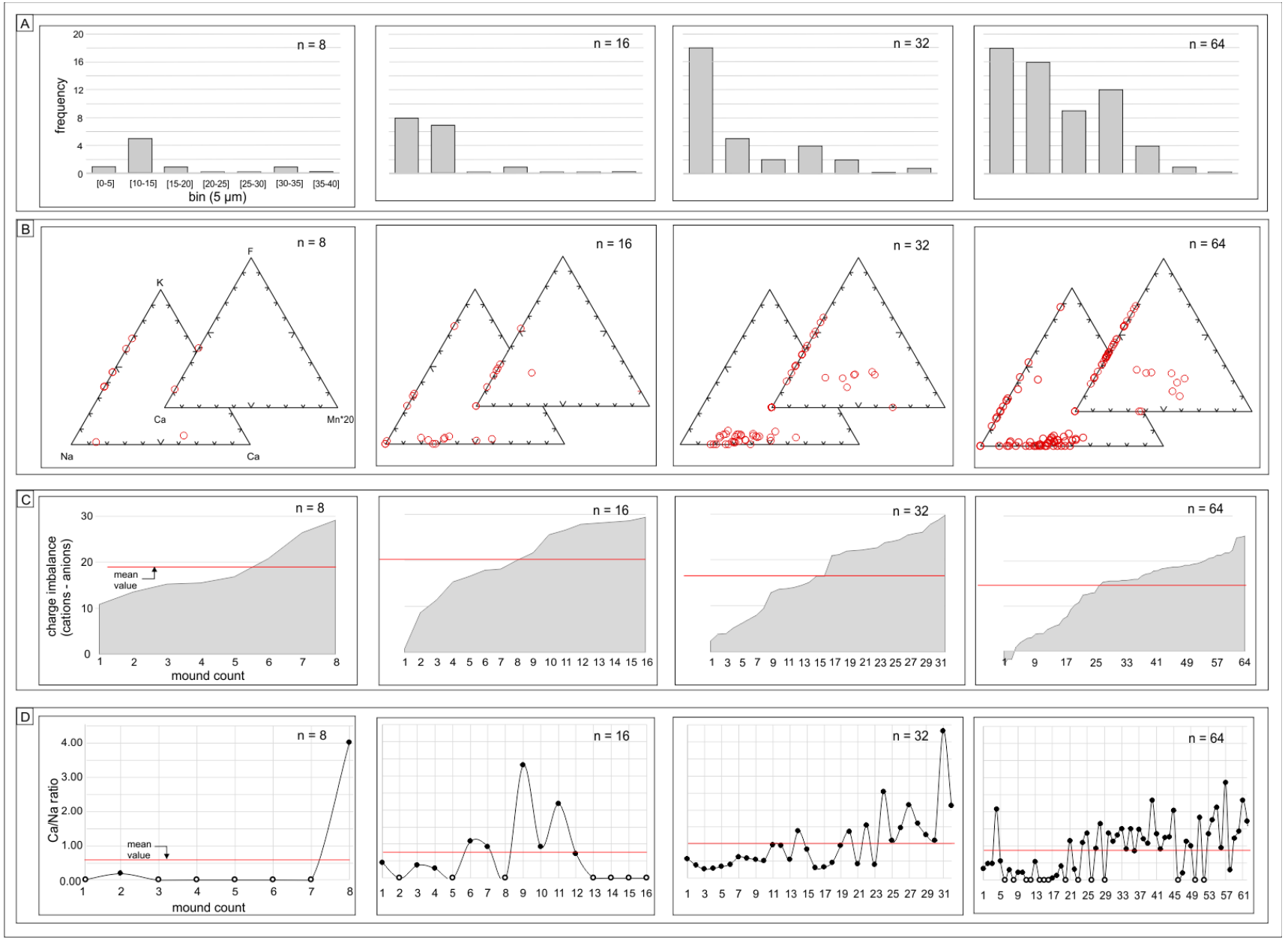
A
n = 8
n = 16
n = 32
n = 64
frequency
bin (5 µm)
[0-5]
[10-15]
[15-20]
[20-25]
[25-30]
[30-35]
[35-40]
B
K
F
Ca
Mn*20
Na
Ca
C
charge imbalance
(cations - anions)
mean
value
mound count
D
Ca/Na ratio
mean
value
mound count

Figure 2.20 (previous page): Chart organization of EDS evaporate mound data collected from four domains of a single quartz chip. (A) Binary charts displaying distribution of mound sizes. Note that relatively small mounds dominate the two larger data sets. (B) Ternary plots (Na–K–Ca and Ca–F–Mn*20) for evaporate mounds. Note that the prominent detection of Mn in a subset of mounds from the two larger data sets. (C) Area charts displaying charge imbalances (∑cations – ∑anions) for evaporate mounds. The important point illustrated here is the consistency of average charge imbalances among the data sets, which demonstrates that volatilization of light elements is insignificant. (D) Binary plot of Ca/Na mound ratios. Note consistency in the range of Ca/Na values between the two larger data sets.

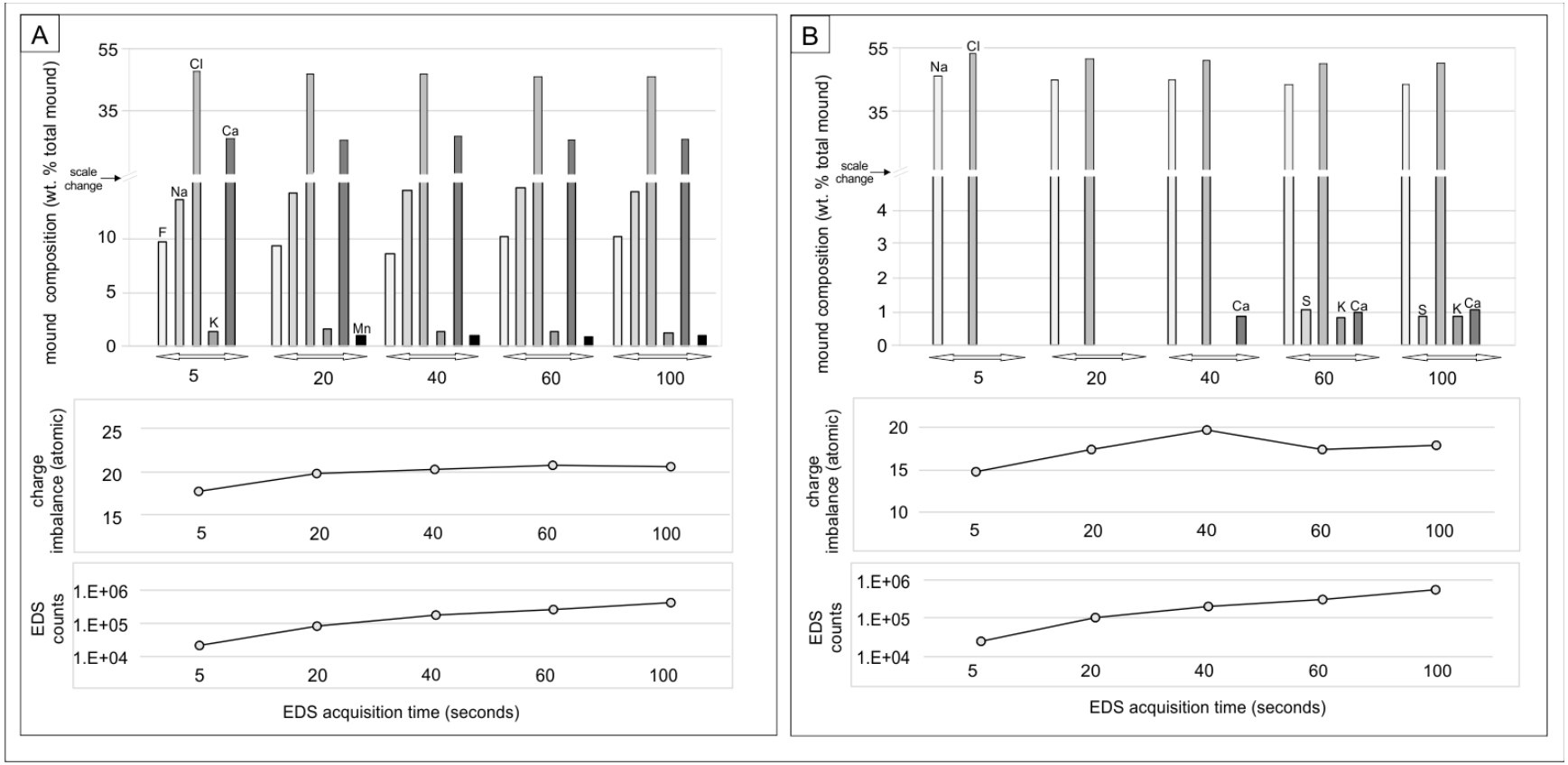

Figure 2.21: Assessment of EDS acquisition time versus results and tabulated data of results generated by different reduction methods.(A) Analytical favourable situation where EDS results are are minimally variable with acquisition time, and 5–second analysis generates representative results. (B) Analytically less favourable situation where representative results require a minimum 60–second analysis

Table 2.5. TABULATED EDS RESULTS FROM REPEAT ANALYSIS OF EVAPORATE MOUND USING VARYING ACQUISITION TIMES AND TWO DATA REDUCTION METHODS

Sample	Acquisition time	Reduction method*	O	Na	Si	S	Cl	K	Ca	As	Pb	Total	∑+	∑-	Σdiff	Σdiff%
			weight percent										atomic weight			
D12-blpeg	5	n/a**	47.89	12.04	28.16		11.9					100	4.54	6.32	-1.79	-16.46
D12-blpeg	20	n/a**	47.38	13.5	25.48		12.86		0.23	0.55		100	4.22	6.29	-2.06	-19.63
D12-blpeg	40	n/a**	49.35	12.17	26.67	0.19	11.14			0.49		100	4.33	6.50	-2.17	-20.02
D12-blpeg	60	n/a**	48.75	12.72	25.59	0.26	11.7	0.17	0.21	0.6		100	4.21	6.44	-2.23	-20.96
D12-blpeg	100	n/a**	49.63	12.15	25.56	0.18	11.14	0.17	0.21	0.56	0.41	100	4.18	6.53	-2.35	-21.95
D12-blpeg	5	2		50.29			49.71					100	2.19	1.40	0.79	21.88
D12-blpeg	20	2		50.93			48.21		0.86			100	2.24	1.36	0.88	24.38
D12-blpeg	40	2		51.94		0.80	47.26					100	2.26	1.38	0.88	24.06
D12-blpeg	60	2		50.95		1.03	46.52	0.67	0.83			100	2.25	1.38	0.88	24.18
D12-blpeg	100	2		51.10		0.83	46.51	0.70	0.87			100	2.26	1.36	0.90	24.79
D12-blpeg	5	3		45.26			54.74					100	1.97	1.54	0.42	12.09
D12-blpeg	20	3		45.7			53.22		1.07			100	2.01	1.50	0.51	14.60
D12-blpeg	40	3		46.27		0.85	52.88					100	2.01	1.54	0.47	13.16
D12-blpeg	60	3		45.45		1.08	51.58	0.86	1.04			100	2.02	1.52	0.50	14.17
D12-blpeg	100	3		45.44		0.89	51.65	0.89	1.12			100	2.03	1.51	0.51	14.55

*: description of data reduction methods 2 and 3 provided in section 2.1.7

**: EDS data for SiO_2 (i.e., background) not collected, precluding application of reduction method 1

2.2.6.4 Stage– versus oven–heating

Two SMB samples were decrepitated at 500°C using oven– and stage–heating techniques and the chips examined for mound variability. It was noted that mound abundance is very similar, and the range of mound sizes, compositions and charge imbalances are comparable (Fig. 2.22), which suggests that the heating method does not impact results. The exception is F, which was detected in the stage–heated chip but not in the oven–heated chip, which may however be attributed to differences in the fluid inclusion types present within single wafers. This could however also be attributed to F volatilisation over the longer heating duration of the oven method mound composition. Fluorine detected in the stage–heated chip was not observed in the oven–heated chip, which may possibly be attributed to chip–scale variation in the entrapment of fluid inclusions given that F was detected in other oven–heated samples during the course of this study.

2.2.7 Comparing evaporate mound microanalysis with microthermometry

The EMA results from a chip of quartz–hosted fluid inclusions cut from a pegmatite sample, the Bayers Lake locality referred to previously, identified four chemically distinct fluids: 1) Na–Ca–Cl, 2) Na–Cl, 3) Na–K–Cl and 4) Na–Ca–Cl–F (Fig. 2.23). The results of microthermometric analysis on the same material indicated it to be dominated by a, low–salinity aqueous fluid with melting temperatures ($T_{m(ice)}$) ranging between –1 and < –5°C and a subordinate fluid or fluids(?) with T_m values for ice and hydrohalite between > –10 and –55°C. The homogenization temperatures (T_h) for these inclusions indicate they are higher for the dominant fluid. Given that both microthermometry and EMA techniques have the sample preparation times (*i.e.*, preparation of polished chips unattached from glass slides), it is noteworthy that the analytical time for acquiring T_m and T_h data for 140 fluid inclusions is on the order of one to two weeks, whereas an equivalent number of fluid inclusions can be analysed, processed and plotted in a 6 – 8 hour

working day. Also relevant is that estimates of T_h can be made using the solvus in the T–density diagram for the aqueous system which can be integrated with the EMA data.

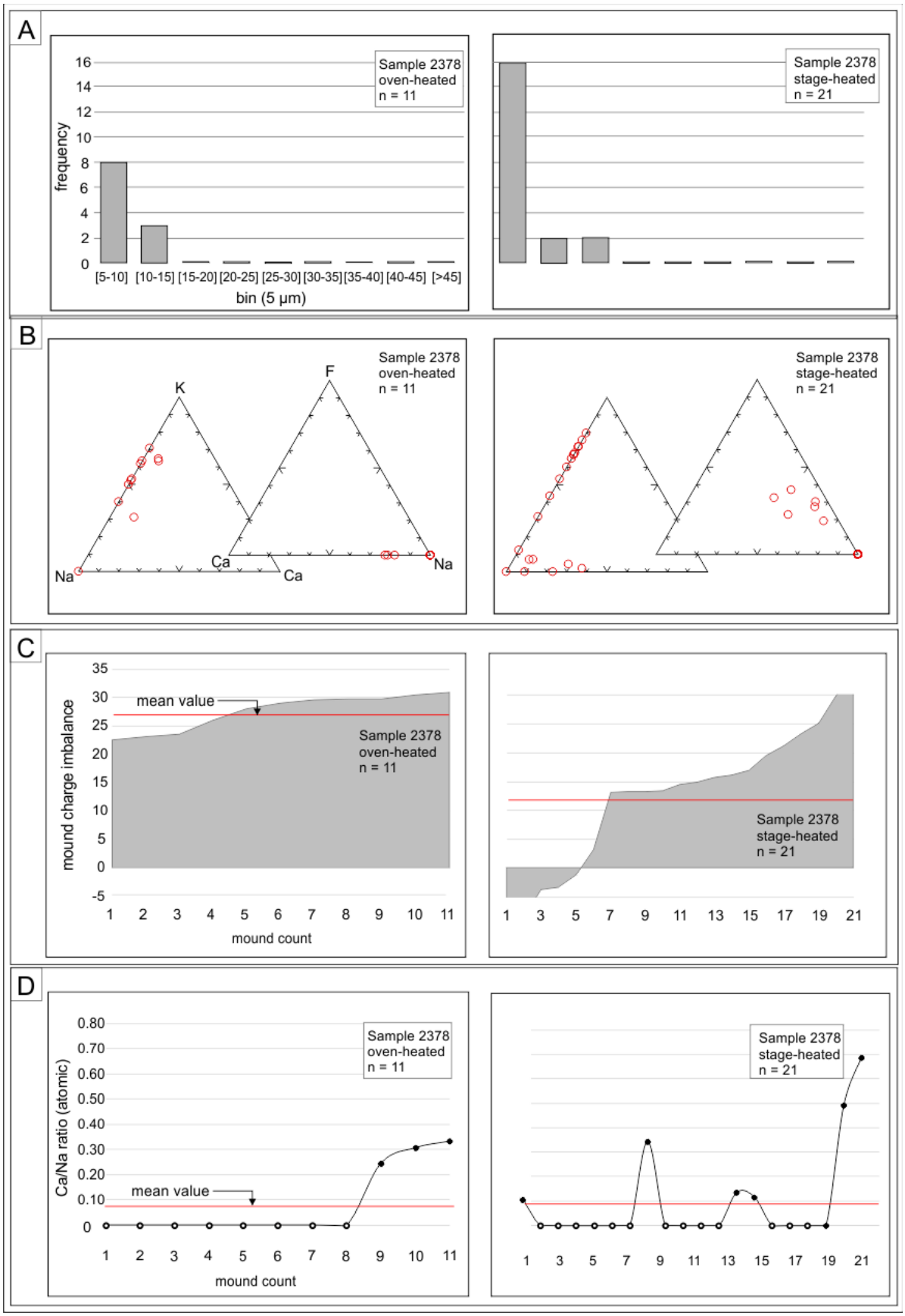
A
Sample 2378
oven-heated
n = 11
frequency
16
14
12
10
8
6
4
2
0
[5-10]
[10-15]
[15-20]
[20-25]
[25-30]
[30-35]
[35-40]
[40-45]
[>45]
bin (5 µm)
Sample 2378
stage-heated
n = 21
B
Sample 2378
oven-heated
n = 11
K
F
Na
Ca
Ca
Na
Sample 2378
stage-heated
n = 21
C
mound charge imbalance
35
30
25
20
15
10
5
0
-5
mean value
Sample 2378
oven-heated
n = 11
1
2
3
4
5
6
7
8
9
10
11
mound count
Sample 2378
stage-heated
n = 21
1
3
5
7
9
11
13
15
17
19
21
D
Ca/Na ratio (atomic)
0.80
0.70
0.60
0.50
0.40
0.30
0.20
0.10
0
mean value
Sample 2378
oven-heated
n = 11
1
2
3
4
5
6
7
8
9
10
11
mound count
Sample 2378
stage-heated
n = 21
1
3
5
7
9
11
13
15
17
19
21

Figure 2.22 (previous page): Chart organization of data collected for oven– and stage–heated quartz chips. (A) Binary plots of mound sizes. (B) Results of EMA plotted in ternary diagrams (Na–K–Ca and Ca–F–Na). (C) Area chart displaying mound charge imbalance (∑cations – ∑anions).

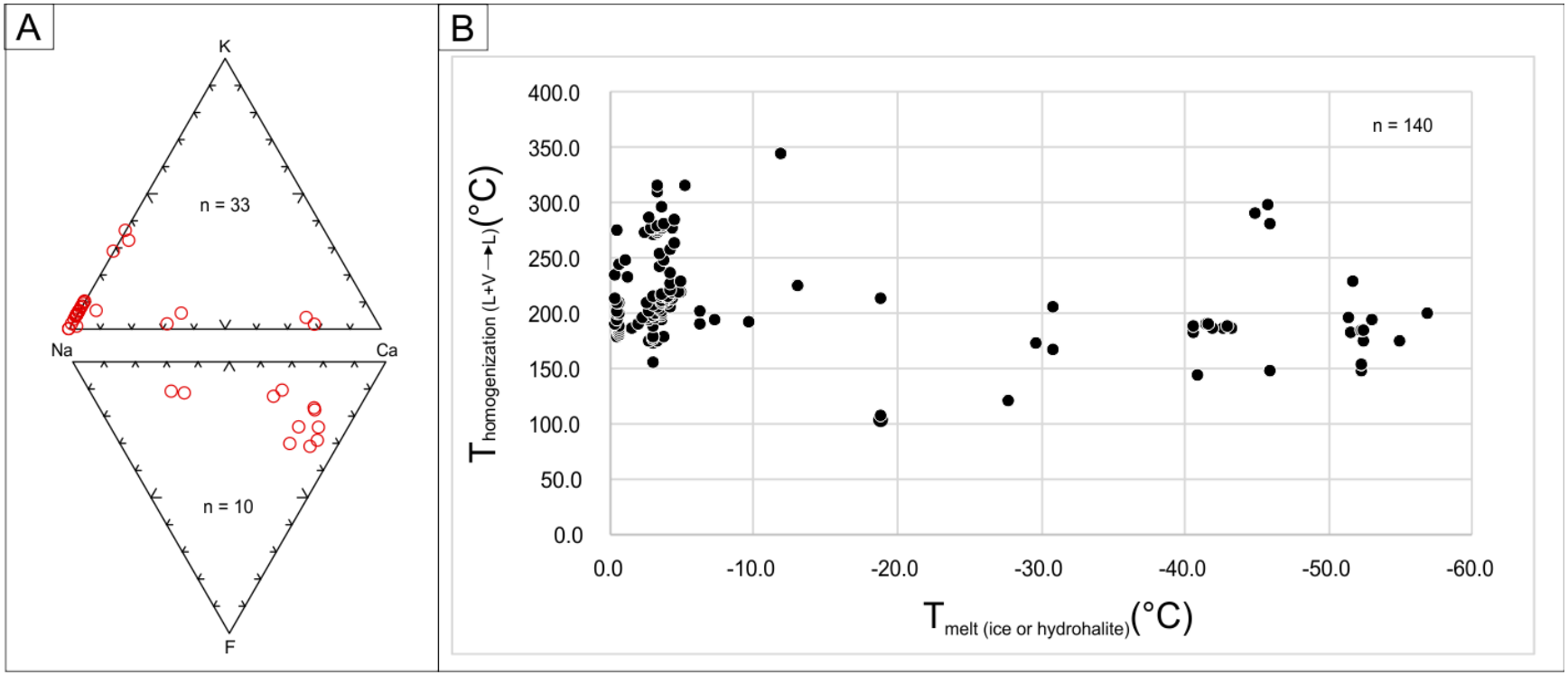

Figure 2.23: Results of EMA and microthermometry of fluid inclusions hosted by quartz pegmatite. (A) Ternary plots of selected elements (Na–K–Ca and Na–Ca–F)) frm EMA which indicte detection of four chemically–distinct fluid types, including NaCl, Na–Ca–Cl, Na–Ca–Cl–F, and Na–K–Cl. (B) Binary plot of homogenization temperature (T_h) versus last–solid melting temperature of fluid inclusions which suggests two general fluid types based on salinity and T_h.

2.3 Discussion

2.3.1 Analytical parameters for evaporate mound generation and SEM–EDS analysis

Analytical parameters for EMA study for the SMB were established during preliminary work on samples from a prospective study area. This approach is recommended for any study since parameters controlling decrepitation temperature may change depending on, for examples, the volatile content (*e.g.*, CO_2, CH_4) and density of the fluid inclusions. In terms of this study of the SMB, or similar settings, whose emplacement is constrained to ca. 3–4 kbar (Kontak & Kyser, 2011), the following approach is recommended: (1) rapid (i.e., 50°C/min) heating to 500°C to avoid volatilisation; (2) collection of SEM–EDS spectra from 16 mounds/chip; (3) a minimum of two quartz chips per sample to evaluate wafer–scale variation in fluid inclusion abundance and chemistry; (4) 60–second acquisition time to guarantee detection of all the solutes, particularly the minor elements at 0.1 wt. % levels; and (5) charge balance assessment of the analyses. In regards to the latter, it is noted that large positive imbalances may be associated with Cl– and F– volatilisation during heating whereas large negative imbalances may reflect SiO_2 precipitation on the walls of inclusions during cooling after initial entrapment (*i.e*., if silica is a significant aqueous species complexed by Cl^- or F^- in the hydrothermal solution).

2.3.2 Limitations of method

2.3.2.1 Origin of evaporate mounds

Ideally, the spatial association between decrepitate pits (i.e., opened inclusions) and evaporate mounds on the surface of the host quartz is the best line of evidence to support a single inclusion origin for evaporate mounds. Pits are roughly circular cavities that are commonly, but not always, adjacent to evaporate mounds and display, on average, 5 – 20 µm long–axis diameters (Fig. 2.11). The evacuation of fluid inclusions with subsequent loss of the fluid phase by opening them during

sample cutting and polishing reasonably explains the occurrence of pits in areas devoid of evaporate mounds.

Modelling of the decrepitation process and mound generation (Haynes *et al.* 1988) requires size and salinity constraints to assess the likely source of implicated fluid inclusions. Microthermometric data (Carruzzo *et al.* 2000, unpublished data from this study) constrains salinity of SMB quartz–hosted fluid inclusions to a wide range from 0 – 45 wt. % $NaCl_{equiv}$. A general constraint on fluid inclusion size of between 2 to 40 μm is supported by microscopic observation of several hundred SMB thin sections from an archive of SMB material. However, results obtained by approximation of mounds as hemiellipsoids (Haynes *et al.* 1988) predicts mounds to be smaller than the associated pit (Table 2.6; data calculated using the theoretical approach of Haynes *et al.* (1988) and microthermometric data from this study and Carruzzo *et al.* (2000). In SMB samples, mound diameters are larger than pit diameters. This ambiguity is resolved in part however by assuming the observed pit area is a cross section through an apical portion of the inclusion cavity as opposed to cutting the cavity's centre. That is to say, it is unlikely that every decrepitated inclusion seen is a halved inclusion. If this assumption, as well as the modelled approximations, in particular the variable porosity, are regarded as valid, the size of decrepitation pits relative to long–axis diameters of roughly spherical decrepitate residues support a single–inclusion origin for evaporate mounds.

2.3.2.2 Secondary fluorescence and charge imbalance

Interference by secondary fluorescence has an unavoidable effect on measured X–ray intensity during EDS analysis of evaporate mounds. Secondary excitation from X–rays generated within the sample is an analytically–defensible explanation for the consistent negative–charge imbalance observed in synthetic Na–Ca–Cl–F mounds with > 20 wt. % F. Precipitation of evaporate mounds

with domains of fluoride salt confirms the chemical bonding of Ca and F atoms in evaporate mounds. The characteristic X–rays produced by excited Ca atoms have sufficiently high energy (Kα = 3.692 keV) to induce lower energy emissions from neighbouring F atoms (Kα = 0.677 keV). Consequently, the secondary X–ray emissions from F atoms will be enhanced by Ca Kα primary X–ray–induced emissions. Furthermore, the lower energy X–ray emissions from exited F atoms cannot surmount the electron–binding energy required to excite Na (Kα = 1.040), Cl (Kα = 2.622) or Ca atoms. In this regard, it is noteworthy that only one of 378 F–bearing mounds analyzed on SMB quartz is devoid of Ca. Given the importance of F in magmatic–hydrothermal processes, it is useful to have a technique that can detect and quantify fluorine. Importantly, despite this secondary fluorescence problem, the resulting over reporting of F and underreporting of Ca does not have a significant impact on normalized mound compositions (*cf.* Sections 2.2.4 and ternary plots in Figs. 2.8 and 2.9), from the perspective of differentiating mound types in single samples.

TABLE 2.6. PREDICTIVE TABLES OF SIZE OF EVAPORATE MOUNDS. PREDICTED SIZES, IN μM, BASED ON THEORETICAL ESTIMATES FOR SHAPE OF FLUID INCLUSION CAVITIES AND EVAPORATE MOUNDS, AND EVAPORATE MOUND POROSITY (SEE TEXT FOR DETAILS).SALINITY RANGE USED TO CALCULATE MOUND SIZE IS BASED ON MICROTHERMOMETRY OF SMB FLUID INCLUSIONS (SEE TEXT FOR DETAILS). TABLE A VALUES CALCULATED USING 15 % MOUND POROSITY AND TABLE B USING 30% MOUND POROSITY.

A

salinity (wt. % $NaCl_{equiv}$)	fluid inclusion diameter (μm)								
	1	5	10	15	20	25	30	35	40
5	0.42	2.08	4.17	6.25	8.34	10.42	12.51	14.59	16.68
10	0.53	2.63	5.25	7.88	10.51	13.13	15.76	18.39	21.01
15	0.60	3.01	6.01	9.02	12.03	15.03	18.04	21.05	24.05
20	0.66	3.31	6.62	9.93	13.24	16.55	19.85	23.16	26.47
25	0.71	3.56	7.13	10.69	14.26	17.82	21.39	24.95	28.52
30	0.76	3.79	7.58	11.36	15.15	18.94	22.73	26.52	30.30
35	0.80	3.99	7.98	11.96	15.95	19.94	23.93	27.91	31.90
40	0.83	4.17	8.34	12.51	16.68	20.85	25.02	29.18	33.35
45	0.87	4.34	8.67	13.01	17.34	21.68	26.02	30.35	34.69

B

salinity (wt. % $NaCl_{equiv}$)	fluid inclusion diameter (μm)								
	1	5	10	15	20	25	30	35	40
5	0.44	2.22	4.45	6.67	8.90	11.12	13.34	15.57	17.79
10	0.56	2.80	5.60	8.41	11.21	14.01	16.81	19.61	22.42
15	0.64	3.21	6.42	9.62	12.83	16.04	19.25	22.45	25.66
20	0.71	3.53	7.06	10.59	14.12	17.65	21.18	24.71	28.24
25	0.76	3.80	7.61	11.41	15.21	19.01	22.82	26.62	30.42
30	0.81	4.04	8.08	12.12	16.16	20.21	24.25	28.29	32.33
35	0.85	4.25	8.51	12.76	17.02	21.27	25.53	29.78	34.03
40	0.89	4.45	8.90	13.34	17.79	22.24	26.69	31.14	35.58
45	0.93	4.63	9.25	13.88	18.50	23.13	27.76	32.38	37.01

2.3.2.3 Formation of mound features due to leakage and related fractionation of solvent elements

The occurrence of solids and physical separation of inclusion phases during decrepitation and mound formation within decrepitation pits suggests that fractionation or physical separation may occur due to incomplete homogenization prior to decrepitation. The latter simply indicates breaching of the fluid inclusion prior to its homogenization due to, for example, the presence of an inherent weakness such as a proximal fracture. In some cases, SE–images clearly show evidence of fluid flow on the surface of the once actively decrepitating quartz chip, which can result in precipitation of a range of evaporative residues that are not discrete evaporate mounds. Fluid flow prior to complete vaporisation of the aqueous solvent phase also apparently leads to solute fractionation, possibly because of the relative salt saturation perpensity during rapid evaporation under such circumstances where compositional domains are identified within mounds. The scale at which fractionation processes occur may not always be discernable, and if so, evaporate mounds may not accurately represent the bulk composition of fluid inclusions, even with raster–mode analyses.

2.3.3 Advantages of method

2.3.3.1 Multi–component analysis and implications

Results from evaporate mound analysis allows quantification of cationic and anionic solute species in a single analytical session. Based on this study, solute species in secondary quartz–hosted fluids inclusions in the SMB may include F^{-}, S^{2-}, Cl^{-}, Na^{+}, K^{+}, Ca^{2+}, Fe^{2+}, Mn^{2+}, Zn^{2+}, and Pb^{2+}. The time–efficient and relatively low cost of the EMA technique make it favourable for use in exploration research provided that fluid inclusions preserve a chemical signature of mineralisation that extends strategically beyond mineralised zones. Detection of base– and precious–metal

mineralization from analysis of fluid inclusions hosted by samples collected from within areas of known mineralization gives reason for optimism (Haynes & Kesler1987a, Chryssoulis & Wilkinson 1983, Wilson *et al.* 1980). Additionally, the occurrence of hydrothermal alteration in rocks distal to mineralised zones is consistent with models for the evolution of mineralised granites (Pisiak *et al.* 2017, De Souza *et al.* 2015). This study does not attempt to answer this question, but it does provide some guidelines for a method by which it may be answered. The recent emergence of chemical discriminants to assess the origin of green rock in porphyry deposit settings (Wilkinson *et al*. 2017), that is barren regional greenschist facies rock or a distal footprint related to a hidden deposit, attests to the potential use of EMA in exploration.

2.3.3.2 Comparing EMA with LA–ICPMS and bulk–crush analysis

The solute chemistry of fluid inclusions is resolvable by EMA, bulk–crush and LA–ICP–MS techniques. The main distinguishing feature of bulk–crush analysis is that is does not resolve the chemistry of individual inclusions. In rare samples that host only a single population of fluid inclusions, which is uncommon, the data may be representative, but specialized sample treatment would still be required in order to measure F (*e.g.*, ion chromatography or fluoride selective electrode). Laser ablation–ICP–MS is generally useful for constraining trace elements and isotope ratios, but is arguable less accessible, considerably more expensive for industry application, and is very time intensive since microthermometry provides the needed internal standard (i.e., salinity) and then each inclusion has to be re–located for subsequent ablation and analysis. Furthermore this method does not allow for quantification of F. In contrast, the EMA method does not require microthermometry or locating individual inclusions. Importantly, when microthermometric data are generated the salinity provides the basis for proportioning the EDS–generated chemistry as is

done with LA–IC–MS analyses (*e.g.*, Pandur *et al.* 2015). A comparative assessment of the three techniques is tabulated below (Table 2.7.

TABLE 2.7. COMPARISON OF PARAMETERS COMMON TO ANALYTICAL METHODS USED TO DETERMINE THE MAJOR SOLUTE CHEMISTRY OF AQUEOUS SALINE FLUID INCLUSIONS

	leachate analysis	*LA-ICP-MS*	*evaporate mound analysis*
sample material	pulverised mineral separate	polished grain	polished grain
detector type	AAS/AES/MS (cations) IC (anions)	MS	EDS
bulk or single inclusion resolution	bulk	single	single
major cation sensitivity	yes	yes	yes
major anion sensitivity	yes	problematic*	yes
relative dilution of fluid inclusion solutes	high	no dilution	no dilution
relative risk of contamination	high	low	low
analyses per day	2-3^	50-100	100s[§]
relative cost ($)	moderate	high	low
relative difficulty in data reduction	moderate	high	low

*: Pettke *et al*., 2012
^: Piperov *et al.,* 2016
[§]: this study
Abbreviations: AAS: atomic absorption spectroscopy; AES: atomic emission spectroscopy; ms: mass spectroscopy; ic: ion chromoatography

2.3.3.3 Detection and quantification of fluorine

The presence of abundant F in late–stage hydrothermal fluid phase is supported by several lines of evidence. Field evidence includes the occurrence of fluorite (*e.g.*, Elmi Assadzedah *et al.* 2017, Richardson *et al.* 1990, O'Reilly *et al.* 1982) and topaz (*e.g.*, Halter *et al*. 1996, O'Reilly 1982, Audétat *et al.* 1998) in mineralised and altered granitoid rocks. Petrological evidence includes, for example, detection of up to 5 wt. % F in melt inclusions hosted by topaz granites in Zinnwald, Erzgerbirge, Germany (Thomas *et al.* 2005). However, detection and quantification of F in hydrothermal fluids through analysis of fluid inclusions is problematic, partly due to the high ionization potential of F, which precludes its detection by LA–ICP–MS. Analytical challenges associated with F explains its absence in the bulk compositional analyses of fluid inclusions as reported in the available literature (*cf*. Kenderes & Appold 2017).

Inaccuracies associated with EDS detection of F in SMB–hosted evaporate mounds are indicated by a charge imbalance between cation and anion elements. A negative charge imbalance suggests an over estimation of anions, and a positive charge imbalance suggests an over estimation of cations. The magnitude of error on the quantised F can be evaluated by proxy. Synthetic NaCl–CaF_2 powder served as an analogue of percent error in the analysis of these powders of known composition and is therefore relatively straightforward (Table 2.3). Relative percent errors calculated from the analysis of synthetic powders provide proxy estimates for error in the analysis of naturally–occurring mounds. For example, in naturally–occurring mounds with F concentrations between 1 and 20 wt. %, charge imbalances ranged from -3.54 to +10.08. A relative percent error range from 18 to 42% is associated with the analysis of synthetic mounds that have a charge imbalances ranging from -3 to -10 (Table 2.8). We acknowledge that there are some analytical inconsistencies between the results of natural powders and natural–occurring mounds.

For example, all charge imbalances associated with natural powders are negative (Table 2.3), whereas charge imbalances associated with SMB–hosted with F concentrations < 20 wt. % are positive (Fig 2.8). However, the uncertainty of error associated with the EDS analysis of mounds with F does not impact the relative wt. % of major solutes in the mounds (*cf*. ternary plots in Figs. 2.8 and 2.9). Despite analytical challenges however, EMA analysis of secondary fluid inclusions hosted by SMB quartz demonstrates that F is a major solute anion in common hydrothermal fluids associated with large felsic intrusions, suggesting reconsideration of the relative role of F and Cl in hydrothermal processes (*e.g.*, metal transport).

TABLE 2.8. AN APPROXIMATION OF PERCENT ERROR IN THE EDS DETECTION OF F IN NATURALLY-OCCURRING EVAPORATE MOUNDS

A	B	C	D	E	F	G
1 - 20	10	125	-3.54, +/-3.37, 1σ	10.06, +/-5.41, 1σ	3 to 10	18 to 42 %
21 - 40	156	47	-9.97, +/-6.84, 1σ	3.57, +/-3.25, 1σ	3 to 10	17 to 21 %

A: Fluorine concentration in mound (range in wt. %)

B: Number of mound analyses with negative charge imbalance

C :Number of mound analyses with positive charge imbalance

$$\left\{ \sum \frac{C_x{}^{n+}}{M_x{}^{n+}} * n \; - \; \sum \frac{C_x{}^{n-}}{M_x{}^{n-}} * n \right.$$, where C = wt. % of element x, M = atomic wt. of element x, and n = atomic charge of element x

D: Average negative charge imbalance

E: Average positive charge imbalance

F: Magnitude of charge imbalance (range)

G: Relative percent error in synthetic mound analyses with charge imbalances within relevant range (adjacent column)

2.4 Conclusions

Evaporate mound analysis (EMA) using SEM–EDS analysis performed on quartz–hosted fluid inclusions from the ca. 380 Ma mineralised South Mountain Batholith (SMB), Nova Scotia, reveals a multi–element composition of secondary magmatic/hydrothermal fluids that are considered to be associated with a cooling felsic intrusive system (i.e., orthomagmatic fluids). Mounds derived from 2–phase (L–V) aqueous inclusions contain the following: Cl^{-}, F^{-}, S^{2-}, Na^{+}, Ca^{2+}, K^{+}, , Mn^{2+}, Fe^{2+}, Zn^{2+}, Al^{3+}, Pb^{2+}, Mg^{2+}, Sn^{2+}, and Cu^{2+}. Analysis by SEM–EDS of synthetic NaCl–CaF_2 powders provides some constraint on errors associated with the EMA analysis, which include average relative errors of 40% for F^{-} and Ca^{2+} and 32% and 15% for Na^{+} and Cl^{-}, respectively. However, analytical errors associated with the EDS system do not have a significant impact on the 'normalized' proportions of these major solute elements, which therefore allows for the differentiation of mound types in natural samples. The detection of F as a major solute element in hydrothermal fluids is rarely reported, and, as far as we are aware, not achievable by other conventional methods that analyze single fluid inclusions. Theoretical constraints based on evaporate mound size, fluid inclusion size and salinity, the latter empirically determined from microthermometric work, suggest discrete evaporate mounds of the size observed in this study are likely of single–inclusion origin. Limitations associated with EMA can be reduced by optimizing analytical procedures for any study area. For the SMB, the focus of this study, these parameters included the following: (1) rapid heating at 50°C/min to 500°C to avoid volatilisation of F and Cl; (2) collection of EDS spectra from 16 mounds/chip to provide a representative sampling; (3) a minimum of two chips per sample were studied to evaluate wafer–scale variation in fluid inclusion

abundance and chemistry (4) a minimum 60–second acquisition time to ensure detection of all major and minor solute elements; and (5) charge balance assessment to assess the quality of data.

The relative simplicity combined with both time and cost efficiency of this methodology compared to other protocols (*e.g.*, LA–ICP–MS) provides a means to assess the major solute chemistry of trapped paleo–hydrothermal fluids in ore deposit settings. As demonstrated here, there is potential for detecting a wide spectrum of important elements which provides the basis to better define elemental associations in ore systems. Thus, it is suggested that the application of EMA should become a more universally applied part of the protocol of ore deposit studies.

2.4 References

ALDERTON, D.H.M., THOMPSON, M., RANKIN, A.H., & CHRYSSOULIS, S.L. 1982. Developments of the ICP–linked Decrepitation Technique for the Analysis of Fluid Inclusions in Quartz. Chemical Geology 37, 203–213.

ALLEN, M.M., YARDLEY, B.W.D., FORBES, L.J., SHMULOVICH, K.I., BANKS, D. A., & SHEPHERD, T.J. 2005. Validation of LA–ICP–MS fluid inclusion analysis with synthetic fluid inclusions. American Mineralogist 90, 1767–1775.

AUDÉTAT, A., GÜNTHER, D., & HEINRICH, C.A. 1998. Formation of a Magmatic–Hydrothermal Ore Deposit: Insights with LA–ICP–MS Analysis of Fluid Inclusions. Science 279, 2091–2094.

BAKKER, R., & BAUMGARTNER, M. 2012. Unexpected phase assemblages in inclusions with ternary H2O–salt fluids at low temperature. Central European Journal of Geosciences 4, 225–237.

BODNAR, R.J. 2003. Interpretation of Data from Aqueous–Electrolyte Fluid Inclusions. *In*: Fluid Inclusions: Analysis and Interpretation. Mineralogical Association of Canada Short Course Publication (I. Samson, A.J. Anderson, & D. Marshall, eds.). Mineralogical Association of Canada, Ottawa, Canada (81 – 100).

BODNAR, R.J. & VITYK, M.O. 1994. Interpretation of microthermometric data for H_2O–NaCl fluid inclusions. *In* Fluid Inclusions in Minerals, Methods and Applications (B. De Vivo & M.L. Frezzotti, eds.). Virginia Tech University, Blacksburg, United States (117–130).

BODNAR, R.J., BINNS, P.R., & HALL, D.L. 1989. Synthetic fluid inclusions – VI. Quantitative evaluation of the decrepitation behaviour of fluid inclusions in quartz at one atmosphere confining pressure. Journal of Metamorphic Geology 7, 229–242.

CARRUZZO, S., KONTAK, D.J., & CLARKE, D.B. 2000. Granite–hosted mineral deposits of the New Ross area, South Mountain Batholith, Nova Scotia, Canada: P, T and X constraints of fluids using fluid inclusion thermometry and evaporate analysis. Transactions of the Royal Society of Edinburgh: Earth Sciences 91, 303–319.

CHRYSSOULIS, S.L. & WILKINSON, N. 1983. High Silver Content of Fluid Inclusions in Quartz from Guadalcazar Granite, San Luis Potosi, Mexico: A Contribution to Ore–Genesis Theory. Economic Geology 78, 302–318.

DE SOUZA, S., DUBÉ, B., MCNICOLL, V.J., DUPUIS, C., MERCIER–LANGEVIN, P., CREASER, R.A., & KJARSGAARD, I.M. 2015. Geology, hydrothermal alteration, and genesis of the world–class Canadian Malartic stockwork–disseminated Archean gold deposit, Abitibi, Quebec, *In* Targeted Geoscience Initiative 4: Contributions to the Understanding of Precambrian Lode Gold Deposits and Implications for Exploration, (B. Dubé & P. Mercier–Langevin eds). Geological Survey of Canada, Open File 7852, Ottawa, Canada, 113–126.

ELMI ASSADZADEH, G., SAMSON, I.M., & GAGNON, J.E. 2016. Identification of Fluid Inclusion Solid Phases Using a Focused Ion Beam Scanning Electron Microscope with Energy Dispersive Spectroscopy: Implications for Interpreting Microthermometric Data and Composition of Fluids in Sn–(–W–Mo) Deposits. Canadian Mineralogist 54, 737–754.

FENG, YONGGANG 2014. Hydrothermal Geochemistry and Mineralizing Processes in the T Zone, Thor Lake Rare–element Deposit, Northwest Territories. Electronic Theses and Dissertations 5106. University of Windsor, Windsor, Canada.

GUILLONG, M., KUHN, R–F., GÜNTHER, D. 2003. Application of a particle separation device to reduce inductively coupled plasma–enhanced elemental fractionation in laser ablation inductively coupled plasma–mass spectrometry. Spectrochimica Acta Part B 58, 211–220.

HAYNES, F.M. & KESLER, S.E. 1987. Fluid inclusion chemistry in the exploration for Mississippi Valley–type deposits: an example from East Tennessee, U.S.A. Applied Geochemistry 2, 321–327.

HAYNES, F. M. & KESLER, S.E. 1987b. Chemical Evolution of Brines during Mississippi Valley–Type Mineralization: Evidence from East Tennessee and Pine Point. Economic Geology 82, 53–71.

HAYNES, F.M., STERNER, S.M., & BODNAR, R.J. 1988. Synthetic fluid inclusions in natural quartz. IV. Chemical analyses of fluid inclusions by SEM/EDA: Evaluation of method. Geochimica et Cosmochimica Acta 52, 969–977.

HEINRICH, C.A. & COUSENS D.R., 1989. Semi–quantitative electron microprobe analysis of fluid inclusion salts from the Mount Isa copper deposit (Queensland, Australia). Geochimica et Cosmochimica Acta 53, 21–28.

HAHN, K. TURNER, E.C., KONTAK, D.J., & FAYEK, M. (2018). A billion years of fluid–flow history through porous carbonate mounds in Mesoproterozoic basin (Borden Basin, Nanisivik District), Nunavut. Geochimica et Cosmochimica Acta 223, 493–51.

KAMENETSKY, V.S., VAN ACHTERBERGH, E., Ryan, C.G., NAUMOV, V.B., MERNAGH, T.P., & Davidson, P. 2002. Extreme chemical heterogeneity of granite–derived hydrothermal fluids: An example from inclusions in a single crystal of miarolitic quartz. Geology 30, 59–62.

KENDERES, S.M. & APPOLD, M.S. 2017. Fluorine concentrations of ore fluids in the Illinois–Kentucky district: Evidence from SEM–EDS analysis of fluid inclusion decrepitates. Geochimica et Cosmochimica Acta 210, 132–151.

KERR, M.J., HANLEY, J.J., KONTAK, D.J., MORRISON, G.G., PETRUS, J., SHARPE, T., & FAYEK, M. (2018). Evidence of upgrading of gold tenor in an auriferous orogenic quartz–carbonate vein system by late magmatic–hydrothermal fluids at the Madrid deposit, Hope Bay Greenstone Belt, Nunavut, Canada. Geochimica et Cosmochimica Acta 241, 180–218.

KONTAK, D.J. 2004. Analysis of Evaporate Mounds as a Compliment to Fluid–Inclusion – Thermometric Data: Case Studies from Granitic Environments in Nova Scotia and Peru. Canadian Mineralogist 42, 1315–1327.

KONTAK, D.J. 1998. A Study of Fluid Inclusions in Sulfide and Nonsulfide Mineral Phases from a Carbonate–Hosted Zn–Pb Deposit, Gays River, Nova Scotia, Canada. Economic Geology 93, 793–817.

KONTAK, D.J. & TUBA, G. 2017. How can fluid inclusions studies better constrain orogenic gold deposit models: case studies from the Superior Province and Meguma Terrane, Canada. SGA Meeting, Québec, Canada, August, 2017. Volume Proceedings of Extended Abstracts.

KONTAK, D.J. & KYSER, T.K. 2011. A fluid inclusion and isotope study of an intrusion–related gold deposit (IRGD) setting in the 380 Ma South Mountain Batholith, Nova Scotia, Canada: evidence for multiple fluid reservoirs. Mineralium Deposita 46, 337–363.

KONTAK, D.J. & CLARK, A.H. (2002): Genesis of the giant, bonanza San Rafael lode tin deposit, Peru: origin and significance of pervasive alteration. Economic Geology 97, 1741–1777.

KONTAK, D.J. & KYSER, K. 2001. Preliminary Fluid Inclusion and Oxygen Isotope Studies of the Flintstone Rock (NTS 21A/04) Silica–clay Deposit, Yarmouth County, Nova Scotia. *In* Mines and Minerals Branch Report on Activities 2000 (M.R. MacDonald, ed.). Nova Scotia Department of Natural Resources Publication, Halifax, Canada (37–48).

KONTAK, D.J. & RYAN, R.J. 2001. Geological Setting and Fluid Inclusion Study of Celestite Mineralization, Beckwith (NTS 11E/13), Nova Scotia. *In* Mines and Minerals Branch Report on Activities 2000 (M.R. MacDonald, ed,). Nova Scotia Department of Natural Resources Publication, Halifax, Canada (49–59).

KONTAK, D.J., ALIMOHAMMADI, M., & WATTS, K. 2014. The Gardners Meadow Sn–Zn–Cu showing of southwest Nova Scotia: A small but not insignificant ca. 360 Ma metallogenic event. Atlantic Geology 50, 42.

KONTAK, D.J., DOSTAL, J., KYSER, K., & ARCHIBALD, D.A. (2002). A petrological, geochemical, isotopic and fluid inclusion study of 370 Ma Pegmatite–Aplite Sheets, Peggys Cove, Nova Scotia, Canada. Canadian Mineralogist 40, 1249–1286.

KONTAK, D.J., ANSDELL, K., DOSTAL, J., HALTER, W., MARTIN, R., & WILLIAMS–JONES, A.E. 2001. The nature and origin of quartz rock crystals in a fluorine–rich leucogranite, East Kemptville Tin Deposit, Nova Scotia, Canada. Transactions of the Royal Society of Edinburgh: Earth Sciences 92, 173–200.

KONTAK, D.J., ANSDELL, K., & ARCHIBALD, D. 1999. New constraints on the age and origin of the Dunbrack Pb–Cu–Zn–Ag deposit, Musquodoboit Batholith, southern Nova Scotia. Atlantic Geology 35, 19–42.

KRETZ, R. 1983. Symbols for rock–forming minerals. American Mineralogist 68, 277–279.

MATHIEU, J., KONTAK, D.J., & TURNER, E.C. 2013. A fluid inclusion study of diagenetic fluids in Proterozoic and Paleozoic carbonate rocks, Victoria Island, NWT. Geofluids 13, 559–578.

METZGER, F.V., KELLY, W.C., NESBITT, B.E., & ESSEN, E.J. 1977. Scanning Electron Microscopy of Daughter Phase in Fluid Inclusions. Economic Geology 72, 141–152.

McDIVITT, J., KONTAK, D.J., LAFRANCE, B., & ROBICHAUD, L. (2018). Contrasting fluid chemistries, alteration characteristics, and metamorphic timing relationships recorded in hybridized ore bodies of the Missanabie–Renabie gold district, Archean Wawa subprovince, Ontario, Canada. Economic Geology 113, 397–420.

NEYEDLEY, K., HANLEY, J.J., FAYEK, M., & KONTAK, D.J. 2017. Textural, fluid inclusion, and stable oxygen isotope constraints on vein formation and gold precipitation at the 007 deposit, Rice lake Greenstone Belt, Bissett, Manitoba, Canada. Economic Geology 112, 629–660.

O'REILLY, G.A., FARLEY, E.J., & CHAREST, M.H. 1982. Metasomatic–Hydrothermal Mineral Deposits of the New Ross–Mahone Bay Area, Nova Scotia. Nova Scotia Department of Mines and Energy Paper 82–2, 15–21.

PALMER, D.A.S. & WILLIAMS–JONES, A.E. 1996. Genesis of the Carbonatite–Hosted Fluorite Deposit at Amba Dongar, India: Evidence from Fluid Inclusions, Stable Isotopes, and Whole Rock–Mineral Geochemistry. Economic Geology 91, 934–950.

PANDUR, K., KONTAK, D.J., & ANSDELL, K.M. 2014. Hydrothermal evolution in the Hoidas Lake vein–type REE deposit, Saskatchewan, Canada: constraints from fluid inclusion microthermometry and evaporate mound analysis. Canadian Mineralogist 52, 717–744.

PETTKE, T., OBERLI, F., AUDÉTAT, A., GUILLONG, M., SIMON, A.C., HANLEY, J.J., & KLEMM, L.M. 2012. Recent developments in element concentration and isotope ratio analysis of individual fluid inclusions by laser ablation single and multiple collector ICP–MS. Ore Geology Reviews 44, 10–38.

PIPEROV, N.B., IVANOVA, L.P., & ALEKSANDROVA, A.N. 2016. A reappraisal of decrepitation–inductively coupled plasma spectroscopy (D–ICP) for bulk analysis of fluid inclusions in minerals. Analytical Methods, 3183–3195.

PISIAK, L.K., CANIL, D., GRONDAHL, C., PLOUFFE, A., FERBEY,T., & ANDERSON, R.G. (2015). Magnetite as a porphyry copper indicator mineral in till: a test using the Mount Polley porphyry copper–gold deposit, south–central British Columbia (NTS 093A). *In* Geoscience BC Summary of Activities Report 2015–1, Victoria, Canada (141–150).

REYNOLDS, T.J. & BEANE, R.E. 1985. Evolution of Hydrothermal Fluid Characteristics at the Santa Rita, New Mexico Porphyry Copper Deposit. Economic Geology 80, 1328–1347.

RICHARDSON, C.K. & PINCKNEY, D.M. 1984. The chemical and thermal evolution of the fluids in the Cave–in–Rock fluorspar district, Illinois: mineralogy, paragenesis, and fluid inclusions. Economic Geology 83, 765–783.

RICHARDSON, J.M., BELL, K., WATKINSON, D.H., & BLENKINSOP, J. 1990. Genesis and fluid evolution of the East Kemptville greisen–hosted tin mine, southwestern Nova Scotia, Canada, *In*

Ore–bearing granite systems; Petrogenesis and mineralizing processes: (H.J. Stein, & J.L. Hannah, eds.). Geological Society of America Special Paper 246, Boulder, United States (181 – 204).

ROEDDER, E. 1984. Fluid Inclusions. Reviews in Mineralogy 12. Mineralogical Society of America, Washington D.C., United States.

SALVI, S., FONTAN, F., MONCHOUX, P., WILLIAMS–JONES, A.E., & MOINE, B. 2000. Hydrothermal Mobilization of High Field Strength Elements in Alkaline Igneous Systems: Evidence from the Tamazeght Complex (Morocco). Economic Geology 95, 559–576.

SAMSON, I.M., WILLIAMS–JONES, A.E., & LUI, W. 1995. The chemistry of hydrothermal fluids in carbonitites: Evidence from leachate and SEM–evaporate analysis of fluid inclusions from Oka, Quebec, Canada. Geochimica et Cosmochimica Acta 59, 1979–1989.

SAMSON, I.M. & WALKER, R.T. 2000. Cryogenic Raman spectroscopic studies in the system NaCl–$CaCl_2$–H_2O and implications for low temperature phase behaviour in aqueous fluid inclusions. Canadian Mineralogist 38, 35–43.

SAVARD, M.M. & CHI, G. 1998. Cation Study of Fluid Inclusion Evaporates in the Jubilee and Gays River (Canada) Zn–Pb Deposits – Characterization of Ore–Forming Brines*. Economic Geology 93, 920–931.

SHEPHERD, T.J., AYORA, C., CENDÓN, D.I., CHENERY, S.R., & MOISSETTE, A. 1998. Quantitative solute analysis of single fluid inclusions in halite by LA–ICP–MS and cryo–SEM–EMA: complimentary microbeam techniques. European Journal of Mineralogy 10, 1097–1108.

THOMAS, R., FÖRSTER, H–J., RICKERS, K., & WEBSTER, J.D. 2005. Formation of extremely F–rich hydrous melt fractions and hydrothermal fluids during differentiation of highly evolved tin–granite magmas: a melt/fluid–inclusion study. Contributions to Mineralogy and Petrology 148, 582–601.

TWEEDALE, F., HANLEY, J.J., & KONTAK, D.J. (2019). Evaporate Mound Analysis of quartz–hosted fluid inclusions from the South Mountain Batholith: detection and evaluation of a multi–element hydrothermal fluids. (in prep.).

TWEEDALE, F., HANLEY, J.J., KONTAK, D.J., & ROGERS, N. 2013. Petrographic observations and evaporate mound analysis of quartz–hosted fluid inclusions: Applications to assess metal fertility in granites. Geological Association of Canada–Mineralogical Association of Canada Annual Meeting, Programs with Abstracts, Winnipeg, Manitoba.

WALSH, J.F., KESLER, S.E., DUFF, D., & CLOKE, P.L. 1988. Fluid Inclusion Geochemistry of high–Grade, Vein–Hosted gold Ore at Pamour Mine, Porcupine Camp, Ontario. Economic Geology 83, 1347–1367.

WALKER, R.T. 1998. Low–temperature Raman spectroscopic analyses of fluid inclusions from granitoid–related mineral deposits and comparison with decrepitate analyses. Electronic Theses and Dissertations Paper 2655, University of Windsor, Ontario.

WILKINSON, J.J., COOKE, D.R., BAKER, M.J., CHANG, Z., WILKINSON, C.C., CHEN, H., FOX, N., Hollings, P., White, N.C., Gemmell, J.B., Loader, M.A., Pacey, A., Sievwright, R.H., Hart, L.A., & Brugge, E.R. 2017. Porphyry indicator minerals and their mineral chemistry as vectoring and fertility tools. *In* Application of indicator mineral methods to bedrock and sediments

(McClenaghan, M.B. & Layton–Matthews, D., eds.). Geological Survey of Canada, Open File 8345, Ottawa, Canada (67–77).

WILSON, J.W.J., KESLER, S.E., CLOKE, P.L., & KELLY, W.C. 1980. Fluid Inclusion Geochemistry of the Granisle and Bell Porphyry Copper Deposits, British Columbia. Economic Geology 75, 45–61.

YARDLEY, B.W.D. & BODNAR, R.J. 2014. Geochemical Perspectives: Fluids in the Continental Crust 3.

ZAW, K., HUNNS, S.R., LARGE, R.R., GEMMELL, J.B., RYAN, C.G., & MERNAGH, T.P. 2003. Microthermometry and chemical composition of fluid inclusions from the Mt Chalmers volcanic–hosted massive sulphide deposits, central Queensland, Australia: implications for ore genesis. Chemical Geology 194, 225–244.

CHAPTER 3: EVAPORATE MOUND ANALYSIS OF QUARTZ–HOSTED FLUID INCLUSIONS FROM THE SOUTH MOUNTAIN BATHOLITH: DETECTION AND EVALUATION OF A MULTI–ELEMENT HYDROTHERMAL FLUIDS.

F. Tweedale[1*], J. Hanley[1], and D. Kontak[2]

1. Department of Geology, Saint Mary's University, Halifax, NS, Canada B3H 3C3

2. Department of Earth Sciences, Laurentian University, Sudbury, Ontario P3E 2C6

* corresponding author: fergus.tweedale@smu.ca

Number of pages: 91

Number of figures: 27

Number of tables: 3

For submission to: Canadian Journal of Earth Sciences

Abstract

In mineralised granitoid intrusions, the bulk composition of evaporate mounds from secondary fluid inclusions cannot be spatially related to mineralised centres at an approximate sample density of 1/100 km^2. Analysis of over 1300 evaporate mounds hosted by quartz in 113 apparently barren samples from the peraluminous South Mountain Batholith of Nova Scotia includes detection of major solutes, Cl^-, Na^+, Ca^{2+}, K^+ and F^-, and minor solutes, S^{2-}, Mn^{2+}, Fe^{2+}, Zn^{2+}, Al^{3+}, Pb^{2+}, Mo^{2+}, Mg^{2+}, Sn^{2+} and Cu^{2+}. Identification of chemically distinct mound types, Na–Ca–Cl, Na–Cl±Ca, Na–Cl, Na–Ca–F–Cl, Na–F–Cl±Ca and Na–K–Cl provides evidence of multiple hydrothermal events. Detection of F as a major solute component in hydrothermal fluids was recognized

throughout the batholith and the distribution of S and K appears to be systematically related to Meguma contact zones, and stage 2 plutons, respectively. A relationship between fluid inclusion chemistry and local hydrothermal alteration of the host granitoids (*e.g.*, chloritisation of biotite, sericitization of feldspars, modal abundance of muscovite, abundance of quartz–hosted fluid inclusions), except for an apparent relationship between relatively high modal abundances of muscovite and Na–K–Cl type evaporate mounds, is not apparent. This result suggests that the solute chemistry of fluid inclusions is a product of fluid:rock interactions that occurred elsewhere, and not the product of hydrothermal processes that have locally altered primary granitoid minerals. However, consistent Pb– and S–detection in a sample proximal to the SMB– contact with the Horton Group suggests that secondary fluid inclusions preserve a regional scale chemical signature of mineralizing fluids sourced from outside the batholith.

3.0 Introduction

The Devonian South Mountain Batholith (SMB) is a 7300 km^2 mineralised (Sn, W, U, Mn, Cu, Zn) polyphase intrusive granitoid complex in south–western Nova Scotia, Canada (Fig. 3.1). Intermittently over the past century, research in mineral exploration of the SMB employed a variety of geophysical, geochemical, biogeochemical and lithogeochemical techniques (see MacDonald 2001 and references therein) that collectively identified numerous mineral prospects and occurrences, as well as past–producing mines (Fig. 3.2), including the east Kemptville Sn–Zn–Cu–Ag deposit (Richardson *et al.* 1990). Application of novel or unconventional exploration techniques to the SMB, including the use of accessory mineral indicators (*e.g.*, tourmaline, Clarke *et al.* 1993) and bulk geochemical indices (Smith & Turek 1976) have been academic, and not exploratory, in pursuit. Similarly, fluid inclusion research in the SMB is restricted to localised areas in the Davis Lake, West Dalhousie, New Ross and Halifax plutons (Smith & Turek 1976,

Kontak *et al.* 2001, Kontak 2004, Carruzzo *et al.* 2000, Kontak & Kyser 2011), and were not applied as a regional exploration vector.

This paper presents the results of a SMB batholith–scale study of the solute chemistry of quartz–hosted secondary fluid inclusions and hydrothermal alteration systematics based on detailed petrographic analysis from a large sample set (n = 119). The objective of this work is to assess the usefulness of integrating fluid inclusion evaporate mound analysis and petrographic alteration indices as an exploration tool.

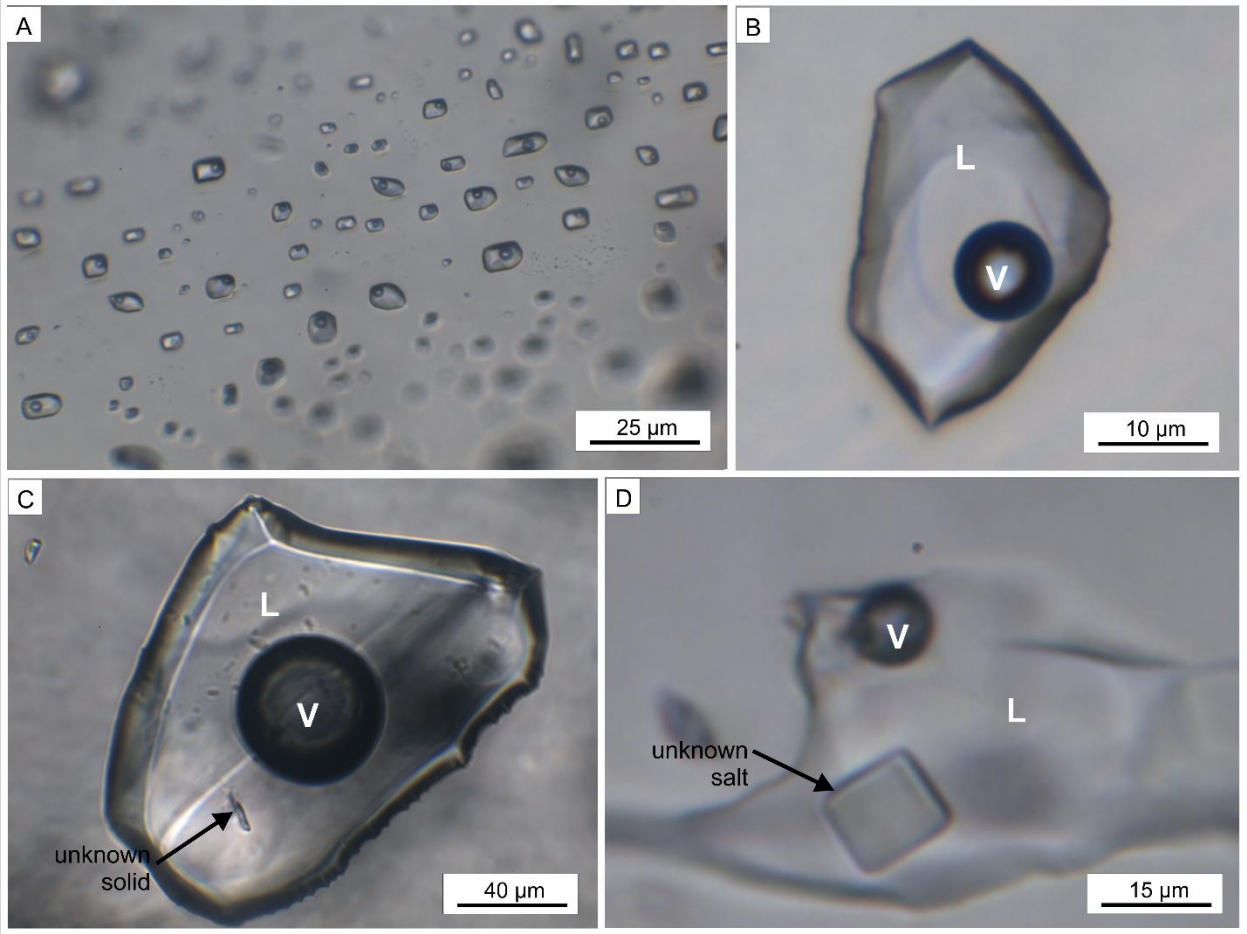

Figure 3.1: Transmitted–light photomicrographs of secondary aqueous fluid inclusions (FI) hosted in magmatic quartz of the South Mountain Batholith. The major solute chemistry of these inclusions is the focus of this study. (A) Abundant equant two–phase (L–V) necked FIs coating a healed fracture plane. Note that the FI display uniform 90/10 L:V ratios. (B) Close of two–phase (L–V) liquid–rich FI apparently lacking any solid phases. (C) Accidental solids of unknown composition in a large aqueous FI pegmatite quartz collected from the Bayers Lake Area near Halifax. (D) A rare 3–phase (L–V–solid) aqueous FI displaying a cubic mineral phase which is likely a halite daughter phase.

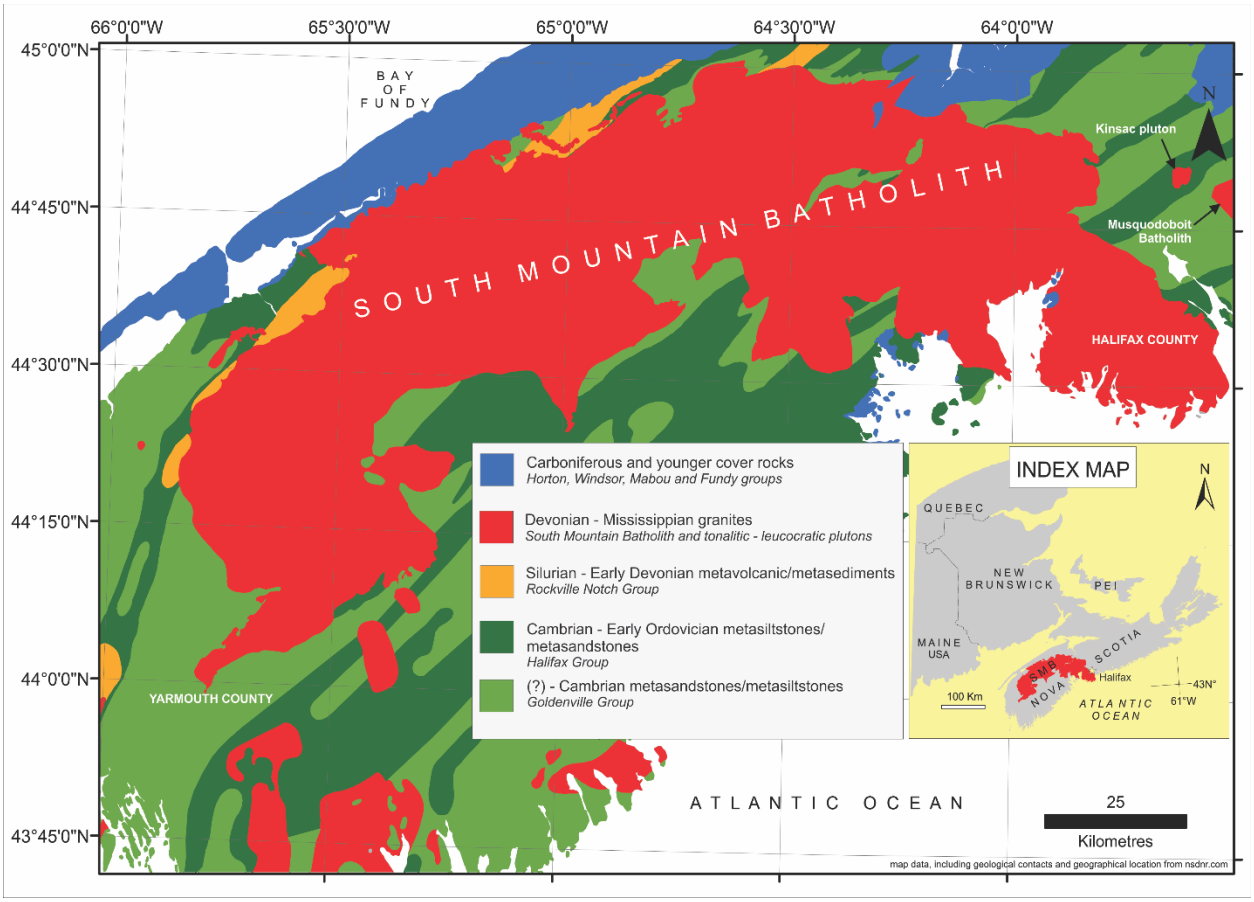

Figure 3.2: Geological setting of the peraluminous South Mountain Batholith (SMB), Nova Scotia, Canada, and its location in the northern Appalachians where it is the largest granitoid intrusion.

3.1 Background

The geochemical and mineralogical complexity of multiphase granitic intrusive environments poses a problem for exploration companies seeking to find the relatively small footprint of an intrusion–related metallic (Sn, W, Sb) ore deposit. For example, Sn(–W) mineralization in both the Late Devonian Ackley Granite, Newfoundland (Tuach *et al.* 1986), and South Mountain Batholith, Nova Scotia (MacDonald 2001), are small targets in these otherwise large intrusive bodies. Added to this challenge is the observation that the distribution of mineralised centres relative to causative intrusive complexes is spatially and temporally variable with many ore styles (*e.g.*, breccias, veins, greisens; Taylor 1979) or in some cases the mineralised centre may occur in the country rock with no apparent progenitor intrusion seen (*e.g.*, Lake George Sb, New Brunswick; Seal *et al.* 1985). Also problematic is the relatively limited exploration strategies that specifically address the varied nature of these ore deposit settings and their small footprints. To be useful in any exploration scenario, analytical approaches must employ a simple and cost–efficient methodology that produces accurate results in a time effective manner.

The potential application of fluid inclusion research to mineral exploration has persisted for decades (see discussion in Roedder 1984), though few companies adopted their potential use as a pathfinder or vector. Research methodologies have however applied, albeit very limited, the bulk analysis of fluid inclusions to regional–scale exploration work in granitic environments during the 1980s and 90s with application in in the SW England Sn–W–base metal ore district (Alderton *et al.* 1982, 1992, Alderton & Rankin 1983, Rankin & Alderton 1983). However, bulk techniques (Yardley *et al.* 1993, Gleeson 2003, Gleeson & Turner 2007, Bottrell & Yardley 1988) typically provide an averaged result from all inclusions present (i.e., many fluid generations) thus reflecting a single geochemical signature for the hydrothermal system versus signals for discrete

hydrothermal fluid events. As the latter is usually the case based on more detailed microthermometric studies of intrusion related Sn–W settings (*e.g.,* Audétat *et al.* 1998, Kontak & Clark 2002, Carruzzo *et al.* 2000), being able to quantify the chemistry of discrete events is preferred. This desire to resolve the compositions of these chemically–distinct hydrothermal fluid events, in particular those related to ore formation led to the development of techniques that analyse single individual inclusions *in–situ*, in particular the LA–ICP–MS method (Pettke *et al.* 2012, Audétat *et al.* 1998, Heinrich *et al.* 1992, Heinrich *et al.* 2003) Although LA–ICP–MS is now becoming for some a routine choice for determining major and trace element concentrations of fluid inclusion solutes, analytical limitations associated with high ionization energies of halogens (Seo *et al.* 2011, Pettke *et al.* 2012), and technical challenges associated with relatively complicated data reduction schemes (Allen *et al.* 2005, Guillong *et al.* 2003) are incompatible with typical mineral exploration timelines. An alternative technique for the chemical analysis of individual fluid inclusions or populations of fluid inclusions is evaporate mound analysis (EMA; Haynes *et al.* 1988, Kontak 2004). The EMA methodology is simple, cost–effective and provides semi–quantitative multicomponent compositional data rapidly, therefore ideally suited to budget–constrained time–sensitive research. Although this method has been available it has not been thoroughly and rigorously evaluated, which we have recently addressed (Tweedale *et al.,* in prep, 2019) in order to promote its use more widely in studying in particular intrusion related ore deposit settings.

3.1.1 Previous studies

Models of granite–related mineralization infer a fluid–mediated process (Burnham 1979, Černy *et al.* 2005, Williams–Jones & Heinrich 2005 and references therein). It may reasonably expected that the mineralizing fluids altered rocks that are proximal to the mineralised centre, and that

hydrothermal alteration is detectable by both petrographic observation and analysis of secondary fluid inclusions. For example, Alderton *et al.* (1992) observed a local–scale spatial relationship between the bulk composition of quartz–hosted fluid inclusions and mineralised centres in the Dartmoor granite, SW England. In another study, Rankin & Alderton (1983) demonstrate a spatial relationship between quartz–hosted fluid inclusion abundance and proximity to granite–hosted mineralization. The application of fluid inclusion chemistry as a guide to batholith–scale exploration however, remains largely untested.

Evaporate mound analysis is a robust technique that is sensitive to both cation and anion elements (Table 3.1). For example, results from EMA research suggest that the bulk composition of fluid inclusions associated with mineralised centres are distinguishable from the composition of inclusions hosted by apparently barren rocks. For example, in MVT environments, ore–mineralizing fluids are relatively Ca–enriched compared to fluids associated gangue mineral phases (Haynes & Kesler 1987b). Other EMA studies document the bulk composition of fluids associated with REE mineralization (Williams–Jones *et al.* 2000, Pandur *et al.* 2015), fluorite and Pb–Zn deposits (Kenderes & Appold 2017), polymetallic (Sn–W–U–Mo–Cu–Mn) granite–hosted mineral deposits (Carruzzo *et al.* 2000) and mineralised nepheline syenites and pegmatites

TABLE 3.1. SUMMARIZED DATA FROM OTHER RESEARCH REPORTING ANALYSIS OF EVAPORATE MOUNDS USING THE SEM-EDS TECHNIQUE

Location and setting	Size of study area	Host mineral	Number of samples	Number of analyses	Major solute cations	Major solute anions	Minor solutes	*Other analytical techniques used	Conclusion relevant to this study	Reference
Guadalcazar granite, Mexico	6 Km^2	Qtz	18	354	Na, K, Ca, Mn, Fe, Zn, Ag, Ba	Cl	Ag	Bt geothermometry, decrepitation-ICP	Ag occurs in 1/18 samples. Mineralized sample proximal to known Ag-deposit	Chryssoulis & Wilkinson (1983)
quartz vein cutting metasediments/metavolcanics, Pamour Mine, Abitibi Greenstone Belt, Ontario	metre-scale quartz vein stockwork	Qtz	3	43	Na, K, Ca, Mg, Zn, Fe, P, Ti	Cl, S	Au, Zn	gas chromotography leachate analysis	detectable S in mounds	Walsh *et al.* (1988)
hypogene quartz kaolinite from strongly deformed area of the South Mountain Batholith, Nova Scotia	2.5 Km^2	Qtz	1	15	Na, K, Ba	Cl	Si, Kln	stable isotopes (O), SEM-EDS analysis of evacuated cavities	abundance of evacuated cavities without any precipitates interpretated as V-rich inclusions	Kontak & Kyser (2001)
altered pegmatitic syenite, Tamazeght complex, High Atlas Mountains, Morrocco	68 Km^2	Ne	10	not specified	Na, Ca, Mn, Fe, K	Cl		SEM-EDS analysis of evacuated cavities	EDS system employed not sensitive to F	Salvi *et al.* (2000)
breccia pipes in Pinatosa; fault-hosted breccia in Red Cloud, Gallinas Mountains, New Mexico	24 Km^2	Qtz, Fl		not specified	Na, K, Ca	Cl, S		raman analysis of solid phases hosted by L-V-S inclusions	identification of two distinct inclusion populations: Na-K-Cl-S (early) and Na-Cl (late)	Williams-Jones *et al.* (2000)
Dunbrack deposit: vein hosted in Musquodoboit Batholith, Nova Scotia	metre-scale quartz veins	Qtz	1	20	Na,K, Ca	Cl	Pb, Cu, Zn, Ag	$^{40}Ar^{39}Ar$ dating, stable isotopes (S, O, D), whole-rock geochemisstry	two distinct mound populations: Na-Cl type and Na-K-Ca-Cl type	Kontak *et al.* (1999)
Oka carbonitite complex, Québec	18 Km^2	Ap, Cal	3	27	Na, K, Ca, Mg	Cl, S		leachate analysis	charge imbalances between 18 - 53%	Samson *et al. (1995)*
Jubilee (J) and Gays River (GR) MVT-type deposits, Nova Scotia	not determined	Dol, Sp, Cal	5	31 (GR) 34 (J)	Na, Ca, K, Mg	Cl	Zn, Pb		analyzed standards to determine appropriate beam SEM voltage for EDS mound analysis	Savard & Chi (1998)
Gays River carbonate-hosted Zn-Pb deposit, Nova Scotia	not determined	Spl, Cal, Brt, Qtz, Fl	1	10	Na, Ca, Mg, Fe	not given	Zn, Pb	gas chromatography	Major solutes: Na, Ca, Mg; Minor solute: Mn; no mound production in Cal or Brt	Kontak (1998)
Pine Point (PP) / East Tennessese (ET) MVT deposits	10 km^2 (ET); 250 km^2 (PP)	Spl, Dol (ET); Spl, Dol, Ga (PP)	not specified	179 (ET); 78 (PP)	Na, Ca, K, Mg, Fe	Cl, S	Zn, Pb		correlation between depressed final melt temperatures and increased Ca: Na ratio	Haynes & Kesler (1987)
Pegmatite, greisen and vein deposits, South Mountain Batholith, Nova Scotia	500 km^2	Qtz	not specified	236	Na, Ca, K, Fe, Ba, Cu, Zn, Ni	Cl, S	Sn, W, U, Mo, Cu and Mn		major solute species: Na, Cl, K, Ca, minor solute species: S, Fe, Ba, Cu, Zn	Carruzzo *et al.* (2000)
Pegmatite-hosted REE deposit in alkaline granite and syenite, T-zone deposit, Thor Lake, NWT	25 km^2	growth zones in Qtz	3	13	Na, Ce	Cl, S	Mg, Al, P, K, Ca, Pr	LA-ICP-MS, raman spectroscopy	REEs in mounds, charge imbalances 5 - 45%	Feng (2014)
East Kemptville tin deposit, Nova Scotia	< 1 km^2	Qtz, Cst	4	c. 200	Na, Fe, Mn, K, Ca	Cl, S	Sr, Ba, Zn, P	gas chromotography	Elevated content of Fe (23 wt. %) and Mn (37 wt. %) in mounds	Kontak *et al.* (2001)

Mineral abbreviations after Kretz (1983).

* All studies, excluding Savard & Chi (1998) and Samson et al., (1995) include microthermometric analysis of fluid inclusions

(Salvi *et al.* 2000). Evaporate mound analysis is the only technique that detects cationic and anionic elements with a single analysis, which makes it amenable to routine mineral exploration. The compositional analysis of cation elements by bulk techniques provides an average value of solute concentrations for all inclusions, and complimentary techniques are required to obtain anion element concentrations (Alderton *et al.* 1982, Gleeson & Turner 2007). Bulk chemical constraints on single fluid inclusions are obtainable using other analytical techniques (*e.g.*, PIXE or LA–ICP –MS), but practical application of these techniques to routine exploration research is limited due to the high cost of analysis, long analytical times, need for specialized equipment, as well as a lack of dedicated technical expertise required to operate the equipment and manage data reduction for industry. In addition, the low ionization potential of halogen solute species, commonly detected in aqueous fluid inclusions from most geological environments (Roedder 1990), precludes detection of F and Cl by mass spectrometry.

This paper presents the results of a regional–scale study (i.e., batholith–scale, ~7300 km^2) integrating fluid–inclusion solute chemistry and hydrothermal alteration mineral systematics of igneous rock samples collected from the variably mineralised South Mountain Batholith (SMB), Nova Scotia, Canada. The primary aim of this research is to assess the value of integrating alteration petrography and evaporate mound analysis for vectoring toward mineralised centres in a large granitic intrusive setting. Abundant accessible outcrop public access to archived slab–sample and thin–section collections housed by the Nova Scotia Department of Natural Resources (NSDNR) makes the SMB an ideal study area for investigation into granite–related mineralization. Additionally the ubiquitous occurrence of quartz–hosted fluid inclusions in the SMB rocks provides ample material for EMA analysis.

3.1.2 Geological setting

The SMB is a large (7300 km^2) granitoid intrusion that dominantly intruded the conformable succession of folded late Neoproterozoic to early Paleozoic Meguma Supergroup metasedimentary rocks which were regionally metamorphosed to mainly lower greenschist facies but locally to lower amphibolite facies prior to intrusion of the SMB (White *et al.* 2012, Hicks *et al.* 1998). Along its western contact, some portions (< 10 % of the SMB perimeter) of the batholith intruded Ordovician to early Devonian metasedimentary and metavolcanic rocks of the Rockville Notch Group (White *et al.* 2012). Horton Group sedimentary rocks hosting Carboniferous (Famennian and Tournaisian) aged fossils non–conformably overlie the northeast corner of the batholith (Martel *et al.* 1993). Ages for the batholith include radiometric estimates of 372 – 361 Ma by Rb–Sr whole–rock isochron analysis (Clarke & Halliday 1980), 367 Ma (mean age from 22 samples) by $^{40}Ar/^{39}Ar$ and K–Ar analyses of muscovite and biotite (Reynolds *et al.* 1981) and 381– 373 Ma by U–Pb zircon dating (Bickerton *et al.* 2018a, Keppie *et al.* 1993).

The batholith is a composite peraluminous intrusion, broadly subdivided into two phases of temporally and lithologically distinct phases (Fig. 3.3). Early Stage 1 plutons are dominantly granodiorites and monzogranites, and later Stage 2 plutons are dominantly monzogranites, leucomonzogranites and leucogranites (MacDonald *et al.* 1992). Contacts between plutons are either intrusive, fault–bounded or gradational. The mineralogy geochemistry and petrogenesis of the SMB are extensively described (*e.g.*, McKenzie & Clarke 1975, Muecke & Clarke 1981, Clarke *et al.* 1997, MacDonald 2001, Clarke *et al.* 2004). Emplacement depth of the SMB is constrained by graphite thermometry (Hilchie & Jamieson 2014) and fluid inclusion microthermomtric studies (Carruzzo *et al.* 2000, Kontak *et al.* 2001, Kontak & Kyser 2011) to 10–12 km. Gravity–based modelling suggests an average basal depth of 7 km (Benn *et al.* 1999). The

provincial gravity map (Fisher 2006) indicates two areas of relatively greater thickness, one centred on the municipality of New Ross, and the other on the Davis Lake pluton

There is a spatial association between the New Ross and Davis Lake plutons and intrusion–related magmatic–hydrothermal styles of mineralization (Sn–Zn–Cu–Ag, Mn–Fe–P, U–Cu, Au–W), and the entire batholith is an area of considerable interest in terms of potential exploration (O'Reilly *et al.* 1982, Chatterjee & Clarke 1985, Carruzzo *et al.* 2000, MacDonald 2001, Baldwin 2017). It is this aspect of the SMB which is explored below using the chemistry of evaporate mounds.

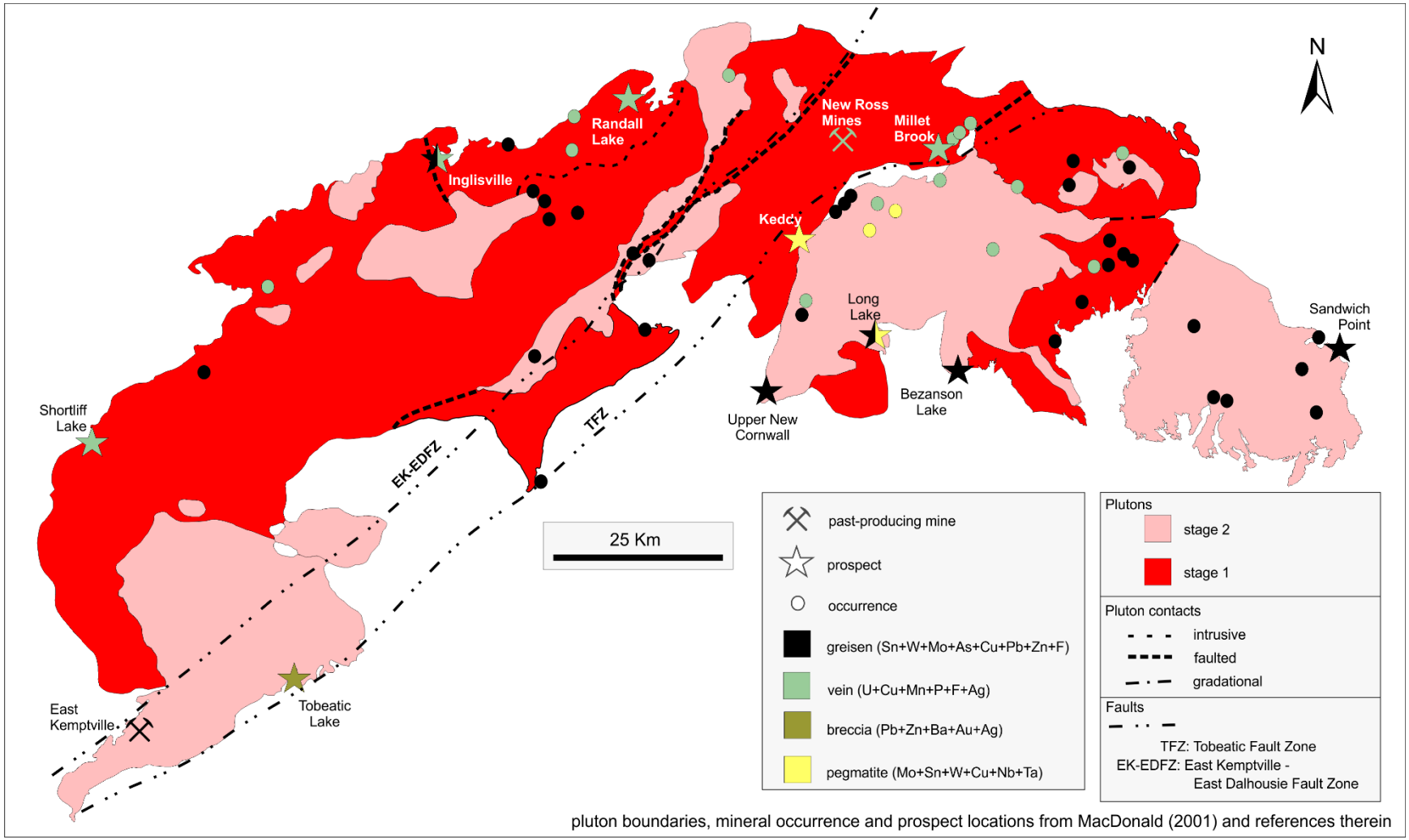

pluton boundaries, mineral occurrence and prospect locations from MacDonald (2001) and references therein

Figure 3.3 (previous page): Map of selected mineral occurrences, prospects and past–producing mines in the South Mountain Batholith (SMB). Although mineral occurrences occur throughout the batholith, known mineralisation types have a local distribution. Large greisen deposits are proximal to SMB–Meguma contact zones. Known vein deposits occur along NE–trending faulting zones located in the interior of the batholith. Occurrence of breccia deposits is restricted to the Tobeatic Fault zone. Known pegmatite deposits are hosted uniquely by the New Ross pluton, although apparently barren pegmatites occur throughout the SMB.

3.2 Methods

3.2.1 Sampling

3.2.1.1 Sample strategy

We superimposed a square grid consisting of 10 km^2 blocks (n = 100) on a map of the entire batholith and sought to collect a sample from each grid block. Field sampling was complimented by acquisition of samples from an archived NSDNR collection and Saint Mary's University research collection. At field localities where more than one igneous lithology is unambiguously exposed, a sample of each rock type was collected. We acknowledge a sample bias. Exposure of flat–lying bedrock in many coastal areas contrasts with the complete burial of bedrock under metre– to decimetre–scale till overburden that blankets large interior parts of the batholith. In addition, road access to some areas is relatively limited. Known mineralised centres were not targeted, except for an archived cassiterite quartz sample from the East Kemptville tin mine, a Mo–bearing quartz–feldspar pegmatite sample collected from the Long Lake prospect, and a greisen sample from the Long Lake prospect. The location of mineralised samples are shown in Figure 3.3. The procedure for preparing fluid inclusions wafers for evaporate mound analysis from slabbed samples is provided in Tweedale *et al.* (in prep, 2019).

3.2.1.2 Sample organization

Preliminary work on deciphering rock type based on the petrographic and geochemical criteria of MacDonald (2001) is not appropriate for this research. A time–efficient method is more appropriate for exploration research such as organization of samples by colour and texture observed in white–light images of fluid–inclusion wafers. High–resolution digital scans of wafers

were evaluated to determine dominant white–light colour and median grain size. As such, red–coloured samples are classified as K–feldspar granites, white samples as monzogranites and grey samples as sericitized granites (Fig. 3.4). Late–stage quartz–rich rocks have a modal abundance of > 90% quartz, and include pegmatites, veins, metre–scale pods and miarolitic cavities. Coarse–, medium– and fine–grained samples were identified following the criteria of MacDonald (2001). Lastly, the entire sample set was subdivided into regional blocks, the boundaries of which are consistent with the National Topographic Series 1: 50 000 scale planimetric base maps.

3.2.2 Evaporate mound analysis

Individual quartz grains or polycrystalline grain patches containing secondary fluid inclusions were cut from fluid inclusion wafers in preparation for evaporate mound production. The mounds were produced via thermal decrepitation following the procedures in Tweedale *et al.* (in prep, 2019). Essentially the evaporate mounds are salt residues that precipitate on the wafer surface from supercritical fluids generated from rapidly overheating fluid inclusions past their homogenization temperature which results in thermal decrepitation of the host quartz grain (Fig. 3.5). For this study the mounds were generated in a temperature–controlled heating oven suing a heating rate of 50°C per minute with final heating at 500°C which was followed by immediate cooling by removal from the oven.

The evaporate mounds were analyzed using two instruments located at the Department of Geology, Saint Mary's University, Halifax, Nova Scotia, Canada: (i) a thermal emission LEO® 1450 scanning electron microscope (SEM) equipped with an Oxford Instrument® X–max 80 mm^2 silicon–drift detector (SDD) energy dispersive X–ray spectrometer (EDS system) and (ii) a field emission Tescan® MIRA 3 LMU SEM coupled with the same SDD–EDS system. The upgrade in equipment was a coincidental occurrence, and entirely unrelated to this study. During imaging and

X–ray analysis of mounds throughout the study, the SEM was run with an accelerating voltage of 20 – 30 keV. The EDS detector is equipped with a thin polymer window that allows detection of light (6<Z12) and heavy (13 < Z < 82) elements in evaporate mounds at concentrations as low 500 – 1000 ppm. The accompanying INCA data reduction software included a Phi–Rho–Z matrix correction scheme and signal counts are calibrated at fixed wavelengths through the analysis of high quality synthetic and natural oxides, metals, alloys and mineral standards. An EDS acquisition time of 45 – 60 seconds was used for spot– and raster–mode analysis of evaporate mounds. Criteria for identifying and analyzing evaporate mounds are fully described in Tweedale *et al.* (in prep, 2019).

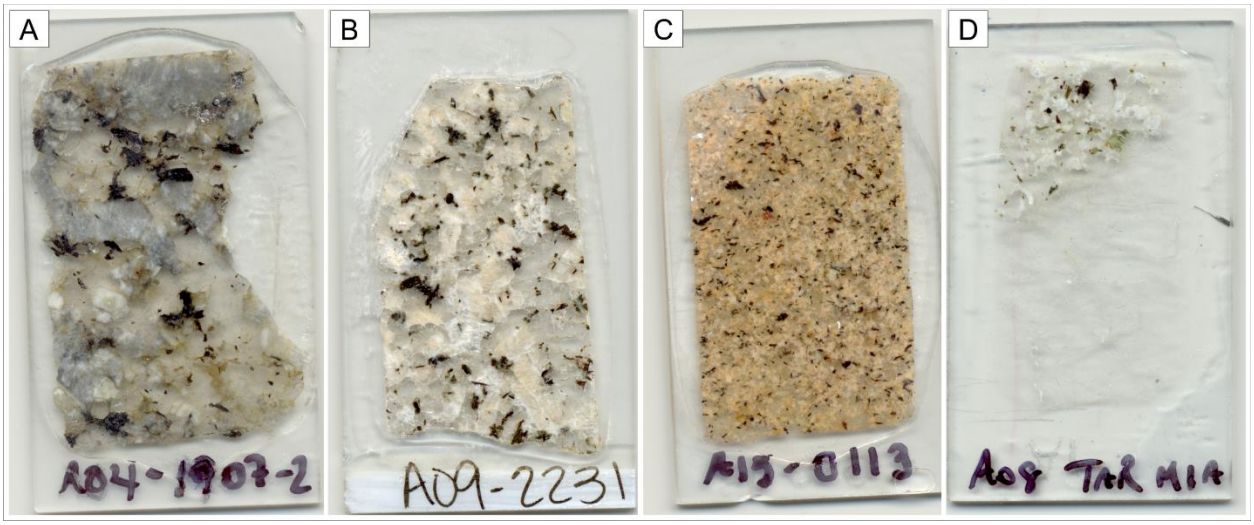

Figure 3.4: White light scans of fluid inclusion wafers displaying the four rock types identified in this study. Each wafer is bonded to standard–sized thin–section glass slides (25 x 46 mm). Grain–size scales are consistent with other research (MacDonald 2001): course–grained (> 0.5 cm), medium–grained (0.1 –0.5 cm) and fine–grained (<0.1 cm). (A) Coarse–grained sericitized granite from the Davis Lake pluton. (B) Medium– to coarse–grained monzogranite from the New Ross pluton. (C) Fine–grained K–feldspar granite from the East Dalhousie pluton. (D) Quartz sample collected from miarolitic cavity exposed in coastline outcrop near Aspotogan Point, Lunenburg County. Note the diffuse contact with the host granite in upper left corner of wafer.

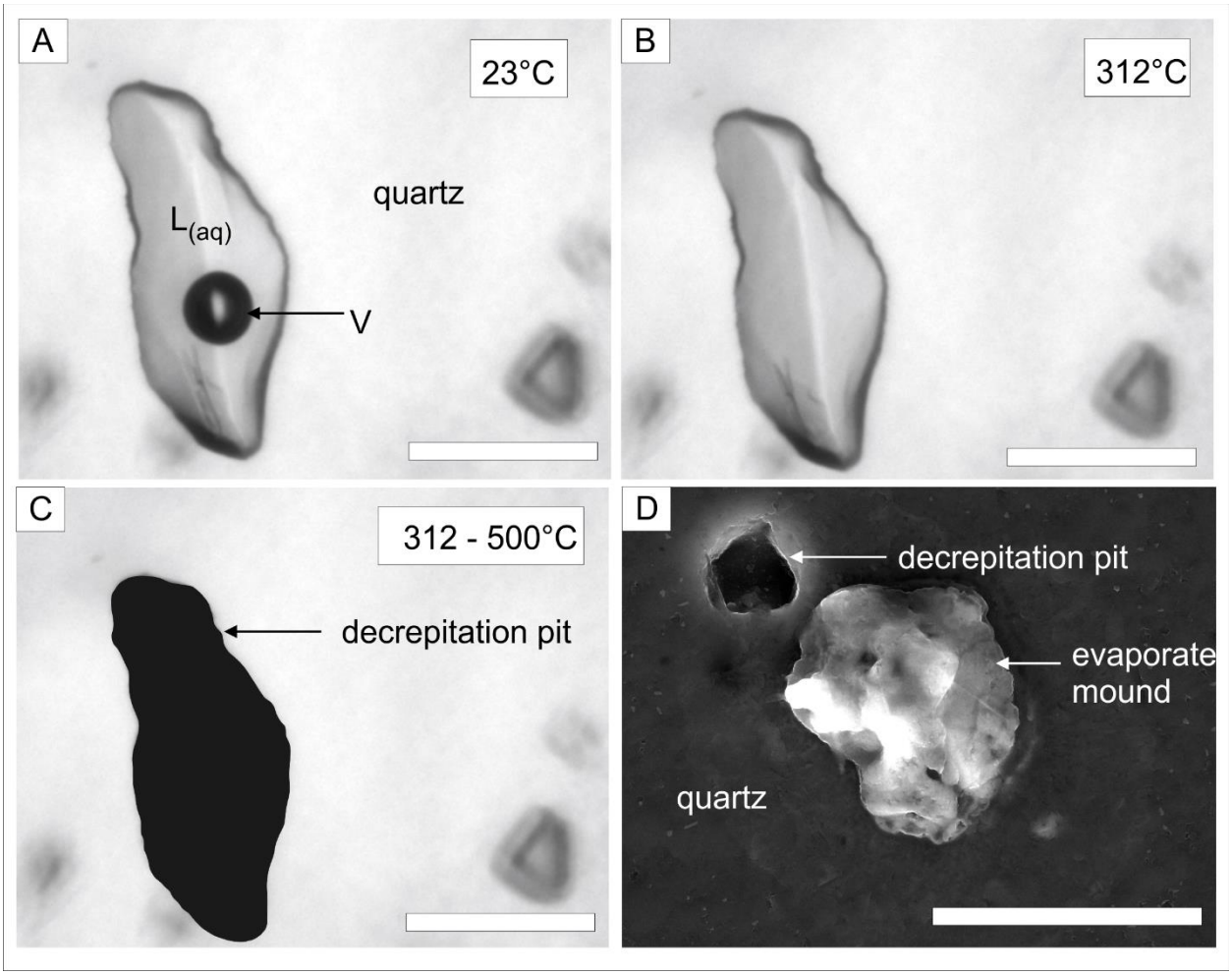

Figure 3.5: Photomicrographs illustrating thermally–induced evaporate mound generation in a heating stage; scale bar is 20 µm. Transmitted–light microscope images show: (A) large two–phase (L–V) liquid–rich aqueous fluid inclusion hosted in quartz at room temperature; (B) the same inclusion homogenized to a single fluid phase; and (C) the same inclusion decrepitated and now occupied by vapor and hence it appears dark due to refraction of light into the quartz host. (D) SEM–SE image of an evaporate mound and adjacent decrepitation pit.

3.2.3 Petrographic alteration indices

Assessments of select mineral replacement textures, modal abundance of muscovite and abundance of quartz–hosted fluid inclusions are considered as proxies for evaluating the degree of fluid:rock interaction and related hydrothermal alteration in SMB granitoids. Using 30 µm–thick thin sections, petrological indices (i.e., proxies) assigned to 64 SMB samples with evaporate mound data were: (1) chloritisation of biotite; (2) sericitisation of feldspars; (3) modal abundance of muscovite; and (4) abundance of quartz–hosted aqueous fluid inclusions (Fig. 3.6). The degree of alteration represented by a mineral replacement texture was determined by the proportion of primary relic biotite and feldspar grains replaced by chlorite and sericite, respectively. We acknowledge that, as in other studies (*e.g.*, Miller 1981), the deciphering of the origin of muscovite in the SMB is problematic (Ham & Kontak 1988). Although a diversity of textures displayed by SMB muscovite were observed (Fig. 3.7), only clearly visible muscovite grains with minimum grain diameters of ~1 mm were point counted. Assessment of all four indices give a quantitative assessment of fluid:rock interaction, and we selected proxies deemed suited for evaluation of the peraluminous granites in the study area. The scarcity of epidote in SMB granites (MacDonald 2001) and extreme variability in albite exsolution abundance and textures at the thin–section scale precluded routine evaluation of saussuritization and perthite coarsening.

Each thin section was visually scanned at low and high magnifications, and an individual score for each alteration parameter was based on comparative analysis with a corresponding alteration index. Incipient degrees of alteration and low abundances for a given index are ranked by a numerical score between 1 and 10, where 10 indicates extensive alteration or high abundances. Finally, a composite alteration ranking for each sample was calculated from the values of each

alteration index; these rankings highlight the broad textural differences between samples that are of interest for this study.

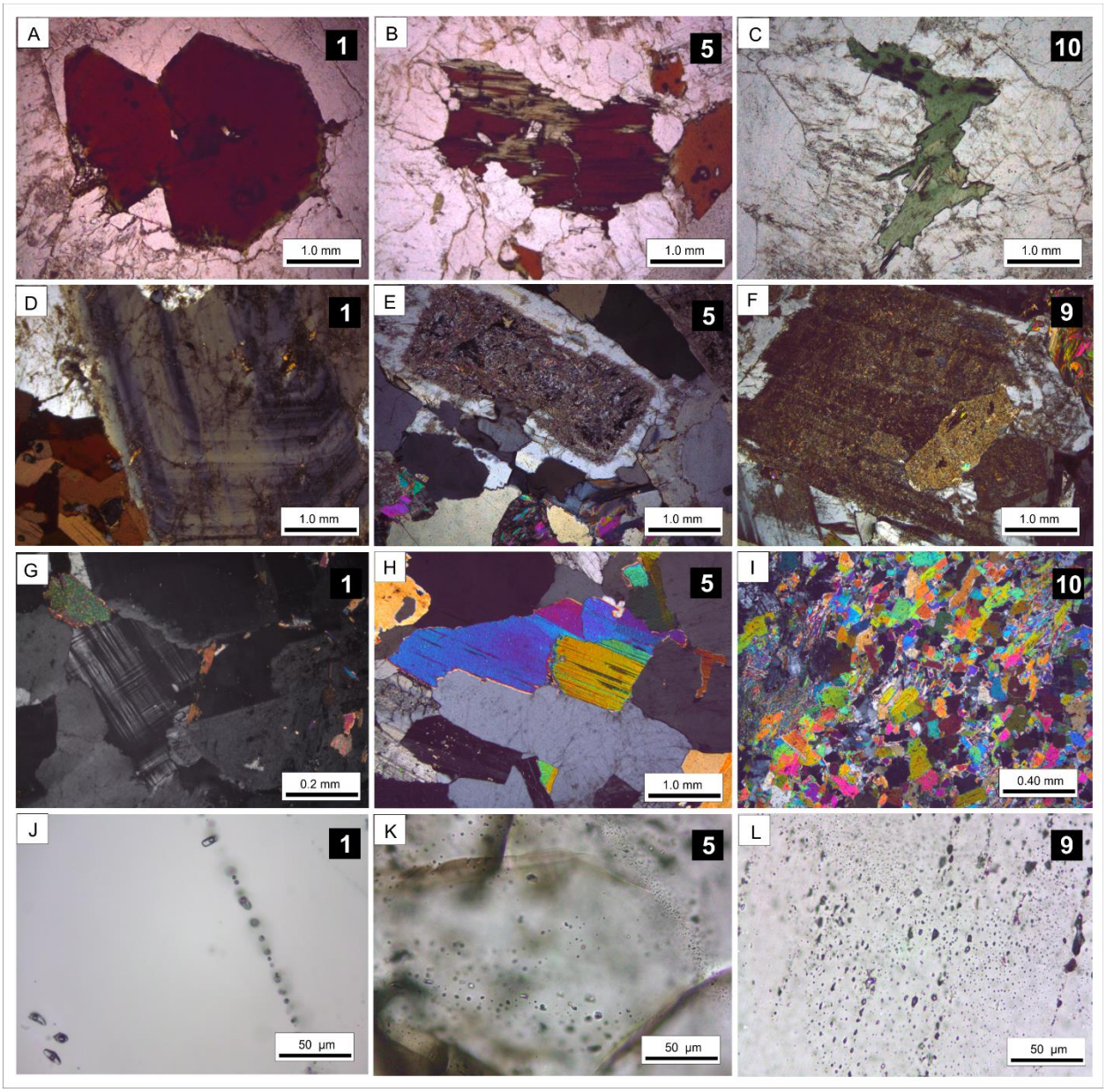

Figure 3.6: Photomicrographs of granitoid samples from the South Mountain Batholith which illustrate the indices used to assess the presence of varying degrees of mineral replacement and hydrothermal textures. The nominal (1 = lowest, 10 = highest) alteration and abundance rankings are shown in top right corner of each plate. (A–C) chloritisation of biotite, (D–F) sericitisation of plagioclase feldspar, (G–I) abundance of muscovite, and (J–L) abundance of quartz–hosted fluid inclusions. These indices were used as proxies for evaluating the relative extent of hydrothermal alteration in samples.

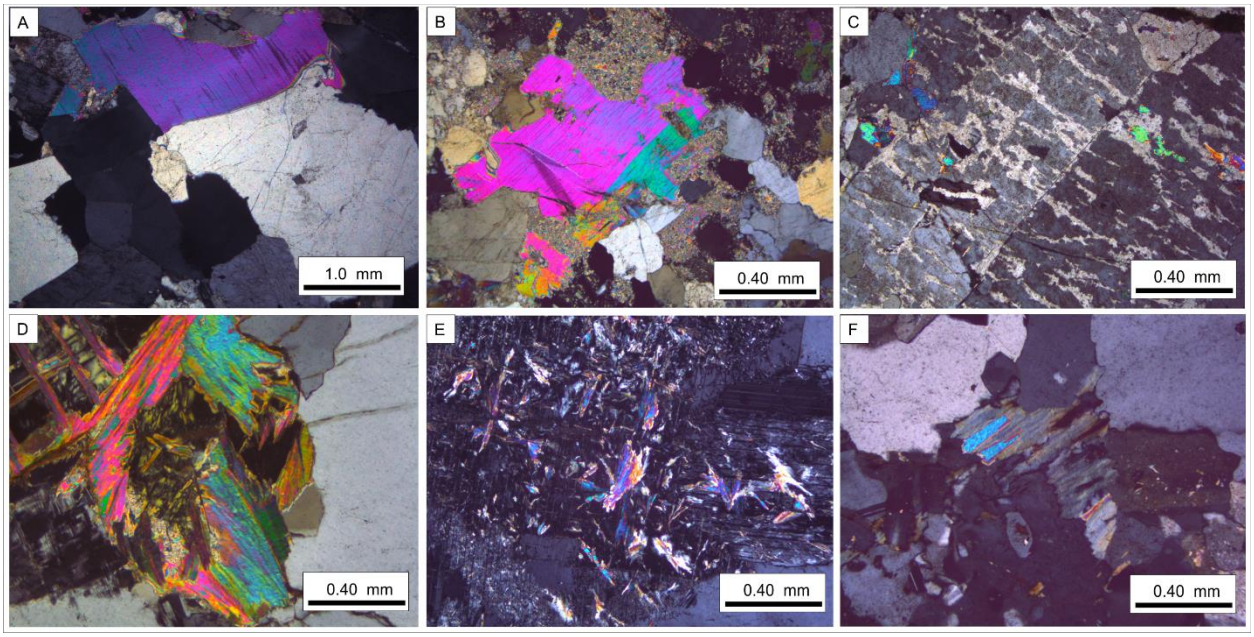

Figure 3.7: Photomicrographs in cross polarized light of granitoid samples from the South Mountain Batholith showing a variety of occurrences and textural relationships of muscovite with other mineral phases. (A) Euhedral coarse–grained muscovite displaying approximately linear grain boundaries. (B) Kinked coarse–grained muscovite similar to previous image. (C) Muscovite replacing small domains in a large perthitic K–feldspar. (D) Muscovite replacement of cordierite (pinitized). (E) Muscovite replacement of plagioclase. (F) Muscovite apparently replacing chlorite.

3.3 Results

We present below the integrated results of using EMA and petrographic assessment of alteration in the SMB in three parts. In the first, the chemical data for >1300 EMA generated from 113 samples, out of 119 and that were prepared from apparently barren granitoid samples are presented (Fig. 3.8). From these EMA variable proportions of least 14 elements were determined via SEM–EDS analysis. The division of mound types are defined by the concentration of major (>10 wt. %) and minor (1 to <10 wt. %) solute elements. To assess regional and host rock variations in evaporate mound chemistry, these results are organized in relation to host–rock grain size, regional location of host rock and host–rock type (summarized in Table 3.2 and Figure 3.9). Secondly, the results of the petrographic study of the 64 granite samples used to assess alteration are presented and integrated with EMA results (summarized in Table 3.3) to investigate possible relationships. Lastly the composition of mounds proximal to known mineralised centres are presented and assessed to see if EMA can provide a vector towards the known mineralization.

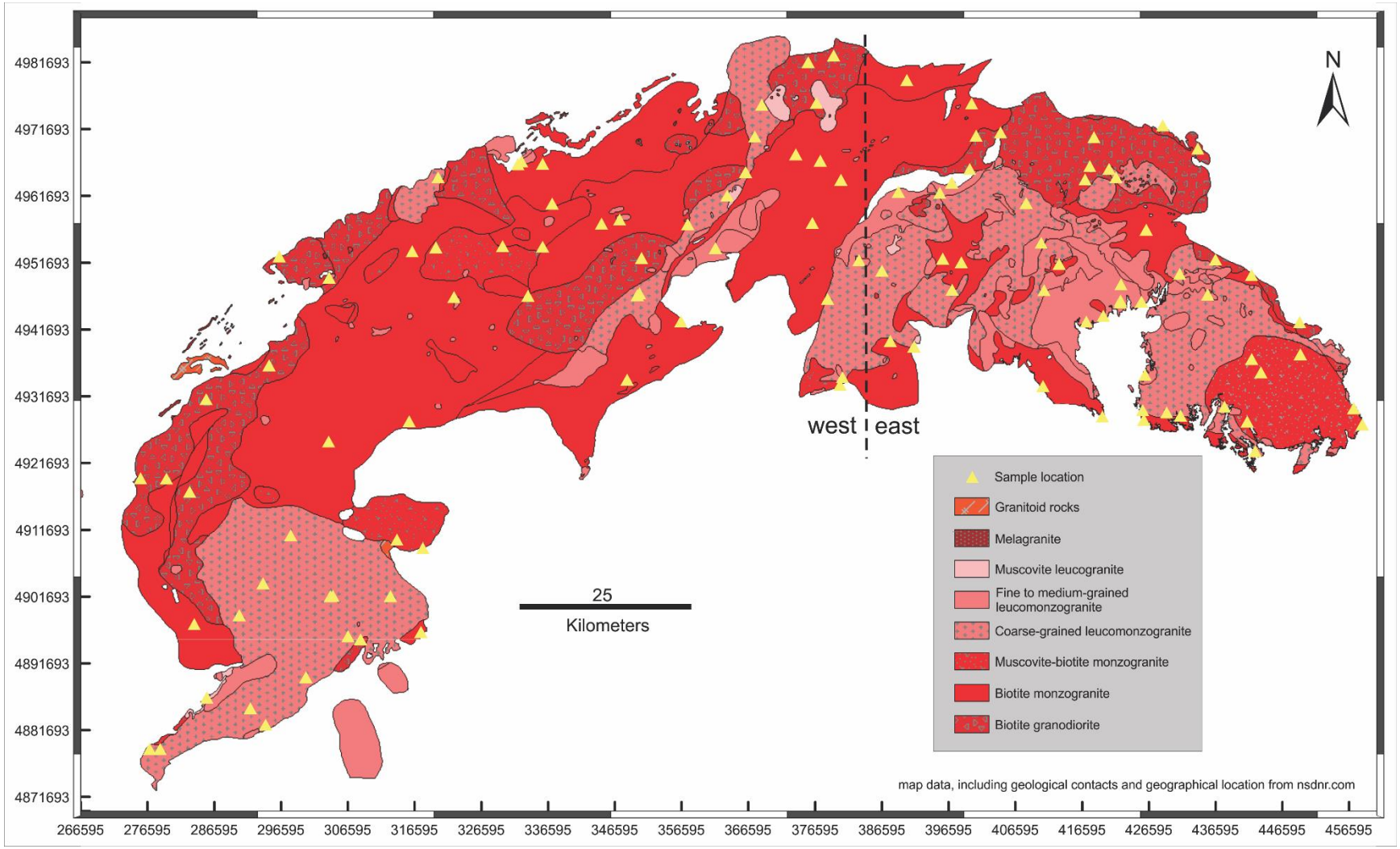
4981693
4971693
4961693
4951693
4941693
4931693
4921693
4911693
4901693
4891693
4881693
4871693
266595
276595
286595
296595
306595
316595
326595
336595
346595
356595
366595
376595
386595
396595
406595
416595
426595
436595
446595
456595
N
west
east
25
Kilometers
Sample location
Granitoid rocks
Melagranite
Muscovite leucogranite
Fine to medium-grained leucomonzogranite
Coarse-grained leucomonzogranite
Muscovite-biotite monzogranite
Biotite monzogranite
Biotite granodiorite
map data, including geological contacts and geographical location from nsdnr.com

Figure 3.8 (previous page): Outline of the South Mountain Batholith with different internal phases showing sample locations of material used in this study. Boundaries of different lithological units are from MacDonald (2001). Note that the west–east divide is arbitrary, but coincides with an NTS map boundary meridian.

TABLE 3.2. TABULATION OF 1370 EVAPORATE MOUNDS INTO CHEMICALLY DISTINCT EVAPORATE MOUND TYPES, ORGANIZED BY REGIONAL LOCATION OF HOST ROCKS

Regional location of host rock	Na-Ca-Cl	Na-K-Cl	Na-Cl	Na-Ca-F-Cl	Na-F-Cl±Ca	Na-Cl±Ca
A03 - A06	108	8	62	8	16	68
A10 - A15	168	39	66	51	27	39
A09 and A16	57	61	57	53	80	72
D05 and D12-D13	53	17	40	76	92	53
Total	386	124	225	188	216	232

TABLE 3.3. DISTRIBUTION OF EVAPORATE MOUND TYPES IN RELATION TO HOST-ROCK GRAIN SIZE, ITS REGIONAL LOCATION AND TO HOST-ROCK TYPE

	Mound total	Na-Ca-Cl	Na-K-Cl	Na-Cl	Na-Ca-F-Cl	Na-F-Cl±Ca	Na-Cl±Ca
		percent of total mounds					
Host-rock grain size							
Coarse	413	33	9	20	11	9	18
Medium	285	35	15	12	9	17	12
Fine	70	33	4	37	4		22
Regional location of host rock							
A03-A06	299	40	3	23	3	6	25
A10-A15	390	43	10	17	13	7	10
A06 and A16	380	15	16	15	14	21	19
D05 and D12 - D13	330	16	5	12	23	28	16
Host-rock type							
sericitised granite	56	75	4	5			16
K-feldspar granite	227	56	12	10	5	7	10
Monzogranite	490	24	10	26	10	14	16
Quartz-pegmatite rocks	85	39	1	46		14	
Mo-pegmatite	214	42	14	22			22
Sn-quartz greisen	19			100			
Greisen	168	13	15	3	54	10	5

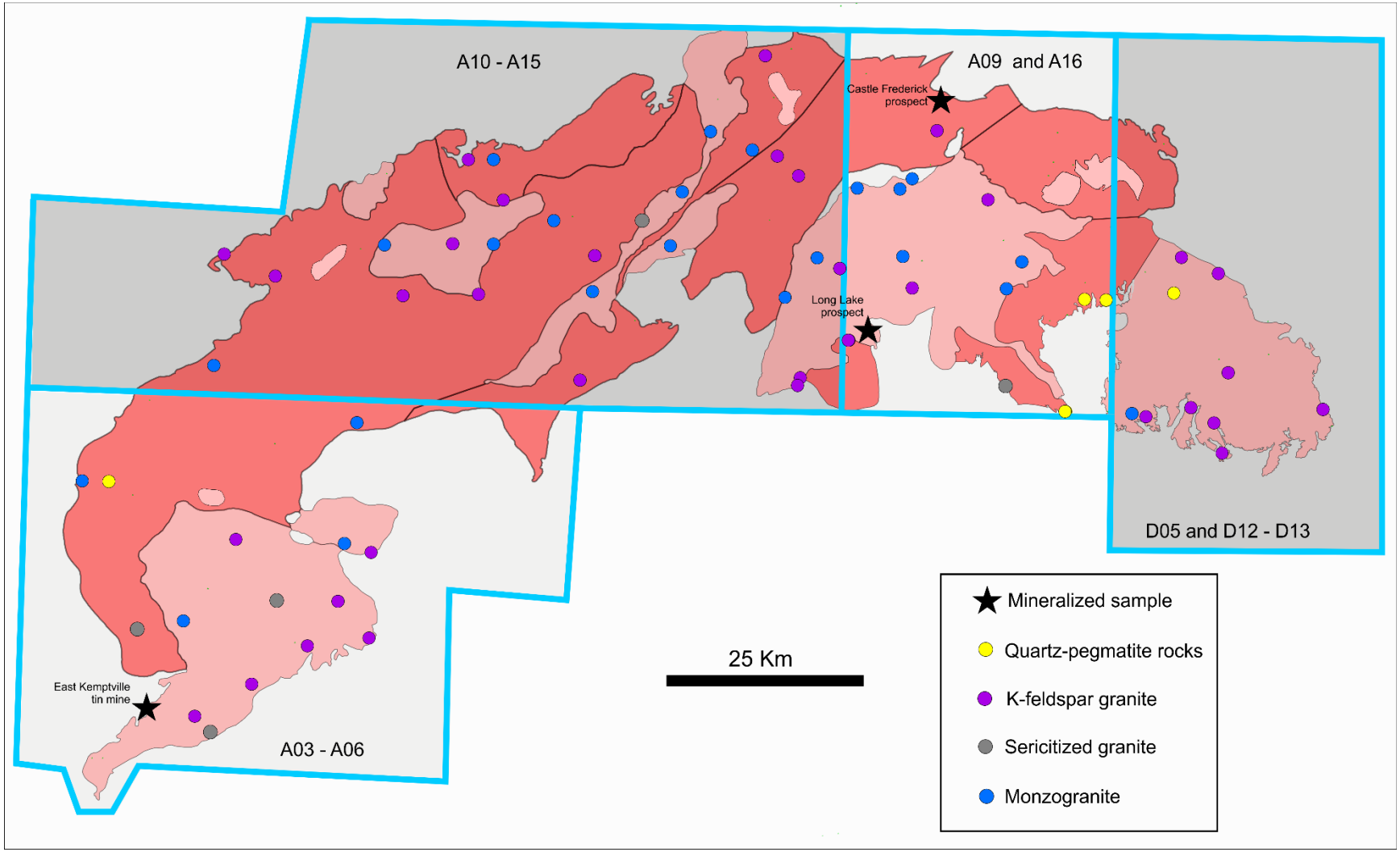

Figure 3.9: Map of the South Mountain Batholith showing sample location by rock type, and boundaries of regional blocks used in this study. Block boundaries are consistent with the NTS series 1: 50 000 map sheet boundaries, but are used in an arbitrary way to organize the EMA data.

3.3.1 Composition of evaporate mounds

All 1317 mounds hosted by apparently barren samples contain Cl^- and Na^+ in major and minor abundance (Fig. 3.10). In addition Ca was detected in approximately 75% of mounds, and in 25%, quantifiable K and F are noted. Importantly, F is always associated with major or minor solute Ca. Concentrations > 10 wt. % Na, K and Ca in the same mound occurs in < 0.01 % of the entire mound population. Sulphur, observed in 115 mounds, and ranges between 0.1 and 11 wt. %, but for 60% (69/115) it is < 3 wt. %. Transition metals observed in 169 mounds range from 0.1 to > 10 wt. %, but the majority (110/170) contained < 3 wt. % for either one or some combination of Mn, Fe, Cu, and/or Zn. Lead concentrations in 22 mounds ranges between 0.5 and 3.3 wt. %.

Commonly, Ca was observed as a major element in mounds that also contained detectable S and/or transition metal elements. Specifically, only 22% (25/115) of mounds that contained detectable S had Ca below detection limits. Of the 222 mounds that had detectable/quantifiable levels of one or more transition metal elements, only 24% had Ca below detection limits. Conversely, all mounds (n = 19) from a Sn–mineralised greisen sample from the East Kemptville tin deposit (*i.e.*, not from an apparently barren location) had Ca below detection limits. Lastly, 68% (142/214) of mounds hosted by a Mo–bearing pegmatite from the Long Lake prospect have detectable calcium.

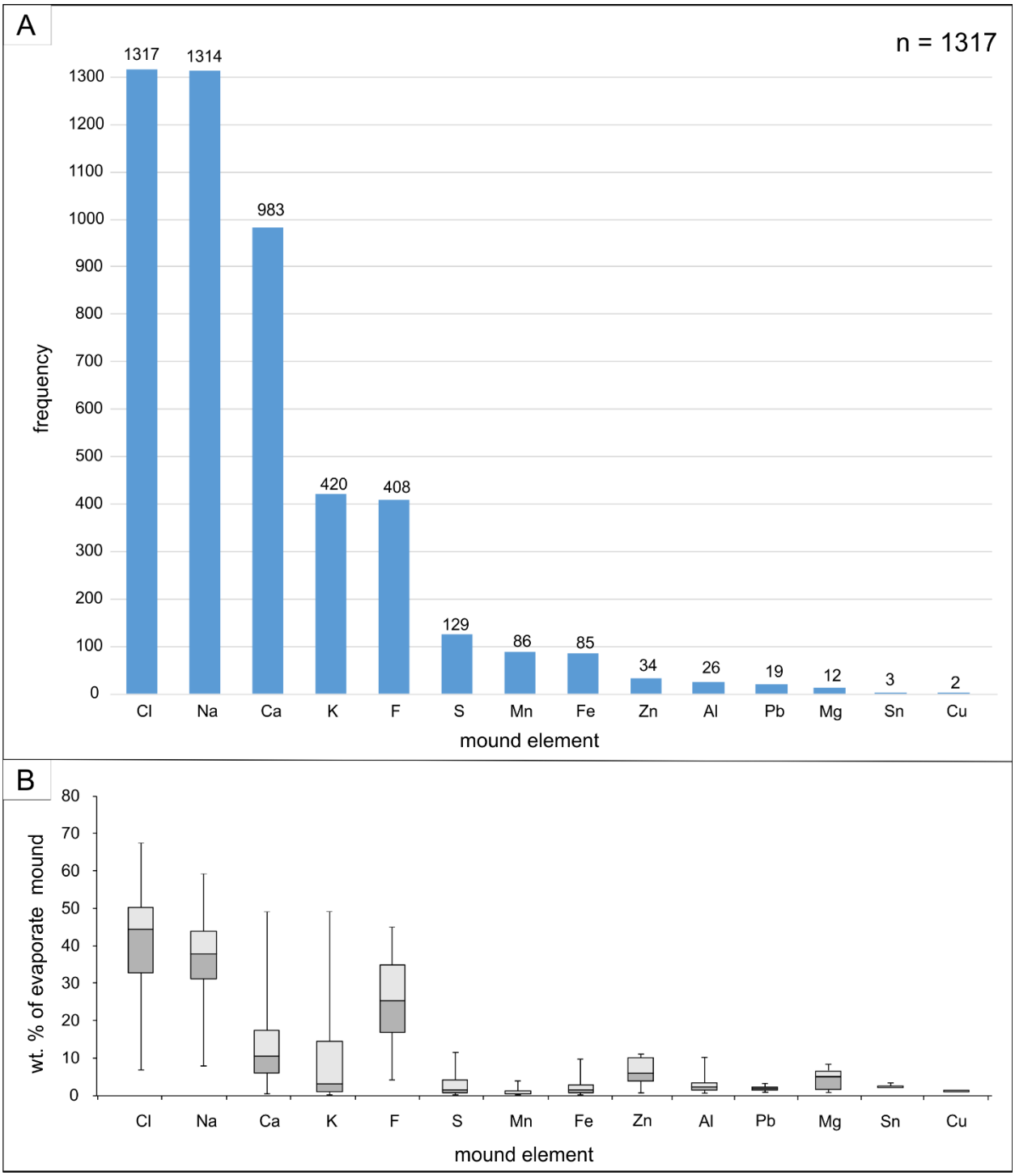
A
n = 1317
frequency
1317
1314
983
420
408
129
86
85
34
26
19
12
3
2
Cl
Na
Ca
K
F
S
Mn
Fe
Zn
Al
Pb
Mg
Sn
Cu
mound element
B
wt. % of evaporate mound
mound element

Figure 3.10 (previous page): Chemical plots illustrating the multi–element diversity of quartz–hosted evaporate mounds analysed in this study. (A) Histogram plot displaying elements detected in mounds in order of decreasing frequency. (B) Box–and–whisker plots summarizing the statistics for single–element concentrations for EMA arranged in order of decreasing frequency.

3.3.2 Types of evaporate mounds

Based on the presence or absence of major solute elements (defined above), we identify six chemically–distinct evaporate mound types (Fig. 3.11). In decreasing order of abundance, mound types include: (1) Na–Ca–Cl, (2) Na–Cl±Ca, (3) Na–Cl (4) Na–F–Cl±Ca, (5) Na–Ca–Cl–F and (6) Na–K–Cl (Table 3–2)

3.3.3 Distribution of select evaporate mound elements

By mapping average mound compositions for select solutes (Ca, K, F, S) across the entire batholith (Fig. 3.12) four general distribution trends emerge: (1) average Ca/Na ratios are higher in samples hosted by Stage 2 plutons than Stage 1 plutons; (2) K–rich mounds are concentrated in samples from Stage 2 plutons; (3) F–rich mounds are more abundant in the eastern half of the batholith; and (4) S–rich mounds are localized near the batholith contact with Meguma metasedimentary host rocks.

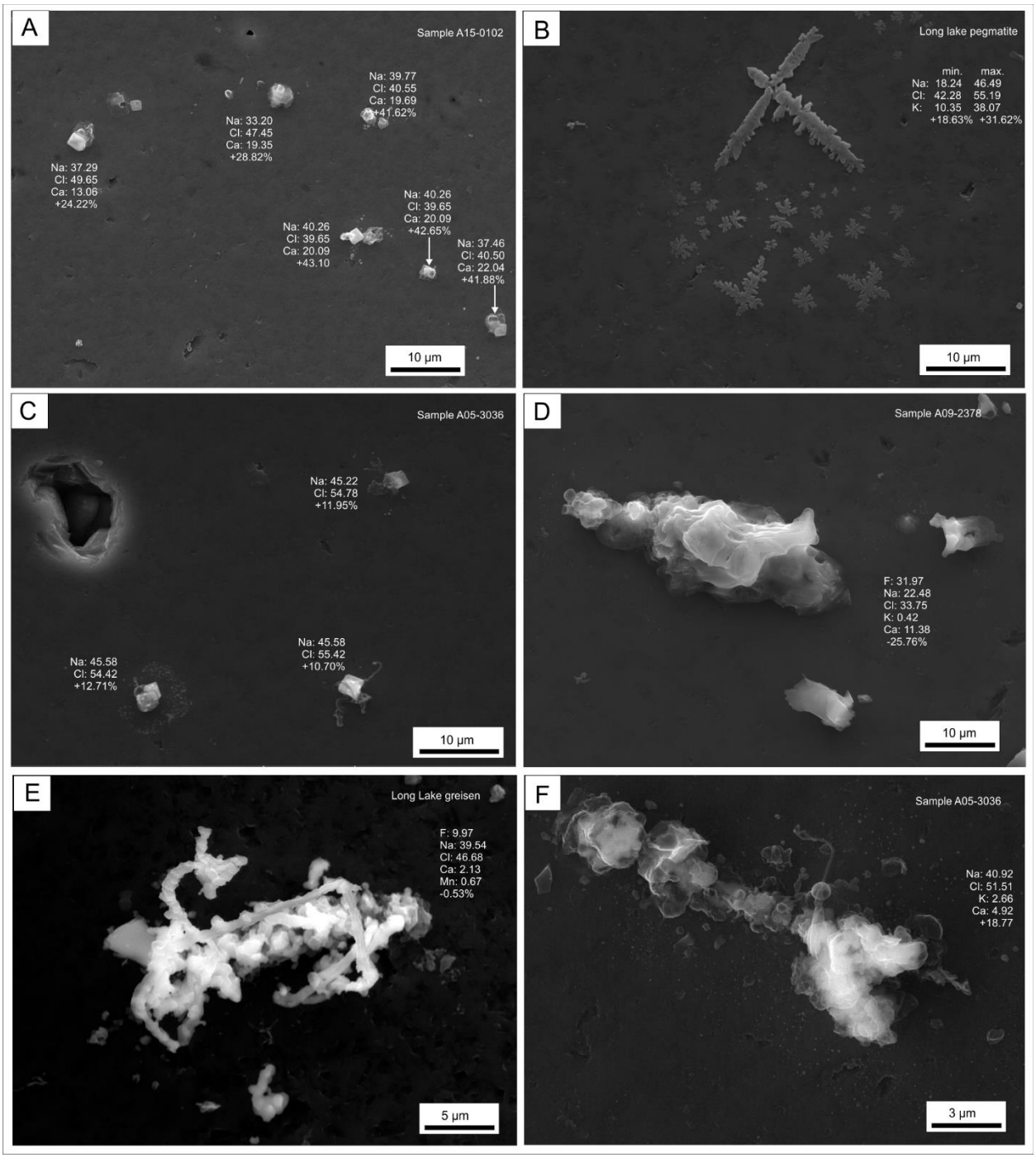

Figure 3.11: SEM–SE images for different evaporate mound types. (A) Sodium–Ca–Cl mounds with roughly uniform element detection as indicated from the mound chemistries shown. (B) Sodium–K–Cl mounds showing a distinctive stellate morphology. (C) Sodium–Cl mounds displaying cubic habit of salt. (D) Sodium–Ca–Cl–F mounds. (E) Sodium–Cl–F mounds with detection of minor Ca. (F) Sodium–Cl mound with minor Ca.

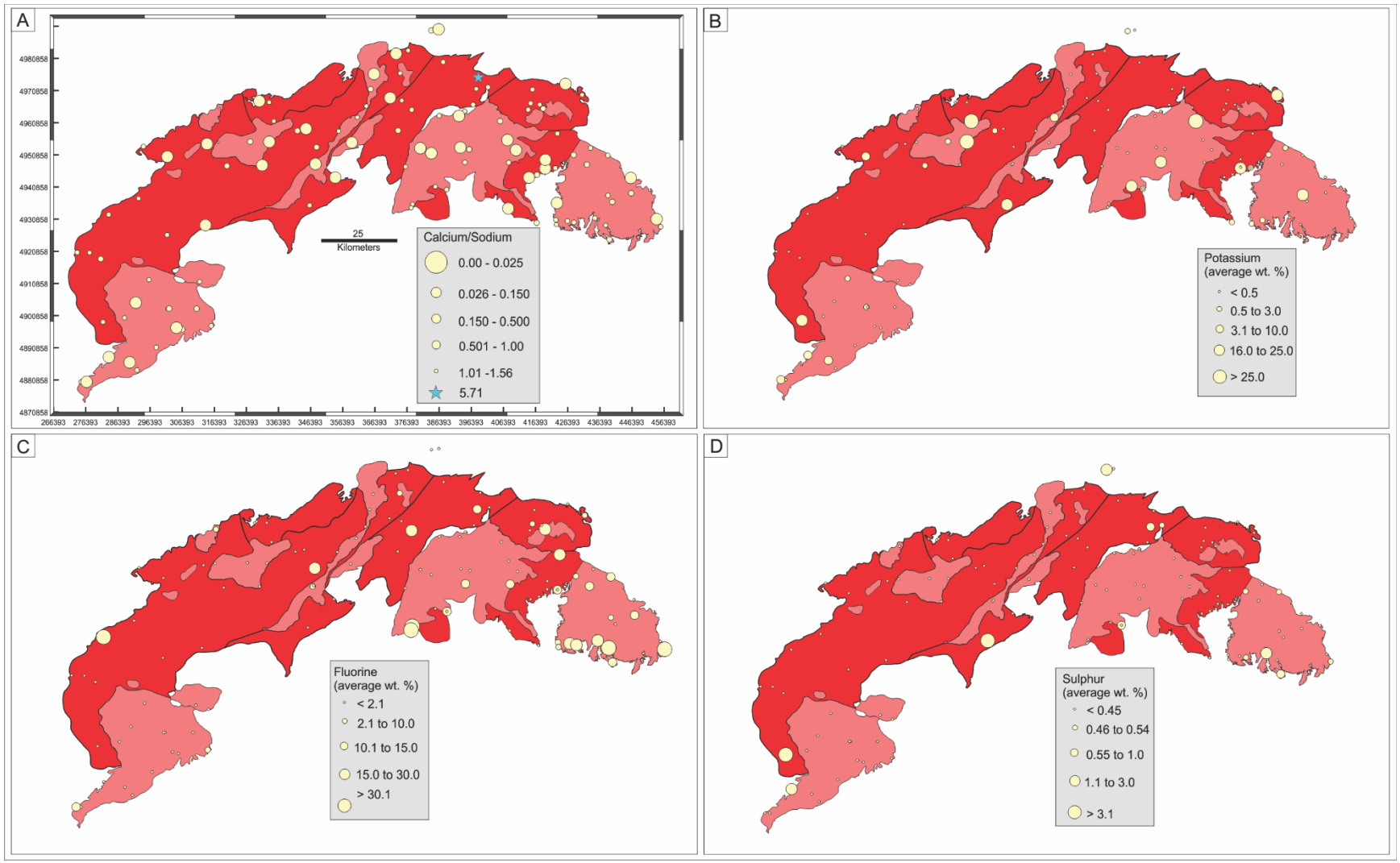
A
4980858
4970858
4960858
4950858
4940858
4930858
4920858
4910858
4900858
4890858
4880858
4870858
266393 276393 286393 296393 306393 316393 326393 336393 346393 356393 366393 376393 386393 396393 406393 416393 426393 436393 446393 456393
25
Kilometers
Calcium/Sodium
0.00 - 0.025
0.026 - 0.150
0.150 - 0.500
0.501 - 1.00
1.01 -1.56
5.71
B
Potassium
(average wt. %)
< 0.5
0.5 to 3.0
3.1 to 10.0
16.0 to 25.0
> 25.0
C
Fluorine
(average wt. %)
< 2.1
2.1 to 10.0
10.1 to 15.0
15.0 to 30.0
> 30.1
D
Sulphur
(average wt. %)
< 0.45
0.46 to 0.54
0.55 to 1.0
1.1 to 3.0
> 3.1

Figure 3.12 (previous page): Proportional symbol maps displaying batholith–wide distribution of select elements and elemental ratios from EMA of samples, Including: (A) Ca/Na, (B) K, (C) F, and (D) S. See text for identification of broad spatial variations.

3.3.4 Fluid types

Six types of evaporate mounds (Section 3.2.2.) represent six types of hydrothermal fluids. These include, in order of decreasing abundance: (1) a Na–Ca–Cl fluid, represented by evaporate mounds with average Ca/(Ca+ Na) = 0.37, ±0.12, 1σ; (2) a Na–Cl±Ca fluid, represented by mounds with average Ca/(Ca+Na) = 0.12, ±0.05, 1σ; (3) a NaCl fluid, represented by mounds with average (Ca+K)/(Ca+K+Na) = 0.01 ±0.03, 1σ; (4) a Na–F–Cl±Ca fluid, represented by mounds with average (Ca/(Ca+Na) = 0.14 ±0.05, 1σ, and average (F/(F+Cl) = 0.47, ±0.18, 1σ; (5) a Na–Ca–Cl–F fluid, represented by mounds with average (Ca/(Ca+Na) = 0.37 ±0.12, 1σ, and average (F/F+Cl) = 0.58, ±0.20, 1σ; and (6) a Na–K–Cl fluid, represented by mounds average K/(K + Na) = 0.45, ±0.20, 1σ. Potassium occurs as a minor solute in all fluids in which it is not a major solute species, and Ca as minor solute occurs in Na–K–Cl fluids. Sulphur occurs as a minor solute in all fluid types, and is most commonly detected in Na–K–Cl fluids. The batholith wide occurrence of these fluids is consistent with results from local–scale EMA research in the Halifax and New Ross plutons (Kontak *et al.* 2002, Carruzzo *et al.* 2000).

The widespread occurrence of F is unique to this study as it was only locally reported before in a F–rich mineralised muscovite greisen setting in the Halifax pluton at Sandwich Point (Fig. 3.3; Kontak & Kyser 2011). Although an unambiguous F–fluid type cannot be resolved by the composition of evaporate mounds, that K is below detection limits in F–bearing mounds suggests decoupling of K and F. Fluorine–bearing mounds occur as two compositionally distinct types: (1) Calcium–F–enriched mounds compose a minimum of 10 wt. % each of Ca and F and (2) Fluorine–bearing mounds that compose detectable F and < 10 wt. % Ca.

Chlorine deficiency in the fluid is indicated by a positive charge imbalance in the EDS mound analysis. Elevated positive–charge imbalances are proportional to the ionic potential of the

dominant cation in the fluid. An average charge imbalance of +19.4 in Na–rich mounds is relatively low compared average deficiencies in Na–K–Cl (+25.8) and Ca–enriched (+35.1) mounds. Charge imbalances associated with mounds with detectable F (n = 322) range from –29.1 to +25.1.

3.3.5 Relationship between mound composition and host–rock grain size

The composition of evaporate mounds is independent of host–rock grain size (Fig. 3.13), which can be considered as a proxy for at least some aspects of magmatic evolution (*e.g.*, duration of crystallization). This result is expected because the chemical nature of fluids are preserved as secondary inclusions and thus temporally isolated from the crystallization of primary minerals that make up the SMB. However, mound generation does appear to be influenced by grain size. Fine–grained samples host relatively fewer mounds compared to medium– and coarse–grained samples. On average, coarse–grained samples host 14 mounds/sample, medium–coarse–grained samples host 12 mounds/sample, and fine–grained samples host 7 mounds/sample. Relatively poor mound generation may reflect the greater resistance of small inclusions to thermal decrepitation (Bodnar *et al.* 1989) and relatively small fluid inclusions are noted to be more abundant in the fine–grained samples. This observation emphasises the need to integrate petrographic observations in this type of work, as emphasized by Tweedale *et al.* (in prep, 2019)

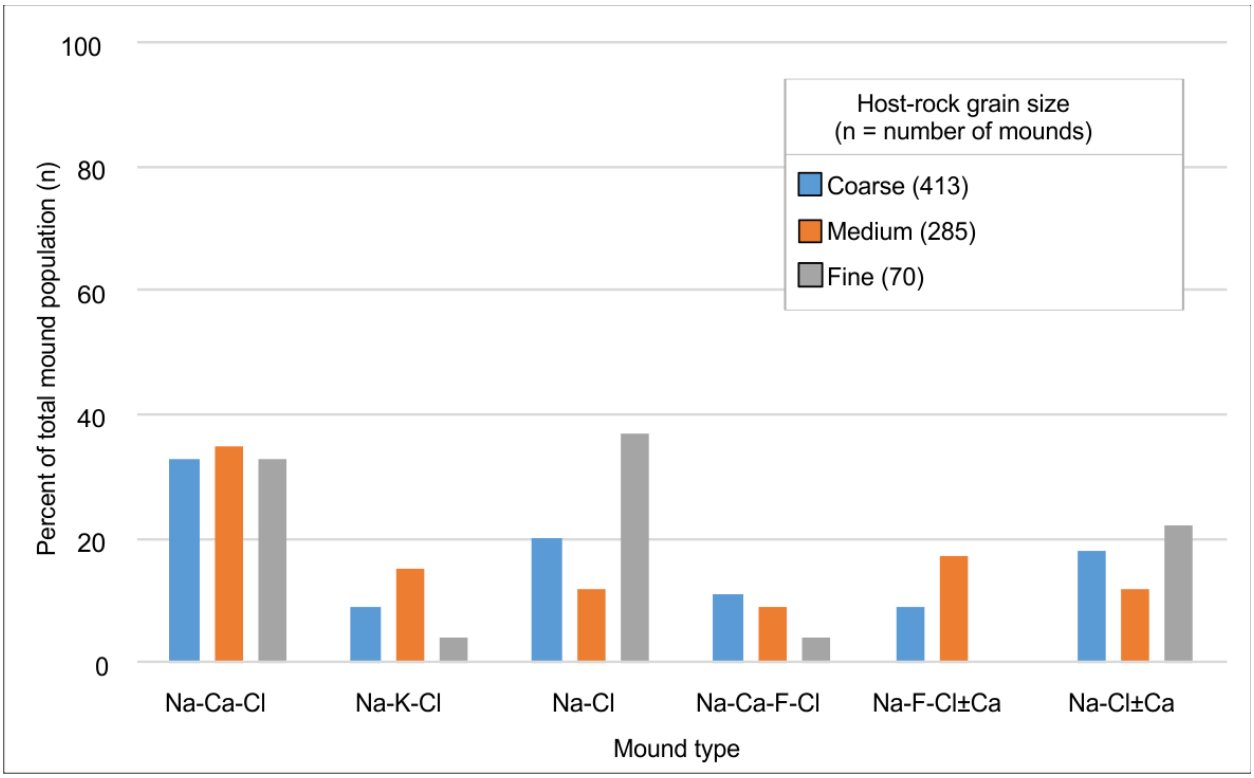

Figure 3.13: Binary plots displaying the relative proportion of evaporate mound types based on subdivision into the type of host rock: coarse–grained (> 0.5 cm), medium–grained (0.1 – 0.5 cm) and fine–grained (<0.1 cm) granites. Note the absence of Na–F–Cl±Ca mounds in the fine–grained granites.

3.3.6 Regional and pluton–scale differences in mound composition

Three trends are discernable at the batholith scale: (1) Ca concentrations > 10 wt. % occurred in 40% of mounds hosted by samples from the western part of the SMB versus and15% of samples from its eastern part; (2) K concentrations > 10 wt. % occurred more frequently in mounds hosted by samples from the Salmontail Lake and New Ross plutons (i.e., NTS regions A09 and A16 in Figure 3.9) than any other part of the batholith; (3) quantifiable F occurred more frequently in mounds from the eastern half of the SMB; and (4) mounds with relatively high S concentrations occur most frequently in samples that are in close proximity to the SMB contact with the Meguma metasedimentary rocks which are known to locally be S rich (White 2010).

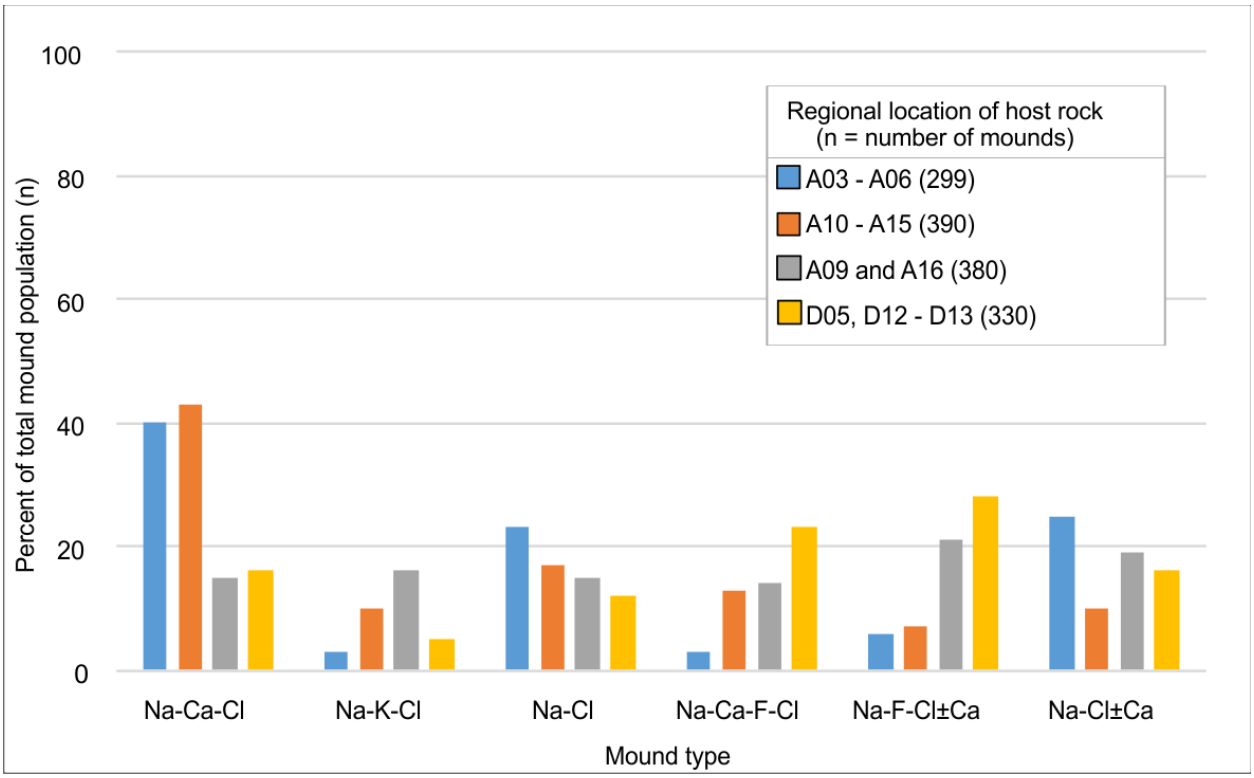

Figure 3.14: Binary plots displaying the relative proportion of evaporate mound types subdivided by their spatial organization into regional blocks. Regional block boundaries are shown in Figure 3.9.

3.3.7 Relationship between mound types and rock types

The six evaporate mound types occur in monzogranites, but Na–Ca–Cl and Na–Cl types are dominant. All six mound types also occur in K–feldspar granite, and the Na–Ca–Cl type is dominant. Sericitised granites host dominantly Na–Ca–Cl mounds, and F was never detected. Sodium–K–Cl mounds are subordinate in each of the above rock types. Sodium–Cl mounds are the dominant type hosted by late–stage quartz–rich rocks. The dominant occurrence of Na–Ca–Cl mounds in sericitised granites, and of NaCl mounds in late quartz rocks (Section 3.2.1.2) are the only obvious relationships (Fig 3.15A).

3.3.8 Relationship between mound types and mineralised host rocks

The dominant type of evaporate mounds hosted by mineralised samples is unique for each sample (Fig. 15B) and the studied samples are discussed separately below.

For the cassiterite bearing greisen sample from East Kemptville, Ca was below the detection limit (i.e., 0.1 wt. %) in all the analyzed mounds (n = 19). Compositional features apparently unique to these mounds include: (1) concentration of K and Mn in all 19 mounds, (2) minor solute detection of Fe in 15 of the mounds, and (3) detection of S (2 – 13 wt. %) in all mounds.

Evaporate mound types hosted by two samples from the Long Lake prospect, a molybdenite–rich pegmatite and a greisen, host compositionally distinct fluid types. Listed in order of decreasing abundance, mound types hosted by the molybdenite–rich pegmatite include Na–Ca–Cl (41%), Na–Cl±Ca (25%), Na–Cl (22%), and Na–K–Cl (12%). Quantifiable F occurs in only one of the 213 mounds analyzed and is therefore an exception for the SMB samples in regards to F (see above). All six mound types defined in this study occur in the greisen sample, a second

example of an intrusion–related mineralised system. The Na–Ca–F–Cl mound type were dominant, accounting for 55% of 163 analyzed mounds. Sodium chloride mounds were the least abundant, accounting for 4% of the total mound analyzed.

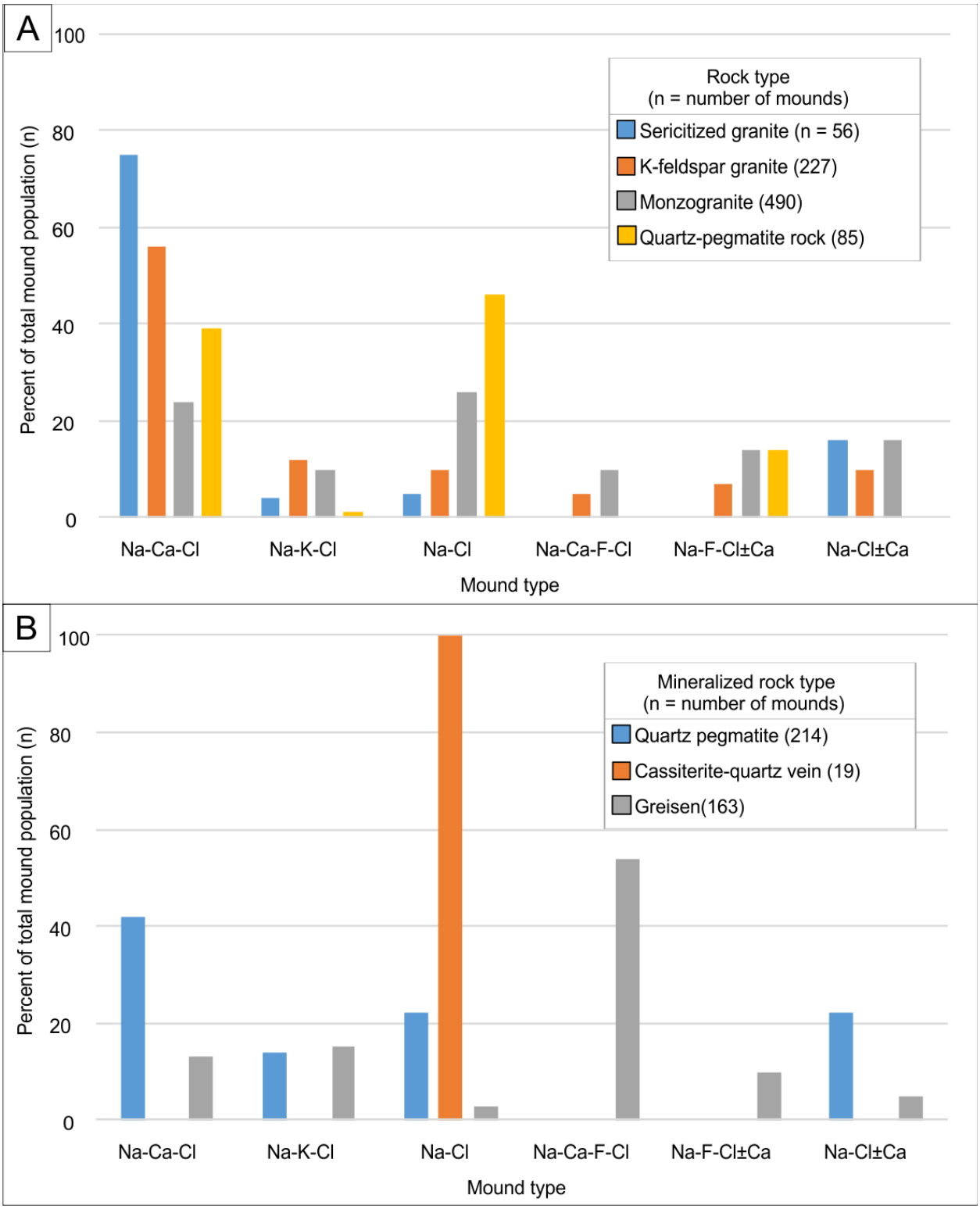

Figure 3.15: Binary plots displaying the relative proportion of evaporate mound types subdivided by type of barren host rock (A) and nature of mineralised rock (B).

3.3.9 Integration of fluid:rock interaction with EMA

The degree and extent of chloritisation of biotite, sericitisation of feldspars, development of muscovite and abundance of secondary fluid inclusions in magmatic quartz in 67 samples were indexed quantitatively as low–, moderate– or high in scoring. The indexed values for 41 of the 67 samples are not considered for further analysis due to either extreme texturally variability at the scale of observation, or due to insufficient EMA data. Only samples with both (1) a high score for one or more of the alteration indices and (2) a minimum of 8 observed mounds were examined for a potential relationship between primary mineral alteration and fluid inclusion chemistry. Evaporate mound chemistry for two samples that displayed the highest composite alteration ranking were also assessed.

Tabulation and graphical display of the integrated alteration and fluid chemistry data for the 26 samples that meet this criteria does not show any relationships between locally preserved fluid chemistry and mineral alteration (Fig. 3.17). The exception is a relationship between K abundance and the muscovite modal abundance in the host rocks may be inferred (Fig. 3.18). Possible explanations for these observations are discussed in a later section.

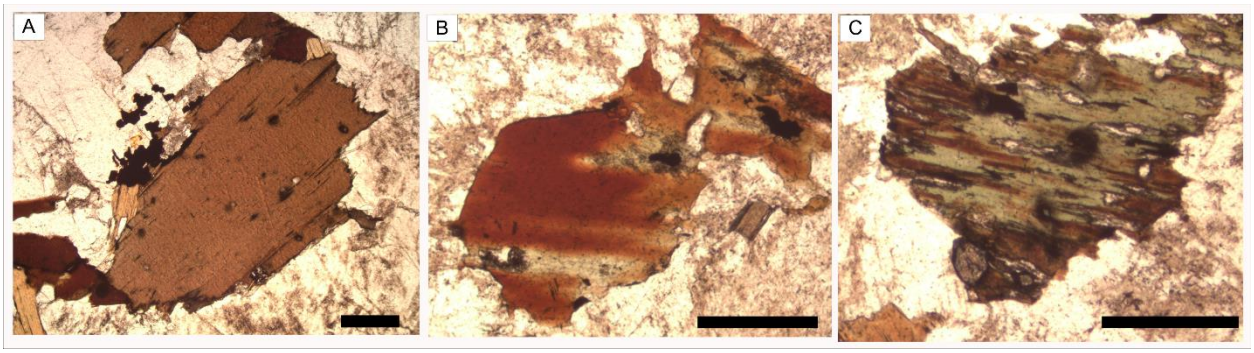

Figure 3.16: Photomicrographs in plane–polarized light of partially chloritized biotite grains in Sample 5280; scale bar = 0.4 mm. Note the extent of chloritisation of biotite varies from grain to grain. (A) Unaltered biotite grain. (B) Moderate alteration of biotite with 15–20% replacement by chlorite. (C) Pseudomorphic replacement (>60% replaced) of primary biotite by chlorite.

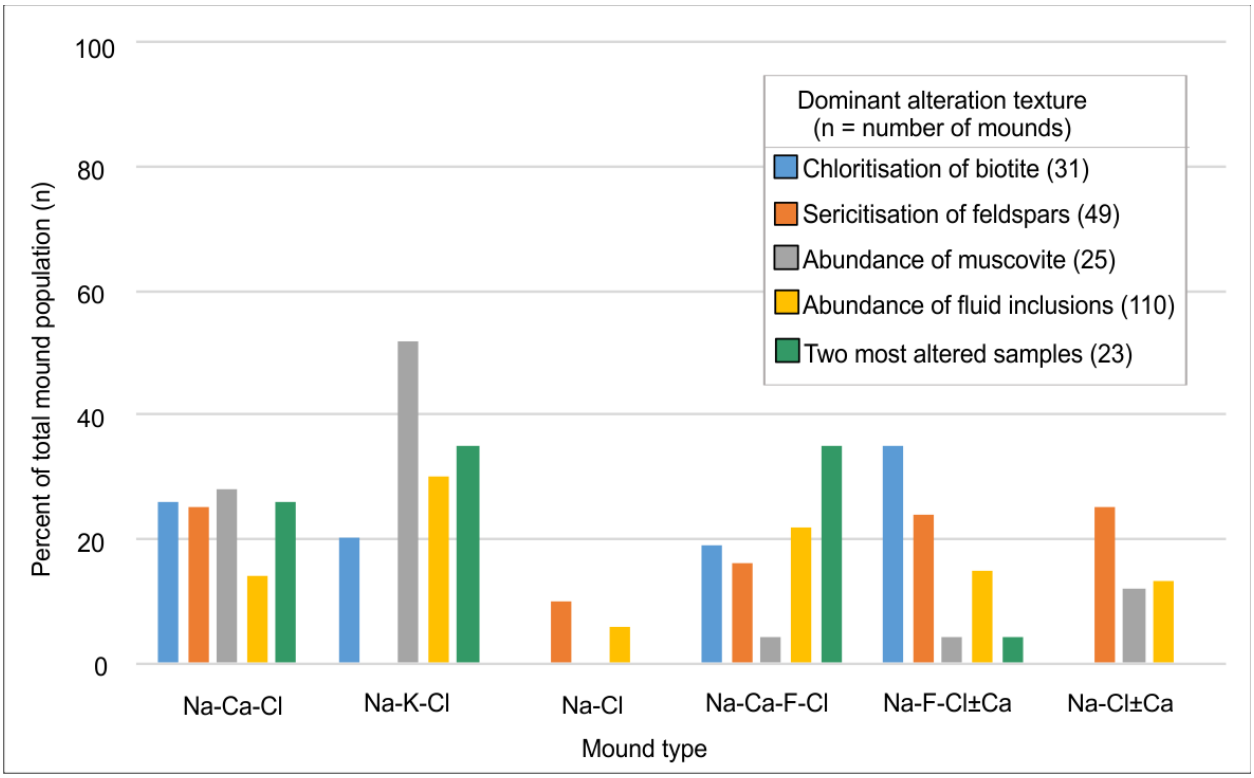

Figure 3.17: Binary plots of evaporate mound types subdivided based on the nature of the altered host rock and also abundance of fluid inclusions. A composite alteration index is the average sum of the four proxies shown here.

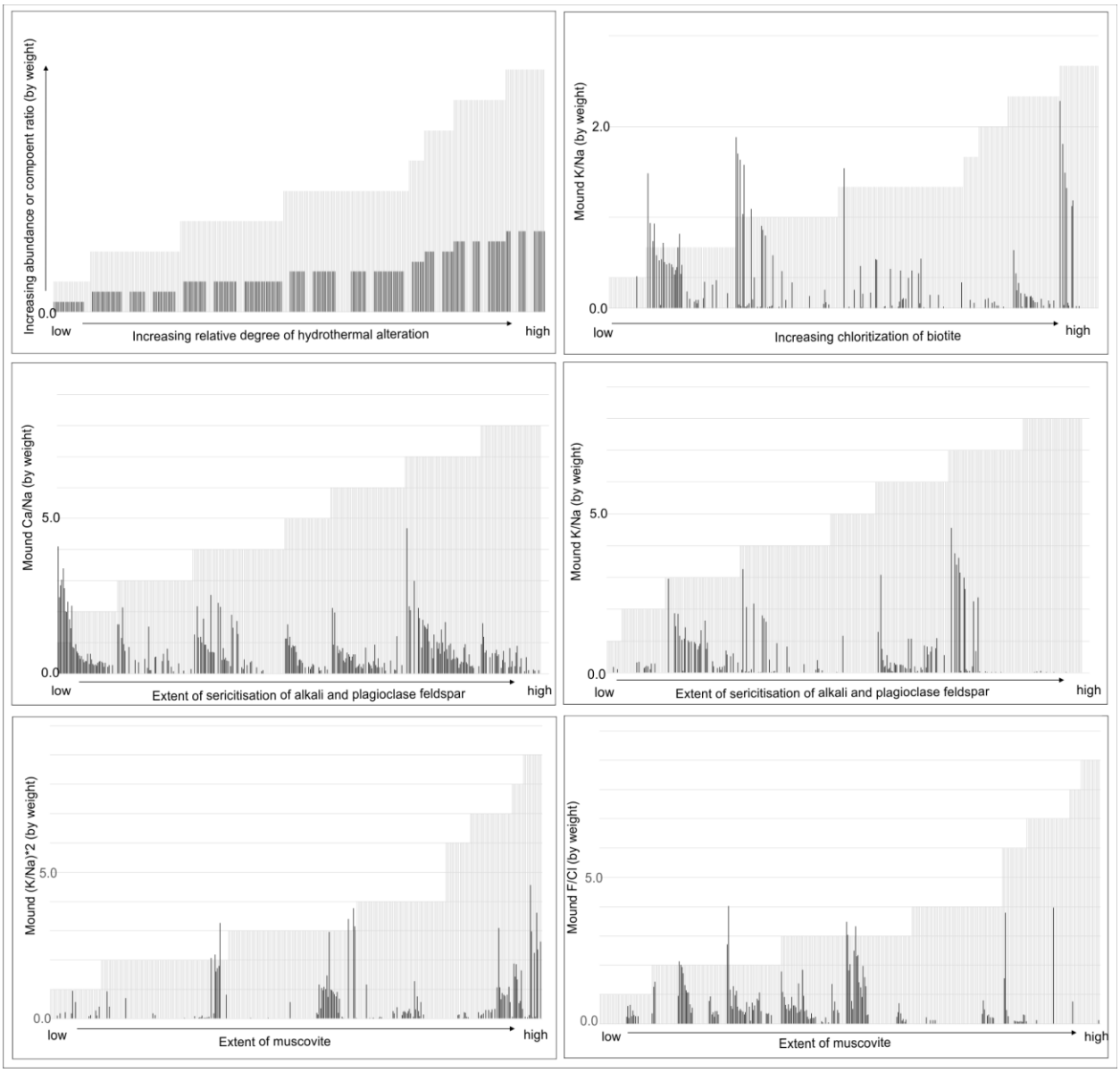

Figure 3.18: Composite binary plots of select mound–element ratios and extent of different mineral alteration types. In all plots, X–axis samples are ordered in increasing degree of alteration, such that least altered samples appear on the left, and Y–axis ratios for select mound–element ratios do not have units. (A) An idealized situation displaying perfect relationship between increasing mound–element ratios and extent of hydrothermal alteration texture, mineral abundance or fluid inclusion abundance. (B) Extent of chloritisation of biotite versus K/Na. (C) Extent of sericitisation of alkali and plagioclase feldspars versus Ca/Na. (D) Extent of sericitisation of alkali and plagioclase feldspars versus K/Na. (E) Extent of muscovite versus (K/Na)*2. (F) Extent of muscovite versus (F/Cl).

3.3.10 Spatial variation peripheral to mineralised centres

In this section the results of two contrasting types and styles of mineralization in the SMB are presented, one is a greisen–hosted Sn–Cu–Zn–Ag deposit setting whereas the other is a massive sulphide vein. These settings were selected to see if there was a detectable change in the chemistry of the EMA proximal the mineralised settings and if so what elements would be relatively enriched.

3.3.10.1 East Kemptville deposit

The setting of this deposit is well described elsewhere (*e.g.*, Halter *et al.* 1996), but essentially it consists of zoned quartz–topaz greisens cored by cassiterite which cut an evolved leucogranite that is part of the zoned Davis Lake Pluton (Dostal *et al.* 2004, Dostal & Chatterjee 2000, Dostal & Chatterjee 1995). For this study therefore, 15 samples distributed in the Davis Lake Pluton and located up to 35 km from the East Kemptville (EK) tin deposit were assessed to determine if there is a systematic spatial variation in the chemistry of the EMA relative to the mineralised centre of an intrusion–related deposit (Fig. 3.19). The results of the EMA are summarized in Figures 3.19, 3.20 & 3.21.

In general the ternary and binary plots of the EMA for the dominant solute components of the mounds (Na–Ca–K) show that away from the mineralised centre there is a dominance of Na–Ca whereas proximal to and within the deposit area there is a switch to a Na–K chemistry. We also note that for the greisen sample in the deposit the EMA include enrichment in S, K, Mn, and Fe (Fig. 3.20), which was also noted the earlier work of Kontak (2004) and more recently by Bickerton *et al.* (2016). As for the 226 mounds hosted by the 14 peripheral samples, S was detected in 12 and mounds from 4 samples, 6 of these in sample A04–8006 (#6 in Fig.3.19) which is noted to show a switch from a Na–Ca to a Na–K mound chemistry. Importantly there is no systematic

spatial enrichment of the mounds in S, Mn or Fe, although we note a more consistent presence of Fe in mounds towards the deposit area (Fig. 3.21).

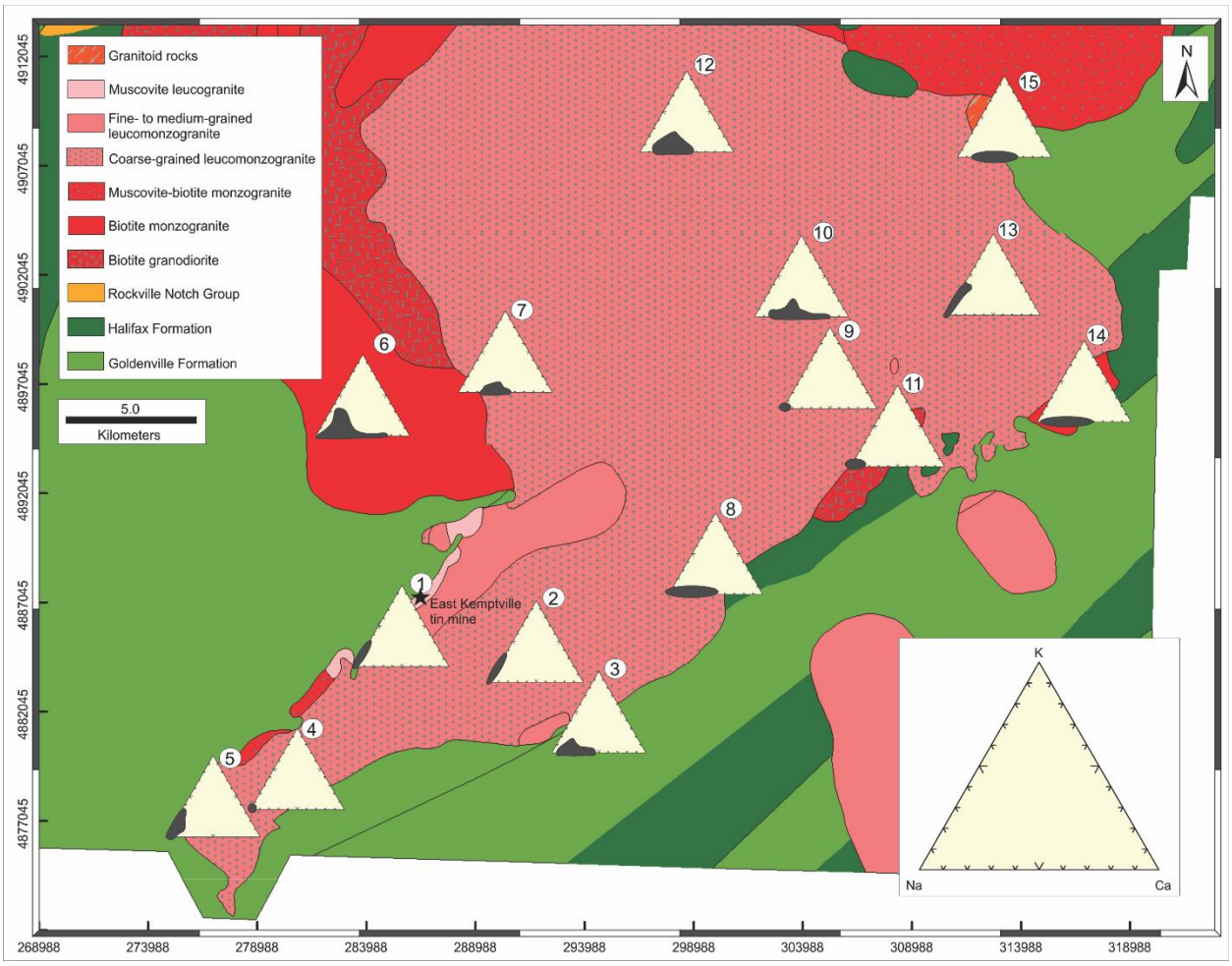

Figure 3.19: Geological map of the Davis Lake pluton (after MacDonald 2001) showing locations of samples used for EMA in regards to the East Kemptville Sn–Zn–Cu–Ag deposit. The inserted Na–K–Ca ternary diagrams (in wt. %) show the compositional range of evaporate mounds in each sample.

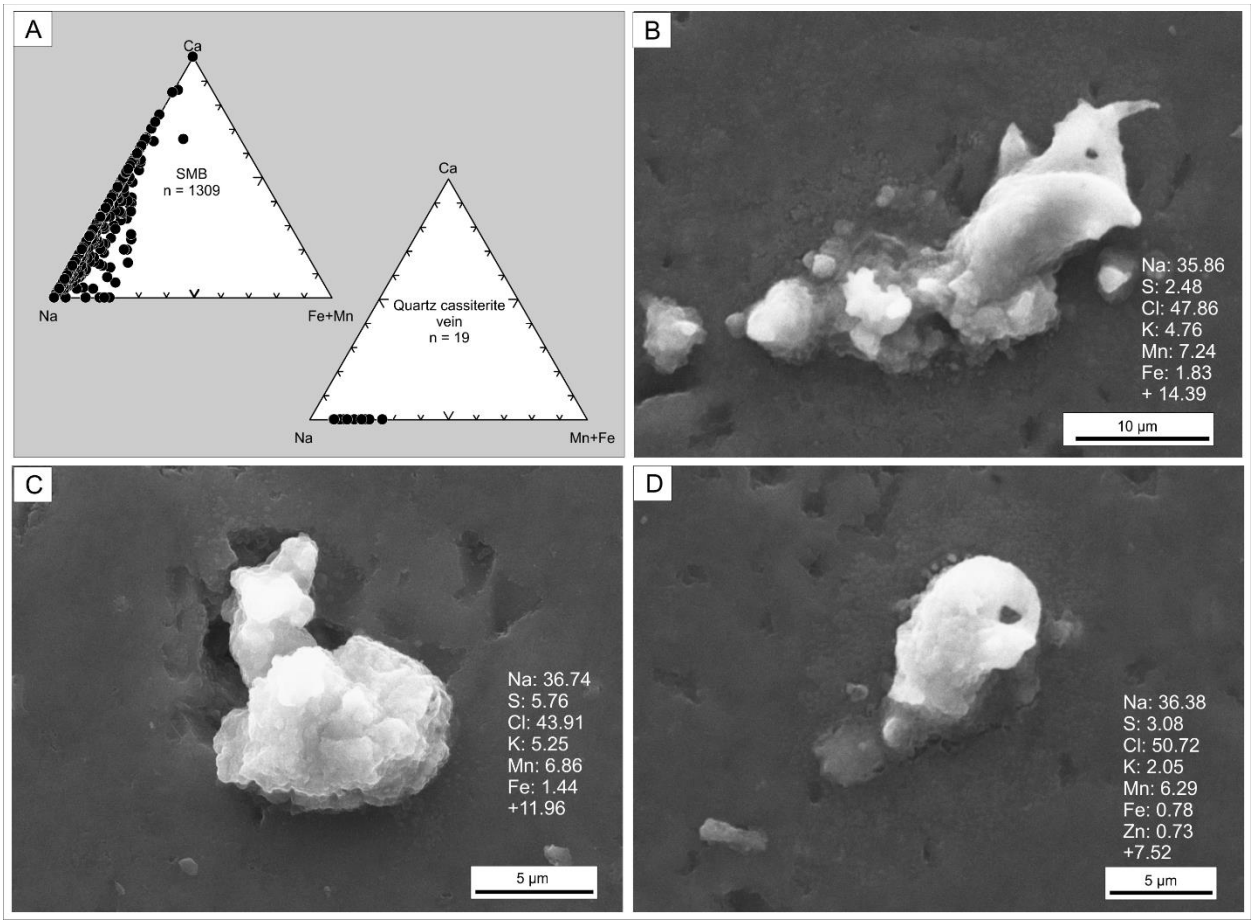

Figure 3.20: Ternary plot (in wt. %) for select solutes and SEM–SE images of evaporate mounds hosted by a cassiterite quartz sample from the East Kemptville deposit.(A) Sodium–Ca–(Fe+Mn) ternary plot for EMA from the South Mountain Batholith (red) and the mineralised quartz sample (blue). (B–D) SEM–SE images of evaporate mounds with compositional data (wt. %) and charge balance (+/- %) superimposed.

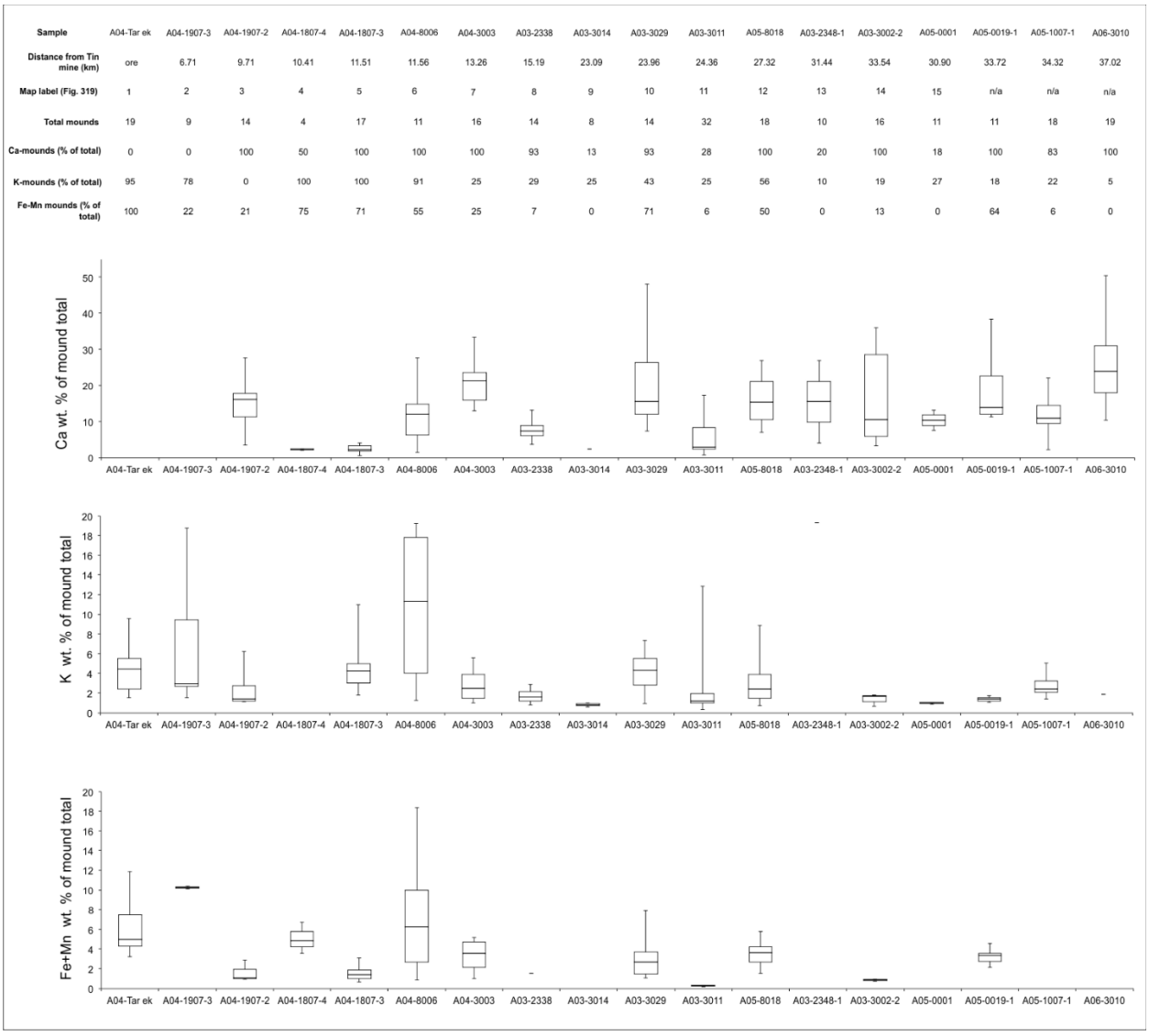

Sample	A04-Tar ek	A04-1907-3	A04-1907-2	A04-1807-4	A04-1807-3	A04-8006	A04-3003	A03-2338	A03-3014	A03-3029	A03-3011	A05-8018	A03-2348-1	A03-3002-2	A05-0001	A05-0019-1	A05-1007-1	A06-3010
Distance from Tin mine (km)	ore	6.71	9.71	10.41	11.51	11.56	13.26	15.19	23.09	23.96	24.36	27.32	31.44	33.54	30.90	33.72	34.32	37.02
Map label (Fig. 319)	1	2	3	4	5	6	7	8	9	10	11	12	13	14	15	n/a	n/a	n/a
Total mounds	19	9	14	4	17	11	16	14	8	14	32	18	10	16	11	11	18	19
Ca-mounds (% of total)	0	0	100	50	100	100	100	93	13	93	28	100	20	100	18	100	83	100
K-mounds (% of total)	95	78	0	100	100	91	25	29	25	43	25	56	10	19	27	18	22	5
Fe-Mn mounds (% of total)	100	22	21	75	71	55	25	7	0	71	6	50	0	13	0	64	6	0

Figure 3.21: Tabulated data and box–and–whisker plots for EMA for samples from the Davis Lake pluton shown in Figure 3.19. The samples are arranged in increasing distance (left to right) from and the East Kemptville Sn–Zn–Cu–Ag deposit.

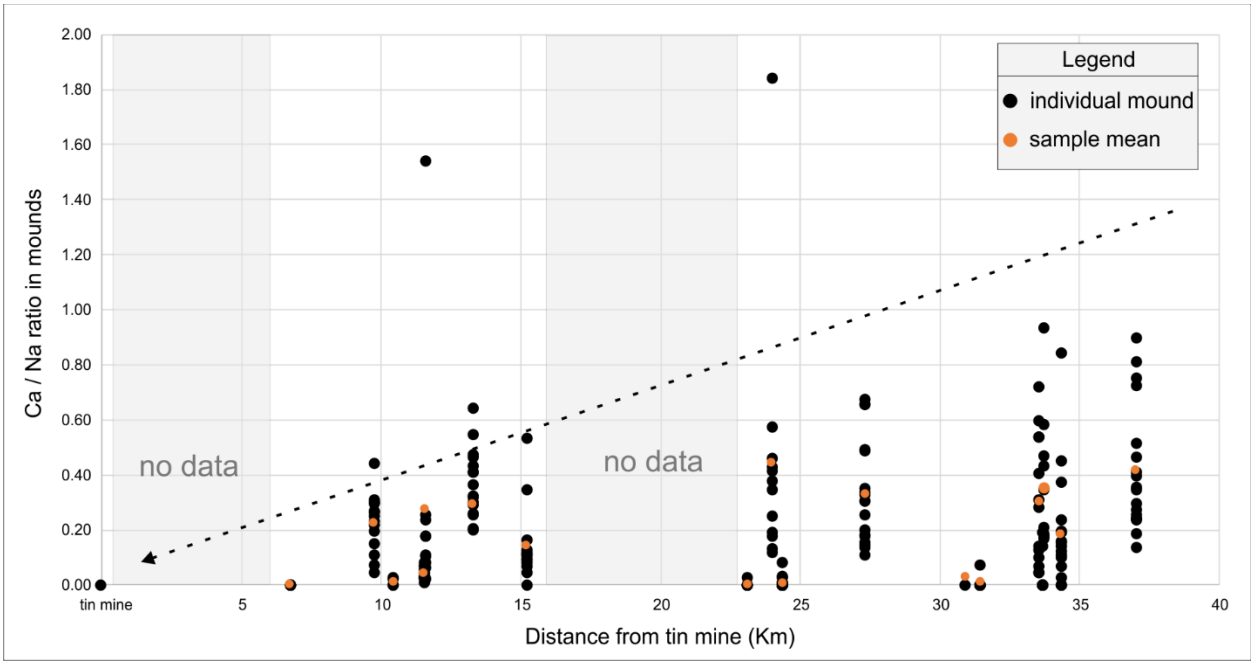

Figure 3.22: Binary plot of Ca/Na ratios for EMA of samples from the Davis Lake pluton (see Fig. 3.19) versus distance from the East Kemptville tin deposit. See Figure 3.19 for sample locations.

3.3.10.2 Castle Frederick Pb–Zn occurrence

The Castle–Frederick sulphide occurrence (CFM) consists of cm–scale (avg. 2, max. 8 cm) steeply dipping veins of massive sulphide mineralization which cut biotite–rich melagranite and biotite monzogranite of the Salmontail Lake pluton (Smith *et al.* 2006). Given the absence of dyke rocks such as porphyritic units in the area, it is likely that these veins relate to an external fluid reservoir (Fig. 3.23). The setting therefore provides an opportunity to study the chemistry of quartz–hosted mounds in granitoid rocks peripheral to the veins which are not directly related to the mineralization and potentially see if there is a chemical halo, preserved as secondary quartz–hosted fluid inclusions, to the mineralization. In order to address the latter, mound chemistry for 12 samples located within a 25 km radius of the sulphide vein occurrence were assessed to determine if there is spatial variation of the EMA. The results of these analyses are summarized in Figures 3.23 to 3.26.

In general, the EMA show there is a consistent Na–Ca chemistry of the mounds with rare cases of K enrichment in two samples, such as in sample A16–1174 (#8 in Fig. 3.23). Noteworthy in regards to the mineralised sample is its enrichment in Ca and S, which is expressed in both the Na–Ca–K ternary plots (Fig. 32.3) and the Ca/Na ratio (Fig. 2.26) and wt. % S (Fig. 3.24) plots. It is also apparent there is no obvious Ca/Na trend in mounds with respect to distance from the mineralization (Fig. 3.26). The consistent presence of elemental concentrations of Pb, Zn and S, of up to 3 wt. %, in mounds of one of the samples (#A16–SMB3 in Fig. 3.23, located ~5 km away from the CFM is unusual and not observed elsewhere in the study area (Fig. 3.24). In addition to these observations, we also note the presence of Al in some of the EMA which occurs in concentrations up to 10 wt. %. The origin of this enrichment is not known, but might relate to accidently trapped solids (*e.g.*, micas and feldspars). The absence of S, Pb and Zn in the mounds

at Castle Frederick is surprising given the nature of the mineralization (i.e., its high grade) and a possible explanation for this is discussed below.

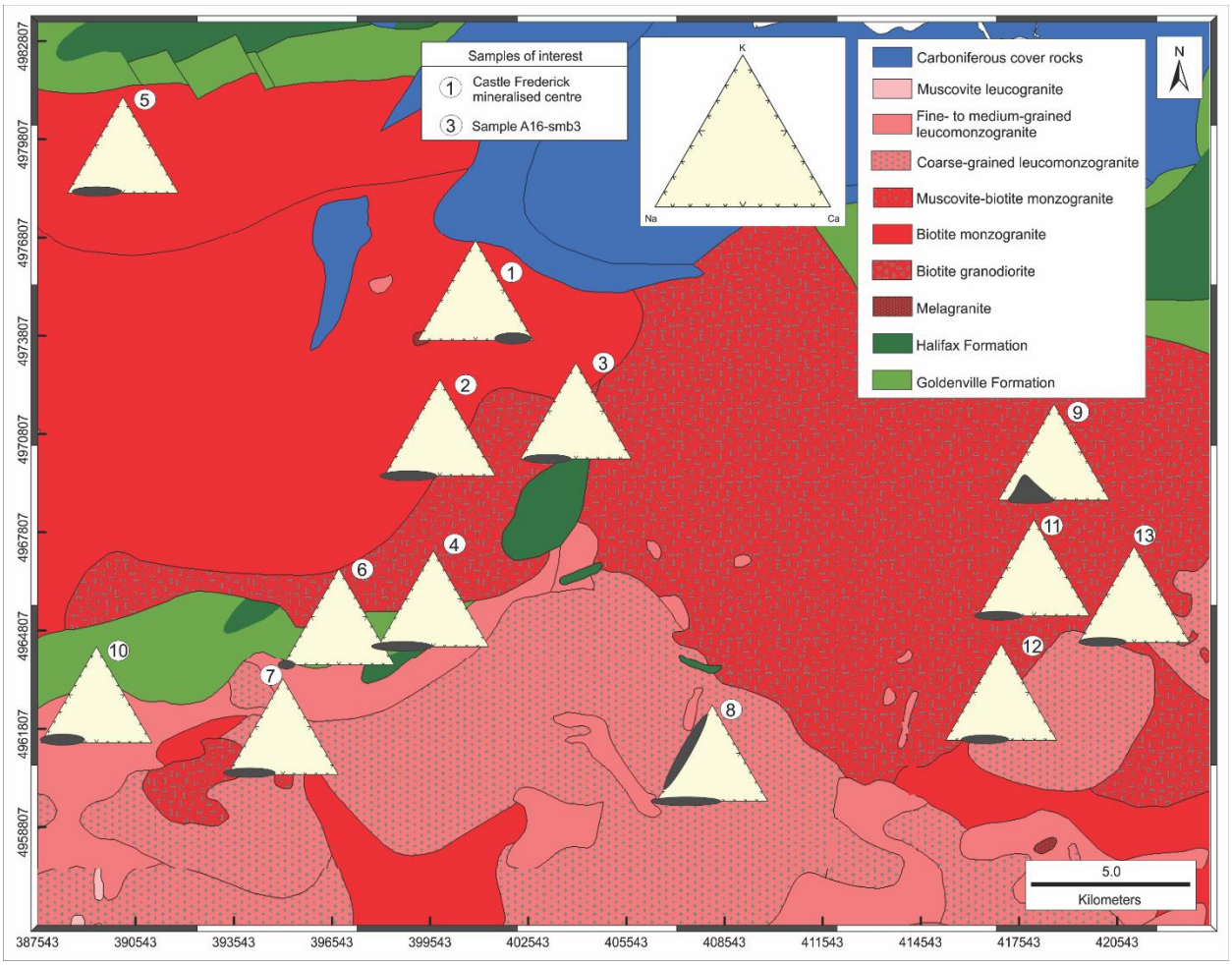

Figure 3.23: Geological map showing locations of samples proximal to the Castle Frederick mineral occurrence in the South Mountain Batholith that were used for EMA. Samples locations are indicated by Na–K–Ca ternary diagrams (in wt. %) showing the compositional range of mounds.

Sample	A16-Tarcf	A16-1281	A16-SMB3	A16-Tar18c	A16-Tar14c	A16-1224	A16-Tar17	A16-Tar14b (Meguma)	A16-1174	A16-Tar14a (Meguma)	A16-Tar10	A16-Tar18b	A16-Tar10.5	A16-Tar8.5	A16-Tar8
Distance from CF occurrence (km)		5.29	5.37	10.29	11.8	13.02	15.22	16.01	16.59	17.42	17.52	18.52	18.78	19.28	21.47
Map Label (Fig. 3.23)	1	2	3	4	5	6	7		8		9	10	11	12	13
Total mounds (tm)	18	15	21	21	8	5	9	2	15	17	7	5	16	7	5
Ca-mounds (% of tm)	100	80	100	95	100	80	89	100	20	71	86	100	88	100	100
K-mounds (% of tm)	5	7	5	29	13		67		73	47	14				
Mn-Fe-Zn-Pb mounds (% of tm)	5	13	81	10	13						14		13	43	60

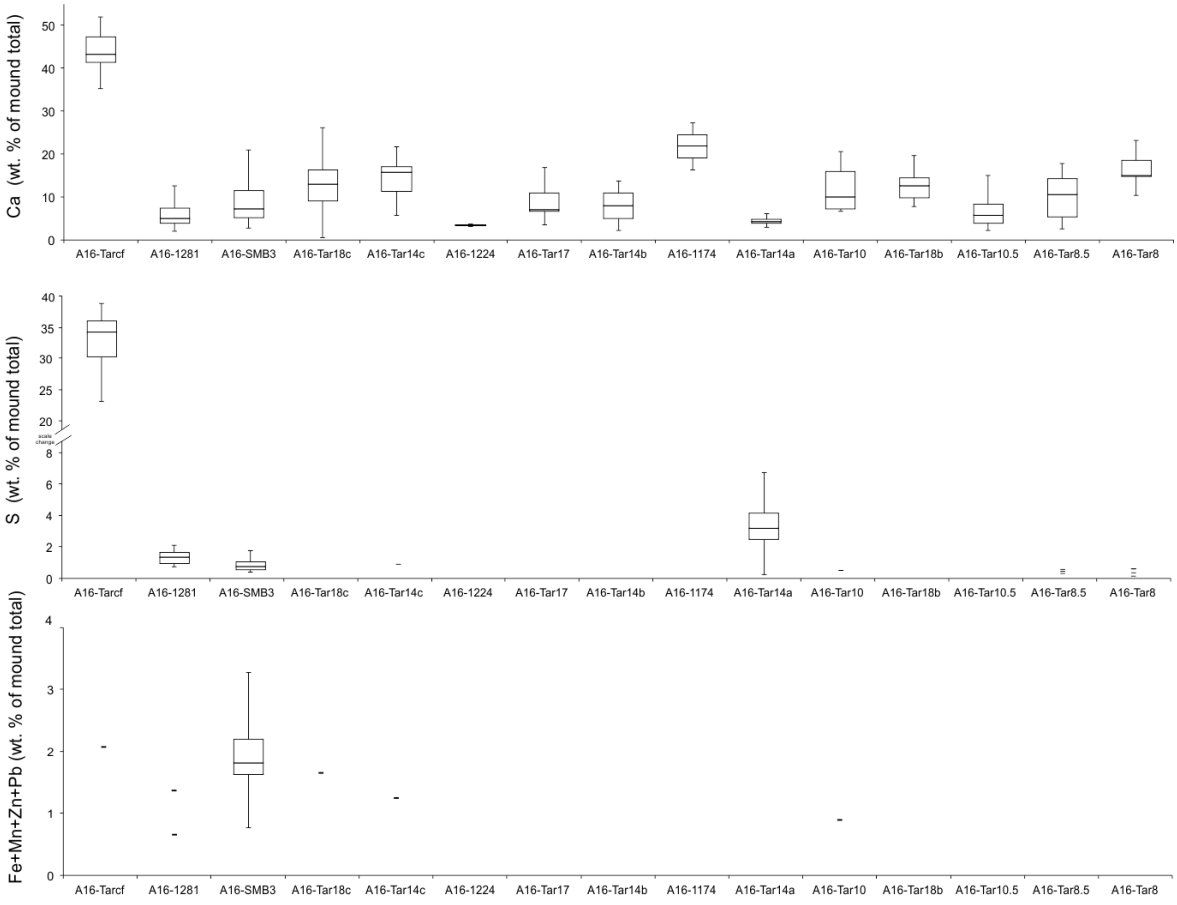

Figure 3.24: Tabulated data and box–and–whisker plots for EMA for samples proximal to the Castle Frederick Pb–Zn mineralised centre shown in Figure 3.23. The samples are arranged in increasing distance (left to right) from the showing.

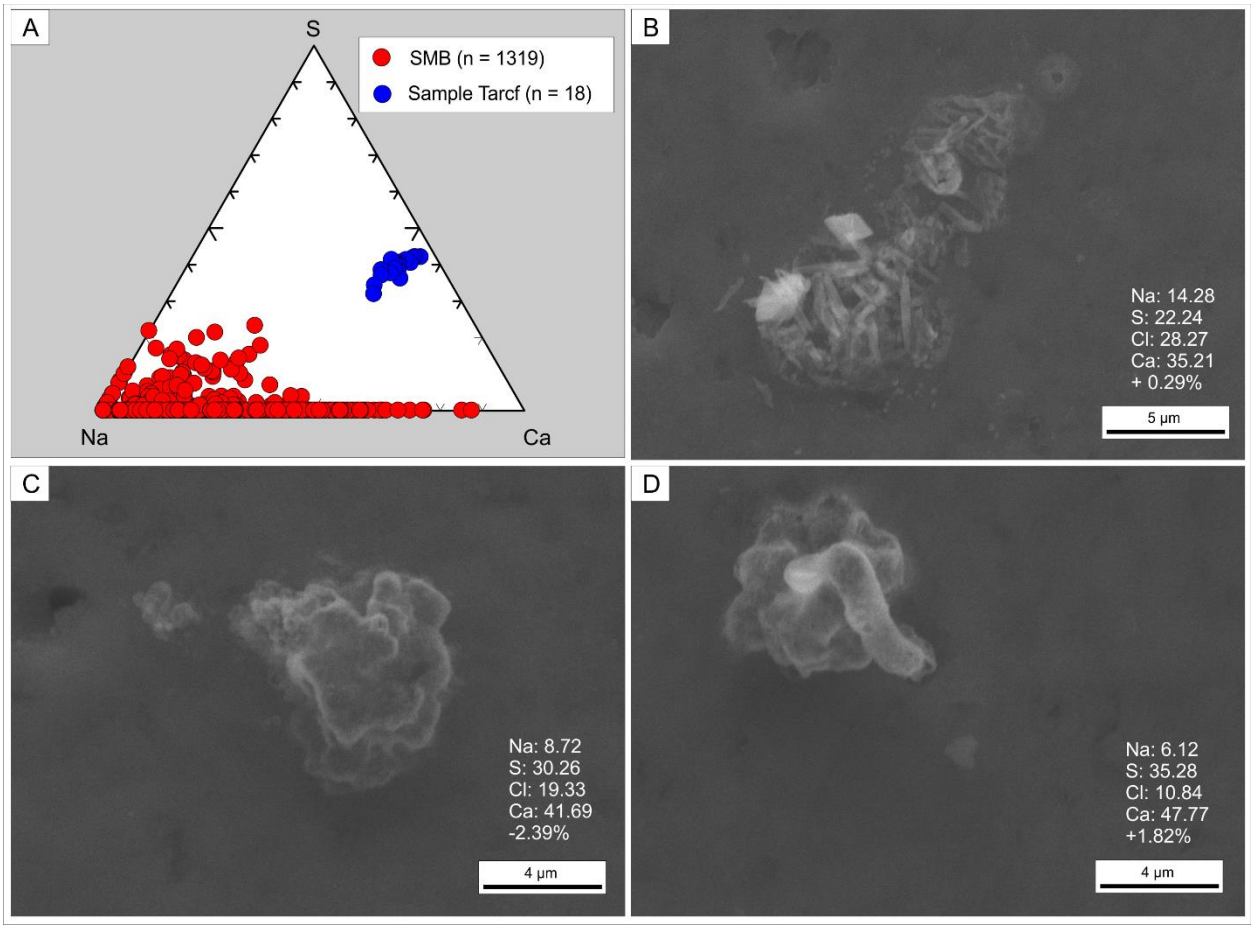

Figure 3.25: Ternary plot for select solutes and SEM–SE images of evaporate mounds for quartz–hosted fluid inclusions from the monzogranite host to the massive sulphide veins at Castle Frederick.(A) Sodium–Ca–S ternary plot (in wt. %) for EMA of Castle Frederick samples (blue) compared to data from the South Mountain Batholith (red). (B–D) SEM–SE images of evaporate mounds with compositional data (wt. %) and charge balance (+/- %) superimposed.

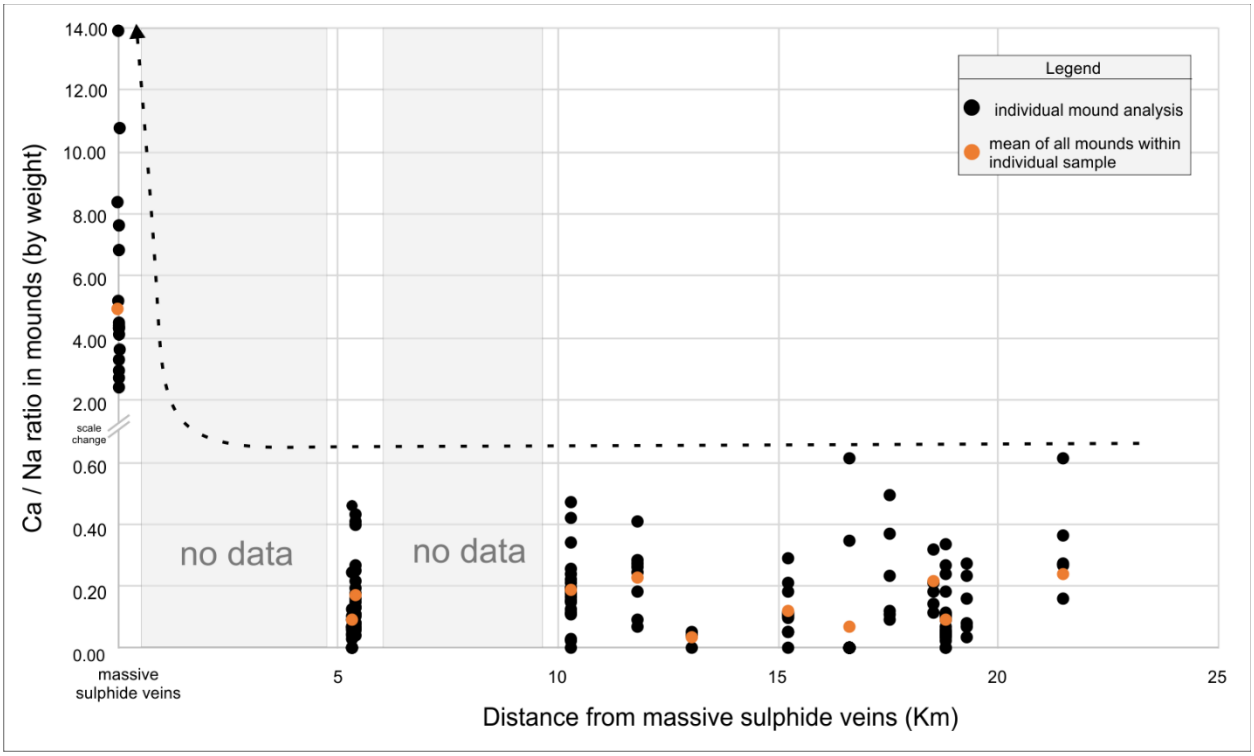

Figure 3.26: Binary plot of Ca/Na ratios in evaporate mounds versus distance from the Castle Frederick Pb–Zn occurrence.

3.4 Discussion

3.4.1 Source of fluids and solutes influencing the fluid inclusion chemistry

As all the quartz–hosted fluid inclusions observed in SMB samples appear to be secondary in origin, it must be considered that sources of both cations and some anions (i.e., S) identified in the EMA may have originated from one or more of the following source reservoirs: 1) late–stage exsolved fluids cognate to the SMB; 2) solid phases of the crystallized SMB due to mineral:fluid reactions; and 3) fluids from the adjacent wall rock and likely generated within the thermal aureole of the SMB. Case 1 is to be expected as part of the normal solidification of crystallizing magmas (*e.g.*, Burnham 1979) with such fluids infiltrating the crystallized mass of the intrusion, in this case the SMB. In case 2, infiltration of the latter orthomagmitic fluid, or possibly another exotic fluid

to the SMB, will lead to mineral:fluid reactions and related exchange of major and minor cations during the subsolidus evolution of the host (*e.g.*, Geiger *et al.* 2002, Plümer & Putnis 2009, Morad *et al.* 2009), and may provide an explanation for the chemical diversity observed in the EMA given that different minerals are present (i.e., plagioclase, K–feldspar, biotite). Thirdly, the influence of the wall rocks must be considered, either in the context of devolitization of fluids due to contact metamorphism or back–reaction of fluids originating in the SMB, as suggested by several earlier studies (Kontak *et al.* 1988, Carruzzo *et al.* 2000, Kontak & Kyser 2011, Kontak *et al.* 2014). In the following sections we address these issues in the context of the chemistry of the EMA.

3.4.1.1 Potential reservoirs for Ca^{2+}

Mounds rich in Ca may relate to albitisation of plagioclase, a common phenomenon in granitoid rocks and generally observed in the cores of plagioclase where the neomorphic phases of sericite and epidote are intergrown with the newly formed albite. This feature, referred to as saussuritization, is common to the SMB (Figs. 3.6D–F) and other granitic intrusions (*e.g.*, Morad *et al.* 2009, Plümer & Putnis 2009). Importantly it is now recognised that such replacement of feldspars and other phases (*e.g.*, leucite by analcime; Putnis *et al.*2007) occurs via a coupled dissolution reprecipitation (CDP) mechanism facilitated by a fluid phase (Putnis 2002, Putnis & Putnis 2007, Niedermeier *et al.* 2009).

The case of albitization of plagioclase ($An_{20–30}$) in A–type Proterozoic granitoids from SE Sweden has been studied in detail by Plümer and Putnis (2009) and is used as a proxy for similar processes in the SMB. These authors propose the following reaction for the temperature range of 200–500°C:

$$Na_{0.8}Ca_{0.2}Al_{1.2}Si_{2.8}O_8 + 0.2Na^+(aq) + 0.2\ H_4SiO_4\ (aq) =$$

$$NaAlSi_3O_8(ab) + 0.2Ca^{2+}(aq) + 0.2Al^{3+} + 0.8OH^-(aq)$$

An important aspect of this reaction is that the Al may contribute to the formation of sericite and/or, along with Ca, the formation of epidote, which depends on the activity of the appropriate phases in the fluid. Given that different assemblages are observed in plagioclase of the SMB (i.e., sericite, epidote, sericite + epidote), it is likely that the reacting fluid had a variable bulk chemistry, which in this case would mainly be its K content or a_{K+} and which is not part of the above reaction.

We can similarly address the alteration of plagioclase to muscovite which is also a common alteration type in igneous rocks of felsic (*e.g.*, Meideno & Allen 1996) or basic (Larsson *et al.* 2002) composition. In the SMB, such alteration varies from cyptic to well developed, the latter being manifest by the presence of coarse muscovite aggregates (Fig. 3.7E). The partial reaction below provides another potential source for Ca.

$$(Na,Ca)Al_2Si_2O_8 + +3SiO_{2(aq)} + K^+_{(aq)} + H^+_{(aq)} =$$

$$K(Al_2)AlSi_3O_{10}(OH)_2 + SiO_{2(aq)} + Na^+_{(aq)} + Ca^{2+}_{(aq)} + Al^{3+}_{(aq)}$$

As with the albitization of plagioclase, this reaction depends on fluid chemistry, in particular acidity and a_{K+}, but both of these are features of magmatic fluids and thus not an issue. We also

note that plagioclase in granitoid rocks generally contains some amount of K_2O and thus this would also contribute to the formation of sericite.

Alternative sources for Ca in the mounds include magmatic fluids and the Meguma metasedimentary wall rocks. In general, late–stage fluid in evolved granitic systems are expected to be depleted in Ca and *in situ* LA–ICP–MS data on melt and fluid inclusions in such systems supports this (*e.g.*, Audétat *et al.* 2000a, Audétat & Li 2017, Zhang & Audétat 2018). Similarly, Bickerton *et al.* (2018b) have shown with *in situ* LA–ICP–MS work that the fluids at the East Kemptville tin deposit are Ca–depleted. Based on this evidence and the low bulk rock CaO contents of the evolved phases of the SMB (<0.66 wt. %; MacDonald (2001)), we suggest that it is likely the late–stage orthomagmatic fluids in the SMB were also deficient in Ca.

As for the wall rock source of Ca, other researchers have suggested the possibility that Ca–bearing fluids derived from the devolatilisation of the Meguma Supergroup rocks represents a possible source (Carruzzo *et al.* 2000, Kontak & Kyser 2011, Kontak *et al.* 2014). Calc–silicate concretions and horizons occur in both the Goldenville and Halifax groups (Chapman 2011, White *et al.* 2008, White 2010, Purves 1974) and would become thermally unstable during the emplacement of the SMB. Ingress of fluids (carrying Ca^{2+}) into the SMB from these metasedimentary rocks via some mechanism of fluid interaction is in fact supported by both isotopic and fluid inclusion studies (Lackey *et al.* 2011, Kontak *et al.* 1988, 2002, Carruzzo *et al.* 2000, Kontak & Kyser 2011, Kontak *et al.* 2014).

3.4.1.2 Potential reservoirs for K^+

The release of K during fluid:rock interaction is a common phenomenon in granitic rocks, in particular where mineralization is noted, due to the acidity of magmatic fluids. The result of these

reactions is the formation of greisens in rare–metal deposits (Sn–W; see Ćerny *et al.* 2005) and phyllic alteration zones in porphyry systems (Seedoorf *et al.* 2005). The alteration results from the disproportionation of SO_2 to H_2S and H_2SO_4 in magmatic systems due to cooling (*e.g.*, Holland 1965, Ohmoto & Rye 1979) and concomitant generation of an acidic fluid. In the case of the SMB, the reduced nature of this S–type peraluminous magma (MacDonald 2001, Clarke *et al.* 2004) would also ensure a higher H_2S/SO_2 than for example oxidized I–type magmas. Combined, the resultant exsolved magmatic fluid would upon cooling have the capacity to react with alkali feldspar to generate muscovite along with formation of secondary quartz and liberation of Na^+ and K^+ ions into solution via the following reaction:

$$3(Na,K)AlSi_3O_8 + 2H^+_{(aq)} = (K)Al_2AlSi_3O_{10}(OH)_2 + 6SiO_2 + 2K^+ + 2Na^+_{(aq)}$$

Thus the presence of K in the EMA is explained by the above reaction which would also contribute to the Na budget of the mounds. In addition, assuming stoichiometric compositions for orthoclase (15 wt. % K_2O) and albite (10% wt. K_2O), Na – K exchange via albitization of alkali feldspar, which is not uncommonly observed petrographically, is a potential source for K^+ via the following reaction:

$$KAlSi_3O_8 + 2H^+_{(aq)} + Na^+_{(aq)} = NaAlSi_3O_8 + K^+_{(aq)}$$

Potassium–rich fluids may be also formed through the partial chloritisation of biotite, which is a common phenomenon in granitic rocks and is seen throughout the SMB (Fig. 3.6). An ideal reaction for this alteration follows:

$$2K(Mg,Fe)_3AlSi_3O_{10}(OH)_2 + 4H^+_{(aq)} + (Mg,Fe)^{2+}_{(aq)} =$$

$$Al(Mg,Fe)_5AlSi_3O_{10}(OH)_8 + 2K^+_{(aq)} + 3SiO_2$$

In reality the appropriate reaction is controlled by the products and reactants, as controlled by chemical analysis. However, this reaction is essentially similar to that derived from an analysis of biotite granite reacting with a 1–2*m* NaCl hydrothermal fluid at 260° under controlled conditions to produce secondary chlorite (Schmidt *et al.* 2018).

3.4.1.3 Potential reservoirs for F^-

Fluorine in granitic rocks manifests as F–bearing minerals (*e.g.*, primary topaz), and fluid inclusions (*e.g.*, Kontak & Kyser 2011, this study) and melt inclusions, as hosted by other peraluminous granites (*e.g.*, Erzgebirge, Germany; Thomas *et al.* 2005, Webster *et al.*, 2004), which substantiates F–enrichment of late hydrous melt phases of evolving granites and in particular mineralised systems. Although the role of F in ore–forming systems was once the subject of debate (*e.g.*, Manning & Pichavant 1985), its partitioning behaviour under experimental conditions distinguishes it unequivocally from Cl and substantiates it as an important ligand in hydrothermal systems (Zhu & Sverjensky 1991).

In the case of the SMB, primary F is manifest as a component of primary muscovite and topaz (Kontak 1990, MacDonald 2001, Clarke & Bogutyn 2003) whereas hydrothermal enrichment is present in muscovite–topaz greisens (O'Reilly *et al.* 1982, Halter *et al.* 1996 Carruzzo *et al.* 2000) and lesser amounts of secondary fluorite in veins and parts of alteration zones (*e.g.*, O'Reilly *et al.* 1982, Kontak *et al.* 1999, Macdonald 2001). Thus the original enrichment of F through magmatic processes is carried into the subsequent hydrothermal stage. As such, the widespread presence of F in the EMA is not surprising, and interesting aspects of which are addressed below.

We do note that whereas the coupling of F^- with Ca^{2+} is consistent with the occurrence fluorite in the SMB (O'Reilly *et al.* 1982), the absence of detectable F–bearing daughter phases (*e.g.*, fluorite or cryolite) in SMB aqueous fluid inclusions is perhaps surprising. For example, approximately half (138/264) of evaporate mounds hosted by the Halifax pluton samples have F up to 40 wt. %, yet fluoride daughter phases, as noted above, were not seen in petrographic work. Another unresolved aspect of the F enrichment in the EMA is its occurrence throughout the SMB, and it does not correlate with, for example, the most evolved phases such as the leucocratic phases. Thus, whereas such enrichment of F can be sourced from magmatic fluids exsolved from the more evolved phases, such as topaz–bearing granites, for the less evolved parts of the SMB we suggest that these fluids originate from deeper, unexposed (i.e., hidden) phases of the batholith.

3.4.2 Fluid chemistry and primary mineral alteration

At the batholith scale, the EMA (and by association fluid chemistry) reflects processes that cannot be easily related genetically to processes operating at mineralised centres. Comparison of proxies for the degree of hydrothermal alteration (*e.g.*, chloritisation of biotite, sericitisation of feldspars, modal abundance of muscovite and abundance of quartz–hosted fluids inclusions) and EMA supports this claim (Fig. 3.17). There is no apparent local relationship between the bulk solute load of locally entrapped fluids and the degree of hydrothermal alteration of the host granitoids. This is confounding given the secondary origin of fluid inclusions and their entrapment after crystallization of primary, and now altered, feldspar and mica minerals. The latter observation suggest that whereas there is local change in the rock mineralogy (*e.g.*, albitization and sericitization of plagioclase), such compositional changes via local mineral alteration through fluid:rock interaction did not apparently markedly effect the solute chemistry of fluids trapped locally. This aspect is further evaluated below.

Mass balance arguments suggest that the observed solute composition of secondary fluid inclusions cannot be the sole product of fluid:rock interaction involving alteration of primary SMB minerals (Fig. 3.27). For modelling purposes, let's assume a briny hydrothermal fluid reservoir, composed of 20 wt. % NaCl and 7 wt. % $CaCl_2$, with a Ca/Na ratio = 0.37, reacts with a Ca–rich rock, and the fluid reservoir is large enough to produce a 1: 1 fluid:rock ratio. Following closed–system interaction of the fluid with a batholith containing a 50% modal abundance of anorthite in and which all the plagioclase is albitized and assuming that: (1) all released Ca^{2+} cations go into the fluid; (2) all albitising Na^{+} came from the fluid; (3) these cations did not participate in other reactions; and (4) these cations did not originate from any other mineral or fluid, the resulting residual fluid Ca/Na will increase to 1.34. By changing the plagioclase to $An_{30,}$ and its modal abundance to 30%, values which are more representative of the SMB (McKenzie & Clarke 1975), and using the same brine composition, the same geologically unrealistic fluid:rock ratio and the same closed–system conditions, the Ca/Na increases to a residual 0.93. In the SMB, Na–Ca–Cl evaporate mounds are the most abundant type, and Ca/Na ratios range from 0 to 1.7 (average = 0.65 ±0.31, 1σ). Therefore, even an idealized hypothetical scenario, designed to unrealistically exaggerate Ca–enrichment in the fluid, albitization cannot fully account for the Ca/Na ratios inferred from the analysis of evaporate mounds.

Our calculation shows that unless fluid:rock ratios were very high, the fluid inclusions did not trap residual fluid compositions that reflect local–scale alteration processes, consistent with the lack of relationship between mound chemistry and alteration indices. Reasonable changes in fluid salinity have a marginal impact on this argument unless the fluid is initially very rich in Ca. Fluids trapped as secondary inclusions have experienced major compositional establishment

elsewhere. In other words, secondary fluids are already modified elsewhere, most likely at depth in the SMB, and those locations cannot be spatially reconciled with the fluid chemistry locally.

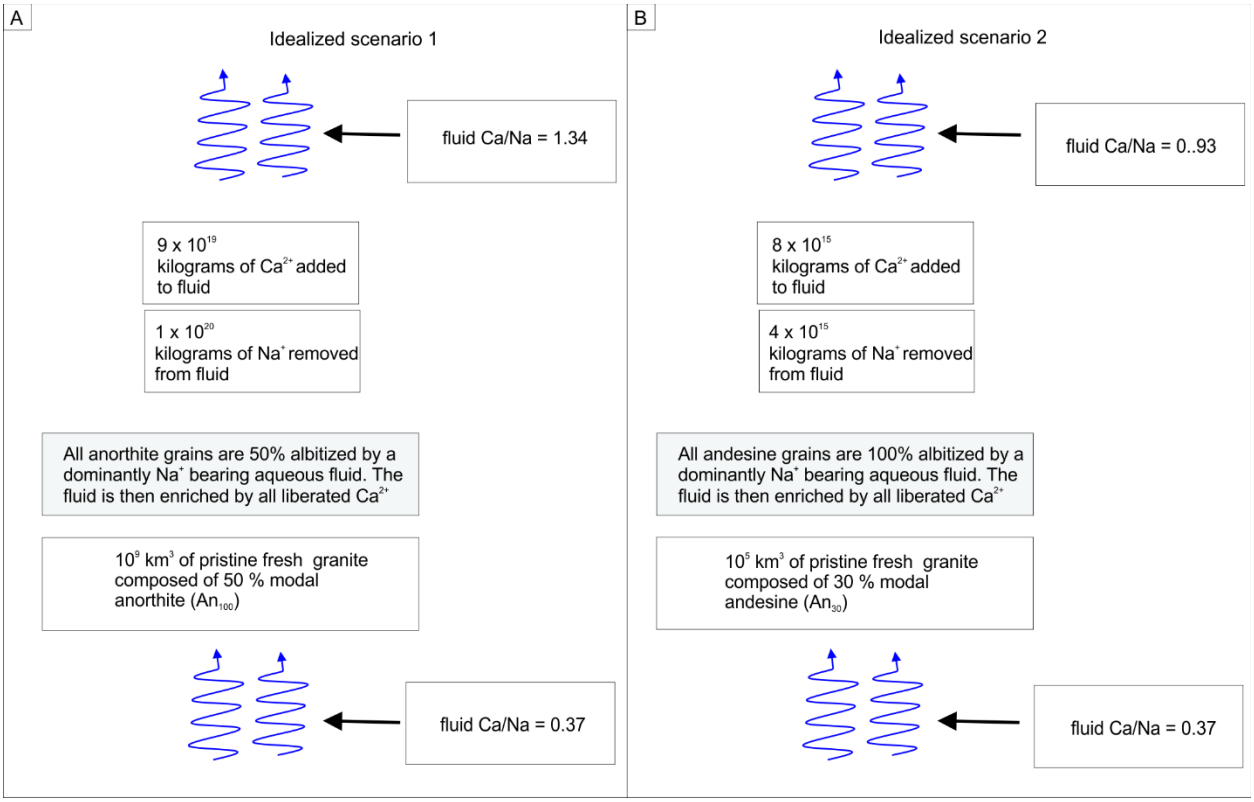

Figure 3.27: Hypothetical models for albitization of (A) anorthite granite, (B) andesine granite batholiths.The idea here is to demonstrate that considerable volumes of water are required to alter hydrothermal fluid Ca/Na ratios. The hydrothermal fluids exiting the altered granites represent the origin of the fluids trapped as secondary fluid inclusion hosted by quartz at the current SMB erosion level.

3.4.3 Fluid chemistry related to intrusion– and non–intrusion related deposits

Regional EMA results suggest that a chemical signature of magmatic–related deposits does extend beyond the mineralised centre, as documented at the East Kemptville deposit area. However, fluid inclusions do appear to preserve evidence of mineralization in rocks proximal to known non–intrusion–related deposits, as indicated by the fluid chemistry in samples within 5 km of the deposit and in the immediate wall rocks where ore is precipitated, as documented at the Castle–Frederick occurrence. These two examples are further explored below.

Locally, near the SMB contact with overlying Carboniferous evaporites of the Visean Windsor Group in the Annapolis Valley, consistent Pb– and S–enrichment of evaporate mounds was detected in a sample located 5 km from a fault–related massive sulphide showing. In addition, the EMA show extreme Ca–enrichment in the showing compared to the surrounding SMB samples. The geological setting of this Pb–Zn occurrence, named by NSDNR as the Castle Frederick occurrence (Smith *et al.* 2006), bears resemblance to MVT–style mineralization in other parts of the Meguma Zone (*e.g.*, Gays River, Smithfield, Kinsac; see Sangster et al (1998)) and is not magmatic in origin. Detection of mineralizing fluids sourced from outside of the batholith does not imply that EMA is only effective in detecting non–magmatic mineralizing fluids, but it does imply that the Castle Frederick Pb–Zn occurrence is part of a more widespread hydrothermal system. An analogous setting is found in the Kinsac vein–type barite–fluorite occurrence hosted in a small peraluminous granitic intrusion related to the 380 Ma Musquodoboit Batholith (Fig. 1), as described by Kontak *et al.* (1999). The fluid inclusions from this occurrence yield low homogenization temperatures (100–130°C) and high salinities (average 24 wt. % NaCl equiv.), but with high Na:Ca ratios (X_{Na}>0.9); we note the latter contrasts therefore with the Castle Frederick data. Based are these data and stable (O, S) and radiogenic (Sr) isotopic studies, the

setting is, as with Castle Frederick, suggested to relate to the widespread Carboniferous Zn–Pb–Ba–F mineralizing event at ca. 300 Ma. As postulated by Kontak *et al.* (1999) for Kinsac, the observed mineralization in the granitic basement immediately beneath the once onlapping carbonate units of the Visean Windsor Group relates to fluid migration along this unconformity where the granites have displayed the Horton Group sedimentary rocks as basement.

Samples proximal to the East Kemptville Sn–Zn–Cu–Ag deposit include 14 locations within 40 km of the mineralised centre (Fig. 3.21). The noted trend of decreasing Ca–enrichment, as reflected in the EMA and hence the fluid phase, andproximal to the deposit contrasts for example with increasing Ca/Na ratios in fluids related to MVT deposits (Haynes & Kesler 1987a, Gleeson & Turner 2007). However, such low Ca/Na ratios may be expected in fluids related to alteration of Ca–depleted rocks such as topaz granites (Taylor & Fallick 1997) and the topaz–muscovite leucogranite that hosts the East Kemptville deposit (Kontak 1990). We also note that the bulk rock chemistry in the strongly zoned Davis Lake pluton is relatively Ca–depleted compared to the rest of the batholith, and rocks proximal (within 5 – 10 km) to the deposit, where the average plagioclase composition is Ab_{99} (Kontak 1991) and essentially devoid of Ca (Dostal & Chatterjee 1995, Dostal *et al.* 2004). Thus the EMA chemistry reflects well the regional zonation of the pluton and proximity of the mineralised centre. This trend is also matched by slight increase in both K and Fe+Mn in the EMA, the latter of which is consistent with Fe enrichment noted in mound analysis and *in situ* LA–ICP–MS measurements of single fluid inclusions for greisen samples from East Kemptville (Bickerton *et al.* 2017, 2018b). This enrichment of Fe in mounds has been noted in other mineralised tin centres (*e.g.*, San Rafael; Kontak & Clark 2002), in addition to LA–ICP–MS data (Audétat *et al.* 2000b, Müller *et al.* 2001).

3.4.4 Implications of fluid enrichment in K, Ca and F

As shown in Figure 3.12, there is widespread but variable enrichment of the evaporate mounds in K, Ca and F in the SMB. Most notable are the elevated Ca and F values. The enrichments of these elements are addressed below in the context of the above discussions.

The noted enrichment of the EMA data in K coincides with samples located within the more evolved stage 2 plutons of the SMB (Fig. 3.12B). Given that bulk–rock enrichment of large–ion–lithophile elements, such as K (also Li, Rb, Cs, etc.), is reasonably expected, the EMA data support the sourcing of the K from a local reservoir such as the late–stage exsolved magmatic fluid phase. As noted already for the SMB, there is no apparent relationship between alteration mineral assemblages related to fluid:mineral reactions, such as chloritization of biotite (see above), and localization of K enrichment. Thus the latter is not considered relevant in the context of effecting the fluid chemistry. Given therefore that K enrichment can be related to the more evolved nature of the host granite, we suggest that the apparent enrichment of the mounds towards the East Kemptville deposit site (Fig. 3.19, 21, 22) is a significant trend as it is spatial coincident with the more evolved nature of the zoned Davis Lake Pluton (Dostal & Chatterjee 1995). Whether such a trend is indicative of mineralization is unlikely, but the elevated Fe and Mn contents, which is also supported by the studies of Bickerton *et al.* (2018b), and local presence of S enrichment is noted, as this is absent in the other phase 2 plutons of the SMB where elevated K is detected. Thus, the latter feature provides evidence of potential for mineralization where, in addition to enrichment of K, there is further support of metal enrichment, in this case Fe and Mn. Of note is that similar conclusions are highlighted in the analyses of mounds in other magmatic hydrothermal settings, including Sn (Kontak & Clark 2002, Kontak 2004) and porphyry (Alimohammadi *et al.* 2014) settings. Thus, this suggests mineralizing events must be highly isolated and do not generate a

regional signal on "background" fluid chemistry, but is a more local phenomenon where ore metals or possibly S are present within the fluids for a relatively short time scale.

The enrichment of the EMA in Ca is noted to be a widespread phenomenon in the secondary fluid inclusions of the SMB. Given the uniqueness of this study, it is not possible to assess this feature in the context of other studies. As we noted above, fluid:mineral interaction, specifically with calcic plagioclase, appears inadequate to account for the observed mound chemistry and its suggests that the Ca–rich nature of the fluid was an inherent feature prior to entering the host–rock environment where it was trapped in quartz. The unresolved question therefore is where did this originate? Two options are considered, one being cognate to the SMB and the other exotic. In the case of the former, we very cautiously suggest that a more mafic component, unexposed at the current level of exposure, may exist at depth and underplates the more felsic SMB. As noted by Clarke *et al.* (1997), mafic intrusions and dyke complexes, such as the Liscomb gabbros (Clarke *et al.* 1993, Kontak & Reynolds 1994) and Weekend dykes (Greenough *et al.* 1988), temporally equivalent to the SMB, are exposed peripheral to the SMB and elsewhere in the Meguma terrane. Is it possible that such material underplates the SMB in a manner that is suggested for the formation of some Andean porphyry deposit settings (*e.g.*, Halter *et al.* 2005). If so, could a Ca–rich fluid be sourced from a reservoir? An alternative source for the Ca–rich fluids is the Meguma metasedimentary rocks which surround and at one time overlay the SMB. As we have noted, this is a Ca reservoir and earlier studies have appealed to it as a source of Ca (*e.g.*, Kontak *et al*, 2002). Where mound chemistry is available for quartz–hosted secondary fluid inclusions, the Ca:Na ratio is noted to vary considerably, as is reported in this study. Thus, a likely scenario is that influx of a Ca–rich fluid sourced in the Meguma metasedimentary rocks mixed with the magmatically sourced, Na–rich fluids in the crystallized SMB. The latter fluid may

also have a Ca component related to albitization, as discussed earlier. Based on the current dataset, this is the preferred interpretation.

The enrichment of F in the EMA across the SMB is the first time such data have been reported in fluids on such a scale. The first order implication of the data is that it reflects batholith wide exsolution of an evolved, late–stage magmatic even in the less evolved stage 1 phases. This suggests therefore the presence, at depth, of more evolved phases that are not presently exposed. Another feature of the data is the abundance of F–rich mounds in the Halifax Pluton. In this regard we highlight two relevant features of this intrusion: 1) the abundance of late–stage leucocratic granitic phases based on mapping (MacDonald & Horne 1988), and 2) the common occurrence locally of pegmatites (± tourmaline) and quartz veins ± muscovite greisen zones, such as noted by Kontak & Kyser (2011). These features attest to evolved nature locally of this phase 2 intrusion of the SMB and thus the not unexpected release of an F–rich fluid as it crystallized.

3.5 Conclusion

The results of integrating evaporate mound analysis with hydrothermal alteration systematics of in SMB granitoid samples reveals a diversity of major and minor solute elements in secondary inclusions hosted by quartz that has not been previously documented, and at the regional–scale of evaluation, does not reflect local hydrothermal processes. The main findings are as follows:

1. Six types of evaporate mounds (Section 3.2.2.) represent six types of hydrothermal fluids. These include, in order of decreasing abundance: (1) a Na–Ca–Cl fluid, represented by evaporate mounds with average Ca/(Ca+ Na) = 0.37, ±0.12, 1σ; (2) a Na–Cl±Ca fluid, represented by mounds with average Ca/(Ca+Na) = 0.12, ±0.05, 1σ; (3) a NaCl fluid, represented by mounds with average (Ca+K)/(Ca+K+Na) = 0.01 ±0.03, 1σ; (4) a Na–F–

Cl±Ca fluid, represented by mounds with average (Ca/(Ca+Na) = 0.14 ±0.05, 1σ, and average F/(F+Cl) = 0.47, ±0.18, 1σ; (5) a Na–Ca–F–Cl fluid, represented by mounds with average (Ca/(Ca+Na) = 0.37 ±0.12, 1σ, and average F(F+Cl) = 0.58, ±0.20, 1σ; and (6) a Na–K–Cl fluid, represented by mounds average K/(K + Na) = 0.45, ±0.20, 1σ.

2. Relationships between mound types and host–rock lithology are not apparent, but ~75% and 55% of evaporate mounds hosted by sericitised and K–feldspar granite samples respectively are Na–Ca–Cl type.
3. Sodium–K–Cl mounds are the least abundant evaporate mound type in the SMB, and F in all these mounds is below detection limits.
4. Assessment of relationships between evaporate mound major solute species and regional/pluton–scale differences reveals four trends: (1) Ca concentrations of > 10 wt. % occurred in 40% of mounds hosted by samples from the western part of the SMB, and 15% of samples from the eastern part; (2) K concentrations in > 10 wt. % occurred more frequently in mounds hosted by samples from the Salmontail Lake and New Ross plutons (i.e., NTS regions A09 and A16) than any other part of the batholith; (3) Quantifiable F occurred more frequently in mounds from the eastern half; and (4) mounds with relatively high S concentrations occur most frequently is samples located in close proximity to the SMB contact with the Meguma Supergroup.
5. There is no apparent relationship between hydrothermal alteration of primary granitoid minerals and the chemistry of locally preserved fluid inclusions, an exception is the relationship between modal abundance of muscovite and Na–K–Cl evaporate mounds.
6. At the resolution of mound chemistry, mounds are not representative of mineralizing fluids, which are either so rare, or discretely organized in samples that they aren't represented in

the fluid inclusion mound record. Alternatively, entrapped mineralizing fluids are preserved as very small inclusions (i.e., < 2 μm diameters) that are difficult to decrepitate (Bodnar *et al.* 1989) and therefore not amenable to EMA.

3.6 References

ALDERTON, D.H.M., RANKIN, A.H., & THOMPSON, M. 1992. Fluid inclusion chemistry as a guide to tin mineralization in the Dartmoor granite, south–west England. Journal of Geochemical Exploration 46, 163–185.

ALDERTON, D. H. M. & RANKIN, A. H. 1983. The character and evolution of hydrothermal fluids associated with the kaolinized St. Austell granite, SW England. Journal of the Geological Society 140, 297–309.

ALDERTON, D.H.M., THOMPSON, M., RANKIN, A.H., & CHRYSSOULIS, S.L. 1982. Developments of the ICP–linked Decrepitation Technique for the Analysis of Fluid Inclusions in Quartz. Chemical Geology 37, 203–213

ALIMOHAMMADI, M., KONTAK, D.J., & KYSER, T.K. 2014. Fluid inclusions and stable isotopes (O, H, S, C) document fluid mixing in the ore–forming systems of the Daraloo and Sarmeshk porphyry Cu deposits, central part of the Dehaj–Sardoeieh Belt, South Iran. Program with Abstracts, 12th Pan–American Current Research on Fluid Inclusions Conference, Denver. CO, 57–58.

ALLEN, M.M., YARDLEY, B.W.D., FORBES, L.J., SHMULOVICH, K.I., BANKS, D. A., & SHEPHERD, T.J. 2005. Validation of LA–ICP–MS fluid inclusion analysis with synthetic fluid inclusions. American Mineralogist 90, 1767–1775.

AUDÉTAT, A. & LI, W. 2017. The genesis of Climax–type porphyry Mo deposits: Insights from fluid inclusions and melt inclusions: Ore Geology Reviews 88, 436–460.

AUDÉTAT, A., GÜNTHER, D., & HEINRICH, C.A. 2000a, Magmatic–hydrothermal evolution in a fractionating granite: A micro–chemical study of the Sn–W–F mineralised Mole granite (Australia): Geochimica et Cosmochimica Acta 64, 3373–3393.

AUDÉTAT, A., GÜNTHER, D., & HEINRICH, C.A. 2000b. Causes for large–scale metal zonation around mineralised plutons: fluid inclusion LA–ICP–MS evidence from the Mole Granite, Australia. Economic Geology 95: 1563–1581.

AUDÉTAT, A., GÜNTHER, D., & HEINRICH, C.A. 1998. Formation of a Magmatic–Hydrothermal Ore Deposit: Insights with LA–ICP–MS Analysis of Fluid Inclusions. Science 279, 2091–2094.Baldwin, G. 2017. A New Look at Mineral Occurrences Associated with the South Mountain Batholith, Southwestern Nova Scotia, *In* Geoscience and Mines Branch, Report of Activities 2016–17; Nova Scotia Department of Natural Resources, Report ME 2017–001, Halifax, Canada (3–4).

BENN, K., HORNE, R.J. KONTAK, D.J., PIGNOTTA, G.S., & EVANS, N.G. 1999. Syn–Acadian emplacement model for the South Mountain Batholith, Meguma Terrane, Nova Scotia: Magnetic fabric and structural analyses; Geological Society of America Bulletin 109, 1279–1293.

BICKERTON, L., KONTAK, D.J., SAMSON, I.M., MURPHY, J.B., & KELLETT, D.A. 2018a. U–Pb geochronology of the South Mountain Batholith, Nova Scotia; in Targeted Geoscience Initiative – 2017 Report of Activities, (N. Rogers, ed.). Geological Survey of Canada, Open File 8358, Ottawa, Canada (61–65). doi:10.4095/306391.

BICKERTON, L., KONTAK, D.J., SAMSON, I., MURPHY, J.B., & ZAJACZ, Z. 2018b. Defining the fluid evolution of a mesothermal magmatic greisen–vein Sn–Cu–Zn–Ag–In deposit, East Kemptville,

Nova Scotia, Canada. Society Economic Geologists Keystone Meeting, Colorado, Program with Abstracts.

BICKERTON, L., KONTAK, D.J., SAMSON, I.M., & MURPHY, J.B. 2017. A mesothermal greisen–hosted Sn–Zn–Cu–Ag–In deposit at East Kemptville, Nova Scotia, Canada. SGA Meeting, Quebec, Canada, Volume Proceedings of Extended Abstracts.

BICKERTON, L., KONTAK, D. J., & SAMSON, I. M. 2016. Defining the PTX of fluids associated with greisen and vein formation at the East Kemptville Sn–Cu–Zn–Ag(–In) deposit, Nova Scotia, Canada. Pan–American Current Research on Fluid Inclusions (PACROFI–XIII) University of Missouri, Columbia, Abstract Volume.

BODNAR R.J., BINNS P.R., & HALL D.L. 1989. SALTY: A Fortran Program to Calculate Compositions of Fluid Inclusions in the System NaCl–KCl–H_20. Journal of Metamorphic Geology 7, 229–242.

BOTTRELL, S.H. & YARDLEY, B.W.D. 1988. The composition of a primary, granite–derived ore fluid from SW England determined by fluid inclusion analysis. Geochimica et Cosmochimica Acta 52, 585–588.

BURNHAM, C.W. 1979. Magmas and hydrothermal fluids. *In* Geochemistry of Hydrothermal Ore Deposits. John Wiley & Sons, Toronto, Canada, 236–277.

CARRUZZO, S., KONTAK, D.J., & CLARKE, D.B. 2000. Granite–hosted mineral deposits of the New Ross area, South Mountain Batholith, Nova Scotia, Canada: P, T and X constraints of fluids using fluid inclusion thermometry and evaporate analysis. Transactions of the Royal Society of Edinburgh: Earth Sciences 91, 303–319.

ČERNY, P., BLEVIN, P.L., CUNEY, M. & London, D. 2005. Granite–related ore deposits. *In* Economic Geology 100th Anniversary Volume 1905–2005 (J.W. Hedenquist, J.F.H. Thompson, R.J. Goldfarb & J.P. Richards, eds.). Society of Economic Geologists, Littleton, United States (337–370).

CHAPMAN, G.G. 2011. Contact metamorphism of calcareous concretions in the Bluestone formation, Halifax Group, Halifax, Nova Scotia. Unpublished B.Sc. thesis, Dalhousie University, Halifax, Nova Scotia.

CHATTERJEE, A. K., STRONG, D.F., CLARKE, D.B., ROBERTSON, J., POLLOCK, D., & MUECKE, G.K. 1985. Geochemistry of the Granodiorite hosting Uranium Mineralisation at Millet Brook. *In* Guide to the granites and mineral deposits of southwestern Nova Scotia (A.K. Chatterjee & D.B. Clarke, eds.). Nova Scotia Department of Energy and Mines, Paper 85–3, Halifax, Canada (63 – 114).

CHRYSSOULIS, S.L. & WILKINSON, N. 1983. High Silver Content of Fluid Inclusions in Quartz from Guadalcazar Granite, San Luis Potosi, Mexico: A Contribution to Ore–Genesis Theory. Economic Geology 78 302–318.

CLARKE, D. B., MACDONALD, M. A., & ERDMANN, S. 2004. Chemical variation in Al_2O_3–CaO–Na_2O–K_2O space: controls on the peraluminosity of the South Mountain Batholith. Canadian Journal of Earth Sciences 41, 785–798.

CLARKE, D.B. & BOGUTYN, P.A. 2003. Oscillatory epitactic–growth zoning in biotite and muscovite from the Lake Lewis Leucogranite, South Mountain Batholith, Nova Scoita, Canada. Canadian Mineralogist 41, 1027–1047.

CLARKE, D.B., MACDONALD, M.A., & TATE, M.C. 1997. Late Devonian mafic–felsic magmatism in the Meguma Zone, Nova Scotia. *In* The nature of magmatism in the Appalachian Orogen. (A.K. Sinha, J.B. Whalen, & J.P. Hogan, eds.). Geological Society of America, Memoir 191, Boulder, United States (107–127).

CLARKE, D.B., CHATTERJEE, A.K., & GILES, P.S. 1993. Petrochemistry, tectonic history, and Sr–Nd systematics of the Liscomb Complex, Meguma Lithotectonic Zone, Nova Scotia. Canadian Journal of Earth Sciences 30, 449–464.

CLARKE, D.B., REARDON, N.C., CHATTERJEE, A.K., & GREGOIRE, D.C. 1989. Tourmaline Composition as a Guide to mineral Exploration: A Reconnaissance Study from Nova Scotia Using Discriminant Function Analysis. Economic Geology 84, 1921–1935.

CLARKE, D.B. & HALLIDAY, A.N. 1980. Strontium isotope geology of the South Mountain Batholith, Nova Scotia. Geochimica et Cosmochimica Acta 44(8), 1045–1058.

DOSTAL, J., CHATTERJEE, A.K., & KONTAK, D.J. 2004. Chemical and isotopic (Pb, Sr) zonation in a peraluminous granite pluton: role of fluid fractionation. Chemical Geology 147, 74–90.

DOSTAL, J. & CHATTERJEE, A.K. 2000. Contrasting behaviour of Nb/Ta and Zr/Hf ratios in a peraluminous granitic pluton (Nova Scoita, Canada). Chemical Geology 163, 207–218.

DOSTAL J. & CHATTERJEE, A.K. 1995. Origin of topaz–bearing and related peraluminous granites of late Devonian Davis Lake pluton, Nova Scotia, Canada. Chemical Geology 123, 67–88.

FENG, YONGGANG. 2014. Hydrothermal Geochemistry and Mineralizing Processes in the T Zone, Thor Lake Rare–element Deposit, Northwest Territories. Electronic Theses and Dissertations. 5106, University of Windsor, Windsor, Canada.

FISHER, B.E. 2006. Digital Version of Nova Scotia Department of Natural Resources Map ME 1979–3, Bouguer Gravity Anomaly Map of Nova Scotia, scale 1:500 000. (J. Keppie, ed.). Nova Scotia Department of Natural Resources, Halifax, Canada.

GEIGER, S, HAGGERTY, R., DILLES, J.H., REED, M.H., & MATTHAI, S.K. 2002. New insights from reactive transport modelling: the formation of the sericitic vein envelopes during early hydrothermal alteration at Butte, Montana. Geofluids 2, 185–201.

GLEESON, S.A. 2003. Bulk Analysis of Volatiles in Fluid Inclusions. *In* Fluid Inclusions: Analysis and Interpretation (I. Samson, A.J. Anderson, & D. Marshall, (eds.). Mineralogical Association of Canada Short Course Publication, Ottawa, Canada (247–278).

GLEESON, S.A. & TURNER, W.A. 2007. Fluid inclusion constraints on the origin of the brines responsible for Pb–Zn mineralization at Pine Point and coarse non–saddle and saddle dolomite formation in the southern Northwest Territories. Geofluids 7, 51–68.

GUILLONG, M., KUHN, R–F., GÜNTHER, D. 2003. Application of a particle separation device to reduce inductively coupled plasma–enhanced elemental fractionation in laser ablation inductively coupled plasma–mass spectrometry. Spectrochimica Acta Part B, 58, 211–220.

GREENOUGH, J.D., RUFFMAN, A., & OWEN, J.V. 1988. Magma injection directions inferred from a fabric study of the Popes Harbour dike, eastern shore, Nova Scotia, Canada. Geology 16, 287–322.

HALTER, W.E., HEINRICH, C.A., & PETTKE, T. 2005. Magma evolution and the formation of porphyry Cu–Au ore fluids: evidence from silicate and sulfide melt inclusions. Mineralium Deposita 39, 845–863.

HALTER, W.E., WILLIAMS–JONES, A.E., & KONTAK, D.J. 1996. The Role of Greisenization in Cassiterite Precipitation at the East Kemptville Tin Deposit, Nova Scotia. Economic Geology 91, 368–385.

HAM, L.J. & KONTAK, D.J. (1988): A textural and chemical study of white mica in the South Mountain Batholith, Nova Scotia: primary versus secondary origin. Maritime Sediments Atlantic Geology 24, 111–121.

HAYNES, F.M. & KESLER, S.E. 1987. Fluid inclusion chemistry in the exploration for Mississippi Valley–type deposits: an example from East Tennessee, U.S.A. Applied Geochemistry 2, 321–327.

HAYNES, F.M., STERNER, S.M., & BODNAR, R.J. 1988. Synthetic fluid inclusions in natural quartz. IV. Chemical analyses of fluid inclusions by SEM/EDA: Evaluation of method. Geochimica et Cosmochimica Acta 52, 969–977.

HEINRICH, C.A., PETTKE, T., HALTER, W.E., AIGNER-TORRES, M., AUDÉTAT, A., GÜNTHER, HATTENDORF, B., BLEINER, D., GUILLONG, M., & HORN, I. 2003. Quantitative multi–element analysis of minerals, fluid and melt inclusions by laser–ablation inductively–coupled–plasma mass–spectrometry. Geochimica et Cosmochimica Acta 67, 3473–3496.

HEINRICH C. A., RYAN C. G., MERNAGH T. P., & EADINGTON P. J. 1992. Segregation of ore metals between magmatic brine and vapor – A fluid inclusion study using pixe microanalysis. Economic. Geology. 87(6), 1566–1583

HICKS, R.J., JAMIESON, R.J., & REYNOLDS, P.H. 1998. Detrital and metamorphic 40Ar/39Ar ages from muscovite and whole–rock samples, Meguma Supergroup, southern Nova Scotia. Canadian Journal of Earth Sciences 36, 22–32.

HILCHIE, L.J. & JAMIESON, R.A. 2014. Graphite thermometry in a low–pressure contact aureole, Halifax, Nova Scotia. Lithos 208–209, 21–3.

HOLLAND, H.D. 1965. Some applications of thermochemical data to problems of ore deposits: II. Mineral assemblages and the compositions of ore–forming fluids. Econ. Geol. 60, 1101–1166.

KENDERES, S.M. & APPOLD, M.S. 2017. Fluorine concentrations of ore fluids in the Illinois–Kentucky district: Evidence from SEM–EDS analysis of fluid inclusion decrepitates. Geochimica et Cosmochimica Acta 210, 132–151.

KEPPIE, J.D 2000. Geological Map of the Province of Nova Scotia. Scale 1: 500 000, Department of Natural Resources, Mines and Energy Branch, Map ME 2000–1, Halifax, Canada.

KEPPIE, J.D., DALLMEYER, R.D., KROGH, T.E., & AFTALION, M. 1993. Dating mineralization using several isotopic methods: An example from the South Mountain Batholith, Nova Scotia, Canada; Chemical Geology 103, 251–270.

KONTAK, D.J. 2004. Analysis of Evaporate Mounds as a Compliment to Fluid–Inclusion Thermometric Data: Case Studies from Granitic Environments in Nova Scotia and Peru. Canadian Mineralogist 42, 1315–1327.

KONTAK, D.J. 1998. A Study of Fluid Inclusions in Sulfide and Nonsulfide Mineral Phases from a Carbonate–Hosted Zn–Pb Deposit, Gays River, Nova Scotia, Canada. Economic Geology 93, 793–817.

KONTAK, D.J. 1991. The East Kemptville topaz–muscovite leucogranite, Nova Scotia. II Mineral Chemistry. Canadian Mineralogist 29, 37–60.

KONTAK, D.J. 1990. The East Kemptville topaz–muscovite leucogranite, Nova Scotia. I Geological setting and whole–rock geochemistry. Canadian Mineralogist 28, 787–825.

KONTAK, D.J. & KYSER, K. 2011. A fluid inclusion and isotope study of an intrusion–related gold deposit (IRGD) setting in the 380 Ma South Mountain Batholith, Nova Scotia, Canada: evidence for multiple fluid reservoirs. Mineralium Deposita 46, 337–363.

KONTAK, D.J. & CLARK, A.H. 2002. Genesis of the giant, bonanza San Rafael lode tin deposit, Peru: origin and significance of pervasive alteration. Economic Geology 97, 1741–1777.

KONTAK, D.J. & KYSER, K. 2001. Preliminary Fluid Inclusion and Oxygen Isotope Studies of the Flintstone Rock (NTS 21A/04) Silica–clay Deposit, Yarmouth County, Nova Scotia. *In* Mines and Minerals Branch Report on Activities 2000 (M.R. MacDonald, ed.). Nova Scotia Department of Natural Resources Publication, Halifax, Canada (37–48).

KONTAK, D.J. & REYNOLDS, P.H. 1994. $^{40}Ar/^{39}Ar$ dating of metamorphic and igneous rocks of the Liscomb Complex, Meguma terrane, southern Nova Scotia, Canada. Canadian Journal of Earth Sciences. 31, 1643–1653.

KONTAK, D.J. & COREY, M.C. 1988. Metasomatic origin of spessartine–rich garnet in the South Mountain Batholith, Nova Scotia. Canadian Mineralogist 26, 315–334.

KONTAK, D.J., ALIMOHAMMADI, M., & WATTS, K. 2014. The Gardners Meadow Sn–Zn–Cu showing of southwest Nova Scotia: A small but not insignificant ca. 360 Ma metallogenic event. Atlantic Geology 50, 42.

KONTAK, D.J., DOSTAL, J., KYSER, K., & ARCHIBALD, D.A. 2002. A petrological, geochemical isotopic and fluid–inclusion study of the 370 Ma pegmatite–aplite sheets, Peggys Cove, Nova Scotia, Canada. Canadian Mineralogist 40, 1249–1286.

KONTAK, D.J., DOSTAL, J., ANSDELL, K., HALTER, W., MARTIN, R.F. & WILLIAMS–JONES, A.E., 2001. The nature and origin of pegmatite in a fluorine–rich leucogranite, East Kemptville, Nova Scotia. Transactions of the Royal Society of Edinburgh: Earth Sciences 92, 173–200.

KONTAK, D.J., HORNE, R.J., ANSDELL, K., & ARCHIBALD, D.A. 1999. Carboniferous barite–fluorite mineralization in the Late Devonian Kinsac Pluton, southern Nova Scotia. Atlantic Geology 35, 109–127.

KONTAK, D.J., ANSDELL, K., & ARCHIBALD, D. 1999. New constraints on the age and origin of the Dunbrack Pb–Cu–Zn–Ag deposit, Musquodoboit Batholith, southern Nova Scotia. Atlantic Geology 35, 19–42.

KONTAK, D.J., STRONG, D.F., & KERRICH, R. 1988. Crystal–melt±fluid phase equilibria verses late–stage fluid–rock interaction in granitoid rocks of the South Mountain Batholith, Nova Scotia: whole rock geochemistry and oxygen isotope evidence. Maritime Sediments and Atlantic Geology 24, 97–110.

KRETZ, R. 1983. Symbols for rock–forming minerals. American Mineralogist 68, 277–279.

LACKEY, J.S., ERDMANN, S., HARK, K.S., NOWAK, R.M., MURRAY, K. E., CLARKE, D.B., & VALLEY, J.W. 2011. Tracing garnet origins in the granitoids rocks by oxygen isotope analysis: examples from the South Mountain Batholith, Nova Scotia. Canadian Mineralogist 40, 317–339.

LARRSSON, D., GRÖNVOLD, K., OSKARSSON, N., & GUNNLAUGSSON, E. 2002. Hydrothermal alteration of plagioclase and growth of secondary feldspar in the Hengill Volcanic Centre, SW Iceland. Journal of Volcanology and Geothermal Research 114, 275–290.

MACDONALD, M.A. 2001. Geology of the South Mountain Batholith, Southwestern Nova Scotia. Nova Scotia Department of Natural Resources, Open File Report ME 2001–2.

MacDONALD, M.A., HORNE, R.J., COREY, M.C., & HAM, L.J. 1992. An overview of recent bedrock mapping and follow–up petrological studies of South Mountain Batholith, southwestern Nova Scotia, Canada. Atlantic Geology 28, 7–28.

MACDONALD, M.A. & HORNE, R.J. 1988. Petrology of the zoned, peraluminous Halifax Pluton, south–central Nova Scotia. Atlantic Geology 24, 33–45.

MANNING, D.A.C. & PICHAVANT, M. 1985. Volatiles and their bearing on the behaviour of metals in granitic systems. *In* Recent Advances in the Geology of Granite–Related Mineral Deposits.

Proceedings of the CIM Conference of Granite–Related mineral Deposits, Special Volume 39 (R.P. Taylor & D.F. Strong, eds.). The Canadian Institute of mining and Metallurgy, Halifax, Canada (13–24).

MARTEL, T.A., MCGREGOR, C.D., & UTTING, J. 1993. Stratigraphic significance of upper Devonian and Lower Carboniferous miospores from the type area of the Horton Group, Nova Scotia. Canadian Journal of Earth Sciences 30, 1091–1098

MCKENZIE, C.B. & CLARKE, D.B. 1975. Petrology of the South Mountain Batholith, Nova Scotia. Canadian Journal of Earth Sciences 12, 1209–1218.Meideno, Q. & Allen, A.R. 1996, Sericitization of plagioclase in the Rosses Granite Complex, Co. Donegal, Ireland. Mineralogical Magazine 60, 927–936.

MILLER, C.F., STODDARD, E.F., BRADFISH, L.J., & DOLLASE, W.A. 1981. Composition of plutonic muscovite: genetic implications. Canadian Mineralogist 19, 25–34.

MORAD, S, EL–GHALI, M.A.K., CAJA, M.A., SIRAT, M., AL–RAMADAN, K., & MANSURBEG, H. 2009, Hydrothermal alteration of plagioclase in granitic rocks from Proterozoic basement of SE Sweden. Geological Journal 45, 105–116.

MUECKE, G.K. & CLARKE, D.B. (1981) Geochemical Evolution of the South Mountain Batholith, Nova Scotia: Rare–Earth Element Evidence. Canadian Mineralogist 19, 133–145.

MÜLLER, B., FRISCHKNECHT, R., SEWARD, T., HEINRICH, C.A., & Gallegos, W.C. 2001. A fluid inclusion reconnaissance study of Huanuni tin deposit (Bolivia), using LA–ICP–MS micro–analysis. Mineralium Deposita 36, 680–688.

NIEDERMEIER, D.R.D., PUTNIS, A., FEISLER, T., GOLLA–SCHINDLE, U., PUTNIS, C.V. 2009. The mechanism of cation and oxygen isotope exchange in alkali feldspars under hydrothermal conditions. Contributions Mineralogy Petrology 157, 65–76.

OHMOTO, H. & RYE, R.O. 1979. Isotopes of sulfur and carbon. *In* Geochemistry of Hydrothermal Ore Deposits (H.L. Barnes, ed.). John Wiley & Sons, New York, United States, 509– 567.

O'REILLY, G.A., FARLEY, E.J., & CHAREST, M.H. 1982. Metasomatic–Hydrothermal Mineral Deposits of the New Ross–Mahone Bay Area Nova Scotia. Nova Scotia Department of Mines and Energy Paper 82–2, 15–21.

PANDUR, K., KONTAK, D.J., & ANSDELL, K.M. 2014. Hydrothermal evolution in the Hoidas Lake vein–type REE deposit, Saskatchewan, Canada: constraints from fluid inclusion microthermometry and evaporate mound analysis. Canadian Mineralogist 52, 717–744.

PETTKE, T., OBERLI, F., AUDÉTAT, A., GUILLONG, M., SIMON, A.C., HANLEY, J.J., & KLEMM, L.M. 2012. Recent developments in element concentration and isotope ratio analysis of individual fluid inclusions by laser ablation single and multiple collector ICP–MS. Ore Geology Reviews 44, 10–38.

PLÜMPER, O. & PUTNIS, A. 2009. The complex hydrothermal history of granitic rocks - Multiple feldspar replacement reactions under subsolidus conditions. Journal of Petrology 50 (5), 967-987.

PURVES, M.F. 1974. Metasomatism of Calcareous Concretions of the Goldenville Formation, Nova Scotia. Unpublished B.Sc. thesis, Dalhousie University, Halifax, Nova Scotia.

PUTNIS, A. 2002. Mineral replacement reactions: from macroscopic observations to microscopic mechanisms. Mineralogical Magazine 66(5), 689–708.

PUTNIS, A. & PUTNIS, C.V. 2007. The mechanism of reequilibration of solids in the presence of a fluid phase. Journal of Solid State Chemistry 180, 1783–1786.

PUTNIS, C.V., GEISLER, T., SCHMID-BEURMANN, P. STEPHAN, T. & GIAMPAOLO, C. 2007. An experimental study of the replacement of leucite by analcime. American Mineralogist 92 (1), 19–26. doi: https://doi.org/10.2138/am.2007.2249

RANKIN, A.H. & ALDERTON, D.H.M. 1983. Fluid Inclusion Petrography of SW England Granites and its Potential in Mineral Exploration. Mineralium Deposita 18, 335–347.

REYNOLDS, P.H., ZENTILLI, M., & MUECKE, G.K. 1981. K–Ar and $^{40}Ar/^{39}Ar$ geochronology of granitoid rocks from southern Nova Scotia: Its bearing on the geological evolution of the Meguma Zone of the Appalachians. Canadian Journal of Earth Sciences 18, 386–394.

ROEDDER, E. 1990. Fluid inclusion analysis – Prologue and epilogue* Geochimica et Cosmochimica Alta 54, 495–507.

ROEDDER, E. 1984. Fluid Inclusions. Reviews in Mineralogy 12. Mineralogical Society of America, Washington D.C., United States.

SALVI, S., FONTAN, F., MONCHOUX, P., WILLIAMS–JONES, A. E., & MOINE, B. 2000. Hydrothermal mobilization of High Field Strength Elements in Alkaline Igneous Systems: Evidence from the Tamazeght Complex (Morocco). Economic Geology 95, 559–576.

SAMSON, I.M., WILLIAMS–JONES, A.E., & LUI, W. 1995. The chemistry of hydrothermal fluids in carbonitites: Evidence from leachate and SEM–evaporate analysis of fluid inclusions from Oka, Quebec, Canada. Geochimica et Cosmochimica Acta 59, 1979–1989.

SANGSTER, D.F., SAVARD, M. & KONTAK, D.J. 1998. A genetic model for mineralization of Lower (Visean) carbonate rocks of Nova Scotia, Canada. Economic Geology 93, 932–952.

SAVARD, M.M. & CHI, G. 1998. Cation Study of Fluid Inclusion Evaporates in the Jubilee and Gays River (Canada) Zn–Pb Deposits – Characterization of Ore–Forming Brines*. Economic Geology 93, 920–931.

SCHMIDT, R.B., BUCHER, K., & STOBER, I. 2018. Experiments on granite alteration under geothermal reservoir conditions and the initiation of fracture evolution. European Journal of Mineralogy 30, 899–916.

SEAL, R.R., CLARK, A.H., & MORRISSY, C.J. 1985. Lake George southwestern New Brunswick: a Silurian, multi–stage, polymetallic (Sb–W–Mo–Au–base metal) hydrothermal centre. *In* Recent Advances in the Geology of Granite–Related Mineral Deposits. (R.P. Taylor & D.F. Strong eds.). Canadian Institute of Mining and Metallurgy Conference on Granite–Related Mineral Deposits, Special Volume 39, Halifax, Canada (252–264).

SEEDORFF, E., DILLES, J.H., PROFETT, Jr., J.M., EINAUDI, M.T., ZURCHER, L., STAVAST, J.A., JOHNSON, D.A., & BARTON, M.D. 2005. Porphyry deposits: Characteristics and origin of hypogene features. *In* Economic Geology 100th Anniversary Volume 1905–2005 (J.W. Hedenquist, J.F.H. Thompson, R.J. Goldfarb & J.P. Richards, eds.). Society of Economic Geologists, Littleton, United States (251–298).

SEO, J.H., GUILLONG, M., AERTS, M., ZAJACZ, Z., & HEINRICH, C.A. 2011. Microanalysis of S, Cl, and Br in fluid inclusions by LA–ICP–MS. Chemcial Geology 284, 35–44.

SMITH, P.K., PRIME, G., & WEIR, D. 2006. Castle Frederick (NTS 21A/16): A New Pb–Zn (–Ag?) Mineral Occurrence. *In* Mineral Resources Branch, Report of Activities 2005; Nova Scotia Department of Natural Resources, Report ME–2006–1, 143–147.

SMITH, T.E. & TUREK, A. 1976. Tin–bearing potential of some Devonian Granitic Rock sin S.W. Nova Scotia. Mineralium Deposita 11. 234–245.

TAYLOR, R.G. 1979. Geology of tin deposits: Elseveir Scientific Publishing, New York, United States.

TAYLOR, R.P. & POLLARD, P.J. 1985 Pervasive hydrothermal alteration in tin–bearing granites and implications for the evolution of ore–bearing magmatic fluids. *In* Recent Advances in the Geology of Granite–Related Mineral Deposits. Proceedings of the CIM Conference of Granite–Related mineral Deposits, Special Volume 39 (R.P. Taylor & D.F. Strong, eds.). The Canadian Institute of Mining and Metallurgy, Halifax, Canada (86–95).

TAYLOR, R.P. & FALLICK, A.E. (1997). The evolution of fluorine–rich felsic magmas: source dichotomy, magmatic convergence and the origins of topaz granite. Terra Nova 9, 105–108.

THOMAS, R., FÖRSTER, H–J., RICKERS, K., & WEBSTER, J. D. 2005. Formation of extremely F–rich hydrous melt fractions and hydrothermal fluids during differentiation of highly evolved tin–granite magmas: a melt/fluid–inclusion study. Contributions to Mineralogy and Petrology 148, 582–601.

TUACH, J., DAVENPORT, P.H., DICKSON, W.L., & STRONG, D.F. 1986. Geochemical trends in the Ackley Granite, southeast Newfoundland: their relevance to magmatic metallogenic processes in high–silica granitoid systerns. Canadian Journal of Earth Sciences 23, 747–76.

TWEEDALE, F., HANLEY, J.J., & KONTAK, D.J. (in prep 2019) Evaporate mound analysis by scanning electron microscopy–energy–dispersive X–ray spectrometry (SEM–EDS): A method for obtaining multi–element compositional constraint on hydrothermal fluids *Canadian Mineralogist, in prep*.

WALSH, J.F., KESLER, S.E., DUFF, D., & CLOKE, P.L. 1988. Fluid Inclusion Geochemistry of high–Grade, Vein–Hosted gold Ore at Pamour Mine, Porcupine Camp, Ontario. Economic Geology 83, 1347–1367.

WEBSTER, J., THOMAS, R., FÖRSTER, H–J., SELTMANN, R., & TAPPEN, C. 2004. Geochemical evolution of halogen–enriched granite magmas and mineralizing fluids of the Zinnwald tin–tungsten mining district, Erzgebirge, Germany. Mineralium Deposita 39, 452–472.

WHITE, C.E. 2010. Stratigraphy of the Lower Paleozoic Goldenville and Halifax groups in southwestern Nova Scotia. Atlantic Geology 46, 136–154.

WHITE C.E., BELL, J.A., MCLEISH, D.F., MACDONALD, M.A., GOODWIN, T.A., & MACNEIL, J.D. 2008.Geology of the Halifax Regional Municipality, central Nova Scotia. *In* Report of Activities (D.R. MacDonald, ed.). Nova Scotia Department of Natural Resources Report ME–2008–1, Halifax, Canada (125–139).

WHITE, C.E., PALACIOS, T., JENSEN, S. & BARR, S.M. 2012. Cambrian–Ordovician acritarchs in the Meguma terrane, Nova Scotia, Canada: Resolution of early Paleozoic stratigraphy and implications for paleogeography. Geological Society of America Bulletin 124 (11/12) 1773–1792.
Williams–Jones, A.E. & Heinrich, C. 2005. Vapor Transport of Metals and the Formation of Magmatic–Hydrothermal Ore Deposits. Economic Geology 100, 1287–1312.

WILLIAMS–JONES, A.E., SAMSON, I.M., & OLIVO, G.R. 2000. The Genesis of Hydrothermal Fluorite–REE Deposits in the Gallinas Mountains, New Mexico. Economic Geology 95, 327–342.

YARDLEY, B.W.D., BANKS, D.A., BOTTRELL, S.H., & DIAMOND, L.W. 1993. Post–metamorphic gold–quartz veins from N.W. Italy: the composition and origin of the ore fluid. Mineralogical Magazine 57, 407–42.

ZHANG, D. & AUDÉTAT 2018. Magmatic–hydrothermal evolution of the barren Huangshan Pluton, Anhui Province, China: A melt and fluid inclusion study. Economic Geology 113, 803–824.

ZHU, C., & SVERJENSKY, D.A. 1991. Partitioning of F–Cl–OH between minerals and hydrothermal fluids. Geochimica et Cosmochimica Acta 55, 1837–1858.

CHAPTER 4: LIMITATIONS OF METHOD, RECOMMENDATIONS FOR FUTURE WORK AND CONCLUSIONS

4.1 Limitations of method and interpretation of results

4.1.1. Unknown origin of mounds

Petrographic observation of fluid inclusions can provide some insight into the mound origin, and as such the sources(s) of mound elements (F, Cl, Na, Ca, Mn etc.) may be somewhat constrained. However, there is no obvious solution to the problem of pinpointing mound origin. Some relevant observations include: (1) in many cases mounds are proximal to decrepitation pits, suggesting that the fluid from which the mound precipitated emanated from the pit; (2) theoretical calculations based on salinity measurements from microthermometric work, and on assumptions about the shapes of fluid–inclusion cavities and evaporate mounds (spherical and hemispherical respectively) provides data that reasonably constrain the size of fluid inclusions from which evaporate mound precipitated (*e.g*., Haynes *et al.*, 1988; this study). The long–axis diameter of mounds provides is a measure of mound size, and all mounds analyzed in this study conform to the size of mounds predicted to precipitate from single inclusions (Tweedale *et al.* in prep, 2019). But there is no absolute certainty about a mound precipitating from a single inclusion.

4.1.2 Fluid mixing prior to volatilisation of the solvent phase

As opposed to discrete fluid inclusion cavities, decrepitation pits may in fact be the intersection points between internal fractures of unknown extent with the surface of observation. Thus pits may be openings to fractures that ruptured during heating runs, thus representing openings to conduits of unknown extent through which fluids released from decrepitated fluid inclusions flowed. If this is the case, mounds may in fact represent the bulk composition of more than one inclusion, and

possibly, discrete mounds may precipitate from the aqueous phase of many inclusions hosted within a fracture plane.

4.1.3 Entrainment of solid phases of unknown origin

Levels of Fe and S in mounds varies from < 1 to > 10 wt. % of the total mound. A likely explanation for the occurrence of > 10 wt. % of these elements in mounds is the contamination by entrainment of Fe–S solids of unknown speciation and origin. In fact, 60 mounds with detectable S in amounts > 3 wt. % are likely contaminated by unknown solids because it is unlikely that such S–rich fluids could exist in a felsic magmatic/hydrothermal system. These analyses are simply not counted. However, detection of 1 – 3 wt. % Fe occurs in 40 mounds devoid of S, and detection of 1 – 3 wt. % S occurs in 34 mounds devoid of Fe. Detection of 1 – 3 wt. % each of S and Fe occurs in 8 mounds. It is difficult to know if these elements existed as fluid inclusion solutes, or if they were entrapped solids of unknown origin.

4.1.4 Scale of analysis

The regional–scale analysis may be too large for effective application of the EMA technique as an exploration tool. A sampling density of 1/100 km^2 was agreed upon at the start of this study with the knowledge that such a strategy is unconventional. The general approach of 'lets see what we can get by doing this' did however produce some encouraging results (i.e., sensing the Castle Frederick occurrence). Alternatively, application of EMA in other research (e.g., Kesler and Haynes, 1987), correlate changes in Na/Ca mound ratios occurring only samples located within within metres of a mineralised zone, which suggests that the formation of mineral deposits are highly focussed hydrothermal events, and that whatever the hydrothermal process may be, it is not reflected in the bulk composition of fluid inclusions entrapped further than a few metres from the deposit. Application of the EMA technique, and its integration with petrographic analysis of

hydrothermal systematics, may be more effective at the local–scale (*e.g.*, Kontak & Kyser 2011, Chryssoulis & Wilkinson 1983, Haynes *et al.* 1987). Results from this research provide empirical criteria for selecting local–scale targets in the SMB (see section below).

4.2 Recommendations for future work

4.2.1 Sampling strategy for local–scale studies: Part I

Results of this study provide empirical criteria for selecting targets destined for local–scale application of the EMA technique in the SMB. Specifically, detection of Mn occurs in mounds hosted by samples from the two mineralised locales analyzed in this study (East Kemptville tin mine and the Long Lake prospect). Of the 119 apparently barren samples analyzed, five host fluid inclusions with detectable Mn (Fig. 4.1). These samples are now targets for local-scale EMA research.

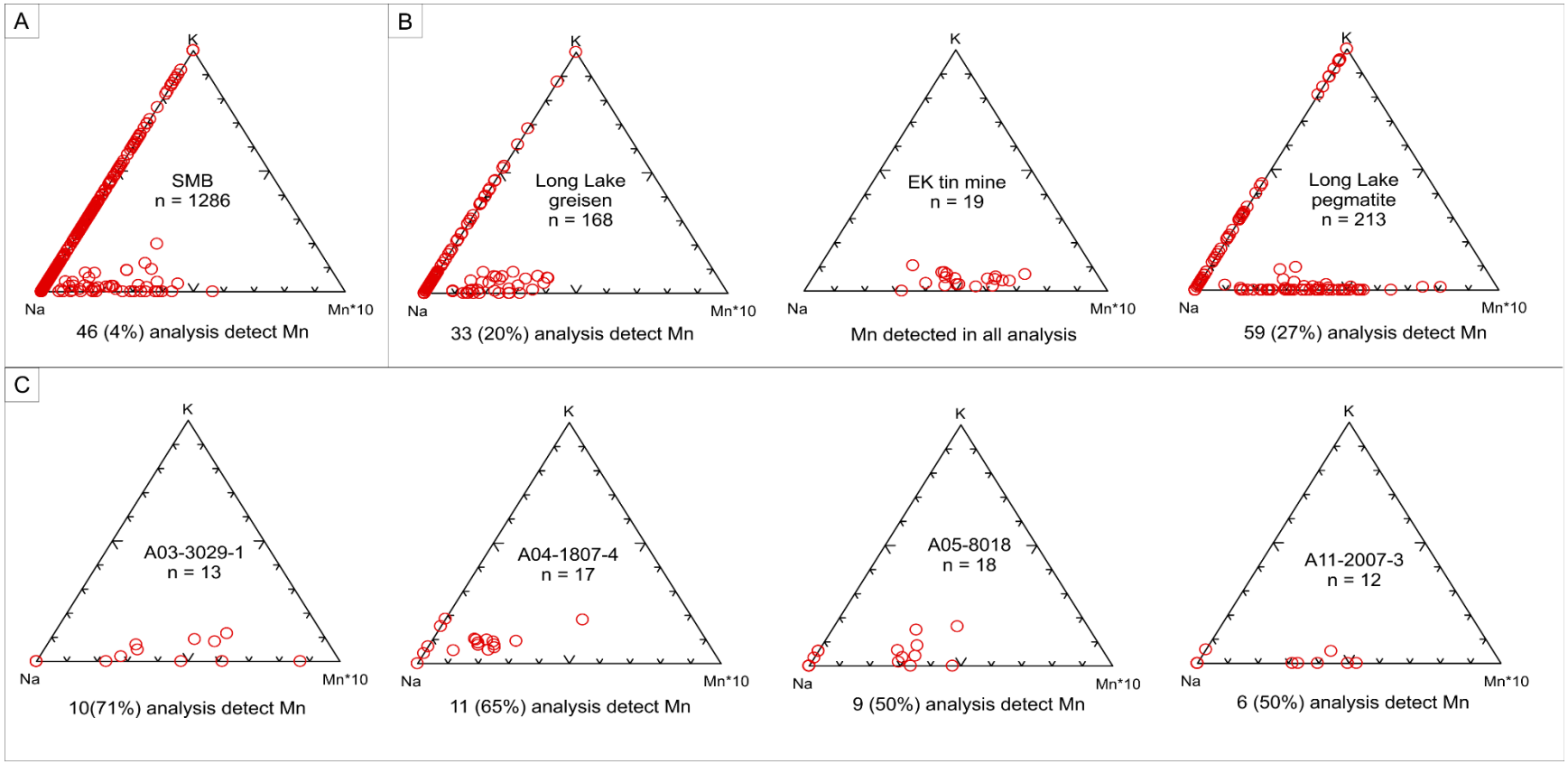

Figure 4.1: Ternary plots (Na–K–Mn*10) of EDS data for evaporate mound analysis for the SMB and select SMB locations. (A) 109 apparently barren SMB samples, (B) three samples, one each from three mineralised localities in the SMB, (C) four samples, one each from four apparently barren SMB localities.

4.2.2 Sampling strategy for local–scale studies: Part II

The objective of this regional–scale study was to acquire a sample set representative of the entire batholith using a grid system (i.e., one sample collected from each grid square). To avoid bias, geological information about SMB–hosted mineral deposits was not consulted. However, such information could be a useful guide for future local–scale studies. For example, SMB–related polymetallic deposits are, in general, spatially associated with leucogranite bodies (Kontak 1990, Clarke *et al.* 1993, Logothetis 1985, O'Reilly *et al.* 1982), which at the current level of erosion account for *ca.* 1 –2 % of the SMB. Local–scale EMA studies specifically targeting leucogranites may provide additional information about known deposits and reveal new deposits.

A specific modal composition of predominantly of alkali feldspar (> 35 %), plagioclase (< 35%), quartz and < 2% mafic minerals (biotite, cordierite, garnet) defines leucogranites. Leucogranites (< 2 % modal mafic minerals) are distinguished from leucomonzogranites, which compose 2 – 6 % mafic minerals. Known leucogranites are themselves texturally heterogeneous. Thus, leucogranites are readily identifiable in thin section. Known leucogranitic bodies exist in the SMB, however, unknown bodies may also occur. Publically available NSDNR bedrock maps display other granitoid intrusions as undifferentiated units, yet unpublished data shows that larger–scale smaller–area mapping of these undifferentiated units reveal greater lithological detail. For example, the *ca*. 25 km^2 Port Mouton pluton, which is well-exposed along the coast of southwestern Nova Scotia composes an outer tonalite–granite perimeter that becomes increasingly monzogranitic toward the centre of the pluton (McCuish 2001). A mandatory first–step for local studies of granitoids in the Meguma terrane would be ground trothing geological contacts and identifying potentially unmapped leucogranite bodies. Following field work, samples would be prepared and analyzed following the procedures described in this research.

4.2.3 Analysis of melt inclusions hosted in Long Lake prospect greisen

During petrographic work, attention was drawn to the abundance of easy–to–find large silicate melt inclusions hosted by a Mo–quartz feldspar pegmatite from the Long Lake prospect that is also inundated with aqueous fluid inclusions (Fig. 4.2). Quartz-hosted fluid inclusions and silicate melt inclusions are commonly considered to preserve the composition of hydrothermal fluids and evolved silicate melts, providing therefore an opportunity to characterize natural processes that are potentially associated with mineralization. Although problems exist with the conclusions drawn from such analysis (e.g., Zajacz *et al*., 2009), to find coexisting fluid and melt inclusions hosted in a single sample compels one to consider further studies that may help to answer basic questions about mineralisation associated with an intrusive (*i.e*., granitic) system. For example, in a study of fluid and melt inclusions associated with granitic intrusions in New Mexico, United States, Audédat & Pettke (2003) demonstrated that the extraction of metals from a felsic hydrous magma is linked to the salinity of the associated hydrothermal fluid. This conclusion is based on analysis of individual fluid and melt inclusions hosted by quartz. The equipment required for melt inclusion analysis (e.g., high–temperature stage mounted on a petrographic microscope) is locally available at the Saint Mary's MOEFL. To date, mounds hosted by the Mo-pegmatite from Long Lake have high Ca contents relative to samples collected from barren parts of the SMB and are devoid of F. On the other hand, consistent detection of F in quartz–hosted fluid inclusion in the Long Lake greisen that hosts the pegmatite suggests the occurrence of multiple hydrothermal events. The\is begs the question of what would the analysis of coexisting fluid and melt inclusions tell us about Mo mineralisation at the Long Lake prospect'?

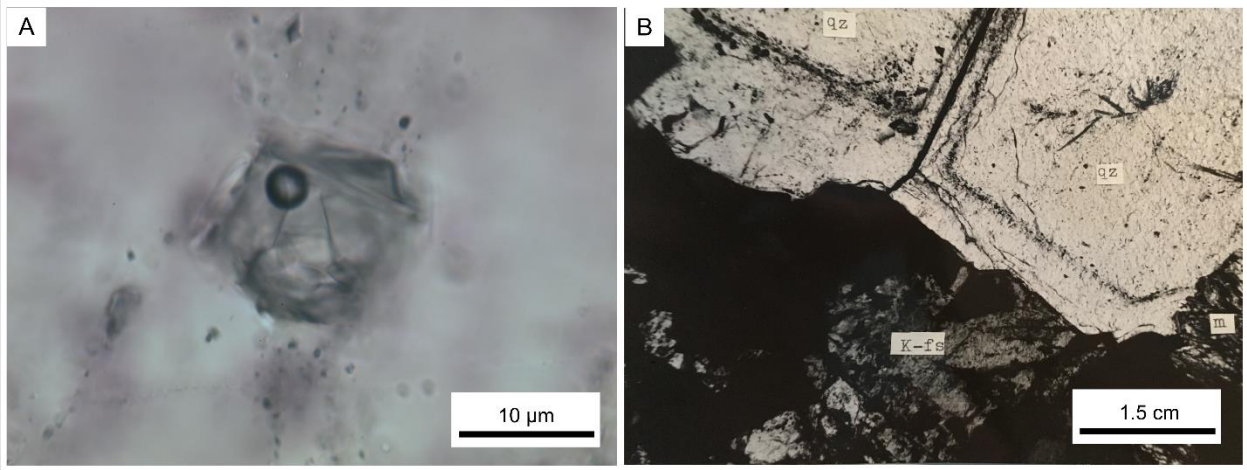

Figure 4.2: Transmitted light photomicrographs of melt and fluid inclusions hosted in quartz from the New Ross pluton. (A) Silicate melt inclusion hosted in Long Lake greisen. (B) Fluid inclusion assemblage trapped within a growth zone of quartz from the Turner tin prospect (copied without permission from Farley 1978)

4.2.4 Analysis of SMB quartz–hosted primary fluid inclusions.

The Turner tin prospect is hosted within leucomonzogranites of the New Ross pluton and documented cases report the occurrence of quartz–hosted fluid inclusions confined to outer growth zones of individual grains (Farley 1978). Primary fluid inclusions were not recognized in the present study; however, if primary inclusions associated with mineralisation can be identified and prepared for analysis, EMA work could constrain the bulk composition of the potentially mineralising fluid.

4.3 Conclusions

1. For application of the EMA technique to exploration research in the SMB, we recommend: (i) rapid (i.e., 50°C/min), stage heating to 500°C to avoid volatilisation of F and Cl; (ii) collection of EDS spectra from 16 mounds/chip, which provides a representative data set at the chip–scale; (iii) a minimum of two chips per sample should be studied to evaluate wafer–scale variation in fluid inclusion abundance and chemistry (iv) a minimum 60–second acquisition time is adequate for detection of all major and minor solute elements typically encountered; (v) charge–balance assessment ($\sum \frac{Cx^{n+}}{Mx^{n+}} * n - \sum \frac{Cx^{n+}}{Mx^{n+}} * n$) of mounds needs to be applied in order to assess quality of data. However, we do not specify a threshold charge–imbalance limit by which an analysis may deemed as acceptable or not. Near–zero charge imbalances are rare, and so as internal consistency within the data set must also be considered
2. Evaporate mounds are discrete sub–spherical salt residues that are morphologically, but not necessarily chemically, distinguished from other salt residues, including salt flats, giant mounds and elongate channels infilling polishing cracks, which are not analysed.
3. Major solute elements of fluid inclusions hosted by SMB quartz are Cl^{-}, Na^{+}, Ca^{2+}, K^{+} and F^{-}.
4. Minor solute elements of fluid inclusions hosted by SMB quartz include S^{2-}, Mn^{2+}, Fe^{2+}, Zn^{2+}, Al^{3+}, Pb^{2+}, Mg^{2+}, Sn^{2+} and Cu^{2+}.
5. Six types of evaporate mounds (Section 3.2.2.) represent six types of hydrothermal fluids. These include, in order of decreasing abundance: (1) a Na–Ca–Cl fluid, represented by evaporate mounds with average Ca/(Ca+ Na) = 0.37, ±0.12, 1σ; (2) a Na–Cl±Ca fluid, represented by mounds with average Ca/(Ca+Na) = 0.12, ±0.05, 1σ; (3) a NaCl fluid,

represented by mounds with average (Ca+K)/(Ca+K+Na) = 0.01 ±0.03, 1σ; (4) a Na–F–Cl±Ca fluid, represented by mounds with average (Ca/(Ca+Na) = 0.14 ±0.05, 1σ, and average F/(F+Cl) = 0.47, ±0.18, 1σ; (5) a Na–Ca–F–Cl fluid, represented by mounds with average (Ca/(Ca+Na) = 0.37 ±0.12, 1σ, and average F(F+Cl) = 0.58, ±0.20, 1σ; and (6) a Na–K–Cl fluid, represented by mounds average K/(K + Na) = 0.45, ±0.20, 1σ. There is no apparent relationship between hydrothermal alteration of primary granitoid minerals and the chemistry of locally preserved fluid inclusions

6. With exception of and apparent coupling between muscovite modal abundance and Na–K–Cl evaporate mound occurrence, fluid inclusion chemistry and local alteration of primary minerals are decoupled, suggesting that the solute chemistry of fluid inclusions is the product of fluid:rock interaction that has occurred elsewhere (*i.e.*, not locally).

4.4. References

AUDÉTAT, A. & PETTKE, T. 2003. The magmatic–hydrothermal evolution of two barren granites: a melt and fluid inclusion study of the Rio del Medio and Canada Pinabete plutons of northern New Mexico (USA). Geochimica et Cosmochimica Acta 67, 1739–1760.

CLARKE, D.B., MACDONALD, M.A., REYNOLDS, P.H., & LONGSTAFFE, F.J. 1993. Leucogranites from the Eastern Part of the South Mountain Batholith, Nova Scotia. Journal of Petrology 34, 653–679.

FARLEY, E.J. 1979. Mineralisation at the Turner and Walker deposits, South Mountain Batholith. Unpublished MSc. Thesis, Dalhousie University, Halifax, Nova Scotia.

HAYNES, F.M. & KESLER, S.E. 1987. Fluid inclusion chemistry in the exploration for Mississippi Valley–type deposits: an example from East Tennessee, U.S.A. Applied Geochemistry 2, 321–327.

HAYNES, F.M., STERNER, S.M., & BODNAR, R.J. 1988. Synthetic fluid inclusions in natural quartz. IV. Chemical analyses of fluid inclusions by SEM/EDA: Evaluation of method. Geochimica et Cosmochimica Acta 52, 969–977.

KONTAK, D.J. 1990. The East Kemptville Topaz–Muscovite Leucogranite, Nova Scotia I, Geological Setting and Whole–Rock Geochemistry. Canadian Mineralogist 28, 787–825.

LOGOTHETIS J. 1985. Economic geology of the New Ross – Vaughan Complex. *In* Guide to the Granites and Mineral Deposits of Southwestern Nova Scotia. (A.K. Chatterjee & D.B. Clarke, eds.). Nova Scotia Department of Mines and Energy, Paper 85–3, Halifax, Canada (41 – 62).

McCuish, K. L. 2001. Schlieren in the South Mountain Batholith and Port Mouton Pluton Meguma Zone, Nova Scotia.

O'Reilly, G.A., Farley, E.J., & Charest, M.H. 1982. Metasomatic–Hydrothermal Mineral Deposits of the New Ross–Mahone Bay Area, Nova Scotia. Nova Scotia Department of Mines and Energy, Paper 82–2, 15–21.

Oreskes, N. & Einaudi, M. T. 1992. Origin of Hydrothermal Fluids at Olympic Dam: Preliminary Results from Fluid Inclusions and Stable Isotopes. Economic Geology 87, 64–90.

Zajacz, Z., Halter, W.E., Pettke, T., & Guillong, M. 2008. Determination of fluid/melt partition coefficients by La–ICPMS analysis of co–existing fluid and silicate melt inclusions: controls on element partitioning. Geochimica et Cosmochimica Acta 72, 2169–2197.

Zajacz, Z., Hanley, J.J., Heinrich, C.A., Halter, W.E., & Guillong, M. 2009. Diffusive reequilibration of quartz–hosted silicate melt and fluid inclusion: are all metal concentrations unmodified? Geochimica et Cosmochimca Acta 73, 3013–3027.

Appendix A

Table A 1. Composition of synthetic $NaCl/CaF_2$ powders.

Table A1

Composition of synthetic powders.

$Nacl/CaF_2$	NaCl	CaF2	NaCl (mg)	CaF_2 (mg)	Total weight	%NaCl	%CaF2	wt. %Na	wt. %Cl	wt. %Ca	wt. %F	TOTAL
95/5	95.00	5.00	189.00	10.90	199.90	94.55	5.45	37.10	57.45	2.80	2.65	100.00
75/25	75.00	25.00	148.00	47.90	195.90	75.55	24.45	29.65	45.90	12.55	11.90	100.00
50/50	50.00	50.00	105.00	80.10	185.10	56.73	43.27	22.26	34.47	22.21	21.06	100.00
100	0.00	100.00			100.00	0.00	100.00	0.00	0.00	51.33	48.67	100.00

Table A 2. EDS analysis of $NaCl/CaF_2$ synthetic powders.

Table A2

EDS analysis of synthetic powders.

Ratio NaCl/CaF2	Sample	Normalized weight %			
		Na	Cl	Ca	F
100/0	1	37.32	62.68	0	0
	2	39.56	60.44	0	0
	3	37.76	62.24	0	0
	Average	38.21	61.79	0.00	0.00
	STD	0.97	0.97	0.00	0.00
	RSTD	2.54	1.57	0.00	0.00

Ratio NaCl/CaF2	Sample	Normalized weight %			
		Na	Cl	Ca	F
50/50	1	24.3	26.42	18.41	30.87
	2	24.53	25.83	18.44	31.2
	3	24.06	26.55	18.68	30.71
	4	24.59	27.21	18.24	29.96
	Average	24.37	26.5025	18.4425	30.685
	STD	0.21	0.49	0.16	0.45
	RSTD	0.86	1.85	0.85	1.48

Ratio NaCl/CaF2	Sample	Normalized weight %			
		Na	Cl	Ca	F
90/10	1	33.66	52.88	5.25	8.21
	2	34.15	52.29	5.44	8.13
	3	35.08	51.27	5.11	8.53
	4	35.68	50.71	4.99	8.63
	Average	34.64	51.79	5.20	8.38
	STD	0.79	0.85	0.17	0.21
	RSTD	2.27	1.64	3.22	2.51

Ratio NaCl/CaF2	Sample	Normalized weight %			
		Na	Cl	Ca	F
40/60	1	20	21.5	23.09	35.41
	2	20.86	20.55	21.67	36.92
	3	20.85	20.8	21.6	36.74
	4	20.95	21.26	21.67	36.13
	Average	20.67	21.0275	22.0075	36.3
	STD	0.39	0.37	0.63	0.59
	RSTD	1.87	1.77	2.84	1.63

Ratio NaCl/CaF2	Sample	Normalized weight %			
		Na	Cl	Ca	F
80/20	1	32.31	46.07	8.32	13.29
	2	33.7	45.05	8.04	13.21
	3	34.13	45.33	7.69	12.86
	4	34.34	44.61	7.74	13.3
	Average	33.62	45.265	7.9475	13.165
	STD	0.79	0.53	0.25	0.18
	RSTD	2.35	1.17	3.19	1.36

Ratio NaCl/CaF2	Sample	Normalized weight %			
		Na	Cl	Ca	F
25/75	1	14.18	14.21	28.71	42.9
	2	14.58	13.11	26.59	45.73
	3	14.97	13.31	26.36	45.37
	4	14.33	14.57	28.65	42.45
	Average	14.52	13.80	27.58	44.11
	STD	0.30	0.61	1.11	1.45
	RSTD	2.06	4.40	4.01	3.29

Ratio NaCl/CaF2	Sample	Normalized weight %			
		Na	Cl	Ca	F
70/30	1	31.12	36.88	11.49	20.51
	2	31.53	36.21	11.31	20.95
	3	31.69	36.85	11.04	20.43
	4	30.87	37.58	11.63	19.92
	Average	31.30	36.88	11.37	20.45
	STD	0.32	0.48	0.22	0.37
	RSTD	1.04	1.31	1.94	1.79

Ratio NaCl/CaF2	Sample	Normalized weight %			
		Na	Cl	Ca	F
0/100	1	0	0	38.59	59.41
	2	0	0	38.26	59.67
	3	0	0	37.82	60.18
	4	0	0	37.41	60.53
	Average	0	0	38.02	59.9475
	STD	0.00	0.00	0.45	0.44
	RSTD	0.00	0.00	1.17	0.73

Ratio NaCl/CaF2	Sample	Normalized weight %			
		Na	Cl	Ca	F
60/40	1	27.56	33.08	14.83	24.53
	2	28.3	33.46	14.51	23.74
	3	28.8	33.49	14.09	23.62
	4	28.63	33.44	14.2	23.72
	Average	28.32	33.37	14.41	23.90
	STD	0.48	0.17	0.29	0.37
	RSTD	1.68	0.50	2.00	1.53

Table A 3. EDS data (weight percent) for repeat analysis of a single evaporate mound.

Table A3

Normalized EDS data from the repeat analysis of single decrepitate mound used in the assessment of EDS instrument precision.

Spectrum	F	Na	Cl	K	Ca	Total
	weight percent of mound total					
1	36.52	19.28	31.43	0.52	12.26	100.00
2	36.39	19.44	31.23	0.56	12.39	100.00
3	36.63	19.29	31.12		12.37	100.00
4	36.52	19.2	31.84		12.44	100.00
5	36.6	19.47	31.1	0.43	12.39	100.00
6	35.98	19.22	31.87	0.48	12.45	100.00
7	35.8	19.28	31.86	0.53	12.53	100.00
8	36.23	19.51	31.41	0.52	12.33	100.00
9	36.47	19.36	31.92		12.24	100.00
10	36.32	19.52	31.56		12.6	100.00
11	36.22	19.15	31.58	0.64	12.41	100.00
12	36.65	19.46	31.66		12.23	100.00
13	36.42	19.32	31.42	0.46	12.37	100.00
14	36.47	19.2	31.93		12.4	100.00
15	36.29	19.36	31.5	0.6	12.24	100.00
16	37.03	19.43	30.73	0.53	12.28	100.00
minimum	35.80	19.15	30.73	0.43	12.23	
maximum	37.03	19.52	31.93	0.64	12.60	
average	36.41	19.34	31.51	0.53	12.37	
standard deviation	0.28	0.12	0.34	0.06	0.11	
realitve standard deviation	0.78	0.61	1.09	11.90	0.86	

Table A 4. Corrected EDS data (weight percent) for mounds composing 1 – 20 wt. % F.

TableA4

Corrected EDS data for mounds contaning detectable (1 - 20 wt. % (uncorrected)) fluorine.

	Sample	Mound size (µm)	F	Fcorr	Na	Nacorr	Cl	Clcorr	K	Ca	Cacorr	V	Cr	Mn	Fe	Cu	Zn	Br	Mo	In	Sn	Pb	Total	Σdiff%	Σdiff%corr	Ca/Na	Ca/Nacorr
1	A03-3014		12.15	8.92	48.1	50.03	36.74	40.58	0.58	2.43	2.95												100	14.14	18.32	0.03	0.03
2	A04-1807-3	7	6.06	3.59	40.69	39.62	49.23	49.49	1.79	2.23	2.64												100	6.03	9.06	0.03	0.04
3	A04-1807-3	10	4.6	2.32	35.91	33.42	50.8	50.42	8.14	0.55	0.03												100	3.52	3.70	0.01	0.00
4	A04-1807-3	10	9.71	6.78	38.46	36.68	44.95	46.73	4.36	1.72	1.85			0.8									100	3.26	4.37	0.03	0.03
5	A04-1807-3	12	8.94	6.11	37.26	35.13	46.13	47.52	4.79	1.81	1.99			1.08									100	2.77	3.69	0.03	0.03
6	A04-1807-3	8	9.16	6.30	37.01	34.81	46.11	47.50	5.05	1.76	1.91			0.92									100	2.12	2.92	0.03	0.03
7	A04-1807-3	20	8.39	5.63	36.93	34.71	47.56	48.45	4.96	1.49	1.49			0.67									100	1.34	2.14	0.02	0.02
8	A04-1807-3	10	12	8.79	38.22	36.37	43.91	46.01	2.89	2.98	3.81												100	0.39	2.37	0.04	0.06
9	A04-1807-3	10	16.58	12.81	34.29	31.42	41.49	44.27	3.19	3.38	4.43			1.06									100	-6.88	-5.94	0.06	0.08
10	A05-0001		10.43	7.41	39.15	37.58	36.28	40.20	0.99	13.16	19.48												100	20.53	26.65	0.19	0.30
11	A09-2155		17.03	13.21	20.33	16.06	27	31.83	21.77	3.24	4.21				0.76	0.98							100	15.45	14.41	0.09	0.15
12	A09-2155		15.85	12.17	43.23	43.08	35.23	39.32	4.21	1.48	1.48												100	6.00	8.02	0.02	0.02
13	A09-2155		15.85	12.17	43.23	43.08	35.23	39.32	4.21	1.48	1.48												100	6.00	8.02	0.02	0.02
14	A09-2370_s	24	11.16	8.05	32.46	29.21	43.77	45.91		12.61	18.64												100	5.66	12.28	0.22	0.37
15	A09-2384		17.05	13.22	47.47	49.10	33.62	37.95		1.86	2.07												100	7.78	11.79	0.02	0.02
16	A09-2384		17.05	13.22	47.47	49.10	33.62	37.95		1.86	2.07												100	7.78	11.79	0.02	0.02
17	A09-2707-4		16.82	13.02	48.03	49.92	32.7	37.14	0.36	1.7	1.82				0.39								100	9.71	13.74	0.02	0.02
18	A09-2707-4		17.73	13.82	48.33	50.37	32.07	36.58	0.45	1.42	1.38												100	8.61	12.69	0.02	0.02
19	A09-2707-4		17.3	13.44	47.4	49.00	33.24	37.61	0.34	1.73	1.87												100	7.69	11.60	0.02	0.02
20	A09-2707-4		18.89	14.85	44.16	44.37	34.05	38.32	0.19	2.7	3.37												100	2.62	6.07	0.04	0.04
21	A09-Tar 16b		15.38	11.75	43.99	44.13	34.43	38.64		6.19	8.78												100	11.02	15.95	0.08	0.11
22	A09-Tar 16b		12.52	9.24	43.53	43.49	38.26	41.80	0.69	4.99	6.93												100	10.81	15.03	0.07	0.09
23	A09-Tar 16b		12.59	9.30	36.29	33.90	39.24	42.57		11.88	17.52												100	10.19	16.30	0.19	0.30
24	A11-2286	10	8.55	5.77	44.55	44.92	36.2	40.13	2.35	8.36	12.12												100	24.28	29.18	0.11	0.15
25	A12-8007	11	10.86	7.79	30.44	26.83	42.1	44.72		16.61	24.72												100	10.06	17.91	0.31	0.53
26	A14-1017	9	7.73	5.05	32.19	28.88	38.09	41.66		21.99	32.83												100	25.53	33.52	0.39	0.65
27	A14-1017	13	19.71	15.57	28.14	24.22	27.89	32.69		24.26	36.23												100	14.32	24.31	0.49	0.86
28	A14-1017	14	19.64	15.51	24.33	20.10	33.45	37.80		22.57	33.70												100	4.97	15.17	0.53	0.96
29	A15-Tar 23		19.07	15.00	28.65	24.79	26.97	31.80		25.31	37.79												100	17.41	27.46	0.51	0.87
30	A15-Tar 23		16.19	12.47	37.54	35.49	31.92	36.44		14.35	21.29												100	14.53	21.48	0.22	0.34
31	A16-1281		13.66	10.24	44.28	44.54	34.51	38.71		6.86	9.81												100	13.30	18.35	0.09	0.13
32	A16-1281		13.39	10.01	46.23	47.31	32.74	37.18		4.75	6.55			0.94									100	13.19	17.54	0.06	0.08
33	A16-1281		16.3	12.56	47.49	49.13	33.08	37.47		2.05	2.36	1.07											100	10.46	14.40	0.02	0.03
34	A16-1281		12.68	9.38	43.45	43.38	37.98	41.58		4.94	6.85												100	8.58	12.69	0.07	0.09
35	A16-1281		14.36	10.86	43.86	43.95	37.72	41.37		3.32	4.34												100	5.26	8.77	0.04	0.06
36	A16-1281		17.75	13.84	41.05	40.10	36.54	40.41		4.07	5.50												100	-0.36	2.87	0.06	0.08
37	A16-Tar 17		4.81	2.51	39.52	38.07	49.12	49.42		6.55	9.34												100	11.04	16.33	0.10	0.14
38	A16-Tar 17		4.81	2.51	39.52	38.07	49.12	49.42		6.55	9.34												100	11.04	16.33	0.10	0.14
39	A16-Tar 17		5.95	3.50	33.5	30.46	49.55	49.68	0.49	10.51	15.43												100	7.64	14.12	0.18	0.29
40	A16-Tar 17		5.95	3.50	33.5	30.46	49.55	49.68	0.49	10.51	15.43												100	7.64	14.12	0.18	0.29
41	A16-Tar 17		11.1	8.00	33.21	30.10	42.5	45.01	1.09	12.1	17.86												100	7.59	13.72	0.21	0.34
42	A16-Tar 17		11.1	8.00	33.21	30.10	42.5	45.01	1.09	12.1	17.86												100	7.59	13.72	0.21	0.34
43	A16-Tar 17		10.94	7.86	38.91	37.27	42.33	44.88	1.17	6.65	9.49												100	7.43	11.68	0.10	0.15
44	A16-Tar 17		10.94	7.86	38.91	37.27	42.33	44.88	1.17	6.65	9.49												100	7.43	11.68	0.10	0.15
45	A16-Tar 17		6.06	3.59	36.9	34.67	49.29	49.52	0.41	7.33	10.54												100	7.36	12.62	0.11	0.17
46	A16-Tar 17		6.06	3.59	36.9	34.67	49.29	49.52	0.41	7.33	10.54												100	7.36	12.62	0.11	0.17
47	A16-Tar 17		9.45	6.55	36.46	34.12	46.23	47.58	1.12	6.74	9.63												100	3.98	8.31	0.11	0.16
48	A16-Tar 17		9.45	6.55	36.46	34.12	46.23	47.58	1.12	6.74	9.63												100	3.98	8.31	0.11	0.16
49	A16-Tar 18c		9.81	6.87	41.33	40.48	37.21	40.96		11.65	17.17												100	20.60	26.62	0.16	0.24
50	A16-Tar 18c		14.62	11.09	40.2	38.97	31.48	36.05	0.61	13.1	19.38												100	18.65	25.18	0.19	0.29
51	A16-Tar 18c		9.94	6.98	42.26	41.74	38.65	42.11		9.14	13.32												100	17.42	22.92	0.12	0.18
52	A16-Tar 18c		9.29	6.41	42.76	42.43	39.37	42.67	0.56	8.02	11.60												100	17.41	22.55	0.11	0.16
53	A16-Tar 8		13.83	10.39	38.56	36.81	36.55	40.42		10.4	15.26						0.66						100	11.50	17.08	0.15	0.24
54	A16-Tar 8		17.51	13.63	29.46	25.71	34.12	38.38		18.5	27.58						0.4						100	8.10	16.40	0.36	0.62
55	A16-Tar 8.5		12.94	9.61	47.84	49.65	36.61	40.47		2.61	3.23												100	12.66	16.96	0.03	0.04
56	A16-Tar 8.5		15.34	11.72	43.81	43.88	34.17	38.42		5.04	7.00						1.64						100	10.95	15.15	0.07	0.09
57	A16-Tar 8.5		18.56	14.55	30.76	27.21	32.33	36.81		17.76	26.46						0.59						100	8.54	16.57	0.33	0.56
58	D12-0095		18.98	14.93	45.58	46.38	30.21	34.89		5.23	7.30												100	9.57	14.73	0.07	0.09
59	D12-0095		17.89	13.96	41.91	41.27	36.35	40.26		3.85	5.16												100	1.20	4.63	0.05	0.07
60	D12-2707-6		11.49	8.34	33.92	30.97	38.95	42.34		10.18	14.92			0.21	1.3		2.26						100	14.78	19.06	0.17	0.28
61	D12-2707-6		17.12	13.29	40.22	38.99	30.51	35.16	0.79	6.4	9.10						4.95						100	11.95	15.71	0.09	0.13
62	D12-2707-6		14.69	11.15	43.54	43.51	34.2	38.45	0.67	3.53	4.66						3.38						100	11.51	14.65	0.05	0.06
63	D12-2707-6		16.09	12.38	41.42	40.60	32.59	37.04	0.75	6.15	8.72						3						100	11.36	15.35	0.09	0.12
64	D12-2707-6		17.27	13.42	38.61	36.87	31.64	36.19	1.38	6.56	9.35						4.54						100	9.52	13.02	0.10	0.15
65	D12-3060		19.72	15.58	43.21	43.05	30.03	34.72		5.73	8.07												100	4.80	9.47	0.08	0.11
66	D12-Tar 14c		13.78	10.35	39.05	37.45	30.78	35.41		16.39	24.39												100	22.44	29.66	0.24	0.37
67	D12-Tar 14c		6.97	4.39	30.44	26.83	41.01	43.91		21.59	32.23												100	22.36	30.76	0.41	0.69

Table A 4 (cont.)

68	D12-Tar 14c		4.77	2.47	41.29	40.43	46.24	47.59		6.55	9.34								100	18.26	23.00	0.09	0.13
69	D12-Tar 14c		5.1	2.76	33.42	30.36	44.28	46.27	0.43	15.12	22.46				1.47				100	17.86	24.75	0.26	0.42
70	D12-Tar 5p		18.14	14.18	47.53	49.19	30.2	34.88		4.13	5.59								100	11.43	16.58	0.05	0.07
71	D12-Tar 5p		19.75	15.60	44.77	45.23	30.1	34.78	0.41	4.97	6.89								100	7.74	12.58	0.06	0.09
72	D12-Tar 5p		17.53	13.65	43.05	42.83	34.96	39.10		4.46	6.10								100	4.64	8.68	0.06	0.08
73	D12-Tar 5p		19.69	15.55	42.97	42.72	32.59	37.04		4.75	6.55								100	3.69	7.94	0.06	0.09
74	D13-smb2	23	5.77	3.34	35.75	33.22	44.92	46.70	1.43	11.36	16.73								100	14.30	20.11	0.18	0.29
75	D13-smb2	24	7.53	4.88	24.69	20.48	49.22	49.48	0.96	17.6	26.22								100	5.10	14.73	0.41	0.73
76	D13-smb2	16	8.28	5.53	31.23	27.75	48.3	48.91		12.18	17.98								100	4.46	11.48	0.22	0.37
77	D13-smb2	26	6.56	4.03	36.27	33.88	50.66	50.34	0.54	5.22	7.28	0.74							100	2.86	6.99	0.08	0.12
78	D13-Tar 14d		17.74	13.83	35.54	32.96	28.54	33.32		15.71	23.35					2.47			100	15.58	22.75	0.25	0.41
79	D13-Tar 14d		19.76	15.61	27.6	23.62	26.04	30.88		24.57	36.69								100	12.13	22.20	0.51	0.89
80	D12-3037-c		18.51	14.51	44.58	44.96	30.97	35.59		5.95	8.41								100	9.49	14.66	0.08	0.11
81	D12-3037-c		19.03	14.97	48.01	49.89	30.33	35.00		2.64	3.28								100	8.89	13.59	0.03	0.04
82	A09-2707-4	14	19.97	15.80	43.99	44.13	29.29	34.03		4.39	6.00	0.47	0.59			1.31			100	7.86	12.09	0.06	0.08
83	A09-Ilgre1	13	12.4	9.14	39.88	38.54	43.25	45.54		2.92	3.72	1.54							100	1.67	4.13	0.04	0.06
84	A09-Ilgre1	20	14.12	10.65	29.63	25.90	42.34	44.89	0.37	13.03	19.28	0.51							100	0.75	7.35	0.25	0.43
85	A09-Ilgre1	23	8.25	5.51	39.54	38.09	49.45	49.62		2.09	2.43	0.67							100	0.52	3.23	0.03	0.04
86	A09-Ilgre1	20	15	11.42	34.87	32.13	41.35	44.17		8.78	12.77								100	-0.04	4.83	0.14	0.23
87	A09-Ilgre1	9	11.48	8.33	36.37	34.00	45.77	47.28	0.43	5.59	7.85	0.36							100	-0.28	3.34	0.09	0.13
88	A09-Ilgre1	21	11.81	8.62	25.37	21.20	47.04	48.11	0.41	14.84	22.03	0.53							100	-1.96	6.22	0.34	0.60
89	A09-Ilgre1	17	15.74	12.07	28.39	24.50	41.99	44.64	0.35	12.68	18.74	0.85							100	-2.70	3.71	0.26	0.44
90	A09-Ilgre1	20	19.94	15.77	25.09	20.90	37.24	40.98		17.31	25.78	0.42							100	-3.20	5.34	0.40	0.71
91	A09-Ilgre1	17	16.54	12.78	23.53	19.27	42.59	45.07	0.51	15.53	23.08	1.3							100	-5.43	2.66	0.38	0.69
92	A09-Ilgre1	12	17.71	13.81	31.13	27.64	41.58	44.34		9.58	14.00								100	-6.94	-1.98	0.18	0.29
93	A09-Tar 9a		13.98	10.52	43.79	43.85	37.94	41.54	0.53	3.76	5.02								100	7.66	11.43	0.05	0.07
94	A15-Tar 20b		10.41	7.39	46.17	47.22	37.2	40.95		6.22	8.83								100	18.41	23.52	0.08	0.11
95	A16-Tar10.75		14.46	10.95	45.69	46.53	36.27	40.19		3.57	4.73								100	9.64	13.85	0.04	0.06
96	A16-Tar10.75		17.17	13.33	46.69	47.97	33.49	37.83		2.64	3.28								100	7.82	11.97	0.03	0.04
97	D05-smb4	24	7.8	5.11	25.52	21.36	40.8	43.76		25.88	38.64								100	21.19	31.05	0.58	1.04
98	D05-smb4	40	8.6	5.81	25.89	21.76	40.78	43.74		24.73	36.93								100	19.10	28.86	0.55	0.97
99	D05-smb4	30	14.78	11.23	29.25	25.47	32.64	37.09		23.34	34.85								100	17.84	26.98	0.46	0.78
100	D05-smb4	32	7.45	4.81	27.05	23.02	43.82	45.95		21.68	32.36								100	16.21	25.62	0.46	0.81
101	D05-smb4	14	12.55	9.27	31.38	27.93	37.17	40.93		18.91	28.20								100	14.91	22.96	0.35	0.58
102	D05-smb4	17	11.76	8.58	28.45	24.57	42.07	44.70		13.69	20.28								100	13.48	19.25	0.28	0.47
103	D05-smb4	18	7	4.41	36.48	34.14	45.13	46.85		8.54	12.40							2.83	100	10.83	15.67	0.13	0.21
104	D05-smb4	39	6.08	3.61	30.53	26.94	49.27	49.51		14.13	20.95								100	8.63	16.57	0.27	0.45
105	D05-smb4	30	10.1	7.12	28.23	24.32	44.1	46.14		17.57	26.17								100	8.47	17.01	0.36	0.62
106	D05-smb4	26	7.89	5.19	32.38	29.11	47.17	48.20		12.57	18.58								100	7.66	14.64	0.22	0.37
107	D05-smb4	12	11.07	7.97	30.99	27.47	43.49	45.71		14.45	21.44								100	6.69	13.98	0.27	0.45
108	D05-smb4	42	4.39	2.14	30.84	27.30	52.98	51.66		11.79	17.38								100	5.58	13.38	0.22	0.37
109	D05-smb4	20	10.73	7.67	32.16	28.85	44.67	46.53		11.45	16.86								100	2.16	8.20	0.20	0.34
110	D05-smb4	24	8.79	5.98	32.16	28.85	49.03	49.37		10.02	14.67								100	1.41	7.57	0.18	0.29
111	D12-0050	45	9.46	6.56	24.09	19.85	42.79	45.22		23.66	35.33								100	13.30	23.67	0.56	1.02
112	D12-0050	18	6.29	3.79	33.77	30.78	47.46	48.38	0.85	10.37	15.21								100	12.52	18.18	0.18	0.28
113	D12-0050	10	7.52	4.87	33.65	30.64	46.4	47.70	1.02	11.42	16.82								100	9.42	15.69	0.19	0.31
114	D12-0050	80	8.51	5.73	29.12	25.32	48.01	48.73	2.77	11.21	16.50	0.38							100	2.92	9.03	0.22	0.37
115	D12-0050	21	7.78	5.09	29.35	25.58	49.09	49.40	3.2	10.59	15.55								100	2.51	8.50	0.21	0.35
116	D12-0050	9	9.28	6.41	39.1	37.51	47.75	48.57	0.56	3.32	4.34								100	1.21	4.35	0.05	0.07
117	D12-0050	10	9.5	6.60	32.72	29.52	49.26	49.51	2.4	6.12	8.67								100	-2.71	0.97	0.11	0.17
118	D12-0050	25	6.68	4.13	30.84	27.30	54.24	52.33	1.8	6.44	9.17								100	-4.82	-0.09	0.12	0.19
119	D12-0066_2	16	7.33	4.70	29.4	25.64	48.64	49.12		14.63	21.71								100	6.66	14.76	0.29	0.49
120	D12-0066_2	21	9.62	6.70	26.61	22.54	47	48.09		16.76	24.95								100	4.22	13.11	0.36	0.63
121	D12-0066_2	20	13.54	10.14	30.59	27.01	44.55	46.45	0.3	11.03	16.22								100	-2.10	3.85	0.21	0.34
122	D12-0066_2	15	19.58	15.45	23.43	19.17	39.41	42.70	0.74	16.84	25.07								100	-6.57	2.07	0.41	0.75
123	D12-0066_2	8	15.27	11.66	28.23	24.32	45.03	46.78		11.47	16.89								100	-7.07	-0.85	0.23	0.40
124	D12-3136	12	17.96	14.03	30.21	26.57	36.72	40.56	4.11	10.99	16.16								100	-0.35	4.67	0.21	0.35
125	D12-Tar10.5		15.14	11.54	46.62	47.87	34.58	38.77		3.66	4.86								100	10.99	15.48	0.05	0.06
126	D12-Tar10.5		19.73	15.59	34.78	32.02	29.3	34.04		16.19	24.08								100	10.88	18.59	0.27	0.43
127	D12-Tar10.5		14.38	10.88	46.85	48.20	35.68	39.70		3.09	3.98								100	10.83	15.11	0.04	0.05
128	D12-Tar10.5		19.6	15.47	43.02	42.79	29.8	34.51		7.58	10.92								100	9.14	14.74	0.10	0.15
129	D12-Tar10.5		16.02	12.32	43.68	43.70	35.32	39.40		4.98	6.91								100	7.74	12.12	0.07	0.09
130	D12-Tar10.5		18.87	14.83	41.85	41.18	32.71	37.15		6.57	9.37								100	5.70	10.52	0.09	0.13
131	D12-Tar6		16.31	12.57	34	31.06	33.13	37.52		14.4	21.36								100	15.20	21.38	0.24	0.39
132	D12-Tar6		16.4	12.65	47.46	49.09	31.85	36.38		4.29	5.84								100	12.78	17.82	0.05	0.07
133	D12-Tar6		16.78	12.99	40.67	39.59	33.23	37.61		9.31	13.58								100	10.18	15.81	0.13	0.20
134	D12-Tar6		14.82	11.26	36.24	33.84	36.76	40.59		12.19	18.00								100	9.18	15.38	0.19	0.31
135	D12-Tar6		17.21	13.37	45.32	46.01	31.81	36.35		4.97	6.89								100	9.15	13.90	0.06	0.09
136	D12-Tar6		18.89	14.85	44.72	45.16	31.56	36.12		4.24	5.76								100	5.76	10.13	0.05	0.07

Table A 5. Corrected EDS data (weight percent) for mounds composing 21 – 40 wt. % F.

TableA5

Corrected EDS data for mounds contaning detectable (21 - 40 wt. % (uncorrected)) fluorine.

#	Sample	Mound size (µm)	F	Fcorr	Na	Nacorr	Mg	Al	P	S	Cl	Clcorr	K	Ca	Cacorr	V	Cr	Mn	Fe	Cu	Zn	Br	Mo	In	Sn	Pb	Total	Σdiff	Σdiff%	Σdiff	Σdiff%corr	Ca/Na	Ca/Nacorr
1	A03-3002-2		25.88	21.03	27.65	23.68					31.64	36.19		14.83	22.02											100	-0.31	-7.45	0.00	0.00	0.31	0.53
2	A03-3002-2		30.26	24.93	28.51	24.64					26.6	31.44	0.64	14	20.76											100	-0.39	-9.04	-0.08	-1.75	0.28	0.48
3	A04-1807-3	5.00	22.73	18.24	35.46	32.86					35.41	39.47	2.25	2.48	3.03		0.28	0.38	1.01							100.00	-0.41	-10.33	-0.37	-9.93	0.04	0.05
4	A04-1807-3	7	21.98	17.58	32.42	29.16					37.15	40.91	3.26	3.77	5.04			0.69	0.72							100	-0.47	-12.00	-0.43	-11.40	0.07	0.10
5	A04-1807-3	22	20.65	16.40	29.49	25.74					39.03	42.40	4.37	3.83	5.13			1.31	0.73		0.6					100	-0.51	-13.20	-0.48	-13.19	0.07	0.11
6	A04-1807-3	5	25.93	21.08	32.01	28.67					32.98	37.39	4.16	3.12	4.03			0.61	1.2							100	-0.58	-14.34	-0.54	-14.39	0.06	0.08
7	A04-1807-3	11	26.71	21.77	28.16	24.24					31.23	35.82	3.1	3.95	5.31			0.85	1.1			4.89				100	-0.78	-19.81	-0.75	-20.29	0.08	0.13
8	A04-1807-3	7	33.09	27.45	31.52	28.09					27.69	32.50	2.39	3.68	4.90			0.88	0.75							100	-0.85	-20.22	-0.78	-19.65	0.07	0.10
9	A04-1807-3	52	20.34	16.13	22.1	17.81					42.37	44.91	11.01	0.95	0.65			2.75	0.48							100	-0.86	-23.37	-0.91	-27.39	0.02	0.02
10	A06-3017		29.79	24.51	27.7	23.73					21.2	25.87	0.7	19.67	29.34						0.94					100	0.07	1.51	0.52	11.45	0.41	0.71
11	A06-3017		34.8	28.98	29.31	25.54					21.86	26.58		14.03	20.80											100	-0.47	-10.72	-0.13	-2.87	0.27	0.47
12	A06-3017		32.38	26.82	33.28	30.19					24.53	29.36	0.8	9.01	13.12											100	-0.48	-11.11	-0.25	-5.96	0.16	0.25
13	A06-3017		34.57	28.78	26.19	22.08					23.87	28.69	0.68	14.69	21.80											100	-0.60	-13.78	-0.26	-5.89	0.32	0.57
14	A09-2132		39.92	33.57	33.38	30.31	4.13				14.84	18.70		7.74	11.17											100	-0.34	-7.29	-0.08	-1.77	0.13	0.21
15	A09-2132		34.96	29.12	13.71	9.98					31.98	36.50	0.27	17.66	26.31						0.85				0.56	100	-1.23	-28.95	-0.78	-18.01	0.74	1.51
16	A09-2161		32.18	26.64	37.56	35.52					24.42	29.25		5.85	8.26											100	-0.46	-10.62	-0.27	-6.48	0.09	0.13
17	A09-2161		39.03	32.77	31.33	27.87					21.37	26.06		8.27	11.99											100	-0.88	-19.91	-0.65	-15.23	0.15	0.25
18	A09-2231		25.36	20.57	37.64	35.62					31.05	35.66		5.95	8.41											100	-0.28	-6.69	-0.12	-2.96	0.09	0.14
19	A09-2231		28.15	23.05	37.72	35.72					28.86	33.62		5.27	7.36											100	-0.39	-9.35	-0.24	-5.90	0.08	0.12
20	A09-2231		29.98	24.68	32.59	29.36					28.32	33.11		9.12	13.29											100	-0.50	-11.88	-0.29	-7.02	0.16	0.26
21	A09-2231		25.81	20.97	34.94	32.22					33.76	38.07		5.49	7.70											100	-0.52	-12.61	-0.39	-9.90	0.09	0.14
22	A09-2231		29.82	24.54	30.83	27.29					29.23	33.97		10.12	14.83											100	-0.55	-12.94	-0.32	-7.74	0.19	0.31
23	A09-2231		31.39	25.93	34.59	31.79					27.05	31.88		6.96	9.97											100	-0.56	-13.22	-0.38	-9.29	0.12	0.18
24	A09-2231		28.67	23.51	32.23	28.93					31.44	36.01		7.66	11.05											100	-0.61	-14.65	-0.44	-10.93	0.14	0.22
25	A09-2231		33.18	27.53	33.8	30.82					26.24	31.08		6.78	9.69											100	-0.68	-15.80	-0.50	-12.11	0.12	0.18
26	A09-2231		34.29	28.53	31.08	27.58					25.57	30.41		9.06	13.20											100	-0.72	-16.69	-0.50	-11.89	0.17	0.27
27	A09-2231		34.15	28.40	29.28	25.51					26.27	31.11		10.3	15.10											100	-0.75	-17.37	-0.51	-12.04	0.20	0.34
28	A09-2231		33.71	28.01	33.67	30.66					26.47	31.31		6.15	8.72											100	-0.75	-17.48	-0.59	-14.28	0.10	0.16
29	A09-2231		38.86	32.62	27.16	23.14					20.96	25.62		13.01	19.25											100	-0.81	-18.06	-0.47	-10.74	0.27	0.48
30	A09-2231		38.74	32.51	32.94	29.78					20.92	25.57		7.4	10.65											100	-0.83	-18.68	-0.61	-14.24	0.13	0.21
31	A09-2350		33.98	28.25	33.64	30.62					21.99	26.72	1.13	7.52	10.83				1.74							100	-0.48	-11.05	-0.28	-6.59	0.13	0.20
32	A09-2350		33.98	28.25	33.64	30.62					21.99	26.72	1.13	7.52	10.83				1.74							100	-0.48	-11.05	-0.28	-6.59	0.13	0.20
33	A09-2384		25.57	20.76	41.34	40.49					27.44	32.26		5.65	7.95											100	-0.04	-0.96	0.15	3.72	0.08	0.11
34	A09-2384		25.57	20.76	41.34	40.49					27.44	32.26		5.65	7.95											100	-0.04	-0.96	0.15	3.72	0.08	0.11
35	A09-2395		25.25	20.47	38	36.08					30.22	34.90	0.51	5.56	7.81				0.46							100	-0.22	-5.36	-0.07	-1.82	0.08	0.12
36	A09-2395		25.25	20.47	38	36.08					30.22	34.90	0.51	5.56	7.81				0.46							100	-0.22	-5.36	-0.07	-1.82	0.08	0.12
37	A09-2395		26.22	21.33	37.72	35.72					31.66	36.21	0.4	3.72	4.96				0.28							100	-0.43	-10.37	-0.32	-8.15	0.06	0.08
38	A09-2395		26.22	21.33	37.72	35.72					31.66	36.21	0.4	3.72	4.96				0.28							100	-0.43	-10.37	-0.32	-8.15	0.06	0.08
39	A09-2707-4		35.59	29.69	42.18	41.63					19.34	23.85		2.89	3.67											100	-0.44	-10.02	-0.24	-5.72	0.04	0.05
40	A09-Tar 16b		25.82	20.98	29.56	25.82					30.93	35.55		13.69	20.28											100	-0.26	-6.27	0.03	0.66	0.27	0.45
41	A10-3017	14	23.33	18.77	23.39	19.13					32.63	37.08		20.65	30.82											100.00	-0.10	-2.41	0.34	7.62	0.51	0.92
42	A10--3078		22.28	17.84	40.44	39.29					29.29	34.03		7.98	11.54											100	0.16	3.80	0.39	9.21	0.11	0.17
43	A10--3078		29.95	24.65	37.36	35.26					22.53	27.29		10.16	14.89											100	-0.08	-1.86	0.21	4.81	0.16	0.24
44	A10--3078		27.67	22.62	42.34	41.85					25.27	30.11		4.72	6.51											100	-0.09	-2.18	0.10	2.50	0.06	0.09
45	A10--3078		36.01	30.06	37.31	35.20					16.79	20.97		9.88	14.46											100	-0.25	-5.66	0.08	1.76	0.15	0.24
46	A10--3078		38.15	31.98	35.59	33.02					17.84	22.17		8.43	12.23											100	-0.54	-12.13	-0.26	-6.03	0.14	0.21
47	A10-3086		25.36	20.57	42.1	41.52					27.88	32.69		4.65	6.40											100	-0.06	-1.40	0.12	2.91	0.06	0.09
48	A10-3086		28.59	23.44	41.21	40.32					23.83	28.64		6.36	9.04											100	-0.07	-1.58	0.16	3.83	0.09	0.13
49	A10-3086		28.45	23.32	40.54	39.42					24.27	29.10	0.79	5.95	8.41											100	-0.10	-2.40	0.11	2.52	0.08	0.12
50	A10-3086		25.41	20.61	41.49	40.70					28.51	33.29		4.58	6.29											100	-0.11	-2.61	0.06	1.45	0.06	0.09
51	A10-3086		36.08	30.13	34.8	32.04					20.8	25.44		8.32	12.06											100	-0.56	-12.63	-0.31	-7.17	0.14	0.22
52	A10-3100	24	20.08	15.90	26.18	22.07					31.38	35.96		22.35	33.37											100	0.31	7.42	0.77	17.29	0.49	0.87
53	A10-3100	17	23.88	19.26	25.8	21.66					32.32	36.80	0.31	16.86	25.10			0.83								100	-0.17	-4.02	0.18	4.21	0.37	0.66
54	A10-3100	16	25.37	20.58	17.74	13.59					31.69	36.24	1.25	23.66	35.33			0.28								100	-0.24	-5.57	0.29	6.45	0.77	1.49
55	A10-3100	30	22.17	17.74	23.82	19.57					35.78	39.78		18.23	27.17											100	-0.23	-5.60	0.15	3.53	0.44	0.80
56	A10-3100	8	21.32	16.99	21.09	16.80					37.64	41.30	0.5	18.46	27.52			0.59	0.39							100	-0.30	-7.31	0.09	2.19	0.50	0.94
57	A10-3100	25	31.71	26.22	17.33	13.21					28.43	33.21	0.48	22.05	32.92											100	-0.61	-13.95	-0.09	-1.94	0.73	1.43
58	A12-1021		25.36	20.57	43.86	43.95					27.76	32.57		3.02	3.87											100	-0.06	-1.44	0.10	2.51	0.04	0.05
59	A14-1017	21	20.3	16.09	24.29	20.06					33.61	37.94		21.8	32.54											100	0.13	3.06	0.58	13.12	0.51	0.93
60	A14-1017	21	26.46	21.55	20.24	15.97					28.24	33.03		25.06	37.42											100	-0.06	-1.37	0.50	10.71	0.71	1.34
61	A14-1017	14	24.51	19.82	21.87	17.58					30.82	35.45		22.8	34.04											100	-0.07	-1.67	0.42	9.32	0.60	1.11
62	A14-1017	23	32.03	26.51	17.66	13.51					26.71	31.55	0.65	22.96	34.28											100	-0.51	-11.66	0.03	0.64	0.75	1.46
63	A14-1017	18	35.95	30.01	19.01	14.78					21.73	26.44	0.51	22.8	34.04											100	-0.53	-11.78	0.03	0.61	0.69	1.32
64	A15-Tar 23		20.47	16.24	37.16	35.01					25.76	30.60		16.61	24.72											100	0.64	15.07	1.04	23.19	0.26	0.41
65	A15-Tar 23		25.61	20.79	30.46	26.86					23.58	28.39		20.35	30.37											100	0.33	7.50	0.79	17.21	0.38	0.65
66	A16-1224		21.2	16.89	43.93	44.05					31.74	36.28		3.13	4.04											100	0.06	1.36	0.21	5.09	0.04	0.05
67	A16-1224		35.08	29.23	41.62	40.87					19.7	24.24		3.6	4.77											100	-0.41	-9.40	-0.21	-4.89	0.05	0.07

Table A 5 (cont.)

68	A16-1281		20.9	16.62	44.23	44.47			1.28	28.53	33.31		5.07	7.05											100	0.19	4.61	0.39	9.36	0.07	0.09
69	A16-1281		23.29	18.73	39.5	38.04			1.58	27.26	32.08		8.38	12.16											100	0.04	1.00	0.27	6.38	0.12	0.18
70	A16-1281		25.25	20.47	40.18	38.94			1.17	26.42	31.26		6.99	10.01											100	-0.05	-1.21	0.16	3.80	0.10	0.15
71	A16-1281		36.71	30.69	27.19	23.17		2.44	1.25	19.19	23.68	0.36	11.38	16.76			1.48								100	-0.47	-10.09	-0.18	-4.06	0.24	0.41
72	A16-Tar 8		32.2	26.66	31.33	27.87				19.96	24.53		14.74	21.88				1.77							100	-0.11	-2.41	0.26	5.90	0.27	0.45
73	A16-Tar 8		27.72	22.67	21.85	17.56				27.26	32.08		23.17	34.60											100	-0.12	-2.81	0.39	8.53	0.61	1.13
74	A16-Tar 8		31.17	25.74	32.2	28.90			0.61	21.28	25.96		14.73	21.87											100	-0.14	-3.26	0.22	4.97	0.26	0.43
75	A16-Tar 8.5		22.96	18.44	38.81	37.13				26.5	31.34		10.48	15.38				1.25							100	0.29	6.96	0.57	13.23	0.15	0.24
76	A16-Tar 8.5		29.63	24.37	32.52	29.28				22.67	27.44		15.18	22.55											100	-0.03	-0.63	0.34	7.67	0.27	0.44
77	A16-Tar 8.5		27.37	22.35	41.75	41.05				25.16	30.00		5.73	8.07											100	-0.05	-1.15	0.16	3.91	0.08	0.11
78	A16-Tar 8.5		34.27	28.51	33.51	30.47				18.79	23.23		13.44	19.90											100	-0.21	-4.62	0.16	3.62	0.23	0.37
79	D05-0015		22.81	18.31	45.26	45.92				29.53	34.25		2.4	2.91											100	0.05	1.32	0.21	5.21	0.03	0.04
80	D05-0015		25.21	20.44	44.76	45.22				26.99	31.82		3.04	3.90											100	0.01	0.23	0.19	4.54	0.04	0.05
81	D05-0015		26.19	21.31	38.4	36.60				28.48	33.26		6.92	9.91											100	-0.17	-3.98	0.03	0.63	0.10	0.16
82	D05-0015		33.03	27.40	40.93	39.94				21.88	26.60		4.16	5.64											100	-0.37	-8.48	-0.17	-4.14	0.06	0.08
83	D12-0042		31.9	26.39	34.61	31.81				20.3	24.90		13.19	19.52											100	-0.09	-2.01	0.27	5.97	0.22	0.35
84	D12-0042		27.55	22.51	38.59	36.85				26.86	31.69		7.01	10.05											100	-0.18	-4.25	0.02	0.58	0.10	0.16
85	D12-0095		23.48	18.90	44.23	44.47				27.26	32.08		5.03	6.99											100	0.17	4.05	0.38	9.14	0.07	0.09
86	D12-0095		21.09	16.79	33.99	31.05				32.22	36.71		12.71	18.79											100	0.09	2.26	0.37	8.76	0.21	0.35
87	D12-0095		24.36	19.68	43.71	43.74				27.54	32.36		4.39	6.00											100	0.06	1.45	0.25	6.09	0.06	0.08
88	D12-0095		23.75	19.14	37.01	34.81				29.38	34.11		9.86	14.43											100	0.02	0.54	0.26	6.28	0.15	0.24
89	D12-0095		34.16	28.41	29.79	26.09				22.01	26.74		14.05	20.83											100	-0.42	-9.57	-0.08	-1.72	0.27	0.46
90	D12-0095		37.42	31.33	32	28.66				19.85	24.41		10.73	15.76											100	-0.60	-13.53	-0.31	-6.98	0.19	0.32
91	D12-2007-3		34.49	28.70	34.4	31.55				20.66	25.29		9.41	13.74			1.04								100	-0.40	-8.99	-0.13	-3.00	0.16	0.25
92	D12-2707-3		24.57	19.87	45.29	45.97				27.54	32.36		2.6	3.22											100	0.03	0.70	0.20	4.88	0.03	0.04
93	D12-2707-3		33.62	27.93	41.21	40.32				20.16	24.75		5.01	6.96											100	-0.30	-6.77	-0.07	-1.59	0.07	0.10
94	D12-2707-3		36.32	30.34	38.49	36.72				19.43	23.95		5.76	8.12											100	-0.50	-11.28	-0.27	-6.34	0.09	0.13
95	D12-2707-3		39.06	32.80	35.93	33.45				17.13	21.36		6.88	9.85											100	-0.63	-14.26	-0.38	-8.97	0.11	0.17
96	D12-2707-6		23.85	19.23	41.78	41.09				23.71	28.52		5.31	7.42				5.35							100	0.32	7.70	0.50	12.18	0.07	0.10
97	D12-3060		22.67	18.19	45.14	45.75				28.18	32.97		4	5.39											100	0.17	4.20	0.37	8.96	0.05	0.07
98	D12-3060		23.28	18.73	42.09	41.51			1.79	27.85	32.66		4.99	6.93											100	-0.04	-1.03	0.13	3.17	0.07	0.10
99	D12-3060		25.23	20.45	41.88	41.23				28.07	32.87		4.83	6.68											100	-0.06	-1.38	0.12	2.96	0.07	0.09
100	D12-3060		25.64	20.82	38.38	36.57				28.47	33.25		7.52	10.83											100	-0.11	-2.59	0.10	2.33	0.11	0.17
101	D12-3060		24.82	20.09	39.96	38.65			3.44	24.61	29.44		7.18	10.31											100	-0.12	-2.77	0.09	2.15	0.10	0.15
102	D12-3060		30.91	25.51	37.33	35.22				25.85	30.69		5.91	8.35											100	-0.44	-10.25	-0.26	-6.26	0.09	0.14
103	D12-3060		27.17	22.18	34.36	31.50			3.37	26.43	31.27	0.38	8.29	12.02											100	-0.47	-10.88	-0.28	-6.61	0.14	0.22
104	D12-3060		32.22	26.68	35.88	33.39			5.83	16.64	20.80		9.42	13.75											100	-0.50	-10.94	-0.22	-4.82	0.15	0.24
105	D12-3060		33.86	28.14	35.92	33.44			6.3	15.09	19.00		8.82	12.83											100	-0.60	-13.01	-0.32	-7.01	0.14	0.22
106	D12-3060		32.1	26.57	33.9	30.94				26.56	31.40		7.45	10.72											100	-0.59	-13.84	-0.40	-9.69	0.13	0.20
107	D12-3083		21.75	17.37	42.58	42.18				29.94	34.64		4.93	6.83			0.8								100	0.14	3.33	0.31	7.63	0.07	0.09
108	D12-3083		29.65	24.38	44.58	44.96				23.01	27.79		2.76	3.47											100	-0.13	-3.12	0.06	1.45	0.04	0.04
109	D12-3083		32.65	27.06	37.5	35.44			1.17	23.01	27.79		5.67	7.98											100	-0.53	-12.11	-0.34	-8.11	0.09	0.13
110	D12-3136		24.43	19.75	41.27	40.40				27.9	32.70	1.05	4.98	6.91	0.37										100	0.01	0.25	0.18	4.39	0.07	0.10
111	D12-3136		27.13	22.14	35.73	33.20				28.36	33.15	1.59	6.55	9.34	0.34	0.29									100	-0.28	-6.81	-0.13	-3.13	0.11	0.16
112	D12-3136		27.97	22.89	35.46	32.86				27.55	32.37	1.15	7.35	10.57		0.52									100	-0.29	-6.96	-0.11	-2.75	0.12	0.18
113	D12-3136		29.17	23.96	37.29	35.17				26.21	31.05	0.84	6.5	9.26											100	-0.31	-7.25	-0.12	-2.99	0.10	0.15
114	D12-3136		34.76	28.95	30.9	27.37				23.41	28.21	3.03	6.74	9.63	0.54									0.63	100	-0.71	-16.68	-0.55	-13.47	0.13	0.20
115	D12-Tar 5p		23.57	18.98	39.65	38.24				27.09	31.92		9.7	14.18											100	0.20	4.83	0.47	11.03	0.14	0.21
116	D12-Tar 5p		21.82	17.43	35.54	32.96		1.86		31.17	35.77	0.38	9.23	13.46											100	0.19	4.58	0.40	9.30	0.15	0.23
117	D12-Tar 5p		23.56	18.97	38.83	37.16				27.47	32.29	0.37	9.76	14.28											100	0.17	4.05	0.43	10.08	0.14	0.22
118	D12-Tar 5p		24.54	19.84	42.49	42.06				26.51	31.35		6.46	9.20											100	0.13	3.10	0.36	8.52	0.09	0.13
119	D12-Tar 5p		25.6	20.78	43.14	42.95				25.97	30.81		5.29	7.39											100	0.06	1.42	0.27	6.51	0.07	0.10
120	D12-Tar 5p		27.4	22.38	39.88	38.54				25.23	30.07		7.48	10.77											100	-0.05	-1.09	0.19	4.41	0.11	0.16
121	D12-Tar 5p		32.44	26.87	41.17	40.26				18.96	23.42		6.8	9.72		0.64									100	-0.09	-2.05	0.18	4.24	0.09	0.14
122	D12-Tar 5p		34.77	28.95	37.87	35.92				20.61	25.24		6.75	9.64											100	-0.43	-9.74	-0.19	-4.51	0.10	0.15
123	D12-3037-c		33.78	28.07	30.66	27.09				18.22	22.60		13.78	20.42						3.57					100	-0.20	-4.49	0.16	3.56	0.26	0.43
124	D12-3037-c		39.79	33.46	36.26	33.86				15.51	19.49		8.45	12.26											100	-0.53	-11.78	-0.23	-5.15	0.13	0.21
125	A03-3002-4	10	24.12	19.47	27.08	23.05	0.61	5.66		32.79	37.22	1.8	7.22	10.37		0.73									100	0.09	2.12	0.20	4.53	0.15	0.26
126	A03-3002-4	12	21.81	17.43	35.39	32.78				37.89	41.51	1.64	6.13	8.69	0.23	0.71		0.48							100	-0.30	-7.29	-0.16	-3.95	0.10	0.15
127	A03-3002-4	8	32.91	27.29	39.77	38.40				22.34	27.09		4.98	6.91											100	-0.38	-8.86	-0.19	-4.42	0.07	0.10
128	A03-3011	29	24.49	19.80	34.55	31.74	2.53			29.56	34.28	0.31	8.25	11.96		0.3									100	0.02	0.42	0.19	4.61	0.14	0.22
129	A03-3024		29.41	24.17	40.39	39.22				25.99	30.83		4.21	5.72											100	-0.31	-7.41	-0.15	-3.66	0.06	0.08
130	A09-2378_2	7	21.46	17.12	38.24	36.39				36.55	40.42		3.75	5.00											100	-0.31	-7.74	-0.21	-5.39	0.06	0.08
131	A09-2378_2	6	24.63	19.92	32.95	29.79				34.79	38.95	0.94	6.69	9.55											100	-0.49	-11.97	-0.35	-8.91	0.12	0.18
132	A09-2378_2	14	24.2	19.54	32.32	29.04				36.01	39.98	0.61	6.86	9.81											100	-0.53	-12.98	-0.39	-9.89	0.12	0.19
133	A09-2378_2	8	25.18	20.41	31.93	28.58				35.07	39.19	0.46	7.36	10.59											100	-0.55	-13.40	-0.40	-10.02	0.13	0.21
134	A09-2378_2	15	29.25	24.03	27.68	23.71				33.33	37.69	0.43	9.31	13.58											100	-0.80	-19.25	-0.61	-15.02	0.19	0.33

Table A 5 (cont.)

135	A09-2378_2	7	38.78	32.55	27.2	23.18				24.14	28.96	0.38	9.5	13.88								100	-1.06	-24.06	-0.82	-19.34	0.20	0.34
136	A09-2378_2	5	35.73	29.81	23.6	19.34				28.44	33.22	1.28	10.95	16.10								100	-1.08	-25.13	-0.83	-19.83	0.27	0.48
137	A09-2378_2	8	38.14	31.97	22.13	17.84				26.2	31.04	0.33	13.21	19.55								100	-1.12	-25.52	-0.80	-18.50	0.34	0.63
138	A09-2378_2	33	31.97	26.45	22.48	18.20				33.77	38.08	0.41	11.37	16.74								100	-1.08	-25.77	-0.83	-20.21	0.29	0.53
139	A09-2378_2	12	35.19	29.33	21.65	17.36				30.06	34.75	0.43	12.68	18.74								100	-1.12	-26.02	-0.82	-19.48	0.34	0.62
140	A09-2378_2	10	39.25	32.97	20.39	16.11				26.68	31.52	0.89	12.79	18.91								100	-1.27	-29.11	-0.96	-22.31	0.36	0.67
141	A09-2707-4	8	34.08	28.34	40.05	38.77				21.96	26.69		3.92	5.27								100	-0.48	-10.95	-0.30	-7.05	0.06	0.08
142	A09-Ilgre1	10	20.06	15.88	27.13	23.10				35.74	39.75		17.06	25.40								100	-0.03	-0.81	0.32	7.45	0.36	0.63
143	A09-Ilgre1	7	22.2	17.77	29.86	26.17				33.71	38.02	0.23	13.69	20.28	0.3							100	-0.12	-2.94	0.16	3.80	0.26	0.44
144	A09-Ilgre1	5	25.99	21.13	27.33	23.32				29.45	34.18		17.23	25.66								100	-0.15	-3.55	0.22	4.99	0.36	0.63
145	A09-Ilgre1	8	21.29	16.97	33.07	29.94				35.14	39.25		10.51	15.43								100	-0.15	-3.67	0.07	1.75	0.18	0.30
146	A09-Ilgre1	8	20.78	16.51	34.94	32.22				35.7	39.72	0.74	7.84	11.32								100	-0.17	-4.25	0.00	-0.12	0.13	0.20
147	A09-Ilgre1	5	24.17	19.51	30.83	27.29				31.96	36.48		13.04	19.29								100	-0.18	-4.38	0.09	2.21	0.24	0.41
148	A09-Ilgre1	7	23.62	19.03	35.15	32.48				32.71	37.15		8.51	12.36								100	-0.21	-5.17	-0.02	-0.51	0.14	0.22
149	A09-Ilgre1	9	21.58	17.22	27.83	23.88				36.34	40.25		14.25	21.14								100	-0.24	-5.87	0.05	1.24	0.29	0.51
150	A09-Ilgre1	12	23.01	18.49	31.15	27.66				34.15	38.40		10.67	15.67	1.02							100	-0.25	-6.11	-0.03	-0.85	0.20	0.32
151	A09-Ilgre1	5	20.56	16.32	33.66	30.65				37.67	41.33	0.27	7.84	11.32								100	-0.28	-7.06	-0.12	-3.05	0.13	0.21
152	A09-Ilgre1	7	31.44	25.98	26.52	22.44		2.98		26.86	31.69		12.2	18.01								100	-0.32	-7.09	-0.06	-1.25	0.26	0.46
153	A09-Ilgre1	16	21.63	17.27	31.29	27.82				36.91	40.71		9.67	14.14	0.51							100	-0.32	-7.87	-0.12	-3.09	0.18	0.29
154	A09-Ilgre1	8	27.49	22.46	25.5	21.34				30.96	35.58		16.06	23.89								100	-0.41	-9.70	-0.07	-1.54	0.36	0.64
155	A09-Ilgre1	6	25.64	20.82	27.48	23.49				33.19	37.57		13.69	20.28								100	-0.41	-9.80	-0.12	-2.92	0.29	0.50
156	A09-Ilgre1	11	29.82	24.54	22.69	18.41				28.68	33.45		18.37	27.38	0.44							100	-0.46	-10.69	-0.05	-1.19	0.46	0.85
157	A09-Ilgre1	5	28.66	23.50	31.41	27.96				29.6	34.32		10.33	15.15								100	-0.46	-10.94	-0.23	-5.59	0.19	0.31
158	A09-Ilgre1	14	29.31	24.08	23	18.73				29.55	34.27		18.15	27.05								100	-0.47	-10.99	-0.07	-1.60	0.45	0.83
159	A09-Ilgre1	5	29.81	24.53	31.75	28.36				28.25	33.04		10.19	14.93								100	-0.48	-11.21	-0.24	-5.82	0.18	0.30
160	A09-Ilgre1	8	27.55	22.51	29.25	25.47				31.97	36.49		11.23	16.53								100	-0.52	-12.42	-0.28	-6.81	0.22	0.37
161	A09-Ilgre1	2	38.67	32.45	27.75	23.79				22.82	27.59		10.76	15.81								100	-0.94	-21.16	-0.66	-15.39	0.22	0.38
162	A09-Tar 9a		27.33	22.32	38.57	36.82				25.27	30.11	0.26	8.57	12.45								100	-0.04	-0.94	0.20	4.81	0.13	0.19
163	A09-Tar 9a		30.73	25.35	37.4	35.31				24.54	29.37		7.33	10.54								100	-0.32	-7.39	-0.10	-2.40	0.11	0.17
164	A10- 2007-7		20.14	15.95	35.8	33.29				32.79	37.22		11.26	16.57								100	0.13	3.25	0.39	9.25	0.18	0.29
165	A10- 2007-7		20.21	16.01	35.58	33.01				33.09	37.48		11.12	16.36								100	0.10	2.56	0.35	8.47	0.18	0.28
166	A15- Tar 22b		27.74	22.68	33.3	30.21				21.32	26.00		17.65	26.29								100	0.27	6.08	0.70	15.33	0.30	0.50
167	A16-smb3_1	25	24.41	19.73	31.08	27.58				34.53	38.73		9.97	14.60								100	-0.41	-9.98	-0.20	-5.01	0.18	0.30
168	A16-Tar10		22.8	18.30	43.22	43.06				27.16	31.99		6.81	9.74								100	0.25	6.04	0.49	11.67	0.09	0.13
169	A16-Tar10		27.14	22.15	40.46	39.31				24.07	28.89		8.33	12.08								100	0.07	1.57	0.33	7.72	0.12	0.18
170	A16-Tar10		34.06	28.32	24.11	19.87				21.29	25.97		20.54	30.65								100	-0.32	-7.17	0.17	3.68	0.49	0.88
171	A16-Tar10		34.79	28.97	27.32	23.31				20.53	25.15		17.36	25.85								100	-0.36	-7.98	0.07	1.52	0.36	0.64
172	A16-Tar10.75		29.97	24.67	33.98	31.04	7.31			22.18	26.92		5.57	7.82		1						100	0.19	4.13	0.32	7.20	0.09	0.14
173	A16-Tar10.75		28.85	23.67	42.55	42.14				20.23	24.82		8.37	12.14								100	0.18	4.10	0.49	11.22	0.11	0.17
174	A16-Tar10.75		24.57	19.87	41.66	40.93				26.92	31.75		6.85	9.80								100	0.10	2.39	0.33	7.77	0.09	0.14
175	A16-Tar10.75		25.87	21.02	43.88	43.98				25.39	30.23		3.78	5.05		1.08						100	0.06	1.37	0.24	5.86	0.05	0.07
176	D05-smb4	29	30.75	25.36	20.41	16.13				20.15	24.74		28.7	42.83								100	0.13	2.94	0.81	16.54	0.81	1.52
177	D12-0050	5	20.49	16.26	34.99	32.28				33.72	38.03		10.8	15.87								100	0.03	0.75	0.27	6.47	0.18	0.28
178	D12-0050	12	21.28	16.96	34.52	31.70				33.39	37.75		10.82	15.90								100	-0.02	-0.51	0.21	5.20	0.18	0.29
179	D12-0066_2	20	24.49	19.80	24.84	20.64				30.71	35.35		19.96	29.78								100	-0.08	-1.88	0.34	7.78	0.46	0.83
180	D12-0066_2	3	33.59	27.90	26.2	22.09				24.03	28.85	2.54	13.64	20.21								100	-0.56	-12.96	-0.25	-5.76	0.30	0.52
181	D12-0066_2	5	24.33	19.66	26.46	22.37				33.62	37.95	9	6.59	9.40								100	-0.52	-13.19	-0.43	-11.47	0.14	0.24
182	D12-3136	8	20.24	16.04	39.99	38.69				32.92	37.33		6.85	9.80								100	0.09	2.13	0.27	6.74	0.10	0.15
183	D12-3136	10	24.78	20.06	20.7	16.42				31.09	35.69	0.83	21.66	32.33	0.95							100	-0.14	-3.43	0.32	7.21	0.60	1.13
184	D12-3136	8	27.5	22.47	33.76	30.77				29.03	33.78	0.38	8.85	12.88	0.47							100	-0.33	-7.85	-0.13	-3.10	0.15	0.24
185	D12-3136	18	32.28	26.73	28.99	25.18		2.59		25.47	30.31	0.61	9.42	13.75	0.64							100	-0.36	-8.05	-0.15	-3.53	0.19	0.31
186	D12-3136	15	33.72	28.02	33.51	30.47				23.85	28.66	0.17	7.14	10.25	0.66	0.19		0.76				100	-0.58	-13.53	-0.40	-9.50	0.12	0.19
187	D12-3136	11	39.48	33.18	29.93	26.25				18.96	23.42		10.97	16.13	0.66							100	-0.74	-16.50	-0.44	-9.99	0.21	0.35
188	D12-3136	20	35.51	29.62	22.11	17.82		1.52		25.68	30.52		13.68	20.27	0.33			0.71	0.47			100	-0.75	-16.98	-0.44	-9.93	0.35	0.65
189	D12-Tar10.5		26	21.14	40.08	38.81				25.99	30.83		7.94	11.48								100	0.04	0.88	0.28	6.55	0.11	0.17
190	D12-Tar10.5		32.64	27.05	35.86	33.36				20.3	24.90		11.2	16.48								100	-0.17	-3.92	0.15	3.34	0.18	0.28
191	D12-Tar6		23.93	19.30	43.43	43.35				26.66	31.50		5.98	8.46								100	0.18	4.17	0.40	9.56	0.08	0.11
192	D12-Tar6		27.99	22.91	35.47	32.87			1.39	22.82	27.59		12.33	18.21								100	-0.05	-1.06	0.27	6.06	0.20	0.32
193	D12-Tar6		29.33	24.10	37.7	35.70			1.87	22.78	27.55		8.32	12.06								100	-0.25	-5.71	-0.01	-0.19	0.13	0.19
194	D12-Tar7		23.61	19.02	42.72	42.37				26.98	31.81		6.7	9.57								100	0.19	4.48	0.42	10.00	0.09	0.13
195	D12-Tar7		20.54	16.30	32.78	29.59				33.4	37.75		13.27	19.64								100	0.06	1.56	0.34	8.20	0.23	0.38
196	D12-Tar7		22.97	18.45	34.81	32.06				30.48	35.14	0.52	10.65	15.64			0.55					100	0.01	0.15	0.24	5.81	0.18	0.28
197	D12-Tar7		28.27	23.16	39.97	38.66				23.91	28.73		7.85	11.34								100	-0.03	-0.76	0.22	5.09	0.11	0.17
198	D12-Tar7		32.12	26.59	34.25	31.37				21.46	26.15		12.16	17.95								100	-0.20	-4.56	0.12	2.78	0.20	0.33
199	D12-Tar7		33.49	27.81	34.74	31.97				19.76	24.31		12.01	17.72								100	-0.21	-4.75	0.12	2.82	0.20	0.32
200	D12-Tar7		32.21	26.67	37.16	35.01				22.24	26.98		8.39	12.17								100	-0.29	-6.62	-0.04	-0.82	0.13	0.20
201	D12-Tar7		28.72	23.56	32.14	28.83				27.26	32.08		11.87	17.51								100	-0.29	-6.81	-0.02	-0.42	0.21	0.35
202	D12-Tar7		32.72	27.12	30.22	26.58				22.87	27.65		14.19	21.04								100	-0.35	-7.87	0.00	-0.04	0.27	0.45
203	D12-Tar7		32.7	27.10	25.94	21.81				23.61	28.42		17.75	26.44								100	-0.37	-8.49	0.04	0.88	0.39	0.70
204	D12-Tar7		33.32	27.66	37.56	35.52				21.82	26.54		7.3	10.49								100	-0.37	-8.52	-0.14	-3.19	0.11	0.17
205	D12-Tar7		32.41	26.85	29.86	26.17				25.17	30.01		12.56	18.56								100	-0.49	-11.31	-0.20	-4.53	0.24	0.41
206	D12-Tar7		32.97	27.35	22.68	18.40				25.9	30.74		18.44	27.49								100	-0.56	-12.81	-0.14	-3.02	0.47	0.86
207	D13-smb2	10	29.51	24.26	24.27	20.04				21	25.66		25.21	37.64								100	0.17	3.75	0.75	15.76	0.60	1.08
208	D13-smb2	14	30.4	25.05	25.09	20.90				23.53	28.33		20.98	31.31								100	-0.13	-2.87	0.35	7.70	0.48	0.86

Table A 6. EDS data (weight percent) for greisen quartz chip 1 heated to 500°C.

Table A6

EDS data for greisen quartz chip 1 heated to 500C.

Sample	Mound size (µm)	F	Na	Al	S	Cl	K	Ca	Mn	Fe	Br	Total	Σ+	Σ-	diif	Σdiff%
chip1	10		17.75			43.20	2.41	35.18	1.46			100.00	2.64	1.22	1.42	36.88
chip1	7		29.85			45.51	1.05	23.59				100.00	2.50	1.28	1.22	32.19
chip1	5		27.31			45.73	3.00	23.95				100.00	2.46	1.29	1.17	31.21
chip1	5	6.44	19.10			38.17	1.07	35.22				100.00	2.62	1.42	1.20	29.77
chip1	10		38.85			42.12	19.03					100.00	2.18	1.19	0.99	29.39
chip1	11	1.59	11.15			45.70	2.47	39.10				100.00	2.50	1.37	1.13	29.11
chip1	24	6.54	10.94			38.89	1.93	41.15	0.55			100.00	2.60	1.44	1.16	28.65
chip1	10		39.33			42.73	17.94					100.00	2.17	1.21	0.96	28.58
chip1	5		42.60			43.61	13.80					100.00	2.21	1.23	0.98	28.40
chip1	5		32.34			46.58	4.42	16.65				100.00	2.35	1.31	1.04	28.30
chip1	8		33.26			47.44		17.91	1.38			100.00	2.39	1.34	1.05	28.24
chip1	4		32.21			47.80		19.99				100.00	2.40	1.35	1.05	28.04
chip1	8	3.50	17.94			43.60	0.95	34.01				100.00	2.50	1.41	1.09	27.79
chip1	14		25.89			48.04	1.23	24.84				100.00	2.40	1.36	1.04	27.77
chip1	5		32.82			47.90		19.28				100.00	2.39	1.35	1.04	27.76
chip1	12	2.45	28.32			44.85	1.90	22.48				100.00	2.40	1.39	1.01	26.55
chip1	13		35.11			43.06	21.83					100.00	2.09	1.21	0.87	26.39
chip1	12	3.07	19.30			44.46	2.64	28.97	1.55			100.00	2.41	1.42	0.99	25.98
chip1	5	4.47	24.96			42.98		27.60				100.00	2.46	1.45	1.02	25.97
chip1	8	5.12	20.98			41.72	2.36	29.16	0.66			100.00	2.45	1.45	1.01	25.79
chip1	10		35.20			48.16	2.61	14.02				100.00	2.30	1.36	0.94	25.70
chip1	10	7.14	13.20			39.76	1.35	38.03	0.52			100.00	2.53	1.50	1.03	25.57
chip1	5	9.09	18.24			36.65	2.09	33.93				100.00	2.54	1.51	1.03	25.37
chip1	25	2.62	21.21			45.99	2.35	27.12	0.70			100.00	2.36	1.44	0.93	24.40
chip1	8	2.59	25.44			46.32	1.35	24.30				100.00	2.35	1.44	0.91	23.98
chip1	25		14.42			50.25	3.56	31.77				100.00	2.30	1.42	0.89	23.82
chip1	35	1.52	23.46			48.48	1.73	24.81				100.00	2.30	1.45	0.86	22.80
chip1	10		20.02			51.00	2.00	26.98				100.00	2.27	1.44	0.83	22.38
chip1	14	6.40	22.21			41.75	2.57	26.26	0.82			100.00	2.37	1.51	0.86	22.07
chip1	12		25.34			50.65	2.87	21.14				100.00	2.23	1.43	0.80	21.92
chip1	26		27.52			50.70	2.21	19.57				100.00	2.23	1.43	0.80	21.86
chip1	6		50.18			49.82						100.00	2.18	1.41	0.78	21.67
chip1	4		35.24			50.93		13.83				100.00	2.22	1.44	0.79	21.50
chip1	10	1.47	32.63			48.97	1.14	15.79				100.00	2.24	1.46	0.78	21.06
chip1	6		34.92			50.77	1.87	12.43				100.00	2.19	1.43	0.76	20.87
chip1	17	2.65	29.38			47.72	0.83	19.42				100.00	2.27	1.49	0.78	20.86
chip1	12		32.85			45.91	21.25					100.00	1.97	1.29	0.68	20.73
chip1	8		37.18			47.23	15.59					100.00	2.02	1.33	0.68	20.42
chip1	10	4.81	29.25			44.95	0.78	20.21				100.00	2.30	1.52	0.78	20.39
chip1	18		17.61			52.47	1.24	28.13	0.55			100.00	2.22	1.48	0.74	20.02
chip1	11	3.14	26.69			47.52	1.43	21.22				100.00	2.26	1.51	0.75	19.96
chip1	10	1.99	25.05			49.21	2.10	21.64				100.00	2.22	1.49	0.73	19.65

Table A 6 (cont.)

chip1	30		39.95		48.78	11.28			100.00	2.03	1.38	0.65	19.11
chip1	8	6.51	22.25		43.20	2.46	24.33	1.25	100.00	2.29	1.56	0.73	18.93
chip1	16	2.23	22.11		49.50	2.15	24.01		100.00	2.22	1.51	0.70	18.82
chip1	16	1.73	26.54		50.45	0.31	20.97		100.00	2.21	1.51	0.70	18.67
chip1	22		20.30		52.58	2.81	23.82	0.49	100.00	2.16	1.48	0.68	18.62
chip1	23	0.17	23.24		52.67	2.11	21.82		100.00	2.15	1.49	0.66	18.07
chip1	16		33.11		52.61	1.05	13.22		100.00	2.13	1.48	0.64	17.81
chip1	8		48.16		51.84				100.00	2.10	1.46	0.63	17.79
chip1	40		25.21		53.05	2.84	18.90		100.00	2.11	1.50	0.62	17.07
chip1	14		26.83		46.61	26.56			100.00	1.85	1.31	0.53	16.83
chip1	12	1.85	38.30		50.34	0.70	8.81		100.00	2.12	1.52	0.61	16.66
chip1	5	6.75	27.83		44.45	0.54	20.42		100.00	2.24	1.61	0.63	16.46
chip1	12	6.44	20.14		45.33	1.54	26.18	0.38	100.00	2.24	1.62	0.62	16.03
chip1	30	0.69	24.39		52.74	2.85	19.34		100.00	2.10	1.52	0.57	15.87
chip1	14		34.61		49.52	15.87			100.00	1.91	1.40	0.51	15.56
chip1	10		26.38		47.26	26.37			100.00	1.82	1.33	0.49	15.50
chip1	4	9.89	31.30		40.58		18.23		100.00	2.27	1.67	0.61	15.39
chip1	35		18.35		45.17	36.47			100.00	1.73	1.27	0.46	15.21
chip1	10	8.92	20.45		41.82	2.93	24.48	1.40	100.00	2.24	1.65	0.59	15.14
chip1	15	5.00	25.09		48.21	0.93	20.77		100.00	2.15	1.62	0.53	14.02
chip1	8	6.17	24.34		46.38	2.43	20.68		100.00	2.15	1.63	0.52	13.73
chip1	10		39.16		52.38	8.46			100.00	1.92	1.48	0.44	13.02
chip1	4	7.62	29.88		44.18	3.05	15.27		100.00	2.14	1.65	0.49	13.01
chip1	6	8.40	28.12		44.15		19.34		100.00	2.19	1.69	0.50	12.92
chip1	8		45.54	15.14	32.19		7.13		100.00	2.34	1.85	0.48	11.57
chip1	10		44.25		54.94	0.81			100.00	1.95	1.55	0.40	11.33
chip1	7	8.84	32.15		43.52	1.98	13.51		100.00	2.12	1.69	0.43	11.27
chip1	20		14.10		46.36	39.54			100.00	1.62	1.31	0.32	10.81
chip1	16	4.15	25.18		51.33	0.48	18.34	0.53	100.00	2.04	1.67	0.38	10.14
chip1	4	9.38	34.41		43.88		12.33		100.00	2.11	1.73	0.38	9.88
chip1	13	6.04	29.11		48.18	2.81	13.86		100.00	2.03	1.68	0.35	9.53
chip1	21	3.27	32.64		53.05		10.51	0.53	100.00	1.96	1.67	0.29	8.12
chip1	35		28.05	1.01	51.14	18.45	1.35		100.00	1.76	1.51	0.25	7.77
chip1	4		45.40	4.93	49.66				100.00	1.98	1.71	0.27	7.24
chip1	11		20.72		51.22	28.06			100.00	1.62	1.44	0.17	5.68
chip1	14		25.11	0.86	51.63	22.40			100.00	1.67	1.51	0.15	4.88
chip1	8		4.43		47.45	48.11			100.00	1.42	1.34	0.08	3.07
chip1	6		-0.11		47.25	52.86			100.00	1.35	1.33	0.01	0.54

Table A 7. EDS data (weight percent) for greisen quartz chip 2 heated to 500°C.

Table A7

EDS data for greisen quartz chip 2 heated to 500C.

Sample	Mound size (µm)	F	Na	Al	S	Cl	K	Ca	Mn	Fe	Br	Total	Σ+	Σ-	diif	Σdiff%
chip2	8		29.06			42.03		28.91				100.00	2.71	1.19	1.52	39.08
chip2	5		34.43			42.80		22.78				100.00	2.63	1.21	1.43	37.15
chip2	15		23.24			44.98		31.78				100.00	2.60	1.27	1.33	34.36
chip2	22	5.38	16.76			41.84	2.03	33.99				100.00	2.48	1.46	1.01	25.73
chip2	19	5.65	22.88			41.21	1.84	28.43				100.00	2.46	1.46	1.00	25.54
chip2	26		23.47			43.81	24.10	8.62				100.00	2.07	1.24	0.83	25.17
chip2	14		39.96			50.00		10.04				100.00	2.24	1.41	0.83	22.70
chip2	30	8.44	14.25			39.59	2.32	35.41				100.00	2.45	1.56	0.89	22.09
chip2	11	6.38	28.25			42.39		22.98				100.00	2.38	1.53	0.84	21.61
chip2	21	9.06	17.65			38.96	1.54	32.79				100.00	2.44	1.58	0.87	21.59
chip2	15	8.12	20.14			40.77		30.98				100.00	2.42	1.58	0.84	21.12
chip2	25	3.47	21.85			46.77	1.20	25.58	1.12			100.00	2.30	1.50	0.80	20.97
chip2	7	9.77	25.38			38.79	0.96	25.11				100.00	2.38	1.61	0.77	19.38
chip2	24	6.50	17.76			44.36		31.38				100.00	2.34	1.59	0.75	18.95
chip2	8	14.65	16.71			33.07	1.68	33.89				100.00	2.46	1.70	0.76	18.18
chip2	11	6.23	25.42			44.64		23.70				100.00	2.29	1.59	0.70	18.10
chip2	20	6.46	23.12			44.28	1.53	24.03	0.58			100.00	2.27	1.59	0.68	17.54
chip2	23	6.79	21.04			44.49		27.13	0.56			100.00	2.29	1.61	0.68	17.36
chip2	18	6.11	27.98			45.18		20.73				100.00	2.25	1.60	0.66	17.04
chip2	5	11.09	33.46			38.02		17.43				100.00	2.33	1.66	0.67	16.81
chip2	10	10.99	21.24			39.09	0.83	27.84				100.00	2.33	1.68	0.65	16.27
chip2	12	8.13	26.68			42.67		21.13	1.38			100.00	2.27	1.63	0.63	16.27
chip2	10	12.56	23.40			37.15		26.89				100.00	2.36	1.71	0.65	15.98
chip2	15	6.34	24.20			45.69		23.77				100.00	2.24	1.62	0.62	15.97
chip2	25	6.29	21.36			45.70	1.11	25.54				100.00	2.23	1.62	0.61	15.89
chip2	14		40.03			50.86	9.11					100.00	1.97	1.43	0.54	15.82
chip2	15	7.21	19.67			44.91		28.21				100.00	2.26	1.65	0.62	15.77
chip2	24	5.86	26.24			46.23	0.46	21.22				100.00	2.21	1.61	0.60	15.68
chip2	19	6.53	21.20			46.08	1.01	25.18				100.00	2.20	1.64	0.56	14.58
chip2	26	6.68	23.94			46.64		22.74				100.00	2.18	1.67	0.51	13.25
chip2	25	8.45	22.75			44.24	0.69	22.85	1.01			100.00	2.18	1.69	0.49	12.68
chip2	23		44.71			55.29						100.00	1.95	1.56	0.39	11.00
chip2	7	12.75	27.73			39.92		19.60				100.00	2.18	1.80	0.39	9.72
chip2	7	9.12	33.05			45.35		12.47				100.00	2.06	1.76	0.30	7.88
chip2	4	10.68	36.19			43.07		10.06				100.00	2.08	1.78	0.30	7.75
chip2	11	8.51	34.68			45.84	1.31	9.66				100.00	2.02	1.74	0.28	7.51
chip2	12		34.16			55.28	10.56					100.00	1.76	1.56	0.20	5.94
chip2	25	11.12	27.66			44.42		16.79				100.00	2.04	1.84	0.20	5.22
chip2	10	10.50	27.02			45.06	1.04	16.38				100.00	2.02	1.82	0.20	5.09
chip2	12		32.35			55.87	11.78					100.00	1.71	1.58	0.13	4.03
chip2	15		30.18			56.19	13.62					100.00	1.66	1.58	0.08	2.35
chip2	22		35.12			58.79	5.51			0.58		100.00	1.69	1.66	0.03	0.93
chip2	19	8.78	13.66			49.96	2.88	24.71				100.00	1.90	1.87	0.03	0.78
chip2	7	10.28	31.07			48.98	0.84	8.83				100.00	1.81	1.92	-0.11	-2.92

Table A 8. EDS data (weight percent) for greisen quartz chip 3 heated to 500°C.

Table A8

EDS data for greisen quartz chip 3 heated to 500C.

Sample	Mound size (µm)	F	Na	Al	S	Cl	K	Ca	Mn	Fe	Br	Total	Σ+	Σ-	diif	Σdiff%
chip3	10	8.74	16.52			38.83		35.91				100.00	2.51	1.56	0.96	23.49
chip3	12	19.37	13.03			29.88		37.72				100.00	2.45	1.86	0.59	13.62
chip3	7	15.25	22.19			38.17		24.39				100.00	2.18	1.88	0.30	7.46
chip3	20	10.48	25.50			44.18	0.36	18.97	0.50			100.00	2.08	1.80	0.29	7.36
chip3	22	8.54	21.00			47.69	0.40	21.84	0.53			100.00	2.03	1.79	0.24	6.21
chip3	20	15.19	20.13			39.46		24.82	0.40			100.00	2.13	1.91	0.22	5.36
chip3	6	20.26	22.37			32.77		24.60				100.00	2.20	1.99	0.21	5.00
chip3	20	11.36	31.97			43.95		12.71				100.00	2.03	1.84	0.19	4.84
chip3	12	9.28	39.14			46.25		3.77	1.56			100.00	1.95	1.79	0.15	4.14
chip3	8	17.29	25.46			37.00	0.22	19.74	0.29			100.00	2.11	1.95	0.15	3.82
chip3	16	11.93	24.22			44.13	0.35	18.53	0.84			100.00	2.02	1.87	0.14	3.72
chip3	8	8.48	34.61			48.12	0.44	7.99	0.37			100.00	1.93	1.80	0.13	3.35
chip3	24	5.72	39.55			51.52		2.52	0.70			100.00	1.87	1.75	0.12	3.23
chip3	14	12.52	18.89			44.18	0.50	22.63	1.27			100.00	2.01	1.91	0.10	2.67
chip3	4	19.02	26.60			35.57		18.81				100.00	2.10	2.00	0.09	2.22
chip3	6	16.70	29.47			38.64		15.19				100.00	2.04	1.97	0.07	1.77
chip3	5	16.80	23.30			39.27		20.62				100.00	2.04	1.99	0.05	1.25
chip3	7	24.52	23.53			29.88		22.07				100.00	2.13	2.13	-0.01	-0.19
chip3	7	18.84	32.15			36.78		12.23				100.00	2.01	2.03	-0.02	-0.49
chip3	10	18.29	27.33			37.91		15.46	1.01			100.00	2.00	2.03	-0.03	-0.86
chip3	13	23.54	17.66			32.10		26.27	0.42			100.00	2.09	2.14	-0.05	-1.17
chip3	8	21.75	20.67			34.45		23.13				100.00	2.05	2.12	-0.06	-1.52
chip3	12	23.13	17.98			32.91		25.98				100.00	2.08	2.15	-0.07	-1.59
chip3	10	13.84	27.70			44.44		14.03				100.00	1.90	1.98	-0.08	-1.97
chip3	7	20.38	22.99			36.78		19.85				100.00	1.99	2.11	-0.12	-2.90
chip3	15	17.19	27.70			40.53		14.07	0.51			100.00	1.93	2.05	-0.12	-3.08
chip3	6	21.53	30.35			35.29		12.83				100.00	1.96	2.13	-0.17	-4.11
chip3	3	23.28	27.71			34.00		15.01				100.00	1.95	2.18	-0.23	-5.57
chip3	3	24.32	28.12			32.76		14.81				100.00	1.96	2.20	-0.24	-5.80
chip3	5	22.29	25.22			36.13		16.36				100.00	1.91	2.19	-0.28	-6.79
chip3	6	26.48	22.87			32.30		18.36				100.00	1.91	2.30	-0.39	-9.35
chip3	2	32.57	23.87			27.69		15.87				100.00	1.83	2.50	-0.67	-15.38

Table A 9. EDS data (weight percent) for quartz Mo–pegmatite chip heated to 300°C.

Table A9

EDS data for quartz Mo-pematite chip heated to 300ºC.

#	Sample	Mound size (µm)	F	Na	Mg	Al	S	Cl	K	Ca	Ti	Mn	Fe	Zn	As	Mo	Total	∑+	∑-	Σdiff	Σdiff%	Ca/Na
1	llpeg_chip3_300	8						52.24						47.76			100	1.46	1.47	-0.01	-0.45	
2	llpeg_chip3_300	24		32.06				58.02		9.92							100	1.89	1.64	0.25	7.18	0.31
3	llpeg_chip3_300	13		42.95				57.05									100	1.87	1.61	0.26	7.45	
4	llpeg_chip3_300	45		45.43				54.57									100	1.98	1.54	0.44	12.43	
5	llpeg_chip3_300	7		36.81				54.52	2.42	6.25							100	1.97	1.54	0.44	12.45	0.17
6	llpeg_chip3_300	20		41.53		2.32		55.38		0.77							100	2.1	1.56	0.54	14.76	0.02
7	llpeg_chip3_300	24		35.63				53.9		10.47							100	2.07	1.52	0.55	15.37	0.29
8	llpeg_chip3_300	42		47.59				52.41									100	2.07	1.48	0.59	16.68	
9	llpeg_chip3_300	5		47.79				52.21									100	2.08	1.47	0.61	17.07	
10	llpeg_chip3_300	5		47.81				52.19									100	2.08	1.47	0.61	17.11	
11	llpeg_chip3_300	7		47.92				52.08									100	2.08	1.47	0.62	17.32	
12	llpeg_chip3_300	5		11.39				40.09	48.52								100	1.74	1.13	0.61	21.12	
13	llpeg_chip3_300	5		33.71				50.03	4.34	11.91							100	2.17	1.41	0.76	21.23	0.35
14	llpeg_chip3_300	18		32.38				46.45	14.84	6.33							100	2.1	1.31	0.79	23.25	0.20
15	llpeg_chip3_300	5		33.93				43.3	22.77								100	2.06	1.22	0.84	25.52	
16	llpeg_chip3_300	10		33.34				47.95		18.71							100	2.38	1.35	1.03	27.61	0.56
17	llpeg_chip3_300	10		12.13				48.59		39.28							100	2.49	1.37	1.12	28.96	3.24
18	llpeg_chip3_300	7		39.46				41.71	18.83								100	2.2	1.18	1.02	30.27	
19	llpeg_chip3_300	44		20.68		5.85	11.15	22.14	24.22	5.13			6.74	4.1			100	2.55	1.32	1.23	31.8	0.25
20	llpeg_chip3_300	45		40.07				39.63						20.3			100	2.36	1.12	1.25	35.79	

Table A 10. EDS data (weight percent) for quartz Mo–pegmatite chip heated to 400°C.

Table A10

EDS data for quartz Mo-pematite chip heated to 400ºC.

#	Sample	Mound size (µm)	F	Na	Mg	Al	S	Cl	K	Ca	Ti	Mn	Fe	Zn	As	Mo	Total	∑+	∑-	Σdiff	Σdiff%	Ca/Na
1	llpeg_chip4_400	5		39.67				56.59									100	1.73	1.6	0.13	3.9	
2	llpeg_chip4_400	8		42.13				57.3		0.57							100	1.86	1.62	0.24	7.04	0.01
3	llpeg_chip4_400	8		38.2				57.5		4.3							100	1.88	1.62	0.25	7.27	0.11
4	llpeg_chip4_400	6		2.47				44.54	52.99								100	1.46	1.26	0.21	7.59	0.00
5	llpeg_chip4_400	5		42.37				56.19	1.44								100	1.88	1.58	0.29	8.51	
6	llpeg_chip4_400	2		2.93				44.21	52.86								100	1.48	1.25	0.23	8.53	
7	llpeg_chip4_400	2		2.63				44.11	53.26								100	1.48	1.24	0.23	8.54	
8	llpeg_chip4_400	5						43.16	56.84								100	1.45	1.22	0.24	8.85	
9	llpeg_chip4_400	2		2.66				43.9	53.45								100	1.48	1.24	0.24	8.99	
10	llpeg_chip4_400	4		43.74				56.26									100	1.9	1.59	0.32	9.05	
11	llpeg_chip4_400	16		29.25				56.87		12.97		0.91					100	1.95	1.6	0.35	9.8	0.44
12	llpeg_chip4_400	8		38.15				56.21		5.65							100	1.94	1.59	0.36	10.09	0.15
13	llpeg_chip4_400	5		2.5				43.36	51.49					2.64			100	1.51	1.22	0.28	10.38	
14	llpeg_chip4_400	5		39.99				54.27	5.73								100	1.89	1.53	0.36	10.4	
15	llpeg_chip4_400	5		4.69				43.77	51.53								100	1.52	1.23	0.29	10.43	
16	llpeg_chip4_400	5		33.5				50.97	15.54								100	1.85	1.44	0.42	12.67	
17	llpeg_chip4_400	23		38.58				54.27		7.16							100	2.04	1.53	0.5	14.15	0.19
18	llpeg_chip4_400	5		6.62				42.21	51.18								100	1.6	1.19	0.41	14.58	
19	llpeg_chip4_400	28		34.66				54.13		11.21							100	2.07	1.53	0.54	15.03	0.32
20	llpeg_chip4_400	8		35.5				53.85		9.51		1.14					100	2.06	1.52	0.54	15.13	0.27
21	llpeg_chip4_400	3		6.41			0.53	42.71	48.39		1.96						100	1.68	1.24	0.44	15.17	
22	llpeg_chip4_400	5		33.42				49.04	17.54								100	1.9	1.38	0.52	15.8	
23	llpeg_chip4_400	5		41.18				51.09	7.73								100	1.99	1.44	0.55	15.97	
24	llpeg_chip4_400	5		38.38				50.29	11.32								100	1.96	1.42	0.54	16	
25	llpeg_chip4_400	3		35.82				49.56	14.62								100	1.93	1.4	0.53	16.04	
26	llpeg_chip4_400	5		40.23				53.23		6.54							100	2.08	1.5	0.57	16.07	0.16
27	llpeg_chip4_400	28		25.37				53.07	1.25	18.44		1.2	0.67				100	2.1	1.5	0.6	16.75	0.73
28	llpeg_chip4_400	6		39.5				49.87	10.63								100	1.99	1.41	0.58	17.18	
29	llpeg_chip4_400	3		48.11				51.89									100	2.09	1.46	0.63	17.69	
30	llpeg_chip4_400	2		30.33				46.72	22.95								100	1.91	1.32	0.59	18.25	
31	llpeg_chip4_400	24		30.21	1.15		0.77	46.32	13.58	2.99			3.06	1.92			100	1.96	1.35	0.61	18.36	0.10
32	llpeg_chip4_400	8		43.43				49.87	6.7								100	2.06	1.41	0.65	18.86	
33	llpeg_chip4_400	3		35.78		2.46	0.86	49.06	11.84								100	2.13	1.44	0.7	19.48	
34	llpeg_chip4_400	15		40.94				48.19	10.87								100	2.06	1.36	0.7	20.47	
35	llpeg_chip4_400	5		30.7				45.05	24.25								100	1.96	1.27	0.68	21.23	
36	llpeg_chip4_400	33		33.16				49.8	2.7	13.09			1.26				100	2.16	1.4	0.76	21.29	0.39
37	llpeg_chip4_400	5		50				50									100	2.17	1.41	0.76	21.33	
38	llpeg_chip4_400	5		37.72				46.4	15.88								100	2.05	1.31	0.74	22	
39	llpeg_chip4_400	3		9.63				39.04	51.33								100	1.73	1.1	0.63	22.26	
40	llpeg_chip4_400	20						51.52		48.48							100	2.42	1.45	0.97	24.95	
41	llpeg_chip4_400	7		38.97				44.74	16.29								100	2.11	1.26	0.85	25.19	
42	llpeg_chip4_400	5		52.55				47.45									100	2.29	1.34	0.95	26.14	
43	llpeg_chip4_400	10		37.93				47.62	2.53	11.92							100	2.31	1.34	0.97	26.45	0.31
44	llpeg_chip4_400	7		30.34				47		21.83		0.83					100	2.44	1.33	1.11	29.58	0.72
45	llpeg_chip4_400	6		23.08	5.31		3.19	36.38	7.22	12.81			12.01				100	2.26	1.23	1.04	29.79	0.56
46	llpeg_chip4_400	7		36.7				45.19	5.63	12.48							100	2.36	1.27	1.09	29.92	0.34
47	llpeg_chip4_400	14		32.66				45.23		20.73		1.38					100	2.51	1.28	1.23	32.52	0.63
48	llpeg_chip4_400	12		28.68	4.61		2.48	36.14	5.91	8.89			9.76	3.54			100	2.33	1.17	1.16	32.99	0.31
49	llpeg_chip4_400	30		35.46				35.76	9.49				7			12.29	100	2.04	1.01	1.03	33.86	0.32
50	llpeg_chip4_400	4		35.9				44.45		19.65							100	2.54	1.25	1.29	33.94	
51	llpeg_chip4_400	5		32.14				43.28	5.55	19.03							100	2.49	1.22	1.27	34.2	
52	llpeg_chip4_400	5		58.09				41.91									100	2.53	1.18	1.34	36.26	
53	llpeg_chip4_400	20		36.3				35.14	10.17	3.35			8.35			6.69	100	2.15	0.99	1.15	36.81	
54	llpeg_chip4_400	36		8.56		0.86		42.99	0.52	43.37		3.7					100	2.78	1.21	1.57	39.26	
55	llpeg_chip4_400	3		35.15				33.97		19.58			11.3				100	2.51	0.96	1.55	44.68	
56	llpeg_chip4_400	3		12.13			3.1	3.03	4	2.19			75.54				100	0.74	0.28	0.46	45.22	
57	llpeg_chip4_400	16		40.43			5.14	23.07	17.65	4.5				9.21			100	2.72	0.97	1.74	47.32	
58	llpeg_chip4_400	8					1.29	34.29	1.65	60.1				2.66			100	3.12	1.05	2.08	49.76	

Table A 11. EDS data (weight percent) for quartz Mo–pegmatite chip heated to 500°C.

Table A11

EDS data for quartz Mo-pematite chip heated to 500ºC.

#	Sample	Mound size (µm)	F	Na	Mg	Al	S	Cl	K	Ca	Ti	Mn	Fe	Zn	As	Mo	Total	∑+	∑-	Σdiff	Σdiff%	Ca/Na
1	llpeg_chip5_500	15		32.57				45.36		20.3		1.77					100	2.49	1.28	1.21	32.19	0.62
2	llpeg_chip5_500	5		40.57				58.81		0.62							100	1.8	1.66	0.14	3.96	0.02
3	llpeg_chip5_500	50		26.3				36.91		33.72		3.07					100	2.94	1.04	1.9	47.68	1.28
4	llpeg_chip5_500	7		31.96				41.29		26.76							100	2.73	1.16	1.56	40.13	0.84
5	llpeg_chip5_500	5		43.54				56.46									100	1.89	1.59	0.3	8.65	
6	llpeg_chip5_500	16		5.76				18.6		68.48		5.45	1.71				100	3.87	0.52	3.34	76.1	11.89
7	llpeg_chip5_500	19		31.64				40.31		26.07		1.41	0.57				100	2.73	1.14	1.59	41.17	0.82
8	llpeg_chip5_500	15		21.38				41.46		34.59		2.57					100	2.75	1.17	1.58	40.32	1.62
9	llpeg_chip5_500	30		33.39			1.29	41.66		21.63		2.04					100	2.61	1.26	1.35	34.97	0.65
10	llpeg_chip5_500	8		34.08			0.49	55.64		9.78							100	1.97	1.6	0.37	10.38	0.29
11	llpeg_chip5_500	5		42.51		1.35		56.14									100	2	1.58	0.42	11.6	
12	llpeg_chip5_500	13		36.96				38.82		24.22							100	2.82	1.09	1.72	44.01	0.66
13	llpeg_chip5_500	16		38.08				44.59		16.03		1.31					100	2.5	1.26	1.25	33.13	0.42
14	llpeg_chip5_500	50		24.74				43.21		29.67		2.39					100	2.64	1.22	1.42	36.89	1.20
15	llpeg_chip5_500	10		25.09			0.73	36.49		35.34		2.36					100	2.94	1.07	1.87	46.47	1.41
16	llpeg_chip5_500	38		44.77				55.23									100	1.95	1.56	0.39	11.12	
17	llpeg_chip5_500	8		29.65		12.58		49.92		7.85							100	3.08	1.41	1.67	37.26	0.26
18	llpeg_chip5_500	10		29.11			0.57	38.51		29.55		2.26					100	2.82	1.12	1.7	43.13	1.02
19	llpeg_chip5_500	40		25.67				39.42		32.78		2.13					100	2.83	1.11	1.72	43.59	1.28
20	llpeg_chip5_500	15		26.45			1.63	29.49		40.63		1.81					100	3.24	0.93	2.31	55.31	1.54
21	llpeg_chip5_500	12		34.73		21.35		43.92									100	3.88	1.24	2.65	51.64	
22	llpeg_chip5_500	7		41				57.45		1.56							100	1.86	1.62	0.24	6.92	0.04
23	llpeg_chip5_500	10		47.63				52.37									100	2.07	1.48	0.59	16.76	
24	llpeg_chip5_500	25		19.62				36.13		42		2.26					100	3.03	1.02	2.01	49.68	2.14
25	llpeg_chip5_500	16		21.23				37.08		39.04		2.65					100	2.97	1.05	1.92	47.89	1.84
26	llpeg_chip5_500	6		41.84				57.5		0.67							100	1.85	1.62	0.23	6.66	0.02
27	llpeg_chip5_500	12		44.4				55.6									100	1.93	1.57	0.36	10.37	
28	llpeg_chip5_500	16		45.27				49.72		5.01							100	2.22	1.4	0.82	22.55	0.11
29	llpeg_chip5_500	10		45.98				54.02									100	2	1.52	0.48	13.52	
30	llpeg_chip5_500	8		46.13				53.87									100	2.01	1.52	0.49	13.82	
31	llpeg_chip5_500	16		33.28			0.69	48.11		17.93							100	2.34	1.4	0.94	25.18	0.54
32	llpeg_chip5_500	24		48.06				51.94									100	2.09	1.47	0.63	17.59	
33	llpeg_chip5_500	20		31.2			1.25	35.31		32.24							100	2.97	1.07	1.89	46.83	1.03
34	llpeg_chip5_500	20		46.26				51.6		2.14							100	2.12	1.46	0.66	18.57	0.05
35	llpeg_chip5_500	15		33.85			0.91	45.39	0	19.84							100	2.46	1.34	1.13	29.62	0.59
36	llpeg_chip5_500	12		43.44				52.16		4.4							100	2.11	1.47	0.64	17.82	0.10
37	llpeg_chip5_500	7		29.38			2.17	34.93		30.08		3.44					100	2.9	1.12	1.78	44.32	1.02
38	llpeg_chip5_500	6		31.88				33.51		30.29						4.32	100	2.99	0.95	2.04	51.94	0.95
39	llpeg_chip5_500	6					6.13	27.19		66.68							100	3.33	1.15	2.18	48.66	
40	llpeg_chip5_500	13		40.51			1.18	44.21		14.1							100	2.47	1.32	1.15	30.24	0.35
41	llpeg_chip5_500	40		50.15				49.85									100	2.18	1.41	0.78	21.61	
42	llpeg_chip5_500	23		27.71			1.16	40.06		28.33		2.74					100	2.72	1.2	1.52	38.68	1.02
43	llpeg_chip5_500	20		45.67				54.33									100	1.99	1.53	0.45	12.91	

Table A 11 (cont.)

44	llpeg_chip5_500	25	33.17				36.34	30.49					100	2.96	1.03	1.94	48.61	0.92
45	llpeg_chip5_500	20	30.02				37.87	32.11					100	2.91	1.07	1.84	46.27	1.07
46	llpeg_chip5_500	10	41.02				56.99	1.99					100	1.88	1.61	0.28	7.91	0.05
47	llpeg_chip5_500	7	37.63				51.81	10.57					100	2.16	1.46	0.7	19.39	0.28
48	llpeg_chip5_500	33	32.32		11.87		40.59	12.12		3.1			100	3.33	1.14	2.19	48.84	0.38
49	llpeg_chip5_500	12	49.34				50.66						100	2.15	1.43	0.72	20.06	
50	llpeg_chip5_500	21	35.35			0.39	44.88	18.64	0.74				100	2.49	1.29	1.2	31.83	0.53
51	llpeg_chip5_500	18	27.05			0.93	33.87	36.37	1.78				100	3.06	1.01	2.04	50.2	1.34
52	llpeg_chip5_500	26	32.05				34.49	31.91	1.55				100	3.04	0.97	2.07	51.55	1.00
53	llpeg_chip5_500	14	23.52				37.1	39.38					100	2.99	1.05	1.94	48.13	1.67
54	llpeg_chip5_500	8	32.85			1.26	34.25	29.84	1.8				100	2.98	1.04	1.94	48.13	0.91
55	llpeg_chip5_500	10	40.38	3.45	6.92		46.53			2.72			100	2.81	1.31	1.5	36.32	
56	llpeg_chip5_500	14	37.63				40.05	22.32					100	2.75	1.13	1.62	41.78	0.59
57	llpeg_chip5_500	12	43.39				53.29	3.32					100	2.05	1.5	0.55	15.47	0.08
58	llpeg_chip5_500	28	47.83				52.17						100	2.08	1.47	0.61	17.15	
59	llpeg_chip5_500	12	41.05				55.1	3.86					100	1.98	1.55	0.42	12.01	0.09
60	llpeg_chip5_500	8	30.87			2.74	32.11	34.28					100	3.05	1.08	1.98	47.87	1.11
61	llpeg_chip5_500	5	53.44				46.56						100	2.32	1.31	1.01	27.8	
62	llpeg_chip5_500	10	43.92				56.08						100	1.91	1.58	0.33	9.41	
63	llpeg_chip5_500	5	44.41				55.59						100	1.93	1.57	0.36	10.39	
64	llpeg_chip5_500	12	38.08			6.19	37.65	18.08					100	2.56	1.45	1.11	27.72	0.47
65	llpeg_chip5_500	5	50.84				49.16						100	2.21	1.39	0.82	22.92	
66	llpeg_chip5_500	5	58.73				41.27						100	2.55	1.16	1.39	37.39	
67	llpeg_chip5_500	16	34.58		14.14	3.78	40.41	7.1					100	3.43	1.38	2.06	42.76	0.21
68	llpeg_chip5_500	8	43.22				56.78						100	1.88	1.6	0.28	8	
69	llpeg_chip5_500	5	45.35				54.65						100	1.97	1.54	0.43	12.27	
70	llpeg_chip5_500	16	31.15		5.39		42.02	18.1			3.34		100	2.96	1.19	1.77	42.81	0.58
71	llpeg_chip5_500	22	20.48			1.55	34.53	38.03	1.37		4.02		100	2.96	1.07	1.89	46.89	1.86
72	llpeg_chip5_500	14	40.43				57.93	1.64					100	1.84	1.63	0.21	5.94	0.04
73	llpeg_chip5_500	5	19.15			20.05	15.99	44.81					100	3.07	1.7	1.37	28.67	2.34
74	llpeg_chip5_500	6	37.17				39.13	11.19		4.26	8.25		100	2.43	1.1	1.32	37.49	0.30
75	llpeg_chip5_500	5	49.36				50.64						100	2.15	1.43	0.72	20.1	
76	llpeg_chip5_500	5	45.39				51.34	3.26					100	2.14	1.45	0.69	19.22	0.07
77	llpeg_chip5_500	14	30.05				39.73	28.93	1.29				100	2.8	1.12	1.68	42.8	0.96
78	llpeg_chip5_500	32	27.86				42.47	28.42	1.25				100	2.68	1.2	1.48	38.15	1.02
79	llpeg_chip5_500	14	51.94				48.06						100	2.26	1.36	0.9	25	
80	llpeg_chip5_500	8	41.4				57.61	0.98					100	1.85	1.62	0.22	6.47	0.02
81	llpeg_chip5_500	14	25.15				35.33	39.52					100	3.07	1	2.07	50.94	1.57
82	llpeg_chip5_500	27	32.64				35.24	32.13					100	3.02	0.99	2.03	50.51	0.98
83	llpeg_chip5_500	14	30.18				42.83	26.27	0.72				100	2.65	1.21	1.44	37.37	0.87

Table A 12. EDS data (weight percent) for Long Lake greisen chip A (n = 8).

Table A12

EDS data for Long Lake greisen chip A (n = 8).

#	Sample	mound size (µm)	F	Na	Al	S	Cl	K	Ca	Mn	Fe	Br	Total	Σ+	Σ-	diff	Σdiff%
1	llgre_01	11	3.90	16.06			49.06	2.67	28.31				100.00	2.50	1.37	1.13	29.11
2	llgre_01	12	4.03	39.38			49.74	0.69	6.15				100.00	2.05	1.56	0.49	13.58
3	llgre_01	35		22.35			41.75	35.90					100.00	1.73	1.27	0.46	15.21
4	llgre_01	14		30.09			43.76	26.16					100.00	1.85	1.31	0.53	16.83
5	llgre_01	20		18.01			43.18	38.80					100.00	1.62	1.31	0.32	10.81
6	llgre_01	10		29.63			44.48	25.89					100.00	1.82	1.33	0.49	15.50
7	llgre_01	12		35.34			43.50	21.16					100.00	1.97	1.29	0.68	20.73
8	llgre_01	13		37.51			40.44	22.05					100.00	2.09	1.21	0.87	26.39

Table A 13. EDS data (weight percent) for Long Lake greisen chip B (n = 16).

Table A13

EDS data for Long Lake greisen chip B (n = 16).

#	Sample	mound size (µm)	F	Na	Al	S	Cl	K	Ca	Mn	Fe	Br	Total	Σ+	Σ-	diff	Σdiff%
1	llgre_01	5		43.69			42.15	14.16					100.00	2.21	1.23	0.98	28.40
2	llgre_01	4	13.65	35.08			38.51		12.76				100.00	2.10	1.77	0.33	8.55
3	llgre_01	6		48.78			51.22						100.00	2.18	1.41	0.78	21.67
4	llgre_01	10		41.08			40.60	18.31					100.00	2.17	1.21	0.96	28.58
5	llgre_01	10		40.74			39.83	19.44					100.00	2.18	1.19	0.99	29.39
6	llgre_01	6					46.54	53.46					100.00	1.35	1.33	0.02	0.71
7	llgre_01	4		36.06			49.87		14.07				100.00	2.40	1.35	1.05	28.04
8	llgre_01	11	5.61	30.77			47.58	1.46	14.58				100.00	2.26	1.51	0.75	19.96
9	llgre_01	10		43.11			56.09	0.79					100.00	1.95	1.55	0.40	11.33
10	llgre_01	23	2.12	27.09			54.11	2.09	14.59				100.00	2.15	1.49	0.66	18.07
11	llgre_01	10	10.89	18.66			40.50	1.48	27.90	0.57			100.00	2.53	1.50	1.03	25.57
12	llgre_01	12	4.86	32.65			44.80	1.97	15.72				100.00	2.40	1.39	1.01	26.55
13	llgre_01	8	6.23	23.47			44.89	1.02	24.39				100.00	2.50	1.41	1.09	27.79
14	llgre_01	10	3.63	35.46			48.94	1.15	10.82				100.00	2.09	1.54	0.55	15.29
15	llgre_01	8		46.79			53.21						100.00	2.10	1.46	0.63	17.79
16	llgre_01	6		37.33			52.16	1.89	8.63				100.00	2.07	1.49	0.58	16.40

Table A 14. EDS data (weight percent) for Long Lake greisen chip C (n = 32).

Table A14

EDS data for Long Lake greisen chip C (n = 32).

#	Sample	mound size (µm)	F	Na	Al	S	Cl	K	Ca	Mn	Fe	Br	Total	Σ+	Σ-	diff	Σdiff%
1	llgre_01	10		38.11			49.34	2.69	9.86				100.00	2.17	1.42	0.75	20.90
1	llgre_01	5	7.35	30.04			43.06		19.55				100.00	2.46	1.45	1.02	25.97
1	llgre_01	12		29.57			52.96	2.93	14.53				100.00	2.23	1.43	0.80	21.92
1	llgre_01	5		36.08			47.57	4.60	11.75				100.00	2.20	1.39	0.81	22.65
1	llgre_01	4	10.79	33.37			42.20	3.09	10.55				100.00	1.99	1.73	0.26	7.05
1	llgre_01	13	8.82	32.24			46.71	2.79	9.44				100.00	1.89	1.75	0.14	3.87
1	llgre_01	7	12.19	35.21			41.22	2.01	9.37				100.00	2.00	1.77	0.23	6.04
1	llgre_01	4	12.80	36.99			41.63		8.58				100.00	2.00	1.80	0.20	5.15
1	llgre_01	21	5.57	34.43			52.40		7.09	0.51			100.00	1.86	1.72	0.14	3.92
1	llgre_01	5	9.89	31.95			43.45	0.56	14.15				100.00	2.24	1.61	0.63	16.46
1	llgre_01	10	7.62	33.22			44.32	0.80	14.04				100.00	2.11	1.63	0.48	12.91
1	llgre_01	8	5.01	29.98			46.72	1.40	16.88				100.00	2.35	1.44	0.91	23.98
1	llgre_01	5	9.99	25.03			38.08	1.17	25.74				100.00	2.62	1.42	1.20	29.77
1	llgre_01	8		36.87			49.08		12.62	1.44			100.00	2.23	1.42	0.81	22.21
1	llgre_01	14		30.67			50.58	1.29	17.46				100.00	2.40	1.36	1.04	27.77
1	llgre_01	4		37.67			52.75		9.58				100.00	2.10	1.50	0.59	16.53
1	llgre_01	10	12.55	25.42			40.42	3.05	17.09	1.46			100.00	2.24	1.65	0.59	15.14
1	llgre_01	8	8.17	26.37			41.52	2.50	20.74	0.70			100.00	2.45	1.45	1.01	25.79
1	llgre_01	25	5.07	26.18			46.64	2.45	18.93	0.73			100.00	2.36	1.44	0.93	24.40
1	llgre_01	14	9.64	27.34			40.95	2.70	18.51	0.86			100.00	2.37	1.51	0.86	22.07
1	llgre_01	15	7.73	29.16			48.02	0.94	14.16				100.00	2.15	1.62	0.53	14.02
1	llgre_01	17	5.03	33.04			47.74	0.84	13.35				100.00	2.09	1.59	0.50	13.62
1	llgre_01	24	10.27	16.19			40.11	2.14	30.67	0.61			100.00	2.60	1.44	1.16	28.65
1	llgre_01	5	13.23	24.04			35.78	2.27	24.67				100.00	2.54	1.51	1.03	25.37
1	llgre_01	8	9.13	28.61			45.59	2.47	14.18				100.00	2.15	1.63	0.52	13.73
1	llgre_01	40		28.98			55.43	2.83	12.76				100.00	1.92	1.59	0.33	9.41
1	llgre_01	25		19.33			54.69	3.72	22.26				100.00	2.30	1.42	0.89	23.82
1	llgre_01	10		24.80			54.51	2.06	18.62				100.00	2.27	1.44	0.83	22.38
1	llgre_01	30	2.71	27.98			53.61	2.81	12.89				100.00	1.91	1.63	0.28	7.92
1	llgre_01	5		36.52			49.92		13.56				100.00	2.22	1.44	0.77	21.18
1	llgre_01	26		31.44			52.86	2.25	13.45				100.00	2.04	1.53	0.52	14.45
1	llgre_01	16	6.64	28.74			51.35	0.47	12.28	0.52			100.00	1.86	1.77	0.09	2.36

Table A 15. EDS data (weight percent) for Long Lake greisen chip D (n = 62).

Table A15

EDS data for Long Lake greisen chip D (n = 62).

#	Sample	Mound size (µm)	F	Na	Al	S	Cl	K	Ca	Mn	Fe	Br	Total	Σ+	Σ-	diff	Σdiff%
1	llgre_01	16	4.53	26.51			50.42	2.18	16.37				100.00	2.22	1.51	0.70	18.82
2	llgre_01	35		30.68		0.98	49.14	17.84	1.37				100.00	1.76	1.50	0.26	7.87
3	llgre_01	8		6.70			45.53	47.77					100.00	1.42	1.34	0.08	3.07
4	llgre_01	8		38.81			45.62	15.57					100.00	2.02	1.33	0.68	20.42
5	llgre_01	11		24.16			48.86	26.98					100.00	1.62	1.44	0.17	5.68
6	llgre_01	14		28.08		0.83	49.54	21.55					100.00	1.67	1.51	0.15	4.88
7	llgre_01	14		36.41			47.99	15.61					100.00	1.91	1.40	0.51	15.56
8	llgre_01	10		39.66			52.08	8.26					100.00	1.92	1.48	0.44	13.02
9	llgre_01	8		47.73		16.45	30.30		5.52				100.00	2.28	1.89	0.39	9.36
10	llgre_01	30		40.86			47.89	11.25					100.00	2.03	1.38	0.65	19.11
11	llgre_01	4		45.07		4.96	49.97						100.00	1.98	1.71	0.27	7.24
12	llgre_01	10	4.25	29.14			49.73	2.12	14.75				100.00	2.22	1.49	0.73	19.65
13	llgre_01	35	3.72	27.96			49.48	1.77	17.06				100.00	2.30	1.45	0.86	22.80
14	llgre_01	16	3.93	30.30			51.26	0.31	14.21				100.00	2.21	1.51	0.70	18.67
15	llgre_01	18		22.26			56.66	1.27	19.25	0.56			100.00	2.22	1.48	0.74	20.02
16	llgre_01	12	5.64	24.52			45.01	2.78	20.42	1.63			100.00	2.41	1.42	0.99	25.98
17	llgre_01	8	9.69	27.14			42.34	2.56	16.98	1.30			100.00	2.29	1.56	0.73	18.93
18	llgre_01	6	11.78	32.10			42.75		13.37				100.00	2.00	1.80	0.20	5.27
19	llgre_01	12	9.58	25.03			45.23	1.59	18.18	0.39			100.00	2.24	1.62	0.62	16.03
20	llgre_01	22		24.72			55.76	2.84	16.18	0.49			100.00	2.16	1.48	0.68	18.62
21	llgre_01	16		35.55			54.36	1.05	9.04				100.00	2.00	1.55	0.46	12.81
22	llgre_01	20	9.60	27.87			43.65	1.58	16.71	0.60			100.00	2.27	1.59	0.68	17.54
23	llgre_01	15	10.55	24.70			45.05		19.70				100.00	2.26	1.65	0.62	15.77
24	llgre_01	25	9.38	26.16			45.62	1.15	17.70				100.00	2.23	1.62	0.61	15.89
25	llgre_01	10	14.03	30.75			42.97	1.05	11.20				100.00	1.85	1.92	-0.07	-1.85
26	llgre_01	10	15.22	26.53			37.65	0.88	19.72				100.00	2.33	1.68	0.65	16.27
27	llgre_01	22	8.57	22.31			42.46	2.18	24.47				100.00	2.48	1.46	1.01	25.73
28	llgre_01	8	20.04	22.37			31.20	1.82	24.57				100.00	2.46	1.70	0.76	18.18
29	llgre_01	4	14.26	38.31			40.36		7.07				100.00	1.98	1.83	0.15	3.97
30	llgre_02	21	13.09	23.25			38.39	1.66	23.62				100.00	2.44	1.58	0.87	21.59
31	llgre_02	30	12.41	19.70			39.68	2.51	25.70				100.00	2.45	1.56	0.89	22.09
32	llgre_02	19	8.81	28.21			40.80	1.95	20.23				100.00	2.46	1.46	1.00	25.54
33	llgre_02	15	11.85	25.62			40.41		22.12				100.00	2.42	1.58	0.84	21.12
34	llgre_02	24	8.80	30.42			45.71	0.47	14.61				100.00	2.21	1.61	0.60	15.68
35	llgre_02	23	10.04	26.04			44.39		18.95	0.58			100.00	2.29	1.61	0.68	17.36
36	llgre_02	24	9.79	23.00			45.04		22.17				100.00	2.34	1.59	0.75	18.95
37	llgre_02	10	17.12	28.61			35.20		19.07				100.00	2.36	1.71	0.65	15.98
38	llgre_02	14		40.60			50.41	8.99					100.00	1.97	1.43	0.54	15.82
39	llgre_02	11	11.66	36.82			43.47	1.31	6.74				100.00	1.94	1.79	0.14	3.82
40	llgre_02	26		27.75			41.67	24.42	6.16				100.00	1.99	1.27	0.72	22.19
41	llgre_02	25	6.04	26.61			47.24	1.24	17.71	1.16			100.00	2.30	1.50	0.80	20.97
42	llgre_02	7	13.72	30.37			37.13	1.01	17.77				100.00	2.38	1.61	0.77	19.38
43	llgre_02	11	9.58	32.73			41.54		16.15				100.00	2.38	1.53	0.84	21.61
44	llgre_02	26	9.75	28.34			46.29		15.62				100.00	2.18	1.67	0.51	13.25
45	llgre_02	19	9.64	25.94			45.98	1.04	17.40				100.00	2.20	1.64	0.56	14.58
46	llgre_02	15	9.41	28.75			45.39		16.44				100.00	2.24	1.62	0.62	15.97
47	llgre_02	12	11.56	31.07			41.24		14.71	1.43			100.00	2.27	1.63	0.63	16.27
48	llgre_02	18	9.13	32.06			44.46		14.35				100.00	2.25	1.60	0.66	17.04
49	llgre_02	11	9.33	29.99			44.20		16.49				100.00	2.29	1.59	0.70	18.10
50	llgre_02	7	12.42	35.72			43.24		8.62				100.00	1.94	1.83	0.11	2.95
51	llgre_02	14		41.42			51.47		7.11				100.00	2.15	1.45	0.70	19.35
52	llgre_02	15		31.80			55.36	12.83					100.00	1.66	1.58	0.08	2.35
53	llgre_02	12		33.62			55.24	11.14					100.00	1.71	1.58	0.13	4.03
54	llgre_02	12		35.18			54.77	10.05					100.00	1.76	1.56	0.20	5.94
55	llgre_02	19	12.05	17.90			50.46	2.90	16.69				100.00	1.90	1.87	0.03	0.78
56	llgre_02	7	13.39	33.33			46.39	0.82	6.07				100.00	1.81	1.92	-0.11	-2.92
57	llgre_02	25	11.89	27.39			43.16	0.71	15.80	1.04			100.00	2.18	1.69	0.49	12.68
58	llgre_02	7	16.96	31.94			37.46		13.64				100.00	1.99	1.92	0.07	1.89
59	llgre_02	5	15.14	37.03			35.54		12.29				100.00	2.17	1.75	0.41	10.50
60	llgre_02	22		34.14	6.29		54.15	4.90			0.52		100.00	2.31	1.55	0.76	19.78
61	llgre_02	25	14.79	31.39			42.31		11.51				100.00	1.87	1.94	-0.07	-1.85
62	llgre_02	23		43.39			56.61						100.00	1.95	1.56	0.39	11.00

Table A 16. Evaluation of EDS results (weight percent) and EDS acquisition time.

Table A16

Evaluation of EDS results and EDS acquisition time.

Sample	Acquisiton time (sec)	F	Na	S	Cl	K	Ca	Mn	As	In	Total	∑+	∑-	diff	∑diff%
AT1	5		13.40		53.42	2.75	30.43				100.00	2.17	1.51	0.66	18.07
AT1	10		12.17		53.81	2.57	31.46				100.00	2.16	1.52	0.65	17.57
AT1	15		13.04		53.07	2.76	31.12				100.00	2.19	1.50	0.69	18.82
AT1	20		12.43		53.41	3.03	31.13				100.00	2.17	1.51	0.66	18.08
AT1	40	1.27	12.90		52.48	2.74	30.61				100.00	2.16	1.48	0.68	18.65
AT1	50	1.82	12.80		52.47	2.84	30.08				100.00	2.13	1.48	0.65	18.02
AT1	60		12.73		53.08	2.74	31.46				100.00	2.19	1.50	0.70	18.87
AT2	5	9.62	13.42		48.66	1.40	26.90				100.00	1.96	1.37	0.59	17.68
AT2	10	10.32	14.02		46.61	1.29	26.59	1.17			100.00	2.01	1.31	0.70	20.97
AT2	15	10.92	14.31		47.02	1.22	25.82	0.72			100.00	1.97	1.33	0.64	19.48
AT2	20	9.21	14.07		47.72	1.62	26.42	0.96			100.00	2.01	1.35	0.66	19.72
AT2	25	9.90	13.71		47.78	1.23	26.22	1.16			100.00	1.98	1.35	0.63	18.97
AT2	30	9.67	14.04		46.82	1.53	26.40	1.54			100.00	2.02	1.32	0.70	21.03
AT2	35	10.14	13.91		47.05	1.28	26.66	0.96			100.00	2.00	1.33	0.68	20.30
AT2	40	8.51	14.31		47.88	1.40	26.96	0.95			100.00	2.04	1.35	0.69	20.28
AT2	60	10.09	14.52		46.86	1.39	26.31	0.83			100.00	2.01	1.32	0.69	20.67
AT2	80	9.88	14.11		46.89	1.30	26.67	1.14			100.00	2.02	1.32	0.70	20.86
AT2	100	10.07	14.21		46.94	1.29	26.48	1.01			100.00	2.01	1.32	0.69	20.55
AT3	5		42.03		57.97						100.00	1.83	1.64	0.19	5.57
AT3	10		41.50		58.50						100.00	1.81	1.65	0.15	4.48
AT3	15		42.04		57.96						100.00	1.83	1.63	0.19	5.59
AT3	20		41.58		58.42						100.00	1.81	1.65	0.16	4.65
AT3	30		41.96		58.04						100.00	1.83	1.64	0.19	5.42
AT3	40		41.16		57.24					1.60	100.00	1.83	1.61	0.22	6.32
AT3	60		42.58		57.42						100.00	1.85	1.62	0.23	6.69
AT3	100		41.56		57.81	0.62					100.00	1.82	1.63	0.19	5.59
AT3.5	5	19.14	3.96		23.10		53.81				100.00	2.86	0.65	2.21	62.86
AT3.5	10	19.07	2.92	1.58	21.84		54.59				100.00	2.85	0.71	2.14	59.91
AT3.5	20	20.43	4.38		20.64		51.42	3.13			100.00	2.87	0.58	2.29	66.27
AT3.5	15	21.60	3.92	0.95	21.22		49.81	2.50			100.00	2.75	0.66	2.09	61.38
AT3.5	25	21.91	3.66	1.02	21.97		49.44	2.00			100.00	2.70	0.68	2.02	59.60
AT3.5	30	21.81	3.76	0.89	21.13		50.22	2.19			100.00	2.75	0.65	2.10	61.67
AT3.5	40	21.24	4.16		21.44		50.74	2.43			100.00	2.80	0.60	2.20	64.50
AT3.5	60	21.48	3.64	0.94	20.89		51.00	2.06			100.00	2.78	0.65	2.13	62.19
AT3.5	100	23.17	3.79	0.95	20.21		49.77	2.11			100.00	2.73	0.63	2.10	62.48
AT4	5		46.61		53.39						100.00	2.03	1.51	0.52	14.77
AT4	10		43.99		51.19				4.81		100.00	2.11	1.44	5.19	8.93
AT4	15		44.14		52.10				3.75		100.00	2.07	1.47	0.60	16.97
AT4	20		45.13		51.94				2.93		100.00	2.08	1.47	0.62	17.35
AT4	25		44.75	1.18	50.84				3.23		100.00	2.08	1.51	0.57	15.86
AT4	30		44.08	1.53	50.85				3.55		100.00	2.06	1.53	0.53	14.77
AT4	40		45.38		50.83		0.88		2.91		100.00	2.13	1.43	0.70	19.64
AT4	60		43.73	1.06	50.09	0.83	1.00		3.29		100.00	2.11	1.48	0.63	17.47
AT4	100		43.78	0.88	50.16	0.86	1.08		3.23		100.00	2.11	1.47	0.64	17.88

Table A 17. EDS data (weight percent) for Sample A09–2378 (oven–heated to 500°C).

Table A17

EDS data (weight percent) for Sample A09-2378 (oven-heated to 500°C).

Sample	Mound size (μm)	F	Na	Cl	K	Ca	Mn	Zn	As	TOTAL	Σ+	Σ-	diff	Σdiff%
A09-2378_oven	5		33.31	44.56	22.13					100.00	2.02	1.26	0.76	23.18
A09-2378_oven	5		22.63	38.22	39.15					100.00	1.99	1.08	0.91	29.63
A09-2378_oven	5		55.10	44.90						100.00	2.40	1.27	1.13	30.87
A09-2378_oven	7		18.17	38.09	43.74					100.00	1.91	1.07	0.84	27.99
A09-2378_oven	7		28.44	39.45	32.10					100.00	2.06	1.11	0.95	29.83
A09-2378_oven	8		28.57	43.10	28.33					100.00	1.97	1.22	0.75	23.61
A09-2378_oven	10		28.68	39.99	31.33					100.00	2.05	1.13	0.92	28.99
A09-2378_oven	10		23.74	38.04	38.22					100.00	2.01	1.07	0.94	30.41
A09-2378_oven	12		30.43	46.47	16.59	6.52				100.00	2.07	1.31	0.76	22.54
A09-2378_oven	15		16.69	40.33	38.52	4.47				100.00	1.93	1.14	0.80	25.93
A09-2378_oven	15		17.52	38.54	38.85	5.09				100.00	2.01	1.09	0.92	29.79

Table A 18. EDS data (weight percent) for Sample A09–2378 (stage–heated to 500°C).

Table A18

EDS data (weight percent) for Sample A09-2378 (stage-heated to 500°C).

Sample	Mound size (μm)	F	Na	Cl	K	Ca	Mn	Zn	As	TOTAL	Σ+	Σ-	diff	Σdiff%
A09-2378 stage	5	16.16	34.40	40.43	2.82	3.22			2.97	100.00	1.85	1.99	-0.14	-3.72
A09-2378 stage	5		11.43	44.34	44.23					100.00	1.63	1.25	0.38	13.12
A09-2378 stage	5		18.25	44.70	37.04					100.00	1.74	1.26	0.48	16.01
A09-2378 stage	5		17.85	44.10	38.05					100.00	1.75	1.24	0.51	16.89
A09-2378 stage	5		19.96	43.25	36.80					100.00	1.81	1.22	0.59	19.46
A09-2378 stage	5		49.84	50.16						100.00	2.17	1.41	0.75	21.05
A09-2378 stage	5		34.60	38.87	26.53					100.00	2.18	1.10	1.09	33.15
A09-2378 stage	7	24.52	32.22	33.57		9.69				100.00	1.89	2.24	-0.35	-8.55
A09-2378 stage	7		13.67	44.27	42.07					100.00	1.67	1.25	0.42	14.45
A09-2378 stage	7		26.73	42.90	30.37					100.00	1.94	1.21	0.73	23.17
A09-2378 stage	7		23.56	41.06	35.38					100.00	1.93	1.16	0.77	24.99
A09-2378 stage	7		39.60	42.12	18.28					100.00	2.19	1.19	1.00	29.68
A09-2378 stage	8	14.91	35.76	42.07	3.02	4.25				100.00	1.85	1.97	-0.13	-3.31
A09-2378 stage	8	10.43	40.11	45.41		4.05				100.00	1.95	1.83	0.12	3.10
A09-2378 stage	10		17.64	46.17	36.19					100.00	1.69	1.30	0.39	13.05
A09-2378 stage	10		41.26	52.91	5.83					100.00	1.94	1.49	0.45	13.16
A09-2378 stage	12		15.77	44.22	40.01					100.00	1.71	1.25	0.46	15.63
A09-2378 stage	14		15.62	44.65	39.73					100.00	1.70	1.26	0.44	14.77
A09-2378 stage	18	11.57	27.55	46.17	1.79	11.81		1.10		100.00	1.87	1.91	-0.04	-1.15
A09-2378 stage	20	18.53	24.23	41.97	0.76	14.51				100.00	1.80	2.16	-0.36	-9.15
A09-2378 stage	20		15.51	45.41	39.08					100.00	1.67	1.28	0.39	13.32

Table A 19. EDS data (weight percent) for Sample A09–2370 (oven–heated to 500°C).

Table A19

EDS data (weight percent) for Sample A09-2370 (oven-heated to 500°C).

Sample	Mound size (μm)	F	Na	Cl	K	Ca	Mn	Zn	As	TOTAL	Σ+	Σ-	diff	Σdiff%
A09-2370 oven	5		16.17	54.85		28.98				100.00	2.15	1.55	0.60	16.30
A09-2370 oven	10		47.32	52.68						100.00	2.06	1.49	0.57	16.17
A09-2370 oven	10		19.96	42.66	37.38					100.00	1.82	1.20	0.62	20.51
A09-2370 oven	15		36.19	46.85	16.96					100.00	2.01	1.32	0.69	20.63
A09-2370 oven	15		36.76	45.03	18.22					100.00	2.07	1.27	0.80	23.84
A09-2370 oven	20		35.38	42.84	21.78					100.00	2.10	1.21	0.89	26.87
A09-2370 oven	25		16.67	45.47	37.86					100.00	1.69	1.28	0.41	13.80
A09-2370 oven	25		33.64	44.88	21.48					100.00	2.01	1.27	0.75	22.79
A09-2370 oven	35		32.42	45.78	21.80					100.00	1.97	1.29	0.68	20.77
A09-2370 oven	37		34.22	46.09	19.69					100.00	1.99	1.30	0.69	21.04
A09-2370 oven	50		15.44	44.08	40.48					100.00	1.71	1.24	0.46	15.72
A09-2370 oven	60		16.28	44.02	39.70					100.00	1.72	1.24	0.48	16.26
A09-2370 oven	70		19.30	41.47	39.23					100.00	1.84	1.17	0.67	22.34
A09-2370 oven	80		19.01	44.87	36.12					100.00	1.75	1.27	0.49	16.08
A09-2370 oven	90		11.33	45.10	43.56					100.00	1.61	1.27	0.34	11.64

Table A 20. EDS data (weight percent) for Sample A09–2370 (stage–heated to 500°C).

Table A20

EDS data (weight percent) for Sample A09-2370 (stage-heated to 500°C).

Sample	Mound size (μm)	F	Na	Cl	K	Ca	Mn	Zn	As	TOTAL	Σ+	Σ-	diff	Σdiff%
A09-2370 stage	5		27.92	45.92		26.15				100.00	2.52	1.30	1.22	32.10
A09-2370 stage	8		16.39	52.49		31.12				100.00	2.27	1.48	0.79	20.97
A09-2370 stage	10		22.61	47.28	30.11					100.00	1.75	1.33	0.42	13.62
A09-2370 stage	15		19.91	57.40	1.43	21.25				100.00	1.96	1.62	0.34	9.61
A09-2370 stage	15		18.48	47.37	34.15					100.00	1.68	1.34	0.34	11.32
A09-2370 stage	15		19.04	55.10	0.79	25.08				100.00	2.10	1.55	0.55	14.93
A09-2370 stage	15		18.38	42.15	29.97	9.50				100.00	2.04	1.19	0.85	26.37
A09-2370 stage	18		25.92	57.90	0.66	15.52				100.00	1.92	1.63	0.29	8.05
A09-2370 stage	20		20.73	58.53	0.76	19.59	0.39			100.00	1.91	1.65	0.26	7.36
A09-2370 stage	20		28.42	54.75	0.66	16.16				100.00	2.06	1.54	0.52	14.31
A09-2370 stage	22	7.91	28.69	45.10		18.31				100.00	2.16	1.69	0.47	12.29
A09-2370 stage	25		23.19	44.52	32.29					100.00	1.83	1.26	0.58	18.73
A09-2370 stage	30		16.61	45.55	37.84					100.00	1.69	1.28	0.41	13.63
A09-2370 stage	35		13.12	47.43	39.44					100.00	1.58	1.34	0.24	8.29

Table A 21. EDS data (weight percent) for Bayers Lake quartz pegmatite samples.

Table A21

EDS data for Bayers Lake quartz pegmatite samples.

#	Sample	Mound size (um)	F	Na	Al	P	S	Cl	K	Ca	Cr	Mn	Fe	Cu	As	Mo	Total	∑+	∑-	diff	∑diff%
1	bayers1	35		28.92				55.11	14.65	1.32							100.00	1.63	1.59	0.05	1.42
2	bayers1	12		27.56				56.74	15.70								100.00	1.54	1.63	-0.09	-2.90
3	bayers1	35		41.07	2.64			52.77	2.05						1.47		100.00	2.20	1.49	0.71	19.31
4	bayers1	25		41.53				55.20	1.50						1.76		100.00	1.94	1.54	0.40	11.59
5	bayers1	14		42.95				55.71	0.39	0.95							100.00	1.97	1.54	0.43	12.21
6	bayers1	140	23.36	17.65				21.26		37.73							100.00	2.57	1.79	0.78	17.85
7	bayers1	65	23.76	6.86			0.65	20.34	0.55	46.26		1.59					100.00	2.64	1.79	0.84	19.03
8	bayers1	40		36.65				48.65	14.71								100.00	1.91	1.41	0.49	14.87
9	bayers1	28		42.99				54.55	2.46								100.00	1.97	1.52	0.45	12.96
10	bayers1	33		40.80				54.56	4.64								100.00	1.91	1.53	0.38	11.03
11	bayers1	10		41.78				53.93	4.29								100.00	1.95	1.51	0.44	12.62
12	bayers1	14		43.07				54.87	2.06								100.00	1.97	1.52	0.44	12.67
13	bayers1	18		40.01				54.13	3.65					2.21			100.00	1.91	1.52	0.38	11.20
14	bayers1	150		35.49				48.31	16.20								100.00	1.88	1.41	0.47	14.42
15	bayers1	20	22.00	5.93				21.24		48.86		1.97					100.00	2.73	1.69	1.04	23.51
16	bayers1	30		40.53				57.33	2.15								100.00	1.85	1.59	0.26	7.57
17	bayers1	44	17.02	11.57				27.12		43.12		1.18					100.00	2.61	1.64	0.98	23.01
18	bayers1	160	17.19	16.79				24.93		41.08							100.00	2.69	1.59	1.09	25.57
19	bayers1	80	18.69	13.95				27.17		38.90		1.29					100.00	2.51	1.73	0.78	18.41
20	bayers1	90	23.70	9.57			0.93	18.95		45.41		1.45					100.00	2.69	1.78	0.91	20.34
21	bayers1	50	21.94	11.69				24.94		39.84		1.59					100.00	2.48	1.82	0.66	15.40
22	bayers1	80	18.21	16.93				28.52		36.34							100.00	2.45	1.75	0.71	16.79
23	bayers1	105	17.45	12.95				25.55		41.94		2.12					100.00	2.65	1.62	1.03	24.19
24	bayers1	45		40.62				54.65	0.77						3.96		100.00	1.96	1.53	0.43	12.28
25	bayers1	18		40.33				57.49	2.17								100.00	1.85	1.60	0.25	7.18
26	bayers1	36		39.15				56.58	4.27								100.00	1.83	1.58	0.25	7.19
27	bayers1	22		42.55				51.54	3.25	2.65							100.00	2.07	1.45	0.62	17.62
28	bayers1	10		43.42				53.50	3.08								100.00	2.00	1.49	0.51	14.54
29	bayers1	6		48.85				51.15									100.00	2.19	1.40	0.78	21.79
30	bayers1	10		46.55				53.45									100.00	2.09	1.47	0.62	17.31
31	bayers1	6		45.52				51.44	3.04								100.00	2.09	1.43	0.66	18.68
32	bayers1	38		40.72				53.41	3.47						2.40		100.00	1.96	1.50	0.46	13.22
33	bayers2	120		7.92				61.89		30.19							100.00	1.90	1.73	0.18	4.85
34	bayers2	140		2.58	1.09			62.68		33.65							100.00	2.02	1.72	0.30	8.15
35	bayers2	90		2.64	0.87			61.73	1.30	32.75		0.71					100.00	2.00	1.69	0.30	8.25
36	bayers2	80		2.47	0.79			60.64	1.49	33.91		0.70					100.00	2.04	1.67	0.37	9.93
37	bayers2	65		7.75	1.19			59.61	0.61	29.51		0.55	0.79				100.00	2.04	1.67	0.37	9.99
38	bayers2	36		38.66			0.32	58.26	2.76								100.00	1.78	1.65	0.13	3.87
39	bayers2	28		40.65				57.08	2.26								100.00	1.86	1.59	0.27	7.95
40	bayers2	48		39.64				58.13	2.22								100.00	1.82	1.62	0.20	5.81
41	bayers2	90		37.28				57.33	3.86							1.54	100.00	1.83	1.61	0.22	6.29
42	bayers2a	60		11.42				46.47	2.16	38.75		1.20					100.00	2.43	1.38	1.06	27.77
43	bayers2a	15	5.97	31.27				45.55	0.57	15.85		0.79					100.00	2.14	1.58	0.55	14.85
44	bayers2a	8		31.94				46.49	2.99	17.38		1.21					100.00	2.28	1.38	0.90	24.70
45	bayers2a	12	5.21	31.18				48.70	0.81	12.76		1.34					100.00	2.02	1.63	0.39	10.83
46	bayers2a	30		31.51				52.40	0.82	14.29		0.99					100.00	2.09	1.52	0.57	15.78
47	bayers2a	70		15.53				47.21	2.21	33.62		1.43					100.00	2.36	1.40	0.96	25.44
48	bayers2a	25	7.10	16.94				41.15	1.44	32.82		0.55					100.00	2.34	1.54	0.81	20.74

Table A 22. Microthermometric data for Bayers Lake quartz pegmatite samples.

Table A22

Microthermometric data for Bayers lake quartz pegmatite (Tm = melting temperature of last solid; Th: homogenizatoin (L to V) temperature).

#	Fluid inclusion	Assemblage	Tm(°C)	Th(°C)	Tm Corrected	Th Corrected	#	Fluid inclusion	Assemblage	Tm(°C)	Th(°C)	Tm (°C) corrected	Th (°C) corrected
1	1	1	-3.6	282.3	-3.3	278.8	73	10	3	-4.3	216.1	-4.0	213.5
2	2	1	-13.5	227.8	-13.1	225.0	74	11	3	-0.6	215.4	-0.3	212.8
3	3	1	-19.3	215	-18.9	212.4	75	8	4	-3.4	274.6	-3.1	271.2
4	4	1	-19.3	107.7	-18.9	106.5	76	9	4	-3.5	274.4	-3.2	271.0
5	5	1	-19.3	105	-18.9	103.9	77	10	5	-4.4	218.3	-4.1	215.6
6	1	1	-3.7	276	-3.4	272.6	78	11	5	-4.6	216.2	-4.3	213.6
7	2	1	-3.6	276	-3.3	272.6	79	1	7	-4.3	217.3	-4.0	214.7
8	3	1	-3.7	277.4	-3.4	274.0	80	2	7	-4.2	213	-3.9	210.4
9	4	1	-4.8	287.8	-4.5	284.2	81	3	7	-5.1	222.2	-4.8	219.5
10	1	1	-3.6	207.4	-3.3	204.9	82	4	7	-5.3	221.4	-5.0	218.7
11	2	1	-3.5	198.5	-3.2	196.1	83	6	7	-5.2	231.3	-4.9	228.5
12	1-1	1	-3.3	175.2	-3.0	173.1	84	7	7	-4.8	266	-4.5	262.7
13	1-2	1	-3.3	190.7	-3.0	188.4	85	8	7	-5.5	318.5	-5.2	314.5
14	1-3	1	-3.1	177.2	-2.8	175.1	86	9	7	-28.2	121.6	-27.7	120.3
15	2	1	-43.3	188.5	-42.7	186.3	87	10	7	-4.5	261.2	-4.2	258.0
16	4	1	-43.5	190.8	-42.9	188.5	88	13	7	-0.8	212.7	-0.5	210.1
17	5	1	-41.1	185.3	-40.5	183.1	89	14	7	-31.3	169.5	-30.8	167.5
18	6	1	-41.1	190.8	-40.5	188.5	90	15	7	-30.2	175.5	-29.7	173.4
19	7	1	-42.1	191.3	-41.5	189.0	91	16	7	-31.3	207.1	-30.8	204.6
20	1	1	-2.9	197.1	-2.6	194.7	92	20	7	-0.8	279	-0.5	275.5
21	3	1	-3.7	318.7	-3.4	314.7	93	21	7	-4.4	211.8	-4.1	209.2
22	4	1	-3.7	312.8	-3.4	308.9	94	22	7	-4.5	239.1	-4.2	236.2
23	5	1	-3.7	312.8	-3.4	308.9	95	1	7	-3.3	199.9	-3.0	197.5
24	6	1	-12.2	347.9	-11.8	343.5	96	2	8	-3.3	178.4	-3.0	176.3
25	1	1	-4	213.2	-3.7	210.6	97	3a	9	-3.3	181.2	-3.0	179.0
26	2	1	-4.5	229.3	-4.2	226.5	98	4	10	-10	193.8	-9.6	191.5
27	3	1	-4.5	224	-4.2	221.3	99	5	11	-3.3	157	-3.0	155.2
28	4	1	-4.5	217.1	-4.2	214.5	100	6	12	-7.6	196.7	-7.2	194.3
29	5	1	-4.5	208.7	-4.2	206.2	101	2b	13	-2.8	276.4	-2.5	273.0
30	6	1	-4	211	-3.7	208.4	102	4a	14	-3.1	203.7	-2.8	201.2
31	7	1	-4	212.5	-3.7	209.9	103	4b	14	-3.1	196.5	-2.8	194.1
32	1	1	-4.1	181.1	-3.8	179.0	104	8a	15	-2.3	193.1	-2.0	190.8
33	2	1	-4.1	283.1	-3.8	279.6	105	8b	15	-6.6	192.8	-6.3	190.5
34	3	1	-4.1	250.1	-3.8	247.0	106	8c	15	-6.6	204.6	-6.3	202.1
35	4	1	-4	280.6	-3.7	277.1	107	1	16	-3.5	202.2	-3.2	199.8
36	5	1	-4	281.9	-3.7	278.4	108	1	19	-2.9	211.8	-2.6	209.2
37	6	1	-4.6	280.6	-4.3	277.1	109	1	22	-4	196.2	-3.7	193.8
38	7	1	-4.6	280.6	-4.3	277.1	110	2	23	-4	202.1	-3.7	199.7
39	1	1	-3.7	176.9	-3.4	174.8	111	3	24	-4	199.8	-3.7	197.4
40	2	1	-3.9	203.2	-3.6	200.8	112	4	25	-4	217.3	-3.7	214.7
41	3	1	-3.9	300	-3.6	296.2	113	5	26	-3.9	219	-3.6	216.3
42	4	1	-3.9	300	-3.6	296.2	114	6	27	-4	211.3	-3.7	208.7
43	5	1	-46.5	150.2	-45.9	148.5	115	1	1a	-3.8	244.9	-3.5	241.9
44	6	1	-46.5	284.1	-45.9	280.6	116	2	1a	-3.8	256.9	-3.5	253.7
45	1	2	-0.8	203.8	-0.5	201.3	117	3	1a	-53	177.3	-52.3	175.2
46	2	2	-0.7	191.7	-0.4	189.4	118	4	1a	-53	186.9	-52.3	184.7
47	3	2	-0.8	195.7	-0.5	193.4	119	1	1a	-43.8	188.8	-43.2	186.5
48	4	2	-0.8	181.1	-0.5	179.0	120	2	1a	-42.5	188.8	-41.9	186.5
49	7	2	-0.7	236.4	-0.4	233.5	121	3	1a	-43.8	188.8	-43.2	186.5
50	8	2	-0.9	187.8	-0.6	185.6	122	4	1a	-42.2	191.7	-41.6	189.4
51	9	2	-1	183.3	-0.7	181.1	123	5	1a	-1.8	188.2	-1.5	186.0
52	12	2	-0.9	190.4	-0.6	188.1	124	2	1a	-52	197.1	-51.3	194.7
53	16	2	-0.9	185.3	-0.6	183.1	125	3	1a	-52.3	232.2	-51.6	229.4
54	17	2	-0.9	212.4	-0.6	209.8	126	3	1b	-3.8	201	-3.5	198.6
55	18	2	-1.4	250.3	-1.1	247.2	127	4	1b	-3.8	206	-3.5	203.5
56	19	2	-1.5	235.8	-1.2	232.9	128	6	1b	-52.9	155	-52.2	153.2
57	21	2	-1	186.6	-0.7	184.4	129	7	1b	-52.9	155	-52.2	153.2
58	22	2	-0.8	201	-0.5	198.6	130	8	1b	-52.9	150	-52.2	148.3
59	23	2	0	265.4	0.3	262.1	131	9	1b	-52.9	186.3	-52.2	184.1
60	24	2	-0.9	201.9	-0.6	199.5	132	6	1b	-2.6	198.5	-2.3	196.1
61	25	2	-0.9	247	-0.6	244.0	133	5	1b	-53.7	196	-53.0	193.6
62	2	2	-45.5	293.3	-44.9	289.6	134	7	1b	-53.7	196	-53.0	193.6
63	7	2	-46.3	301.8	-45.7	298.0	135	5	1c	-3.3	216.8	-3.0	214.2
64	2-2	2	-41.5	145	-40.9	143.3	136	6	1c	-4.6	221.7	-4.3	219.0
65	2	2	-57.6	202.9	-56.9	200.5	137	3	2b	-3.3	179.9	-3.0	177.8
66	3	2	-55.6	176.1	-54.9	174.0	138	4	2b	-3.5	201	-3.2	198.6
67	6	2	-52.2	184.6	-51.5	182.4	139	5	2b	-4	199.7	-3.7	197.3
68	3	3	-3.6	280.1	-3.3	276.6	140	6	2c	-3.1	289.7	-2.8	286.1
69	4	3	-3.4	280.1	-3.1	276.6	141	7	2c	-3.3	210.4	-3.0	207.9
70	5	3	-3.2	280.8	-2.9	277.3							
71	6	3	-3.4	280.7	-3.1	277.2							
72	9	3	-4.2	217.9	-3.9	215.3							

Appendix B

Table B 1: EDS results (weight percent) for evaporate mounds hosted A03 samples.

Table B1

EDS results (weight percent) for evaporate mounds hosted by A03 samples.

Sample	Site	Position	Mound size (µm)	F	Na	Mg	Al	S	Cl	K	Ca	Mn	Fe	Cu	Zn	Mo	In	Sn	Pb	Total	∑+	∑-	Σdiff	Σdiff%
A03-2338	1	1	10		38.78				53.99		7.23									100	2.05	1.52	0.52	14.68
A03-2338	2	1	5		43.47				52.96		3.57									100	2.07	1.49	0.57	16.13
A03-2338	3	1	8		39.08				53.43	1.33	6.15									100	2.04	1.51	0.53	15.03
A03-2338	4	1	10		39.28				53.2		7.52									100	2.08	1.50	0.58	16.26
A03-2338	4	2	1		54.18				45.82											100	2.36	1.29	1.06	29.15
A03-2338	5	1	12		39.93				51.9		8.17									100	2.14	1.46	0.68	18.85
A03-2338	6	1	8		32.94				47.17		19.89									100	2.42	1.33	1.09	29.14
A03-2338	7	1			36.49				51.21	1.89	10.41									100	2.15	1.44	0.71	19.73
A03-2338	8	1	5		39.87				51.22		8.91									100	2.18	1.44	0.73	20.25
A03-2338	8	2	7		39.86				55.51		4.63									100	1.96	1.57	0.40	11.29
A03-2338	8	3	4		41.78				52.3		5.92									100	2.11	1.48	0.64	17.75
A03-2338	9	1	7		41.43				50.21		6.82		1.53							100	2.20	1.42	0.78	21.60
A03-2338	10	1	20		37.47				54.38	0.8	7.35									100	2.02	1.53	0.48	13.59
A03-2338	11	1	8		25.46				48.04	2.85	23.65									100	2.36	1.36	1.01	27.05
A03-2348-1	1	1			43.29				56.71											100	1.88	1.60	0.28	8.12
A03-2348-1	1	2			49.63				50.37											100	2.16	1.42	0.74	20.60
A03-2348-1	1	3			41.32				58.68											100	1.80	1.66	0.14	4.10
A03-2348-1	1	4			44.64				55.36											100	1.94	1.56	0.38	10.84
A03-2348-1	2	1	1		40.21				59.79											100	1.75	1.69	0.06	1.80
A03-2348-1	2	2	1		44.96				55.04											100	1.95	1.55	0.40	11.47
A03-2348-1	2	3	1		48.11				51.89											100	2.09	1.46	0.63	17.67
A03-2348-1	6	1	2		44.94				55.06											100	1.95	1.55	0.40	11.44
A03-2348-1	8	2	30		33.05			7.45	36.08	19.32	4.1									100	2.14	1.48	0.65	18.06
A03-3002-2	1	1		30.26	28.51				26.6	0.64	14									100	1.96	2.34	-0.39	-9.03
A03-3002-2	2	1		25.88	27.65				31.64		14.83									100	1.94	2.25	-0.31	-7.43
A03-3002-2	18	1	2		39.04				33.47		27.49									100	3.07	0.94	2.13	52.95
A03-3002-2	18	2	2		27.48				37.93		34.59									100	2.92	1.07	1.85	46.38
A03-3002-2	19	1	2		33.59				34.89		31.53									100	3.03	0.98	2.05	51.02
A03-3002-2	19	2	2		36.72				28.74		34.54									100	3.32	0.81	2.51	60.75
A03-3002-2	21	1			34.51				29.49		36									100	3.30	0.83	2.47	59.71
A03-3002-2	28	1	3		42.67				48.07		3.23					6.04				100	2.14	1.36	0.79	22.48
A03-3002-2	28	2	2		46.82				41.74		11.44									100	2.61	1.18	1.43	37.77
A03-3002-2	28	3	5		41.29				53.75		4.96									100	2.04	1.52	0.53	14.80
A03-3002-2	29	1	3		43.65				46.76		9.6									100	2.38	1.32	1.06	28.63
A03-3002-2	29	2	1		44.1				52.46		3.45									100	2.09	1.48	0.61	17.09
A03-3002-2	29	3	1		45.09				46.99		7.92									100	2.36	1.33	1.03	27.99
A03-3011	2	1	3		50.34				49.66											100	2.19	1.40	0.79	21.96
A03-3011	2	1			49.65				47.05	3.3										100	2.24	1.33	0.92	25.68
A03-3011	2	2			50.04				48.93	1.03										100	2.20	1.38	0.82	22.97
A03-3011	2	3			50.23				48.77	1.01										100	2.21	1.38	0.84	23.29
A03-3011	2	4			50.51				48.06	1.44										100	2.23	1.36	0.88	24.47
A03-3011	4	1			52.56				47.44											100	2.29	1.34	0.95	26.14
A03-3011	4	2			54.38				45.62											100	2.36	1.29	1.08	29.52
A03-3011	8	1	6		46.54				50.87		2.59									100	2.15	1.43	0.72	20.01
A03-3011	8	2	5		46.19				53.81											100	2.01	1.52	0.49	13.91
A03-3011	9	1	4		50.87				49.13											100	2.21	1.39	0.83	22.96
A03-3011	9	2	8		47.45				50.23		2.32									100	2.18	1.42	0.76	21.20
A03-3011	10	1	4		49.77				43.2		7.03									100	2.51	1.22	1.30	34.72
A03-3011	10	2	2		51.57				48.43											100	2.24	1.37	0.88	24.29
A03-3011	11	1	2		50.03				49.97											100	2.18	1.41	0.77	21.37
A03-3011	11	2	2		46.27				53.73											100	2.01	1.52	0.50	14.07
A03-3011	12	1			46.4				53.6											100	2.02	1.51	0.51	14.33
A03-3011	12	2			43.31				56.05		0.64									100	1.92	1.58	0.33	9.56
A03-3011	12	3			45.28				54.72											100	1.97	1.54	0.43	12.11
A03-3011	13	1	6		46.95				53.05											100	2.04	1.50	0.55	15.41
A03-3011	13	2	4		46.98				53.02											100	2.04	1.50	0.55	15.47
A03-3011	14	1	8		44.86				54.42		0.72									100	1.99	1.53	0.45	12.82
A03-3011	15	1	16		45.74				53.45	0.81										100	2.01	1.51	0.50	14.27
A03-3011	15	2	8		43.04				56.96											100	1.87	1.61	0.26	7.61
A03-3011	15	3	6		43.94				56.06											100	1.91	1.58	0.33	9.43
A03-3011	15	4	5		44.95				55.05											100	1.95	1.55	0.40	11.45
A03-3011	16	1	5		45.05				53.59	1.36										100	1.99	1.51	0.48	13.75
A03-3011	16	2			48.34				51.66											100	2.10	1.46	0.64	18.12
A03-3011	16	3			48.5				51.5											100	2.11	1.45	0.66	18.43
A03-3014	2	1			53.01				46.99											100	2.31	1.33	0.98	27.00
A03-3014	2	4			55.61				44.39											100	2.42	1.25	1.17	31.79
A03-3014	4	1			49.71				49.27	1.02										100	2.19	1.39	0.80	22.32

Table B1 (cont.)

A03-3014	5	1			50.75				49.25						100	2.21	1.39	0.82	22.75
A03-3014	5	2			54.25				45.75						100	2.36	1.29	1.07	29.30
A03-3014	5	3			55.35				44.65						100	2.41	1.26	1.15	31.31
A03-3014	6	1			53.19				46.81						100	2.31	1.32	0.99	27.34
A03-3014	6	2		12.15	48.1				36.74	0.58	2.43				100	2.23	1.68	0.55	14.15
A03-3029-1	2	1	8		33.81				53.39	0.95	10.57	1.28			100	2.07	1.51	0.56	15.74
A03-3029-1	3	1	7		33				40.6		26.39				100	2.75	1.15	1.61	41.23
A03-3029-1	4	1	13		25.07				47.55	5.53	18.14	3.7			100	2.27	1.34	0.93	25.75
A03-3029-1	4	2	4		35.81				51.19		11.94	1.07			100	2.19	1.44	0.75	20.57
A03-3029-1	4	3	3		11.91				41.85		38.26	7.97			100	2.72	1.18	1.54	39.43
A03-3029-1	5	1	4		40.79				49.72		9.49				100	2.25	1.40	0.84	23.15
A03-3029-1	6	1	12		27.39				42.68		27.42	2.5			100	2.65	1.20	1.45	37.53
A03-3029-1	7	1	6		30.23				42.41		22.58	4.78			100	2.62	1.20	1.42	37.23
A03-3029-1	7	2	4		45.96				54.04						100	2.00	1.52	0.47	13.46
A03-3029-1	8	1	12		29.82				52.54	3.23	13.04	1.38			100	2.08	1.48	0.60	16.79
A03-3029-1	8	2	50		25.68				50.52	5.41	15.56	2.83			100	2.13	1.42	0.71	19.93
A03-3029-1	9	1	10		35.72				52.57	2.68	7.31	1.72			100	2.05	1.48	0.57	16.03
A03-3029-1	14	1	11		19.93				56.03	7.33	13.1	3.62			100	1.84	1.58	0.26	7.58
A03-3002-4	2	1	10	24.12	27.08	0.61	5.66		32.79	1.8	7.22		0.73		100	2.29	2.19	0.10	2.12
A03-3002-4	2	5	12	21.81	35.39				37.89	1.64	6.13	0.23	0.71		100	1.92	2.22	-0.30	-7.16
A03-3002-4	4	3	8	32.91	39.77				22.34		4.98				100	1.98	2.36	-0.38	-8.86
A03-3011	6	4	38		35.76	0.75		0.66	46.77	12.88	2.93		0.24		100	2.10	1.36	0.74	21.39
A03-3011	7	3	29	24.49	34.55	2.53			29.56	0.31	8.25		0.3		100	2.14	2.12	0.02	0.42
A03-3024	1	3			53.01				46.99						100	2.31	1.33	0.98	27.00
A03-3024	3	2		29.41	40.39				25.99		4.21				100	1.97	2.28	-0.31	-7.39
A03-3024	4	1			53.27				46.73						100	2.32	1.32	1.00	27.48
A03-3024	7	4			52.02				39.64		8.34				100	2.68	1.12	1.56	41.11
A03-3024	8	1			53.26				46.74						100	2.32	1.32	1.00	27.47
A03-3024	9	1			51.06				48.94						100	2.22	1.38	0.84	23.34
A03-3024	9	2			51.99				48.01						100	2.26	1.35	0.91	25.09
A03-3024	9	3			52.5				47.5						100	2.28	1.34	0.94	26.05
A03-3024	13	2			50.8				46.39		2.81				100	2.35	1.31	1.04	28.47

Table B 2. EDS results (weight percent) for evaporate mounds hosted A04 samples.

Table B2

EDS results (weight percent) for evaporate mounds hosted by A04 samples.

Sample	Site	Position	Mound size (μm)	F	Na	Mg	Al	S	Cl	K	Ca	Mn	Fe	Cu	Zn	Mo	In	Sn	Pb	Total	∑+	∑-	Σdiff	Σdiff%
A04-8006	1	1	26		40.41			5.12	26	17.56	7.61		3.3							100	2.70	1.05	1.65	43.97
A04-8006	3	1	14		40.3			7.97	27.3	18.7	5.74									100	2.52	1.27	1.25	33.04
A04-8006	6	1	14		14.6				46.16		39.24									100	2.59	1.30	1.29	33.15
A04-8006	7	1	5		36.09				46.31	2.84	14.75									100	2.38	1.31	1.07	29.10
A04-8006	8	1	7		33.23				45.86	6.15	14.75									100	2.34	1.29	1.05	28.78
A04-8006	11	1	8		39.53			7.88	28.91	19.23	4.45									100	2.43	1.31	1.13	30.12
A04-8006	14	1	13		40.11			5.32	15.36	16.51	12.45		10.25							100	3.16	0.77	2.39	60.97
A04-8006	19	1	12		38.59				55.89		1.42		0.83			3.26				100	1.85	1.58	0.27	7.91
A04-8006	22	1	16		36.05			2.9	50.69	1.23	6.66		2.46							100	2.02	1.61	0.41	11.28
A04-8006	27	1	12		39.07			5.92	15.9	17.93	11.99		9.18							100	3.09	0.82	2.27	58.10
A04-3003	1	1	22		30.39				50.35	3.31	15.95									100	2.20	1.42	0.78	21.58
A04-3003	2	1	5		38.12				48.57		13.31									100	2.32	1.37	0.95	25.78
A04-3003	2	2	3		37.32				41.85		20.83									100	2.66	1.18	1.48	38.56
A04-3003	3	1	8		30.58				40.23		29.19									100	2.79	1.13	1.65	42.12
A04-3003	3	2	6		32.25				40.53	1.61	23.12		2.49							100	2.69	1.14	1.54	40.30
A04-3003	3	3	4		34.13				44.07		21.79									100	2.57	1.24	1.33	34.82
A04-3003	3	4	5		29.84				45.45		24.72									100	2.53	1.28	1.25	32.76
A04-3003	4	1	5		36.46				28.89		29.51		5.15							100	3.24	0.81	2.43	59.83
A04-3003	4	2	5		30.91				47.06		22.03									100	2.44	1.33	1.12	29.60
A04-3003	4	3	14		35.77				46.02		18.22									100	2.46	1.30	1.17	31.00
A04-3003	5	1	5		29.85				36.72		33.43									100	2.97	1.04	1.93	48.24
A04-3003	5	2	5		35.89				39.2		20.35		4.57							100	2.74	1.11	1.63	42.49
A04-3003	5	3	14		30.14				41.6	5.56	22.69									100	2.59	1.17	1.41	37.56
A04-3003	6	1	10		36.65				50.37		12.98									100	2.24	1.42	0.82	22.41
A04-3003	6	2	8		34.56				49.88		15.56									100	2.28	1.41	0.87	23.66
A04-3003	6	3	9		33.7				49.19	1.02	15.08	1.01								100	2.28	1.39	0.89	24.35
A04-1907-3	2	1			41.37			3.6	25.92	18.75			10.37							100	2.65	0.96	1.69	47.00
A04-1907-3	3	1			51.25				22.79	15.87			10.08							100	3.00	0.64	2.35	64.67
A04-1907-3	3	1	11		49.07				48.14	2.79										100	2.21	1.36	0.85	23.78
A04-1907-3	3	2	12		48.45				51.55											100	2.11	1.45	0.65	18.33
A04-1907-3	4	1	13		44.2				53.19	2.61										100	1.99	1.50	0.49	14.00
A04-1907-3	4	5	5		47.36				49.71	2.93										100	2.13	1.40	0.73	20.70
A04-1907-3	5	1	7		45.73				51.21	3.06										100	2.07	1.44	0.62	17.72
A04-1907-3	5	2	5		47.1				51.37	1.53										100	2.09	1.45	0.64	18.05
A04-1907-2	9	1	5		38.26				43.97		17.77									100	2.54	1.24	1.30	34.31
A04-1907-2	9	2	10		31				50.71	1.21	16.15	0.92								100	2.20	1.43	0.77	21.31
A04-1907-2	10	1	7		43.74				52.7		3.56									100	2.08	1.49	0.59	16.58
A04-1907-2	10	2			36.53				47.45		16.02									100	2.37	1.34	1.04	27.91
A04-1907-2	11	1	5		44.35				49.91		5.75									100	2.21	1.41	0.80	22.20
A04-1907-2	11	2	7		42				47.06		10.93									100	2.36	1.33	1.04	28.06
A04-1907-2	12	1	8		36.44				49.02	1.15	12.33	1.07								100	2.26	1.38	0.88	24.05
A04-1907-2	13	1	11		39.89				43.86		16.25									100	2.53	1.24	1.30	34.36
A04-1907-2	13	2			37.92				42.66		19.42									100	2.60	1.20	1.40	36.76
A04-1907-2	14	1			38.99				43.19		17.82									100	2.57	1.22	1.35	35.68
A04-1907-2	14	2			35.84				36.61		27.54									100	2.91	1.03	1.88	47.61
A04-1907-2	14	4			38.7				46.46		14.84									100	2.41	1.31	1.10	29.58
A04-1907-2	15	1	13		33.43				46.94	1.54	18.09									100	2.38	1.32	1.06	28.52
A04-1907-2	16	1			32.09				52.72	6.26	6.08	2.86								100	1.96	1.49	0.47	13.68
A04-1807-4	1	1			50.37				44.05		2.02	1.84	1.72							100	2.42	1.24	1.18	32.16
A04-1807-4	2	1			50.31				42.46		2.36	2.46	2.4							100	2.48	1.20	1.28	34.90
A04-1807-4	2	2			52.49				40.75			3.15	3.61							100	2.53	1.15	1.38	37.47
A04-1807-4	2	3			52.77				47.23											100	2.30	1.33	0.96	26.55
A04-1807-3	1	2	5	22.73	35.46				35.41	2.25	2.48	0.38	1.01							100	1.69	2.20	-0.50	-12.94
A04-1807-3	1	3	5	25.93	32.01				32.98	4.16	3.12	0.61	1.2							100	1.61	2.30	-0.69	-17.57
A04-1807-3	4	1	10	4.6	35.91				50.8	8.14	0.55									100	1.78	1.68	0.11	3.15
A04-1807-3	4	2	20	4.03	35.39				52.7	6.44	1.45									100	1.74	1.70	0.04	1.21
A04-1807-3	4	3	52	20.34	22.1				42.37	11.01	0.95	2.75	0.48							100	1.33	2.27	-0.94	-26.19
A04-1807-3	5	1	2		43.73				54.03		2.24									100	1.96	1.52	0.43	12.47
A04-1807-3	5	2	10	12	38.22				43.91	2.89	2.98									100	1.81	1.87	-0.06	-1.61
A04-1807-3	5	3	20	8.39	36.93				47.56	4.96	1.49	0.67								100	1.78	1.78	0.00	-0.01
A04-1807-3	6	1	8	9.16	37.01				46.11	5.05	1.76	0.92								100	1.80	1.78	0.02	0.47
A04-1807-3	7	1	7	6.06	40.69				49.23	1.79	2.23									100	1.87	1.71	0.16	4.58
A04-1807-3	7	2	12	8.94	37.26				46.13	4.79	1.81	1.08								100	1.81	1.77	0.04	1.02
A04-1807-3	7	3	10	9.71	38.46				44.95	4.36	1.72	0.8								100	1.84	1.78	0.06	1.74
A04-1807-3	8	1	10	16.58	34.29				41.49	3.19	3.38	1.06								100	1.68	2.04	-0.37	-9.84
A04-1807-3	9	1	22	20.65	29.49				39.03	4.37	3.83	1.31	0.73		0.6					100	1.54	2.19	-0.65	-17.50
A04-1807-3	10	1	7	21.98	32.42				37.15	3.26	3.77	0.69	0.72							100	1.61	2.20	-0.59	-15.50
A04-1807-3	11	1	7	33.09	31.52				27.69	2.39	3.68	0.88	0.75							100	1.55	2.52	-0.97	-23.78
A04-1807-3	11	2	11	26.71	28.16				31.23	3.1	3.95	0.85	1.1							100	1.44	2.35	-0.91	-24.04

Table B 3. EDS results (weight percent) for evaporate mounds hosted A05 samples.

Table B3

EDS results (weight percent) for evaporate mounds hosted by A05 samples.

Sample	Site	Position	Mound size (μm)	F	Na	Mg	Al	S	Cl	K	Ca	Mn	Fe	Cu	Zn	Mo	In	Sn	Pb	Total	∑+	∑-	Σdiff	Σdiff%
A05-8018	1	1	26		23.43				51.44	8.91	10.4	2.22	3.6							100	1.98	1.45	0.52	15.31
A05-8018	1	2	9		35.37				49.15	2.31	9.65	1.85	1.68							100	2.21	1.39	0.82	22.82
A05-8018	2	1	35		25.04				50.71	6.55	15.27	1.22	1.22							100	2.11	1.43	0.68	19.12
A05-8018	2	2	18		31.44				45.83	1.66	16.83	1.35	2.89							100	2.40	1.29	1.11	30.02
A05-8018	2	3	14		34.32				49.53	3.3	8.71	1.32	2.81							100	2.16	1.40	0.76	21.45
A05-8018	2	4	8		37.44				53.05	2.48	7.03									100	2.04	1.50	0.55	15.43
A05-8018	2	5	8		28.91				50.09	4.06	15.44	1.51								100	2.19	1.41	0.77	21.49
A05-8018	3	1			38.77				47.61		13.63									100	2.37	1.34	1.02	27.58
A05-8018	3	2			40.44				49.94		9.62									100	2.24	1.41	0.83	22.75
A05-8018	4	1	14		26.51				51.01		22.48									100	2.27	1.44	0.84	22.51
A05-8018	5	1	20		27.86				48.19		23.95									100	2.41	1.36	1.05	27.81
A05-8018	6	1	20		20.42				56.25		23.33									100	2.05	1.59	0.47	12.79
A05-8018	6	2	20		29.4				49.92	0.69	17.35	1.21	1.44							100	2.26	1.41	0.85	23.17
A05-8018	7	1	12		34.38				51.15		10.84	1.73	1.89							100	2.17	1.44	0.72	20.05
A05-8018	7	2	5		40.09				46	1.39	12.52									100	2.40	1.30	1.11	29.88
A05-8018	8	1	13		29.1				49.31		16.6	2.61	2.38							100	2.27	1.39	0.88	24.10
A05-8018	9	1	24		19.85				55.47	1.29	23.39									100	2.06	1.56	0.50	13.75
A05-8018	10	1	12		23.61				49.42		26.96									100	2.37	1.39	0.98	25.97
A05-3036	6	1			43.59				51.39		5.02									100	2.15	1.45	0.70	19.38
A05-3036	6	2	9		44.83				50.53		4.65									100	2.18	1.43	0.76	20.98
A05-3036	6	3	6		43.23				52.41		4.36									100	2.10	1.48	0.62	17.33
A05-3036	6	4	11		43.39				53.6	3.01										100	1.96	1.51	0.45	13.02
A05-3036	6	7	5		45.21				50.05		4.74									100	2.20	1.41	0.79	21.89
A05-3036	9	3			40.74				51.09	3.02	5.16									100	2.11	1.44	0.67	18.77
A05-3036	10	1	9		43.49				51.17		5.34									100	2.16	1.44	0.71	19.85
A05-3036	11	1	7		43.58				54.44	1.98										100	1.95	1.54	0.41	11.80
A05-3036	12	1			45.93				54.07											100	2.00	1.53	0.47	13.42
A05-3036	12	2	7		45.84				54.16											100	1.99	1.53	0.47	13.24
A05-3036	13	1	9		40.76				52.29	1.94	5.02									100	2.07	1.47	0.60	16.86
A05-3036	13	2	10		29.94				54.39	5.06	10.6									100	1.96	1.53	0.43	12.21
A05-3036	14	1			34.67				47.79	4.43	13.12									100	2.28	1.35	0.93	25.61
A05-3036	15	1	4		38.8				49.96	2.43	8.8									100	2.19	1.41	0.78	21.67
A05-3036	16	1	15		34.21				55.3	6.93	3.56									100	1.84	1.56	0.28	8.32
A05-3036	17	1			42.83				57.17											100	1.86	1.61	0.25	7.21
A05-3036	18	1	7		37.97				49.57	4.53	7.92									100	2.16	1.40	0.76	21.47
A05-3036	18	2	6		40.14				49.68		10.18									100	2.25	1.40	0.85	23.33
A05-3036	20	2	7		42.7				54.8	2.5										100	1.92	1.55	0.38	10.83
A05-3036	20	3	8		42.93				55.09	1.98										100	1.92	1.55	0.36	10.49
A05-3036	21	1	12		42.62				55.02	2.36										100	1.91	1.55	0.36	10.45
A05-3036	22	1	10		30.67				43.31	5.28	20.75									100	2.50	1.22	1.28	34.43
A05-3036	23	1			53.26				46.74											100	2.32	1.32	1.00	27.47
A05-3036	24	1	4		45.19				54.81											100	1.97	1.55	0.42	11.95
A05-3036	24	2	6		44.56				55.44											100	1.94	1.56	0.37	10.70
A05-3036	24	3	7		45.57				54.43											100	1.98	1.54	0.45	12.71
A05-3036	25	1	9		38.6				51.66	8.43	1.32									100	1.96	1.46	0.50	14.73
A05-3036	26	1	4		44.61				55.39											100	1.94	1.56	0.38	10.80
A05-3036	27	1	6		41.14				58.86											100	1.79	1.66	0.13	3.75
A05-3036	27	2	12		44.3				55.7											100	1.93	1.57	0.36	10.17
A05-3036	28	1	4		45.52				54.48											100	1.98	1.54	0.44	12.61
A05-3036	29	1			45.01				54.99											100	1.96	1.55	0.41	11.59
A05-3036	30	1			43.53				50.82		5.65									100	2.18	1.43	0.74	20.56
A05-1007	1	1	7		24.43				39.58		35.99									100	2.83	1.12	1.71	43.39
A05-1007	1	3	3		39.89				46.82		13.29									100	2.39	1.32	1.07	28.76
A05-1007	2	1	4		41.75				49.42		8.83									100	2.25	1.39	0.86	23.47
A05-1007	3	1	3		40.07				48.93		10.99									100	2.28	1.38	0.90	24.63
A05-1007	7	1	4		36.52				46.24	2.25	14.99									100	2.38	1.30	1.08	29.22
A05-1007	7	2			40.74				45.31		13.95									100	2.46	1.28	1.18	31.55
A05-1007	7	4			42.87				23.43		33.7									100	3.52	0.66	2.86	68.37
A05-1007	8	1	2		43.69				51.08		5.23									100	2.16	1.44	0.72	19.91
A05-1007	8	2	4		40.06				46.69	2.55	10.69									100	2.33	1.32	1.02	27.82
A05-1007	9	1	2		42.88				49.54		7.58									100	2.24	1.40	0.84	23.10
A05-1007	10	1	3		34.36				41.97	1.43	22.24									100	2.62	1.18	1.44	37.79
A05-1007	14	1			45.99				37.53	5.28	11.19									100	2.68	1.06	1.63	43.44
A05-1007	14	2			54.26				35.65		10.09									100	2.86	1.01	1.85	47.91
A05-1007	14	3			54.45				45.55											100	2.37	1.28	1.08	29.66
A05-1007	15	1			46.76				53.24											100	2.03	1.50	0.53	15.06
A05-1007	15	2			46.05				51.72		2.23									100	2.11	1.46	0.65	18.30

Table B3 (cont.)

A05-1007	15	3			46.2		53.8					100	2.01	1.52	0.49	13.95
A05-0019-1	4	1			28.82		24.27		46.91			100	3.59	0.68	2.91	68.00
A05-0019-1	4	2	2		31.21		37.13		31.65			100	2.94	1.05	1.89	47.42
A05-0019-1	4	3	4		39.29		48.75		11.95			100	2.30	1.38	0.93	25.26
A05-0019-1	4	4	7		32.43		38.84		26.59	2.14		100	2.81	1.10	1.72	43.97
A05-0019-1	4	5	6		38.69		46.57		12.21	1.71	0.82	100	2.38	1.31	1.07	28.94
A05-0019-1	4	6			42.91		43.18		13.91			100	2.56	1.22	1.34	35.52
A05-0019-1	5	1	4		37.31		44.44		13.7	2.34	2.21	100	2.47	1.25	1.22	32.68
A05-0019-1	6	1	7		38.77		46.32		11.29	2.03	1.6	100	2.38	1.31	1.07	29.13
A05-0019-1	7	1	10		38.08		45.43	1.06	11.91	2	1.52	100	2.40	1.28	1.12	30.47
A05-0019-1	8	1	12		28.22		49.81	1.71	16.92	2.29	1.05	100	2.24	1.40	0.83	22.83
A05-0019-1	9	1			24.62		53.86		18.54	1.86	1.11	100	2.10	1.52	0.58	16.12
A05-0001	1	1		10.43	39.15		36.28	0.99	13.16			100	2.39	1.57	0.81	20.54
A05-0001	1	1		9.66	45.93	0.97	43.45					100	2.00	1.79	0.20	5.36
A05-0001	1	2			47.39		52.61					100	2.06	1.48	0.58	16.29
A05-0001	1	3			47.68		52.32					100	2.07	1.48	0.60	16.85
A05-0001	1	4			48.74		51.26					100	2.12	1.45	0.67	18.91
A05-0001	2	1			46.74	0.66	52.6					100	2.03	1.52	0.51	14.29
A05-0001	2	2			49.31		50.69					100	2.14	1.43	0.72	20.01
A05-0001	2	3			48.89	2.32	48.79					100	2.13	1.52	0.61	16.61
A05-0001	2	4			50.87		49.13					100	2.21	1.39	0.83	22.98
A05-0001	3	1			47.99	1.57	49.53	0.9				100	2.11	1.49	0.62	17.07
A05-0001	4	1		40.9	30.26		20.32	0.98	7.53			100	1.72	2.73	-1.01	-22.71

Table B 4. EDS results (weight percent) for evaporate mounds hosted A06 samples.

Table B4

EDS results (weight percent) for evaporate mounds hosted by A06 samples.

Sample	Site	Position	Mound size (μm)	F	Na	Mg	Al	S	Cl	K	Ca	Mn	Fe	Cu	Zn	Mo	In	Sn	Pb	Total	∑+	∑-	Σdiff	Σdiff%
A06-3017	3	1			51.14				48.86											100	2.22	1.38	0.85	23.49
A06-3017	3	2			52.43				47.57											100	2.28	1.34	0.94	25.92
A06-3017	4	1			55.21				44.79											100	2.40	1.26	1.14	31.06
A06-3017	5	1		29.79	27.7				21.2	0.7	19.67				0.94					100	2.23	2.17	0.07	1.53
A06-3017	6	1		32.38	33.28				24.53	0.8	9.01									100	1.92	2.40	-0.48	-11.09
A06-3017	7	1		40.14	30.81				19.3		9.75									100	1.83	2.66	-0.83	-18.52
A06-3017	8	1		43.44	29.43				16.98		10.15									100	1.79	2.77	-0.98	-21.50
A06-3017	9	1		43.89	25.87				18.08	2.23	9.93									100	1.68	2.82	-1.14	-25.40
A06-3017	10	1		34.57	26.19				23.87	0.68	14.69									100	1.89	2.49	-0.60	-13.76
A06-3017	10	2		34.8	29.31				21.86		14.03									100	1.98	2.45	-0.47	-10.70
A06-3017	10	3			51.86				48.14											100	2.26	1.36	0.90	24.85
A06-3010	1	1	4		33.89				35.64		30.47									100	2.99	1.01	1.99	49.73
A06-3010	1	2	4		43.48				46.14		10.39									100	2.41	1.30	1.11	29.85
A06-3010	1	3	5		41.8				40.62		17.58									100	2.69	1.15	1.55	40.33
A06-3010	2	1	5		37.03				38.34	1.84	22.8									100	2.79	1.08	1.71	44.20
A06-3010	2	1	3		42.39				40.22		17.39									100	2.71	1.13	1.58	41.00
A06-3010	2	2	3		46.32				29.91		23.77									100	3.20	0.84	2.36	58.28
A06-3010	2	3	4		36.5				17.53		45.97									100	3.88	0.49	3.39	77.40
A06-3010	2	3	2		50.9				32.71		16.38									100	3.03	0.92	2.11	53.32
A06-3010	2	4	8		40.92				40.88		18.19									100	2.69	1.15	1.53	39.95
A06-3010	3	1	3		31.89				23		45.11									100	3.64	0.65	2.99	69.73
A06-3010	3	1	5		40.82				39.82		19.37									100	2.74	1.12	1.62	41.88
A06-3010	3	2	10		41.78				29.35		28.87									100	3.26	0.83	2.43	59.47
A06-3010	3	3	5		39.67				36.39		23.94									100	2.92	1.03	1.89	47.98
A06-3010	3	4	9		35.27				39.54		25.19									100	2.79	1.12	1.68	42.89
A06-3010	4	1	14		41.1				41.5		17.41									100	2.66	1.17	1.49	38.82
A06-3010	6	1	4		35.08				18.87		46.04									100	3.82	0.53	3.29	75.56
A06-3010	6	2	5		38.7				29.97		31.33									100	3.25	0.85	2.40	58.68
A06-3010	7	1	18	44	17.21				11.81		26.99									100	2.10	2.65	-0.56	-11.70
A06-2327	1	1	3		31.31				37.02	31.67										100	2.17	1.04	1.13	35.07
A06-2327	4	1	2		49.48				50.52											100	2.15	1.42	0.73	20.33
A06-2327	10	1	5		47.87				52.13											100	2.08	1.47	0.61	17.22
A06-2315	5	1	5		47.32				39.92		12.76									100	2.69	1.13	1.57	41.05
A06-2315	5	2	3		30.77				28.93		40.3									100	3.35	0.82	2.53	60.82
A06-2315	5	3	2		26.98				32.43		40.59									100	3.20	0.91	2.28	55.52
A06-2315	6	1	20		27.31				47.92	14.32	2.7					7.75				100	1.85	1.35	0.50	15.57
A06-2315	7	1	7		30.14				38.49		31.37									100	2.88	1.09	1.79	45.19
A06-2315	8	1			25.83				30.83		43.34									100	3.29	0.87	2.42	58.15
A06-2315	9	1	4		31.54				31.48		36.98									100	3.22	0.89	2.33	56.74
A06-2315	9	2	5		30.24				34.46		35.3									100	3.08	0.97	2.10	51.98
A06-2315	10	1			31.14				36.82		32.04									100	2.95	1.04	1.91	47.96

Table B 5. EDS results (weight percent) for evaporate mounds hosted A08 samples.

Table B5

EDS results (weight percent) for evaporate mounds hosted by A08 samples.

Sample	Site	Position	Mound size (μm)	F	Na	Mg	Al	S	Cl	K	Ca	Mn	Fe	Cu	Zn	Mo	In	Sn	Pb	Total	∑+	∑-	Σdiff	Σdiff%
A08-Tar mia	1	2	10		42.83				51.2		5.96									100	2.01	1.44	0.57	16.42
A08-Tar mia	2	1	14		40.34				53.83		5.83									100	1.90	1.52	0.38	11.17
A08-Tar mia	2	2	8		39.82				53.81		6.37									100	1.89	1.52	0.37	10.95
A08-Tar mia	3	1	10		39.15				50.23		10.61									100	1.97	1.42	0.55	16.28
A08-Tar mia	4	1	6		35.87				51.86		12.27									100	1.87	1.46	0.40	12.13
A08-Tar mia	5	1	5		36.63				56.77	0.46	5.37	0.77								100	1.75	1.60	0.15	4.53
A08-Tar mia	5	2	5		39.36				57.46		3.18									100	1.79	1.62	0.17	5.00
A08-Tar mia	6	1	6		40.3				53.24		6.46									100	1.91	1.50	0.41	12.08
A08-Tar mia	6	2	12		39.83				56.12		3.74	0.31								100	1.83	1.58	0.25	7.28
A08-Tar mia	6	4	5		39.48				56.35		4.17									100	1.82	1.59	0.23	6.80
A08-Tar mia	7	2	5		43.36				52.98	3.66										100	1.98	1.49	0.49	13.97
A08-Tar mia	8	2	1		48.21				49.05	2.74										100	2.17	1.38	0.78	22.07
A08-Tar mia	9	1	5		38.12				55.11	1.58	5.19									100	1.83	1.55	0.27	8.09
A08-Tar mia	10	1	10		38.76			1.99	48.68	6.38	4.18									100	1.95	1.44	0.52	15.30
A08-Tar mia	12	1			39.86				55.39		4.75									100	1.85	1.56	0.29	8.49

Table B 6. EDS results (weight percent) for evaporate mounds hosted A09 samples.

Table B6

EDS results (weight percent) for evaporate mounds hosted by A09 samples.

Sample	Site	Position	Mound size (μm)	F	Na	Mg	Al	S	Cl	K	Ca	Mn	Fe	Cu	Zn	Mo	In	Sn	Pb	Total	∑+	∑-	Σdiff	Σdiff%
A09-2132	1	4		39.92	33.38	4.13			14.84		7.74									100	2.18	2.52	-0.34	-7.27
A09-2132	4	3		51.84	16.23		5.4		12.19	2.14	11.76				0.43					100	1.96	3.07	-1.11	-22.08
A09-2132	5	1		49.32	19.1				17.8		12.93				0.85					100	1.50	3.10	-1.60	-34.70
A09-2132	5	2		57.73	16.83				10.27		14.02				1.15					100	1.47	3.33	-1.86	-38.82
A09-2132	7	1		34.96	13.71				31.98	0.27	17.66				0.85			0.56		100	1.52	2.74	-1.22	-28.61
A09-2132	7	3		53.21	18.97				15.1		10.93				1.8					100	1.43	3.23	-1.80	-38.71
A09-2155	4	2			51.55			0.54	46.52	1.39										100	2.28	1.35	0.93	25.72
A09-2155	4	3			53.48			0.59	45.24	0.69										100	2.34	1.31	1.03	28.20
A09-2155	5	1		15.85	43.23				35.23	4.21	1.48									100	2.06	1.83	0.23	6.02
A09-2155	6	1			8.14				40.12	51.75										100	1.68	1.13	0.55	19.44
A09-2155	7	1		17.03	20.33	2.79	4.55	1.55	27	21.77	3.24		0.76	0.98						100	2.40	1.75	0.64	15.46
A09-2155	8	1			31.03			4.22	32.43	22.9	5.61		3.8							100	2.35	1.18	1.17	33.25
A09-2161	1	1		48.64	20.58				17.19		13.59									100	1.57	3.05	-1.47	-31.87
A09-2161	2	1		45.41	21.91				21.11		11.56									100	1.53	2.99	-1.46	-32.24
A09-2161	3	1		51.98	18.42				15.46		14.15									100	1.51	3.17	-1.66	-35.58
A09-2161	4	1		55.04	18.68				12.98		13.3									100	1.48	3.26	-1.79	-37.70
A09-2161	5	1		52.99	16.51				13.96		16.53									100	1.54	3.18	-1.64	-34.70
A09-2161	6	1		49.79	22.2				15.13		12.87									100	1.61	3.05	-1.44	-30.92
A09-2161	7	1		53	21.25				13.13		12.62									100	1.55	3.16	-1.61	-34.07
A09-2161	8	1		39.03	31.33				21.37		8.27									100	1.78	2.66	-0.88	-19.89
A09-2161	9	1		54.04	20.53				11.49		13.94									100	1.59	3.17	-1.58	-33.21
A09-2161	10	1		32.18	37.56				24.42		5.85									100	1.93	2.38	-0.46	-10.60
A09-2161	11	1		47.12	23.67				17.43		11.79									100	1.62	2.97	-1.35	-29.50
A09-2161	12	1		49.36	18.25				17.89		14.5									100	1.52	3.10	-1.59	-34.31
A09-2161	14	1		52.16	21.59				13.31		12.93									100	1.58	3.12	-1.54	-32.66
A09-2161	15	1		43.99	27.16				17.54		11.31									100	1.75	2.81	-1.06	-23.36
A09-2161	16	1		40.51	29.36				20.2		9.94									100	1.77	2.70	-0.93	-20.76
A09-2231	1	1		34.15	29.28				26.27		10.3									100	1.79	2.54	-0.75	-17.36
A09-2231	2	1		28.67	32.23				31.44		7.66									100	1.78	2.40	-0.61	-14.63
A09-2231	3	1		25.81	34.94				33.76		5.49									100	1.79	2.31	-0.52	-12.60
A09-2231	4	1		29.82	30.83				29.23		10.12									100	1.85	2.39	-0.55	-12.92
A09-2231	5	1		29.98	32.59				28.32		9.12									100	1.87	2.38	-0.50	-11.86
A09-2231	6	1		38.86	27.16				20.96		13.01									100	1.83	2.64	-0.81	-18.04
A09-2231	7	1		34.29	31.08				25.57		9.06									100	1.80	2.53	-0.72	-16.68
A09-2231	8	1		33.18	33.8				26.24		6.78									100	1.81	2.49	-0.68	-15.79
A09-2231	9	1		31.39	34.59				27.05		6.96									100	1.85	2.42	-0.56	-13.20
A09-2231	10	1		25.36	37.64				31.05		5.95									100	1.93	2.21	-0.28	-6.67
A09-2231	11	1		50.49	24.75				14.14		10.62									100	1.61	3.06	-1.45	-31.09
A09-2231	12	1		40.51	36.47				14.75		8.26									100	2.00	2.55	-0.55	-12.09
A09-2231	13	1		28.15	37.72				28.86		5.27									100	1.90	2.30	-0.39	-9.33
A09-2231	14	1		33.71	33.67				26.47		6.15									100	1.77	2.52	-0.75	-17.46
A09-2231	15	1		42.45	27.02				19.46		11.07									100	1.73	2.78	-1.06	-23.40
A09-2231	16	1		38.74	32.94				20.92		7.4									100	1.80	2.63	-0.83	-18.66
A09-2350	5	1			47.55				37.89	14.56										100	2.44	1.07	1.37	39.09
A09-2350	5	2			47.08			1.68	36.62	12.3	2.33									100	2.48	1.14	1.34	37.08
A09-2350	7	1			50.96				37.06	8.38	3.61									100	2.61	1.05	1.57	42.82
A09-2350	8	3		33.98	33.64				21.99	1.13	7.52		1.74							100	1.93	2.41	-0.48	-11.04
A09-2350	9	1			33.93			2.75	36.14	24.37				2.81						100	2.19	1.19	1.00	29.50
A09-2350	9	2			30.46			1.43	39.63	28.48										100	2.05	1.21	0.85	25.96
A09-2350	10	1			37.31				37.67	25.02										100	2.26	1.06	1.20	36.10
A09-2350	11	1			31.69				38.84	29.47										100	2.13	1.10	1.04	32.12
A09-2350	11	2			37.52				31.76	30.71										100	2.42	0.90	1.52	45.93
A09-2370 stage	3	1	36		16.93				44.48	38.59										100	1.72	1.25	0.47	15.74
A09-2370 stage	3	2	22		22.34				44.3	33.36										100	1.83	1.25	0.58	18.72
A09-2370 stage	3	3	20		22.53				38.3	29.74	9.43									100	2.21	1.08	1.13	34.36
A09-2370 stage	4	1	23		22.77				56.16	1.33	19.74									100	2.01	1.58	0.43	11.84
A09-2370 stage	6	1	25		27.99				57	0.61	14.4									100	1.95	1.61	0.34	9.66
A09-2370 stage	6	2	14		19.92				50.34		29.74									100	2.35	1.42	0.93	24.68
A09-2370 stage	6	3	8						59.08	1.75	39.17									100	2.00	1.67	0.33	9.08
A09-2370 stage	7	1	24		30.55				53.49	0.63	15.33									100	2.11	1.51	0.60	16.62
A09-2370 stage	7	2	24	11.16	32.46				43.77		12.61									100	2.04	1.82	0.22	5.67
A09-2370 stage	7	5	10		31.1				43.04		25.85									100	2.64	1.21	1.43	37.05
A09-2370 stage	9	1	35		20.61				42.19	37.2										100	1.85	1.19	0.66	21.66
A09-2370 stage	10	1	18		22.22				53.42	0.74	23.62									100	2.16	1.51	0.66	17.91
A09-2370 stage	10	2	21		23.38				57.49	0.7	18.06	0.36								100	1.95	1.62	0.33	9.18
A09-2370 stage	11	1	30		26.96				41.13	31.91										100	1.99	1.16	0.83	26.32
A09-2370 stage	11	2	18		26.24				44.3	29.47										100	1.90	1.25	0.65	20.53

Table B6 (cont.)

A09-2384	2	1		25.57	41.34				27.44		5.65			100	2.08	2.12	-0.04	-0.95
A09-2384	3	1			51.49				48.51					100	2.24	1.37	0.87	24.15
A09-2384	3	2			48.08				49.36		2.56			100	2.22	1.39	0.83	22.90
A09-2384	3	3			52.57				47.43					100	2.29	1.34	0.95	26.18
A09-2384	4	1		47.48	30.63				15.25		6.65			100	1.66	2.93	-1.27	-27.54
A09-2384	4	2		52.83	32.09				6.95		8.13			100	1.80	2.98	-1.18	-24.60
A09-2384	4	3			21.4				55.35		23.25			100	2.09	1.56	0.53	14.51
A09-2384	4	5			54.27				45.73					100	2.36	1.29	1.07	29.33
A09-2384	5	1		17.05	47.47				33.62		1.86			100	2.16	1.85	0.31	7.79
A09-2395	2	2			49.05			0.21	48.92	0.38				100	2.28	1.39	0.89	24.23
A09-2395	2	3			48.35				51.65					100	2.10	1.46	0.65	18.15
A09-2395	4	2		26.22	37.72				31.66	0.4	3.72	0.28		100	1.85	2.27	-0.43	-10.35
A09-2395	4	3		25.25	38				30.22	0.51	5.56	0.46		100	1.96	2.18	-0.22	-5.35
A09-2707-5v	8	3	12		38.52				49.1		12.39			100	2.29	1.38	0.91	24.71
A09-2707-5v	8	4	6		43.02				55.04		1.94			100	1.97	1.55	0.42	11.81
A09-2707-5v	12	2			55.77				44.23					100	2.43	1.25	1.18	32.08
A09-2707-5v	14	1	13		33.24		1.2	6.03	42.04	0.46	7.26	9.77		100	2.30	1.56	0.74	19.18
A09-2707-5v	15	1	5		36.14				49.28		14.58			100	2.30	1.39	0.91	24.65
A09-2707-5v	18	1	14		40.24				52.43	1.07	6.25			100	2.09	1.48	0.61	17.12
A09-2707-5v	21	1	16		38.6				54.01	0.77	6.61			100	2.03	1.52	0.51	14.22
A09-3003	1	2			40.26				55.48		4.26			100	1.96	1.56	0.40	11.29
A09-3003	1	3			33.53				47.98	1.63	16.86			100	2.34	1.35	0.99	26.73
A09-3003	2	1			36.61				54.26	1.46	7.67			100	2.01	1.53	0.48	13.59
A09-3003	3	1	16		35.41				52.45	0.97	11.17			100	2.12	1.48	0.64	17.84
A09-3003	3	2	9		41.55				51.05		7.39			100	2.18	1.44	0.74	20.34
A09-3003	4	1	7		36.22				50.08		13.7			100	2.26	1.41	0.85	23.04
A09-3003	5	1			37.47				52.07	2.33	8.14			100	2.10	1.47	0.63	17.58
A09-3003	6	1	12		37.12				53.22	0.83	8.82			100	2.08	1.50	0.57	16.06
A09-3003	7	1			42.59				51.51		5.9			100	2.15	1.45	0.69	19.27
A09-3003	8	1	7		40.99				54.22		4.79			100	2.02	1.53	0.49	13.86
A09-3003	8	2	10		40.65				56.33		3.01			100	1.92	1.59	0.33	9.38
A09-3003	8	3	4		42.03				53.22		4.75			100	2.06	1.50	0.56	15.80
A09-3003	9	1	11		39.94				54.73		5.33			100	2.00	1.54	0.46	12.94
A09-3003	10	1	14		35.34				53.91	1.63	9.12			100	2.03	1.52	0.51	14.43
A09-3003	10	2	12		41.93				54.31		3.76			100	2.01	1.53	0.48	13.52
A09-Tar 16	2	1			51.98				48.02					100	2.26	1.35	0.91	25.08
A09-Tar 16	2	2			48.52				51.48					100	2.11	1.45	0.66	18.48
A09-Tar 16	2	3			46.41				53.59					100	2.02	1.51	0.51	14.37
A09-Tar 16	6	1			53.22				46.78					100	2.32	1.32	1.00	27.39
A09-Tar 16	6	2			49.14				50.86					100	2.14	1.43	0.70	19.68
A09-Tar 16	6	3			49.41				50.59					100	2.15	1.43	0.72	20.20
A09-Tar 16	7	1			45.81				54.19					100	1.99	1.53	0.46	13.18
A09-Tar 16	7	2			45.83				54.17					100	1.99	1.53	0.47	13.22
A09-Tar 16	8	1			46.65				53.35					100	2.03	1.50	0.52	14.84
A09-Tar 16	8	2			45.17				54.83					100	1.96	1.55	0.42	11.91
A09-Tar 16	8	3			45.7				54.3					100	1.99	1.53	0.46	12.96
A09-Tar 16b	1	1			49.19				49.02		1.79			100	2.23	1.38	0.85	23.43
A09-Tar 16b	2	1			49.63				50.37					100	2.16	1.42	0.74	20.62
A09-Tar 16b	2	2			47.81				41.42		10.77			100	2.62	1.17	1.45	38.27
A09-Tar 16b	3	1		25.82	29.56				30.93		13.69			100	1.97	2.23	-0.26	-6.25
A09-Tar 16b	4	1			50.87				49.13					100	2.21	1.39	0.83	22.98
A09-Tar 16b	5	1			50.33				43.3		6.37			100	2.51	1.22	1.29	34.49
A09-Tar 16b	6	1		12.52	43.53				38.26	0.69	4.99			100	2.16	1.74	0.42	10.82
A09-Tar 16b	6	2			49.92				44.44		5.63			100	2.45	1.25	1.20	32.35
A09-Tar 16b	7	1		15.38	43.99				34.43		6.19			100	2.22	1.78	0.44	11.03
A09-Tar 16b	7	2			49.98				45.36		4.66			100	2.41	1.28	1.13	30.58
A09-Tar 16b	7	3			49.94				43.14		6.92			100	2.52	1.22	1.30	34.83
A09-Tar 16b	7	4			50.5				44.03		5.47			100	2.47	1.24	1.23	33.08
A09-Tar 16b	8	2			35.1	1.65	3.32	3.9	47.41	1.07	5.04	1.74		100	2.37	1.58	0.79	20.04
A09-Tar 16b	9	1		12.59	36.29				39.24		11.88			100	2.17	1.77	0.40	10.20
A09-Tar 16b	10	1			43.63				43.19		13.18			100	2.56	1.22	1.34	35.44
A09-Tar 16b	10	2			51.1				48.9					100	2.22	1.38	0.84	23.42
A09-Tar 16b	10	3			49.48				50.52					100	2.15	1.42	0.73	20.33
A09-Tar 16b	12	2			47.03				49.26		3.71			100	2.23	1.39	0.84	23.24
A09-Tar 16b	12	3			50				45.1		4.9			100	2.42	1.27	1.15	31.08
A09-Tar 16b	12				49.93				50.07					100	2.17	1.41	0.76	21.19
A09-Tar 20a	6	1			45.03				54.97					100	1.96	1.55	0.41	11.63
A09-Tar 20a	6	2			49.5				50.5					100	2.15	1.42	0.73	20.37
A09-Tar 20a	7	1			50.18				49.82					100	2.18	1.41	0.78	21.67
A09-Tar 20a	8	2			48.29				47.96		3.75			100	2.29	1.35	0.93	25.68
A09-Tar mia	1	2	10		42.83				51.2		5.96			100	2.01	1.44	0.57	16.42
A09-Tar mia	2	1	14		40.34				53.83		5.83			100	1.90	1.52	0.38	11.17
A09-Tar mia	2	2	8		39.82				53.81		6.37			100	1.89	1.52	0.37	10.95
A09-Tar mia	3	1	10		39.15				50.23		10.61			100	1.97	1.42	0.55	16.28

Table B6 (cont.)

A09-Tar mia	2	1	14		40.34				53.83		5.83						100	1.90	1.52	0.38	11.17
A09-Tar mia	2	2	8		39.82				53.81		6.37						100	1.89	1.52	0.37	10.95
A09-Tar mia	3	1	10		39.15				50.23		10.61						100	1.97	1.42	0.55	16.28
A09-Tar mia	4	1	6		35.87				51.86		12.27						100	1.87	1.46	0.40	12.13
A09-Tar mia	5	1	5		36.63				56.77	0.46	5.37	0.77					100	1.75	1.60	0.15	4.53
A09-Tar mia	5	2	5		39.36				57.46		3.18						100	1.79	1.62	0.17	5.00
A09-Tar mia	6	1	6		40.3				53.24		6.46						100	1.91	1.50	0.41	12.08
A09-Tar mia	6	2	12		39.83				56.12		3.74	0.31					100	1.83	1.58	0.25	7.28
A09-Tar mia	6	4	5		39.48				56.35		4.17						100	1.82	1.59	0.23	6.80
A09-Tar mia	7	2	5		43.36				52.98	3.66							100	1.98	1.49	0.49	13.97
A09-Tar mia	8	2	1		48.21				49.05	2.74							100	2.17	1.38	0.78	22.07
A09-Tar mia	9	1	5		38.12				55.11	1.58	5.19						100	1.83	1.55	0.27	8.09
A09-Tar mia	10	1	10		38.76			1.99	48.68	6.38	4.18						100	1.95	1.44	0.52	15.30
A09-Tar mia	12	1			39.86				55.39		4.75						100	1.85	1.56	0.29	8.49
A09-2378_chip2	3	1	5		47.41				52.59								100	2.06	1.48	0.58	16.33
A09-2378_chip2	3	2	3		51.98				48.02								100	2.26	1.35	0.91	25.08
A09-2378_chip2	3	3	3		49.38				50.62								100	2.15	1.43	0.72	20.14
A09-2378_chip2	4	1	2		48.27				51.73								100	2.10	1.46	0.64	18.00
A09-2378_chip2	6	1	4		48.45				51.55								100	2.11	1.45	0.65	18.35
A09-2378_chip2	6	3	5		43.19				56.81								100	1.88	1.60	0.28	7.94
A09-2378_chip2	9	3	5		39.12			0.71	53.61	3.61	2.94						100	1.94	1.56	0.38	10.99
A09-2378_chip2	11	1	6		28.89				48.02	23.1							100	1.85	1.35	0.49	15.40
A09-2378_chip2	11	2	9		28.15				47.66	24.19							100	1.84	1.34	0.50	15.65
A09-2378_chip2	11	3	5		13.32				43.51	43.16							100	1.68	1.23	0.46	15.67
A09-2378_chip2	11	4	5		20.95				44.87	34.18							100	1.79	1.27	0.52	17.04
A09-2378_chip2	11	5	7		25.22				47.23	27.55							100	1.80	1.33	0.47	14.98
A09-2378_chip2	12	1	13		27.73				47.17	25.09							100	1.85	1.33	0.52	16.28
A09-2378_chip2	13	1	10		37.83				46.7	15.46							100	2.04	1.32	0.72	21.55
A09-2378_chip2	14	2	5	35.73	23.6				28.44	1.28	10.95						100	1.61	2.68	-1.08	-25.12
A09-2378_chip2	15	1	20	8.58	21.96	1.73	1.9	0.44	41.66	22.77			0.97				100	1.93	1.65	0.27	7.59
A09-2378_chip2	18	1	7	21.46	38.24				36.55		3.75						100	1.85	2.16	-0.31	-7.73
A09-2378_chip2	19	1	10	39.25	20.39				26.68	0.89	12.79						100	1.55	2.82	-1.27	-29.10
A09-2378_chip2	20	1	8	25.18	31.93				35.07	0.46	7.36						100	1.77	2.31	-0.55	-13.39
A09-2378_chip2	21	1	8	38.14	22.13				26.2	0.33	13.21						100	1.63	2.75	-1.12	-25.50
A09-2378_chip2	22	1	14	24.2	32.32				36.01	0.61	6.86						100	1.76	2.29	-0.53	-12.97
A09-2378_chip2	23	1	15	29.25	27.68				33.33	0.43	9.31						100	1.68	2.48	-0.80	-19.24
A09-2378_chip2	23	2	6	24.63	32.95				34.79	0.94	6.69						100	1.79	2.28	-0.49	-11.96
A09-2378_chip2	24	1	33	31.97	22.48				33.77	0.41	11.37						100	1.56	2.64	-1.08	-25.76
A09-2378_chip2	25	1	7	38.78	27.2				24.14	0.38	9.5						100	1.67	2.72	-1.06	-24.04
A09-2378_chip2	25	2	12	35.19	21.65				30.06	0.43	12.68						100	1.59	2.70	-1.11	-26.01
A09-2378_chip2	25	3	8	40.61	26.76				23.4		9.24						100	1.63	2.80	-1.17	-26.51
A09-2378_chip2	25	4	5	42.86	27.58				20.09		9.46						100	1.67	2.82	-1.15	-25.61
A09-2707-4	1	3	10		49.7			0.75	49.55								100	2.16	1.44	0.72	19.88
A09-2707-4	1	4	14	19.97	43.99				29.29		4.39	0.47	0.59		1.31		100	2.20	1.88	0.32	7.85
A09-2707-4	5	1	8	34.08	40.05				21.96		3.92						100	1.94	2.41	-0.48	-10.95
A09-2707-5	4	1	5		46.22				53.78								100	2.01	1.52	0.49	13.99
A09-2707-5	4	2	5		47.21				52.79								100	2.05	1.49	0.56	15.94
A09-2707-5	5	1	13		49.04				50.96								100	2.13	1.44	0.70	19.49
A09-2707-5	6	1	5		46.17				53.83								100	2.01	1.52	0.49	13.89
A09-2707-5	8	4	8		46.86				53.14								100	2.04	1.50	0.54	15.25
A09-2707-5	8	5	7		54.83				45.18								100	2.39	1.27	1.11	30.35
A09-2707-5	9	1	8		40.64				40.8	18.56							100	2.24	1.15	1.09	32.17
A09-2707-5	9	2	20		35.68				47.88	16.44							100	1.97	1.35	0.62	18.72
A09-2707-5	9	3	25		28.91		3.04	1.68	47.58	16.11	2.68						100	2.14	1.45	0.69	19.36
A09-2707-5	9	4	10		38.22				45.28	16.5							100	2.08	1.28	0.81	24.02
A09-2707-5	9	5	15		34.76			1.24	43.81	15.9	4.29						100	2.13	1.31	0.82	23.79
A09-2707-5	9	6	8		38.06				40.84	21.1							100	2.20	1.15	1.04	31.17
A09-2707-5	9	8	5		36.87				41.19	21.93							100	2.16	1.16	1.00	30.15
A09-2707-5	9	9	10		34.95				44.93	20.12							100	2.03	1.27	0.77	23.24
A09-2707-5	9	10	12		35.22				47.7	17.08							100	1.97	1.35	0.62	18.81
A09-2707-5	9	11	5		35.92				46.55	17.53							100	2.01	1.31	0.70	20.99
A09-Tar 9a	2	2			53.4				46.6								100	2.32	1.31	1.01	27.73
A09-Tar 9a	6	1			49.68				50.32								100	2.16	1.42	0.74	20.72
A09-Tar 9a	6	3			44.1	4.35		2.56	46.82		2.17						100	2.38	1.48	0.90	23.40
A09-Tar 9a	7	2		27.33	38.57				25.27	0.26	8.57						100	2.11	2.15	-0.04	-0.92
A09-Tar 9a	8	1		30.73	37.4				24.54		7.33						100	1.99	2.31	-0.32	-7.37
A09-Tar 9a	9	1		13.98	43.79				37.94	0.53	3.76						100	2.11	1.81	0.30	7.67
A09-tar9a	2	2				53.4				46.6							100	2.32	1.31	1.01	27.73
A09-tar9a	6	1				49.68				50.32							100	2.16	1.42	0.74	20.72
A09-tar9a	6	3				44.1	4.35		2.56	46.82							100	2.38	1.48	0.90	23.40
A09-tar9a	7	2			27.33	38.57				25.27	0.26						100	2.11	2.15	-0.04	-0.92
A09-tar9a	8	1			30.73	37.4				24.54							100	1.99	2.31	-0.32	-7.37
A09-tar9a	9	1			13.98	43.79				37.94	0.53						100	2.11	1.81	0.30	7.67

Table B 7. EDS results (weight percent) for evaporate mounds hosted A10 samples.

Table B7

EDS results (weight percent) for evaporate mounds hosted by A10 samples.

Sample	Site	Position	Mound size (µm)	F	Na	Mg	Al	S	Cl	K	Ca	Mn	Fe	Cu	Zn	Mo	In	Sn	Pb	Total	∑+	∑-	Σdiff	Σdiff%
A10-0060-2	8	2	3		26.72				54.01	7.07	12.21									100	1.95	1.52	0.43	12.33
A10-2007-6	1	1	4		42.91				51.33		5.76									100	2.15	1.45	0.71	19.59
A10-2007-6	1	2	6		43.59				48.94		7.47									100	2.27	1.38	0.89	24.33
A10-2007-6	4	1	2		37.6				41.68		20.73									100	2.67	1.18	1.49	38.85
A10-2007-6	5	1	8		40.68				51.3		8.02									100	2.17	1.45	0.72	19.97
A10-2007-6	5	2	8		39.39				51.98		8.63									100	2.14	1.47	0.68	18.76
A10-2007-6	5	3	8		40.91				54.57		4.52									100	2.00	1.54	0.47	13.13
A10-2007-6	6	1	7		43.1				49.81		7.08									100	2.23	1.40	0.82	22.64
A10-2007-6	11	1			45.92				54.08											100	2.00	1.53	0.47	13.38
A10-3012	2	1	10		45.62				49.53		4.85									100	2.23	1.40	0.83	22.87
A10-3012	2	2			44.38				37.88		17.74									100	2.82	1.07	1.75	44.97
A10-3017	2	4	5		30.54				36.69		32.77									100.00	2.96	1.03	1.93	48.24
A10-3017	3	1	14	23.33	23.39				32.63		20.65									100.00	2.05	2.15	-0.10	-2.39
A10-3017	5	1	4		36.44				40.22		23.33									100.00	2.75	1.13	1.61	41.58
A10-3017	6	1	11		26.98				38.82		34.20									100.00	2.88	1.09	1.79	44.91
A10-3017	6	1		46.42	24.07				18.33		11.17									100	1.60	2.96	-1.36	-29.71
A10-3017	6	2	6		28.58				38.82		32.60									100.00	2.87	1.09	1.78	44.77
A10-3017	7	1	3		35.13				31.57		33.30									100.00	3.19	0.89	2.30	56.35
A10-3017	7	2	12		35.28				38.63		26.10									100.00	2.84	1.09	1.75	44.50
A10-3017	7	2		48.16	25.29				16.72		9.84									100	1.59	3.01	-1.42	-30.79
A10-3017	8	1	3		36.40				32.54		31.06									100.00	3.13	0.92	2.22	54.69
A10-3017	13	1	13		34.06			3.86	42.32	15.79	3.97									100.00	2.08	1.43	0.65	18.45
A10-3017	14	1	9		31.04				49.97	6.36	12.63									100.00	2.14	1.41	0.73	20.65
A10-3017	16	1	4		44.38				47.31		8.32									100.00	2.35	1.33	1.01	27.48
A10-3017	16	2	7		39.21				51.95		8.84									100.00	2.15	1.47	0.68	18.87
A10-3017	16	3	5		44.63				46.20		9.17									100.00	2.40	1.30	1.10	29.60
A10-3017	16	4	5		45.42				49.94		4.64									100.00	2.21	1.41	0.80	22.09
A10-3017	16	5	6		45.29				54.71											100.00	1.97	1.54	0.43	12.15
A10-3056	5	1	19		37.36				38.63		24.02									100	2.82	1.09	1.73	44.30
A10-3078	2	2			40.98				42.73		16.29									100	2.59	1.21	1.39	36.57
A10-3078	2	3			36.36				36.18		27.46									100	2.95	1.02	1.93	48.61
A10-3078	3	1			44.5			8.27	15.59	15.59	7.53		8.52							100	3.01	0.96	2.06	51.86
A10--3078	2	1		41.38	34.38				18.04		6.2									100	1.80	2.69	-0.88	-19.64
A10--3078	3	1		40.85	21.16				21.14		16.84									100	1.76	2.75	-0.99	-21.87
A10--3078	5	1		47.99	22.72				11.29		18									100	1.89	2.84	-0.96	-20.25
A10--3078	8	1		27.67	42.34				25.27		4.72									100	2.08	2.17	-0.09	-2.17
A10--3078	9	1		40.07	31.27				15.11		13.54									100	2.04	2.54	-0.50	-10.93
A10--3078	10	1		38.15	35.59				17.84		8.43									100	1.97	2.51	-0.54	-12.11
A10--3078	11	1		29.95	37.36				22.53		10.16									100	2.13	2.21	-0.08	-1.84
A10--3078	12	1		46.42	29.42				13.36		10.81									100	1.82	2.82	-1.00	-21.58
A10--3078	13	1		48.5	24.99				12.06		14.45									100	1.81	2.89	-1.08	-23.08
A10--3078	14	1		36.01	37.31				16.79		9.88									100	2.12	2.37	-0.25	-5.64
A10--3078	15	1		46.22	28.36				11.87		13.55									100	1.91	2.77	-0.86	-18.34
A10--3078	16	1		22.28	40.44				29.29		7.98									100	2.16	2.00	0.16	3.81
A10-3085	1	1			13.98			2.43	47.89	29.48	5.46									100	1.66	1.50	0.16	4.94
A10-3085	1	2			24.1			3.03	43.49	25.09	4.29									100	1.90	1.42	0.49	14.70
A10-3085	1	3			39.2				58.05	2.76										100	1.78	1.64	0.14	4.04
A10-3085	1	4			25.72			4.16	41.8	16.99	11.33									100	2.12	1.44	0.68	19.11
A10-3085	2	1	8		39.05				52.58	1.11	7.26									100	2.09	1.48	0.61	16.95
A10-3085	3	1	6		44.58				55.42											100	1.94	1.56	0.38	10.72
A10-3085	4	1	3		47.99			13.36	38.64											100	2.09	1.92	0.16	4.08
A10-3085	6	1	2		45.03				54.97											100	1.96	1.55	0.41	11.61
A10-3085	6	2			45.94				54.06											100	2.00	1.52	0.47	13.42
A10-3085	6	3			43.92				56.08											100	1.91	1.58	0.33	9.39
A10-3085	7	1	7		43.22				56.78											100	1.88	1.60	0.28	7.98
A10-3085	7	2	4		45.57				54.43											100	1.98	1.54	0.45	12.69
A10-3085	7	3	4		45.17				53.49		1.34									100	2.03	1.51	0.52	14.75
A10-3086	1	1		36.08	34.8				20.8		8.32									100	1.93	2.49	-0.56	-12.61
A10-3086	2	2		28.45	40.54				24.27	0.79	5.95									100	2.08	2.18	-0.10	-2.38
A10-3086	3	1			54.67				44.44	0.89										100	2.40	1.25	1.15	31.40
A10-3086	4	1		25.36	42.1				27.88		4.65									100	2.06	2.12	-0.06	-1.38
A10-3086	8	1		28.59	41.21				23.83		6.36									100	2.11	2.18	-0.07	-1.56
A10-3086	8	2		25.41	41.49				28.51		4.58									100	2.03	2.14	-0.11	-2.60
A10-3086	8	3		44.99	35.63				15		4.38									100	1.77	2.79	-1.02	-22.43
A10-3100	1	1			30.23				41.49		28.28									100	2.73	1.17	1.56	39.92
A10-3100	1	2	10		41.43				44.24		14.33									100	2.52	1.25	1.27	33.70
A10-3100	2	1			36.8				36.92		26.29									100	2.91	1.04	1.87	47.32

Table B7 (cont.)

A10-3100	3	1	25	31.71	17.33		28.43	0.48	22.05							100	1.87	2.47	-0.61	-13.96
A10-3100	3	2	20		26.89		46.62		26.5							100	2.49	1.31	1.18	30.91
A10-3100	3	3	30	22.17	23.82		35.78		18.23							100	1.95	2.18	-0.23	-5.61
A10-3100	4	1			32.18		46.9		20.92							100	2.44	1.32	1.12	29.75
A10-3100	5	1			38.64		48.75		12.62							100	2.31	1.38	0.93	25.37
A10-3100	5	2	5		39.4		52.56		8.04							100	2.11	1.48	0.63	17.57
A10-3100	6	2			27.82		35.52		36.66							100	3.04	1.00	2.04	50.41
A10-3100	7	1	39		21.51		37.19		41.3							100	3.00	1.05	1.95	48.14
A10-3100	7	2	24	20.08	26.18		31.38		22.35							100	2.25	1.94	0.31	7.41
A10-3100	7	3		16.9	23.61		31.31	0.8	27.38							100	2.41	1.77	0.64	15.29
A10-3100	7	4	20		30.03		44.27		25.7							100	2.59	1.25	1.34	34.91
A10-3100	8	1	40	24.01	5.1		34.22		36	0.66						100	2.04	2.23	-0.19	-4.39
A10-3100	8	2	38	32.93	10.73		22.44		33.91							100	2.16	2.37	-0.21	-4.60
A10-3100	8	3	16	25.37	17.74		31.69	1.25	23.66	0.28						100	1.99	2.23	-0.24	-5.58
A10-3100	8	4	8	21.32	21.09		37.64	0.5	18.46	0.59	0.39					100	1.89	2.18	-0.30	-7.32
A10-3100	8	5	17	23.88	25.8		32.32	0.31	16.86	0.83						100	2.00	2.17	-0.17	-4.02
A10-3100	8	6			23.61		33.5		42.89							100	3.17	0.94	2.22	54.04
A10-3129	1	2	20		36.58		32.89	19.34	4.03		7.16					100	2.54	0.93	1.61	46.49
A10-3129	1	3	10		31.3		40.48	15.73	3.65		1.49		7.36			100	2.15	1.14	1.01	30.62
A10-3129	2	1	1		38.02		46.42						15.56			100	1.98	1.31	0.67	20.35
A10-3129	2	2	4		45.63	5.06	49.31									100	1.98	1.71	0.28	7.54
A10-3129	7	1	6		27.23	4.94	44.63	16.49	3.12			3.58				100	1.87	1.57	0.30	8.78
A10-3129	10	1	2		34.27	4.53	44.86		16.34							100	2.29	1.55	0.74	19.38
A10-3129	10	2	7		36.12		39.71		15.44				8.73			100	2.51	1.12	1.39	38.30
A10-3129	11	1	10		32.08		41.94		25.97							100	2.67	1.18	1.49	38.58
A10-3129	15	1	1		38.47		56.16		5.37							100	1.94	1.58	0.35	10.02
A10-3129	18	1	5		39.99		51.46	3.18	5.36							100	2.08	1.45	0.63	17.88
A10-3129	18	2	5		39.99		51.78	3.14	5.09							100	2.07	1.46	0.61	17.25
A10-3129	21	1	20		27.42	9.33	32.88	23.4	6.96							100	2.13	1.51	0.62	17.11
A10-3129	23	1	6		25.6		44.12		25.88						4.39	100	2.50	1.24	1.25	33.49
A10-3129	23	2	9		26.45		47.34	2.61	23.6							100	2.37	1.34	1.04	28.02
A10-3129	24	1	1		35.95		37.18		26.87							100	2.88	1.05	1.83	46.63
A10-3129	24	2	1		38.06		36.85		25.1							100	2.89	1.04	1.85	47.05
A10- 2007-7	2	2		47.57	25.74		13.41	0.4	12.89							100	1.77	2.88	-1.11	-23.82
A10- 2007-7	4	1		20.21	35.58		33.09		11.12							100	2.10	2.00	0.11	2.57
A10- 2007-7	4	4		50.13	24.12		14.71		11.05							100	1.60	3.05	-1.45	-31.22
A10- 2007-7	6	2		20.14	35.8		32.79		11.26							100	2.12	1.98	0.13	3.27
A10- 2007-7	6	3		53.21	23.03		13.31		10.45							100	1.52	3.18	-1.65	-35.17

Table B 8. EDS results (weight percent) for evaporate mounds hosted A11 samples.

Table B8

EDS results (weight percent) for evaporate mounds hosted by A11 samples.

Sample	Site	Position	Mound size (µm)	F	Na	Mg	Al	S	Cl	K	Ca	Mn	Fe	Cu	Zn	Mo	In	Sn	Pb	Total	∑+	∑-	Σdiff	Σdiff%
A11-2007-3	4	1	4		30.61				42.45		26.94									100	2.68	1.20	1.48	38.16
A11-2007-3	4	2	10		21.29				46.97		30.34	1.4								100	2.49	1.32	1.17	30.56
A11-2007-3	4	3	5		33.66				29.57		36.78									100	3.30	0.83	2.46	59.64
A11-2007-3	4	4			17.02				46.2		34.9	1.88								100	2.55	1.30	1.25	32.36
A11-2007-3	5	1			22.26				39.9		37.84									100	2.86	1.13	1.73	43.47
A11-2007-3	5	2			27.74				44.54		27.72									100	2.59	1.26	1.33	34.67
A11-2007-3	5	3			22.25				44.04		33.71									100	2.65	1.24	1.41	36.16
A11-2007-3	6	1	3		32.23				42.68		23.48	1.6								100	2.63	1.20	1.43	37.22
A11-2007-3	6	3	15	0	20.46				52.35		25.18	2.01								100	2.22	1.48	0.74	20.10
A11-2007-3	7	1	6		23.89				39.18	2.22	32.85	1.86								100	2.80	1.11	1.70	43.44
A11-2007-3	8	1	6		29.28				34.99	1.75	33.97									100	3.01	0.99	2.03	50.65
A11-2007-3	9	1	6		25.89				46.97		25.96	1.18								100	2.46	1.32	1.14	30.07
A11-2007-4	2	1	7		41.04				50.37		8.59									100	1.79	1.42	0.36	11.37
A11-2007-4	2	2	8		49.96				50.04											100	2.17	1.41	0.76	21.25
A11-2007-4	2	3	6		48.69				51.31											100	2.12	1.45	0.67	18.81
A11-2007-4	2	5	6		45.88				54.12											100	2.00	1.53	0.47	13.32
A11-2007-4	2	6	12		43.97				51.27	4.76										100	2.03	1.45	0.59	16.90
A11-2007-4	2	8	6		46.91				53.09											100	2.04	1.50	0.54	15.35
A11-2007-4	3	1	5		42.91				53.09	4										100	1.97	1.50	0.47	13.60
A11-2007-4	3	2	6		43				43.63	3.86			9.52							100	2.14	1.23	0.91	26.97
A11-2007-4	3	3	6		47.46				52.54											100	2.06	1.48	0.58	16.43
A11-2007-4	3	4	7		54.66				45.34											100	2.38	1.28	1.10	30.05
A11-2007-4	3	5	5		50.74				49.26											100	2.21	1.39	0.82	22.74
A11-2007-4	3	6	5		35.02				64.98											100	1.52	1.83	-0.31	-9.22
A11-2007-4	3	7	8		39.49				41.76	18.75										100	2.20	1.18	1.02	30.20
A11-2007-4	6	2	5		42.98				53.37	2.25	1.4									100	1.96	1.51	0.46	13.17
A11-2007-4	8	1	17		45.36				41.62	13.02										100	2.31	1.17	1.13	32.53
A11-2007-4	11	1	5		40.54				46.36		13.1									100	2.09	1.31	0.78	23.03
A11-2007-4	11	2	1		43.84				56.16											100	1.91	1.58	0.32	9.25
A11-2007-4	12	1	10		25.62				46.93		27.45									100	1.80	1.32	0.48	15.23
A11-2007-4	12	2	1		39.81				60.19											100	1.73	1.70	0.03	0.99
A11-2007-4	12	3	1		32.68				67.34											100	1.42	1.90	-0.48	-14.39
A11-2249-2	6	1	2		46.39				53.61											100	2.02	1.51	0.51	14.33
A11-2249-2	6	3	2		53.89				46.11											100	2.34	1.30	1.04	28.63
A11-2249-2	7	1	1		36.4				63.6											100	1.58	1.79	-0.21	-6.23
A11-2249-2	7	2	1		59.3				40.7											100	2.58	1.15	1.43	38.40
A11-2249-2	7	3	1		49.18				50.82											100	2.14	1.43	0.71	19.76
A11-2249-2	7	4	1		58.74				41.26											100	2.56	1.16	1.39	37.41
A11-2249-2	8	3	1		34.1				65.9											100	1.48	1.86	-0.38	-11.23
A11-2268	1	1	20		37.81				42.38	14.11	3.54									100	2.09	1.26	0.83	24.75
A11-2268	1	2	5		48.63				51.37											100	2.12	1.45	0.67	18.70
A11-2268	1	3	2		48.77				45.55	5.68										100	2.27	1.28	0.98	27.65
A11-2268	3	2	10		40.63				47.59	11.78										100	2.07	1.34	0.73	21.29
A11-2268	3	3	6		40.97				49.16	9.88										100	2.03	1.39	0.65	18.95
A11-2268	4	1	8		42.69				49.85	7.46										100	2.05	1.41	0.64	18.58
A11-2268	4	2	5		43.07				51.78	5.14										100	2.00	1.46	0.54	15.71
A11-2268	4	3	2		59.3				40.7											100	2.58	1.15	1.43	38.40
A11-2286	1	1	14		48.31				51.69											100	2.10	1.46	0.64	18.08
A11-2286	2	1	12		47.61				45.71		6.67									100	2.24	1.29	0.95	26.88
A11-2286	4	1	10	8.55	44.55				36.2	2.35	8.36									100	2.21	1.47	0.74	20.00
A11-2286	4	2	5		42.98				47.36	4.06	5.6									100	2.11	1.34	0.78	22.54
A11-2286	5	1	5		36.07	5.9			39.2	6.13	11.54									100	2.26	1.14	1.11	32.81
A11-2286	5	3	10		43.17				44.87	4.61	7.36									100	2.18	1.27	0.91	26.52
A11-2286	5	4	12		42.77				47.99	3.15	6.09									100	2.09	1.35	0.74	21.45
A11-2286	6	1	7		45.55				46.72		7.73									100	2.17	1.32	0.86	24.53
A11-2286	7	1	8		34.9	5.24			38.68	5.57	11.2									100	2.16	1.23	0.93	27.38
A11-2286	7	2	8		43.88				47.46		8.67									100	2.13	1.34	0.79	22.70
A11-2286	10	2	8		46.34				46.85	6.81										100	2.19	1.32	0.87	24.73
A11-2286	10	3	6		47.33				52.67											100	2.06	1.49	0.57	16.17
A11-2286	10	4	5		47.24				52.76											100	2.05	1.49	0.57	16.00
A11-2286	11	1	6		47.62				52.38											100	2.07	1.48	0.59	16.74
A11-2286	12	1	5		45.5				49.68		4.82									100	2.10	1.40	0.70	19.94
A11-2286	12	2	12		48.47				51.53											100	2.11	1.45	0.65	18.39
A11-2286	12	3	10		46.83				46.88		6.29									100	2.19	1.32	0.87	24.79
A11-2286	13	2	15		45.31				40.22	6.55	7.92									100	1.97	1.13	0.84	26.94
A11-2286	13	3	9		43.43				43.53	4.55	8.48									100	1.89	1.23	0.66	21.22
A11-2286	13	4	6		46.4				48.35		5.24									100	2.02	1.36	0.65	19.35

Table B8 (cont.)

A11-2007-2	7	2		55.83	44.17			100	2.43	1.25	1.18	32.19
A11-Tar ft3	1	1	5	22.96	42.98	34.06		100	1.87	1.21	0.66	21.33
A11-Tar ft3	1	2	6	42.17	54.72	3.11		100	1.91	1.54	0.37	10.71
A11-Tar ft3	1	3	15	34.81	48.32	16.87		100	1.95	1.36	0.58	17.61
A11-Tar ft3	1	4	11	33.6	48.83	17.57		100	1.91	1.38	0.53	16.23
A11-Tar ft3	1	5	6	34.76	47.63	17.61		100	1.96	1.34	0.62	18.72
A11-Tar ft3	2	1	8	40.57	52.07	7.35		100	1.95	1.47	0.48	14.15
A11-Tar ft3	2	3	5	40.85	54.92	4.23		100	1.89	1.55	0.34	9.78
A11-Tar ft3	5	1	25	36.07	44.35	16.36	3.23	100	2.07	1.25	0.82	24.62
A11-Tar ft3	5	2	22	35.87	46.77	17.36		100	2.00	1.32	0.69	20.61
A11-Tar ft3	5	3	18	36.81	46.49	16.71		100	2.03	1.31	0.72	21.48
A11-Tar ft3	5	4	5	36.58	47.78	13.49	2.14	100	1.99	1.35	0.64	19.23
A11-Tar ft3	5	5	5	32.1	49.31	18.59		100	1.87	1.39	0.48	14.74
A11-Tar ft3	6	1	10	36.8	43.85	15.56	2.17	100	2.05	1.29	0.77	22.93
A11-Tar ft3	6	2	30	35.55	46.91	17.55		100	2.00	1.32	0.67	20.25
A11-Tar ft3	7	1	35	39.4	45.69	14.91		100	2.10	1.29	0.81	23.83
A11-Tar ft3	8	1	12	30.96	46.27	22.77		100	1.93	1.31	0.62	19.29
A11-Tar ft3	8	2	16	33.84	47.86	18.3		100	1.94	1.35	0.59	17.94

Table B 9. EDS results (weight percent) for evaporate mounds hosted A12 samples.

Table B9

EDS results (weight percent) for evaporate mounds hosted by A12 samples.

Sample	Site	Position	Mound size (μm)	F	Na	Mg	Al	S	Cl	K	Ca	Mn	Fe	Cu	Zn	Mo	In	Sn	Pb	Total	∑+	∑-	Σdiff	Σdiff%
A12-Tar 23b	2	1	10		37.03				51.77		11.2									100	2.16	1.46	0.70	19.33
A12-Tar 23b	2	2			39.63				44.61		15.76									100	2.50	1.26	1.24	32.98
A12-Tar 23b	3	2	10		41.94				44.12		13.94									100	2.51	1.24	1.26	33.67
A12-Tar 23b	3	3	4		44.6				47.15		8.25									100	2.34	1.33	1.01	27.61
A12-Tar 23b	3	4	3		43.47				43.22		13.31									100	2.54	1.22	1.32	35.20
A12-Tar 23b	4	1	1		43.42				39.78		16.79									100	2.71	1.12	1.59	41.47
A12-Tar 23b	13	2	2		36.17				48.97	1.34	13.52									100	2.27	1.38	0.89	24.36
A12-Tar 23b	14	1	1		36.3			7.71	27.93	13.3	14.76									100	2.64	1.27	1.37	35.13
A12-Tar 23b	17	2	5		39.68				46.47		13.85									100	2.41	1.31	1.09	29.45
A12-8007	1	1	2		39.15				41.91		18.94									100	2.65	1.18	1.47	38.26
A12-8007	1	2	3		41.98				51.85		6.17									100	2.13	1.46	0.67	18.65
A12-8007	1	3			41.15				40.42		18.43									100	2.71	1.14	1.57	40.76
A12-8007	2	1	11	10.86	30.44				42.1		16.61									100	2.15	1.76	0.39	10.05
A12-8007	3	1	2		40.61				39.76		19.63									100	2.75	1.12	1.62	42.00
A12-8007	4	1	1		41.05				36.31		22.64									100	2.91	1.02	1.89	48.00
A12-8007	5	1	10		38.36				39.89		21.76									100	2.75	1.13	1.63	41.99
A12-8007	5	2	15		37.68				39		23.32									100	2.80	1.10	1.70	43.62
A12-8007	5	3	2		46.54				32.91		20.55									100	3.05	0.93	2.12	53.32
A12-8007	7	2	14		52.67				47.33											100	2.29	1.34	0.96	26.35
A12-1021	2	1		25.36	43.86				27.76		3.02									100	2.06	2.12	-0.06	-1.42
A12-1021	4	1		47.36	26.66				15.59	0.13	10.27									100	1.68	2.93	-1.26	-27.28
A12-1021	6	1		55.05	24.64				10.47		9.84									100	1.56	3.19	-1.63	-34.28
A12-1021	6	2		55.65	24.7				10.74		8.9									100	1.52	3.23	-1.71	-36.07
A12-1021	7	1		55.18	24.83				10.68		9.31									100	1.54	3.21	-1.66	-34.97
A12-1021	7	2		54.26	28.44				9.78		7.52									100	1.61	3.13	-1.52	-32.03
A12-1021	7	3			53.3				46.7											100	2.32	1.32	1.00	27.54
A12-1021	8	1		53.97	25.55				10.66		9.82									100	1.60	3.14	-1.54	-32.47
A12-1021	8	2		56.08	24.57				10.12		9.23									100	1.53	3.24	-1.71	-35.83
A12-1019	2	2	12		37.7				33.84		28.46									100	3.06	0.95	2.11	52.44
A12-1019	2	3	9		37.05				40.09		22.86									100	2.75	1.13	1.62	41.75
A12-1019	2	4	8		31.53				30.2		38.27									100	3.28	0.85	2.43	58.77
A12-1019	2	5	7		41.87				48.92		9.21									100	2.28	1.38	0.90	24.60
A12-1019	4	1	5		35.37				25.66		38.97									100	3.48	0.72	2.76	65.59

Table B 10. EDS results (weight percent) for evaporate mounds hosted A14 samples.

Table B10

EDS results (weight percent) for evaporate mounds hosted by A14 samples.

Sample	Site	Position	Mound size (μm)	F	Na	Mg	Al	S	Cl	K	Ca	Mn	Fe	Cu	Zn	Mo	In	Sn	Pb	Total	∑+	∑-	Σdiff	Σdiff%
A14-1032	4	2	4		45.59				53.02	1.39										100	2.02	1.50	0.52	14.87
A14-1032	8	1	6		37.07				50.48		12.45									100	2.23	1.42	0.81	22.13
A14-1032	12	1	6		37.09				45.11		17.8									100	2.50	1.27	1.23	32.56
A14-1032	13	2			36.88				49.36	1.45	12.31									100	2.26	1.39	0.86	23.65
A14-1032	14	1	4		42.19				43.17		14.64									100	2.57	1.22	1.35	35.62
A14-1032	14	2	5		43.41				44.01		12.58									100	2.52	1.24	1.27	33.91
A14-1017	1	1	22		26.93				28.62		44.45									100	3.39	0.81	2.58	61.53
A14-1017	1	3			24.06				37.24		38.7									100	2.98	1.05	1.93	47.84
A14-1017	2	1	9		33.4				28.73		37.87									100	3.34	0.81	2.53	60.97
A14-1017	3	1	13	19.71	28.14				27.89		24.26									100	2.43	1.82	0.61	14.31
A14-1017	4	1	2		32.59				24.88		42.53									100	3.54	0.70	2.84	66.91
A14-1017	4	2	3		34.71				29.69		35.59									100	3.29	0.84	2.45	59.37
A14-1017	5	1	14	24.51	21.87				30.82		22.8									100	2.09	2.16	-0.07	-1.68
A14-1017	6	1	21	20.3	24.29				33.61		21.8									100	2.14	2.02	0.13	3.05
A14-1017	7	1	14	19.64	24.33				33.45		22.57									100	2.18	1.98	0.21	4.96
A14-1017	8	1	7		36.61				34.37		29.01									100	3.04	0.97	2.07	51.64
A14-1017	10	1	21	26.46	20.24				28.24		25.06									100	2.13	2.19	-0.06	-1.37
A14-1017	10	2	5		43.19				56.81											100	1.88	1.60	0.28	7.92
A14-1017	11	1	9	7.73	32.19				38.09		21.99									100	2.50	1.48	1.02	25.53
A14-1017	12	1	18	35.95	19.01				21.73	0.51	22.8									100	1.98	2.51	-0.53	-11.79
A14-1017	13	1	22		28.69				36.74		34.57									100	2.97	1.04	1.94	48.30
A14-1017	13	2	23	32.03	17.66				26.71	0.65	22.96									100	1.93	2.44	-0.51	-11.67
A14-1017	13	3	18		30.34				42.53		27.12									100	2.67	1.20	1.47	38.04
A14-1017	13	4	10		32.61				34.52		32.87									100	3.06	0.97	2.08	51.70
A14-1007	1	1	35		37.78				38.33	13.54	10.35									100	2.51	1.08	1.42	39.71
A14-1007	1	2	4		42.04				44.21	13.76										100	2.18	1.25	0.93	27.22
A14-1007	1	4	2		34.09				23.46		42.45									100	3.60	0.66	2.94	68.95
A14-1007	3	1	22		33			10.89	23.62	14.98	17.51									100	2.69	1.35	1.35	33.35
A14-1007	5	1	12		33.25				40.58		26.17									100	2.75	1.14	1.61	41.25
A14-0003	1	2			25.78				23.53		50.69									100	3.61	0.66	2.94	68.92
A14-0003	2	1	2		29.85				20.29		49.87									100	3.74	0.57	3.17	73.48
A14-0003	6	1	8		42.66				48.42		8.91									100	2.29	1.37	0.93	25.34
A14-0003	8	4	5		6.86				39.41	53.73										100	1.67	1.11	0.56	20.15
A14-0003	10	1	3		42.17				41.32		16.51									100	2.64	1.17	1.48	38.81
A14-0003	13	1	3		37.75				36.32		25.93									100	2.91	1.02	1.89	47.97
A14-0003	19	1	2		11.86				34.21	53.92										100	1.89	0.96	0.93	32.52
A14-0003	19	2	3		7.53				38.5	53.98										100	1.71	1.09	0.62	22.27

Table B 11. EDS results (weight percent) for evaporate mounds hosted A15 samples.

Table B11

EDS results (weight percent) for evaporate mounds hosted by A15samples.

Sample	Site	Position	Mound size (μm)	F	Na	Mg	Al	S	Cl	K	Ca	Mn	Fe	Cu	Zn	Mo	In	Sn	Pb	Total	∑+	∑-	Σdiff	Σdiff%
A15-Tar 20b	2	1		10.41	46.17				37.2		6.22									100	2.32	1.60	0.72	18.42
A15-Tar 20b	2	2			48.05			0.75	42.45		8.76									100	2.53	1.24	1.28	34.02
A15-Tar 20b	4	1							45.43	54.57										100	1.40	1.28	0.11	4.27
A15-Tar 20b	7	2			51.16				42.86		5.98									100	2.52	1.21	1.31	35.23
A15- Tar 22b	4	1			35.79				33.56		30.65									100	3.09	0.95	2.14	53.06
A15- Tar 22b	5	2		27.74	33.3				21.32		17.65									100	2.33	2.06	0.27	6.10
A15- Tar 22b	6	1			37.14				34.66		28.19									100	3.02	0.98	2.04	51.12
A15- Tar 22b	6	2			39.98				29.88		30.14									100	3.24	0.84	2.40	58.75
A15- Tar 22b	6	3			40.99				33.39		25.62									100	3.06	0.94	2.12	52.95
A15- Tar 22b	8	1			40.31				28.82		30.87									100	3.29	0.81	2.48	60.41
A15- Tar 22b	10	1			28.37				34.27		37.36									100	3.10	0.97	2.13	52.44
A15- Tar 22b	10	2			33.13				27.71		39.15									100	3.39	0.78	2.61	62.57
A15-Tar 23	1	1		19.07	28.65				26.97		25.31									100	2.51	1.76	0.74	17.43
A15-Tar 23	2	2			34.44				33.2		32.36									100	3.11	0.94	2.18	53.75
A15-Tar 23	2	3			39.57				36.49		23.94									100	2.92	1.03	1.89	47.82
A15-Tar 23	3	1		25.61	30.46				23.58		20.35									100	2.34	2.01	0.33	7.52
A15-Tar 23	8	1		16.19	37.54				31.92		14.35									100	2.35	1.75	0.60	14.54
A15-Tar 23	8	2			43.74				38.04		18.22									100	2.81	1.07	1.74	44.76
A15-Tar 23	16	1			35.57				32.08		32.35									100	3.16	0.90	2.26	55.50
A15-Tar 23	16	3			38.33				36.75		24.92									100	2.91	1.04	1.87	47.48
A15-Tar 23	16	4		20.47	37.16				25.76		16.61									100	2.45	1.80	0.64	15.09
A15-Tar 22	2	5			41.4	2.18	3.66	6.84	20.9	9.08	6.47				9.48					100	2.89	1.02	1.87	47.95
A15-Tar 22	2	6			45.64			6.82	21.29	16.71	9.55									100	2.89	1.03	1.86	47.59
A15-Tar 22	3	1			47.13			5.77	18.08	20.11	8.91									100	3.01	0.87	2.14	55.15
A15-Tar 22	5	1			47.58	2.59		4	29.67	6.55	9.61									100	3.00	1.09	1.92	46.89
A15-Tar 22	6	1			35.17			9.05	36.29		19.5									100	2.50	1.59	0.91	22.36
A15-Tar 15	1	2			55.73				44.27											100	2.42	1.25	1.18	32.00
A15-Tar 15	1	3			59.91				40.09											100	2.61	1.13	1.48	39.48
A15-Tar 15	2	1			50.69				49.31											100	2.20	1.39	0.81	22.64
A15-Tar 15	2	2			52.03				47.97											100	2.26	1.35	0.91	25.17
A15-Tar 15	2	3			54.23				45.77											100	2.36	1.29	1.07	29.26
A15-Tar 15	3	1			45.57				52.27	2.16										100	2.04	1.47	0.56	16.04
A15-Tar 15	3	2			50.82				49.18											100	2.21	1.39	0.82	22.89
A15-Tar 15	4	1			47.94				52.06											100	2.09	1.47	0.62	17.36
A15-Tar 15	4	2			50.72				49.28											100	2.21	1.39	0.82	22.70
A15-Tar 15	4	3			54.5				45.5											100	2.37	1.28	1.09	29.76
A15-Tar 15	5	1		3.28	41.02				50.32	3.24	2.13									100	1.97	1.59	0.38	10.70
A15-Tar 15	5	2			42.88				52.02	2.73	2.37									100	2.05	1.47	0.59	16.65
A15-Tar 15	5	3		3.83	40.71				49.9	2.59	2.97									100	1.99	1.61	0.38	10.47
A15-Tar 15	6	2			42.29				55.08	1.14		1.48								100	1.92	1.55	0.37	10.62
A15-Tar 15	6	3			44.25				55.75											100	1.92	1.57	0.35	10.07
A15-0113	2	2	5		20.73				32.8		46.47									100	3.22	0.93	2.30	55.37
A15-0113	4	1	9		21.88			37.22			40.9									100	2.99	2.32	0.67	12.62
A15-0113	5	1	3		43.45				56.55											100	1.89	1.60	0.29	8.44
A15-0113	5	2	13		22.99				44.16		32.85									100	2.64	1.25	1.39	35.87
A15-0113	6	1	8		32.64				41.23		26.13									100	2.72	1.16	1.56	40.15
A15-0113	6	2	3		43.62				56.38											100	1.90	1.59	0.31	8.79
A15-0113	6	3	1		48.3				51.7											100	2.10	1.46	0.64	18.04
A15-0113	7	1	6		27.68				36.94		35.39									100	2.97	1.04	1.93	48.05
A15-0113	7	2			31.59				26.19		42.22									100	3.48	0.74	2.74	64.98
A15-0113	7	3			44.44				55.56											100	1.93	1.57	0.37	10.44
A15-0113	8	1	9		5.19				36.83		57.97									100	3.12	1.04	2.08	50.02
A15-0113	9	1	1		31.7				27.75		40.55									100	3.40	0.78	2.62	62.59
A15-0113	9	2	2		30.77				35.04		34.19									100	3.04	0.99	2.06	50.98
A15-0113	9	3	3		27.9				31.69		40.4									100	3.23	0.89	2.34	56.64
A15-0111	6	1	13		21.24			22.17	13.77	39.78	3.04									100	2.09	1.77	0.32	8.32
A15-0102	1	2	6		38.71				35.7		25.59									100	2.96	1.01	1.95	49.24
A15-0102	2	1	8		45.26				54.74											100	1.97	1.54	0.42	12.09
A15-0102	4	1	7		40.98				49.1		9.92									100	2.28	1.38	0.89	24.37
A15-0102	5	1	6		28.71				44.87		26.42									100	2.57	1.27	1.30	33.96
A15-0102	5	2	4		32.13				43.19		24.68									100	2.63	1.22	1.41	36.67
A15-0102	5	3	3		29.46				26.08		44.46									100	3.50	0.74	2.76	65.27
A15-0102	6	1	4		31.69				30.52		37.79									100	3.26	0.86	2.40	58.26
A15-0102	6	2	2		34.99				26.1		38.91									100	3.46	0.74	2.73	64.94
A15-0102	6	3	1		44.48				55.52											100	1.93	1.57	0.37	10.54
A15-0102	7	2	5		40.01				41.51		18.48									100	2.66	1.17	1.49	38.91
A15-0102	8	1	5		36.88				30.7		32.42									100	3.22	0.87	2.36	57.64

Table B11 (cont.)

A15-0102	9	1	6		37.2				49.43		13.37				100	2.29	1.39	0.89	24.22
A15-0102	9	2	7		33.15				47.33		19.52				100	2.42	1.34	1.08	28.82
A15-0102	9	3	5		39.47				40.04		20.49				100	2.74	1.13	1.61	41.62
A15-0102	9	4	8		40.02				39.17		20.8				100	2.78	1.10	1.67	43.10
A15-0102	9	5	5		40.51				39.4		20.08				100	2.76	1.11	1.65	42.65
A15-0102	9	6	7		37.3				40.12		22.58				100	2.75	1.13	1.62	41.68
A15-0102	15	1	13		24.67				51.59		23.74				100	2.26	1.46	0.80	21.62
A15-0102	15	3	4		42.57				51.19		6.24				100	2.16	1.44	0.72	19.94
A15-0102	16	1	9		22.91				56.36		20.73				100	2.03	1.59	0.44	12.19
A15-0068	3	1		35.31	19.41		1.58		29.51	1.15	12.64	0.41			100	1.68	2.69	-1.01	-23.12
A15-0068	3	2		45.58	26.83				17.74		9.86				100	1.66	2.90	-1.24	-27.21
A15-0068	5	1	12		31.46				43.32	1.26	23.96				100	2.60	1.22	1.37	36.00
A15-0068	6	1	22		23.36	9.4	2.66	4.85	18.15	4.07	24.78		11.02		100	3.89	0.81	3.08	65.39
A15-0068	7	1	25	7.79	18.22				45.52		27.86	0.61			100	2.21	1.69	0.51	13.11
A15-0068	7	2	14		31.67				48.93		19.4				100	2.35	1.38	0.97	25.92
A15-0068	7	3	8		32.9				47.44		19.67				100	2.41	1.34	1.07	28.65
A15-0068	7	4	24		30.04				49.12		20.83				100	2.35	1.39	0.96	25.74
A15-0068	7	5	5		35.37				46.84		17.79				100	2.43	1.32	1.11	29.49
A15-0068	8	1	7		26.11				40.1		33.79				100	2.82	1.13	1.69	42.77
A15-0068	8	1			47				42.14		10.86				100	2.59	1.19	1.40	37.03
A15-0068	8	2	8		34.26				50.71		15.03				100	2.24	1.43	0.81	22.07
A15-0068	8	3	6		32.63				45.35		22.02				100	2.52	1.28	1.24	32.63
A15-0068	8	4	5		32.76				47.93		19.32				100	2.39	1.35	1.04	27.73
A15-0068	8	5	4		38.03				45.6		16.37				100	2.47	1.29	1.18	31.54
A15-0068	9	1	12		27.66				47.92		24.41				100	2.42	1.35	1.07	28.35
A15-0068	9	1		27.06	40.79				27.17		4.98				100	2.02	2.19	-0.17	-3.98
A15-0068	11	1	12		31.16				51.69		17.15				100	2.21	1.46	0.75	20.53
A15-0068	11	2	10		30.28				48.37	8.88	12.47				100	2.17	1.36	0.80	22.72
A15-0068	11	3	9		25.98				45.95		28.07				100	2.53	1.30	1.23	32.27
A15-0068	12	1	9		34.78				50		13.52		1.71		100	2.25	1.41	0.84	22.92
A15-0068	12	2	32		30.2				51.09		17.95	0.77			100	2.24	1.44	0.80	21.65
A15-0068	12	3	12		27.57				49.65		22	0.78			100	2.33	1.40	0.93	24.83
A15-0068	13	1	12		28.98				50.11		19.94	0.97			100	2.29	1.41	0.88	23.69
A15-0068	14	1	10		28.47				47.96		23.58				100	2.42	1.35	1.06	28.19
A15-0068	14	2	14		19.68				44.97		34.57	0.78			100	2.61	1.27	1.34	34.58
A15-0068	15	1	7		28.55				42.77		28.68				100	2.67	1.21	1.47	37.81
A15-0068	15	2	9		25.11				51.01	1.71	22.17				100	2.24	1.44	0.80	21.83
A15-0068	15	3	6		29.82				38.55		31.62				100	2.88	1.09	1.79	45.12
A15-0068	16	1	80					34.68			45.63		19.69		100	2.98	2.16	0.82	15.92
A15-0060-2	4	1			51.92				47.52		0.56				100	2.29	1.34	0.95	26.09
A15-0060-2	5	1		25.84	38.27				26.13	1.78	4.63		3.34		100	2.06	2.10	-0.04	-0.87
A15-0060-2	5	2		8.96	48.43				42.61						100	2.11	1.67	0.43	11.46
A15-0060-2	5	3		29.05	38.97				25	3.34	3.64				100	1.96	2.23	-0.27	-6.48
A15-0050	1	1	16		26.65				50.42	1.07	21.86				100	2.28	1.42	0.85	23.11
A15-0050	1	2	9		38.77				46.01		15.22				100	2.45	1.30	1.15	30.66
A15-0050	2	1			42.85				52		5.15				100	2.12	1.47	0.65	18.22
A15-0050	2	2			37.57				36.57		25.86				100	2.92	1.03	1.89	47.85
A15-0050	3	1	6		31.59				38.94		29.47				100	2.84	1.10	1.75	44.28
A15-0050	4	1	7		25.37				41.17		33.47				100	2.77	1.16	1.61	40.97
A15-0050	4	4	1		41.85				52.52		5.63				100	2.10	1.48	0.62	17.29
A15-0050	5	1	2		40.41				40.2		19.4				100	2.73	1.13	1.59	41.24
A15-0050	6	1	1		49.4				50.6						100	2.15	1.43	0.72	20.16
A15-0050	6	3	2		44.13				44.69		11.18				100	2.48	1.26	1.22	32.54
A15-0050	10	1	3		25.94				41.22		32.84				100	2.77	1.16	1.60	40.82
A15-0027	2	1			18.39				57.36	3.43	20.82				100	1.93	1.62	0.31	8.71
A15-0027	3	1		23.85	16.69				43.67	1.5	14.1	0.19			100	1.47	2.49	-1.02	-25.77
A15-0027	3	2		24.14	33.57				30.21	0.79	11.29				100	2.04	2.12	-0.08	-1.89
A15-0027	3	3		39.51	21.45				25.31	0.65	13.08				100	1.60	2.79	-1.19	-27.10
A15-0027	4	1		26.37	33.86				30.92	0.47	8.38				100	1.90	2.26	-0.36	-8.58
A15-0027	5	1		20.49	36.27				33.73	1.37	8.13				100	2.02	2.03	-0.01	-0.28
A15-0027	7	1		26.75	29.45				32.53	0.92	9.75	0.6			100	1.79	2.33	-0.53	-12.98
A15-0027	9	1			49.69				50.31						100	2.16	1.42	0.74	20.73
A15-0027		1		25.79	36.03				31.36	0.53	6.29				100	1.89	2.24	-0.35	-8.40
A15-0027		2		15.68	45.95				37.02		1.34				100	2.07	1.87	0.20	4.98
A15-0014	2	3		28.24	40.67				27.61		3.48				100	1.94	2.27	-0.32	-7.66

Table B 12. EDS results (weight percent) for evaporate mounds hosted A16 samples.

Table B12

EDS results (weight percent) for evaporate mounds hosted by A16 samples.

Sample	Site	Position	Mound size (μm)	F	Na	Mg	Al	S	Cl	K	Ca	Mn	Fe	Cu	Zn	Mo	In	Sn	Pb	Total	∑+	∑-	Σdiff	Σdiff%
A16-1174	1	1			41.41				40.64	17.95										100	2.26	1.15	1.11	32.70
A16-1174	2	1			43.94				37.98	18.08										100	2.37	1.07	1.30	37.81
A16-1174	3	1			44.44				38.49	17.08										100	2.37	1.09	1.28	37.17
A16-1174	4	1			38.25				41.37	20.38										100	2.19	1.17	1.02	30.38
A16-1174	5	1			57.28				42.72											100	2.49	1.20	1.29	34.81
A16-1174	6	1			52.72				32.47	14.81										100	2.67	0.92	1.76	48.95
A16-1174	7	1			43.85				41.65	14.5										100	2.28	1.17	1.10	31.96
A16-1174	8	1			44.6				31.06	24.34										100	2.56	0.88	1.69	49.05
A16-1174	9	1			42.89				39.4	17.72										100	2.32	1.11	1.21	35.20
A16-1174	10	1			8.67				40.84	50.49										100	1.67	1.15	0.52	18.31
A16-1174	11	1			24.47				37.78	37.75										100	2.03	1.07	0.96	31.15
A16-1174	13	1			37.57				42.25	20.18										100	2.15	1.19	0.96	28.68
A16-1174	14	1		60.55	15.46				7.64		16.35									100	1.49	3.40	-1.91	-39.14
A16-1174	16	1			45.3				27.47		27.23									100	3.33	0.77	2.55	62.24
A16-1224	1	1			51.31				48.69											100	2.23	1.37	0.86	23.81
A16-1224	2	1		35.08	41.62				19.7		3.6									100	1.99	2.40	-0.41	-9.38
A16-1224	3	1		21.2	43.93				31.74		3.13									100	2.07	2.01	0.06	1.37
A16-1277	8	2	4		38.37				49.33		12.3									100	2.28	1.39	0.89	24.25
A16-1277	9	1	13		35.31				49.7		14.99									100	2.28	1.40	0.88	23.92
A16-1277	9	2			28.53				36.88		34.59									100	2.97	1.04	1.93	48.08
A16-1277	10	2	1						43.27	56.73										100	1.45	1.22	0.23	8.63
A16-1277	12	1	5		41				44		15									100	2.53	1.24	1.29	34.20
A16-1277	12	2	5		38.68				42.12		19.21									100	2.64	1.19	1.45	37.94
A16-1281	1	2			50.35				49.65											100	2.19	1.40	0.79	21.99
A16-1281	2	1		25.25	40.18			1.17	26.42		6.99									100	2.10	2.15	-0.05	-1.19
A16-1281	3	1		36.71	27.19		2.44	1.25	19.19	0.36	11.38		1.48							100	2.08	2.55	-0.47	-10.08
A16-1281	4	1			50.06				46.77		3.16									100	2.34	1.32	1.02	27.80
A16-1281	5	1		16.3	47.49				33.08		2.05									100	2.21	1.79	0.42	10.47
A16-1281	6	1		13.66	44.28			0.69	34.51		6.86									100	2.27	1.74	0.53	13.31
A16-1281	7	1			49.9				50.1											100	2.17	1.41	0.76	21.14
A16-1281	8	1		13.39	46.23			1.95	32.74		4.75	0.94								100	2.28	1.75	0.53	13.20
A16-1281	9	1		43.65	23.79			1.75	11.82		18.99									100	1.98	2.74	-0.76	-16.04
A16-1281	10	1		12.68	43.45			0.96	37.98		4.94									100	2.14	1.80	0.34	8.59
A16-1281	12	1		20.9	44.23			1.28	28.53		5.07									100	2.18	1.98	0.19	4.62
A16-1281	13	1		23.29	39.5			1.58	27.26		8.38									100	2.14	2.09	0.04	1.02
A16-1281	14	1		17.75	41.05			0.6	36.54		4.07									100	1.99	2.00	-0.01	-0.34
A16-1281	15	1		14.36	43.86			0.74	37.72		3.32									100	2.07	1.87	0.21	5.27
A16-1281	16	1			51.96				48.04											100	2.26	1.36	0.91	25.04
A16-smb3_chip2	1	1	34		36.19				56.09		5.07								2.65	100	1.88	1.58	0.29	8.53
A16-smb3_chip2	1	2	5		38.87				54.32		3.67								3.14	100	1.93	1.53	0.40	11.57
A16-smb3_chip2	2	1	14		31.61				58.82	0.41	7.14								2.02	100	1.78	1.66	0.12	3.51
A16-smb3_chip2	2	2	15		36.16			0.73	57.11		4.1								1.91	100	1.81	1.66	0.16	4.53
A16-smb3_chip2	2	3	12		31.22			1.76	51.82		13.57								1.63	100	2.07	1.57	0.49	13.59
A16-smb3_chip2	2	4	9		29.77			0.65	46.86		21.16								1.56	100	2.38	1.36	1.02	27.20
A16-smb3_chip2	3	1	15		30.18			1.07	48.09		20.66									100	2.34	1.42	0.92	24.44
A16-smb3_chip2	3	2	12		34.86			0.96	55.16		6.19								2.83	100	1.88	1.62	0.26	7.52
A16-smb3_chip2	4	1	8		35.55			0.48	57.54		4.82								1.62	100	1.82	1.65	0.16	4.74
A16-smb3_chip2	4	2	10		33.37			0.51	53.18		11.19								1.75	100	2.04	1.53	0.51	14.30
A16-smb3_chip2	4	3	14		34.65			0.35	58.69		6.32									100	1.82	1.68	0.15	4.15
A16-smb3_chip2	5	1	14		30.49		0.72	0.37	57.96		8.21								2.25	100	1.86	1.66	0.20	5.70
A16-smb3_chip2	5	2	11		37.47				58.69		3.85									100	1.82	1.66	0.17	4.79
A16-smb3_chip2	5	3	16		38.78		1.32	0.37	54.95		2.77								1.81	100	2.01	1.57	0.43	12.10
A16-smb3_chip2	6	1	12	0	27.62		2.41	0.99	53.95		12.85								2.19	100	2.15	1.58	0.57	15.22
A16-smb3_chip2	7	1	18	0	30.97			0.95	59.16		7.06								1.87	100	1.73	1.73	0.01	0.19
A16-smb3_chip2	7	2	18	0	30.45			1.65	54.84		11.43								1.63	100	1.93	1.65	0.28	7.71
A16-smb3_chip2	9	1	9		30.55				46.57		22.89									100	2.47	1.31	1.16	30.59
A16-smb3_chip2	9	2	14		37.43			0.59	50.7		9.64								1.63	100	2.14	1.47	0.67	18.66
A16-smb3_chip2	10	2	18		35.99				55.22		6.59								2.19	100	1.94	1.56	0.38	10.82
A16-smb3_chip2	10	3	15		34.83				51.33		10.56								3.28	100	2.10	1.45	0.66	18.47
A16-Tar 14b	3	1			44.2		3.68		50		2.12									100	2.44	1.41	1.03	26.70
A16-Tar 14b	15	1			47.19				39.09		13.72									100	2.74	1.10	1.63	42.57
A16-Tar 14c	2	1		5.1	33.42			0.17	44.28	0.43	15.12									100	2.24	1.55	0.69	18.27
A16-Tar 14c	3	trum			33.71				49.9		16.39									100	2.28	1.41	0.88	23.75
A16-Tar 14c	5	1		4.77	41.29		1.15		46.24		6.55									100	2.25	1.56	0.70	18.27
A16-Tar 14c	6	1		6.97	30.44				41.01		21.59									100	2.40	1.52	0.88	22.37
A16-Tar 14c	7	1			39.5				41.8		18.69									100	2.65	1.18	1.47	38.43
A16-Tar 14c	8	3		13.78	39.05				30.78		16.39									100	2.52	1.59	0.92	22.46

Table B12 (cont.)

A16-Tar 14c	13	1			41.57			44.29		12.89		1.25				100	2.50	1.25	1.25	33.29
A16-Tar 14c	17	1			47.84			46.4		5.76						100	2.37	1.31	1.06	28.82
A16-Tar 17	4	1		5.95	33.5			49.55	0.49	10.51						100	1.99	1.71	0.28	7.65
A16-Tar 17	5	1			33.29			49.95		16.76						100	2.28	1.41	0.88	23.71
A16-Tar 17	5	2		11.1	33.21			42.5	1.09	12.1						100	2.08	1.78	0.29	7.60
A16-Tar 17	12	1			45.82			53.15	1.03							100	2.02	1.50	0.52	14.79
A16-Tar 17	13	1		6.06	36.9			49.29	0.41	7.33						100	1.98	1.71	0.27	7.37
A16-Tar 17	14	1		9.45	36.46			46.23	1.12	6.74						100	1.95	1.80	0.15	3.99
A16-Tar 17	15	1		10.94	38.91			42.33	1.17	6.65						100	2.05	1.77	0.28	7.44
A16-Tar 17	15	2		4.23	41.59			50.74		3.43						100	1.98	1.65	0.33	8.98
A16-Tar 17	15	2		4.23	41.59			50.74		3.43						100	1.98	1.65	0.33	8.98
A16-Tar 17	16	1		4.81	39.52			49.12		6.55						100	2.05	1.64	0.41	11.05
A16-Tar 18	1	5			39.41	2.03	8.46	46.77	0.81	2.07		0.45				100	2.08	1.85	0.23	5.94
A16-Tar 18	3	3		52.34	19.99					14.41						100	1.59	2.76	-1.17	-26.85
A16-Tar 18b	2	1	6		39.38			48.08		12.53						100	2.34	1.36	0.98	26.57
A16-Tar 18b	2	2	4		40.27			45.21		14.52						100	2.48	1.28	1.20	32.00
A16-Tar 18b	6	1	4		40.5			51.74		7.77						100	2.15	1.46	0.69	19.11
A16-Tar 18b	7	1			39.66			50.45		9.88						100	2.22	1.42	0.79	21.82
A16-Tar 18b	7	2	4		35.71			44.74		19.55						100	2.53	1.26	1.27	33.41
A16-Tar 18c	1	1			46.86			50.79	0.66	1.68						100	2.14	1.43	0.71	19.78
A16-Tar 18c	2	1			44.82			45.73	0.53	8.91						100	2.41	1.29	1.12	30.23
A16-Tar 18c	2	2		9.81	41.33			37.21		11.65						100	2.38	1.57	0.81	20.61
A16-Tar 18c	2	3			40.92			43.88	0.88	13.6	0.72					100	2.51	1.24	1.27	33.90
A16-Tar 18c	2	4			46.44			41.95		11.61						100	2.60	1.18	1.42	37.44
A16-Tar 18c	2	5			45.87			33.7		20.43						100	3.01	0.95	2.06	52.06
A16-Tar 18c	2	8			42.48			42.03		15.49						100	2.62	1.19	1.44	37.71
A16-Tar 18c	2	9			47.73			39.55		12.73						100	2.71	1.12	1.60	41.70
A16-Tar 18c	3	1			41.61			44.4	1.17	12.83						100	2.48	1.25	1.23	32.89
A16-Tar 18c	3	3			35.98			36.48		26.04	1.5					100	2.92	1.03	1.89	47.88
A16-Tar 18c	3	4		14.62	40.2			31.48	0.61	13.1						100	2.42	1.66	0.76	18.66
A16-Tar 18c	4	1			31.9			49.22		18.88						100	2.33	1.39	0.94	25.32
A16-Tar 18c	4	2			31.71			42.46		25.83						100	2.67	1.20	1.47	38.04
A16-Tar 18c	4	4			45.16			54.84								100	1.96	1.55	0.42	11.89
A16-Tar 18c	4	5			41.18			43.03		15.79						100	2.58	1.21	1.37	36.00
A16-Tar 18c	4	7			45.59			39.02		15.39						100	2.75	1.10	1.65	42.85
A16-Tar 18c	4	8			51.42			46.2		2.38						100	2.36	1.30	1.05	28.76
A16-Tar 18c	5	2		9.94	42.26			38.65		9.14						100	2.29	1.61	0.68	17.43
A16-Tar 18c	5	4			43.97			37.94		18.1						100	2.82	1.07	1.75	44.92
A16-Tar 18c	5	8		9.29	42.76			39.37	0.56	8.02						100	2.27	1.60	0.68	17.43
A16-Tar 8	2	3		13.83	38.56			36.55		10.4			0.66			100	2.22	1.76	0.46	11.51
A16-Tar 8	2	4		17.51	29.46			34.12		18.5			0.4			100	2.22	1.88	0.33	8.12
A16-Tar 8	2	5		27.72	21.85			27.26		23.17						100	2.11	2.23	-0.12	-2.80
A16-Tar 8	3	2		31.17	32.2		0.61	21.28		14.73						100	2.14	2.28	-0.14	-3.24
A16-Tar 8	3	3		32.2	31.33			19.96		14.74			1.77			100	2.15	2.26	-0.11	-2.39
A16-Tar 8.5	1	1		15.34	43.81			34.17		5.04			1.64			100	2.21	1.77	0.44	10.96
A16-Tar 8.5	4	1		34.27	33.51			18.79		13.44						100	2.13	2.33	-0.21	-4.61
A16-Tar 8.5	5	2		29.63	32.52			22.67		15.18						100	2.17	2.20	-0.03	-0.62
A16-Tar 8.5	5	3		22.96	38.81			26.5		10.48			1.25			100	2.25	1.96	0.29	6.98
A16-Tar 8.5	6	1		18.56	30.76			32.33		17.76			0.59			100	2.24	1.89	0.35	8.56
A16-Tar 8.5	9	1		12.94	47.84			36.61		2.61						100	2.21	1.71	0.50	12.67
A16-Tar 8.5	9	2		27.37	41.75			25.16		5.73						100	2.10	2.15	-0.05	-1.14
A16-smb3_chip1	1	1	8		38.82			56.76		4.42						100	1.91	1.60	0.31	8.78
A16-smb3_chip1	1	2	5		41.27			53.52		5.21						100	2.06	1.51	0.55	15.31
A16-smb3_chip1	2	3	25	24.41	31.08			34.53		9.97						100	1.85	2.26	-0.41	-9.96
A16-smb3_chip1	3	1	5		43.89			56.11								100	1.91	1.58	0.33	9.35
A16-smb3_chip1	3	2	5		44.85		6.03	49.13								100	1.95	1.76	0.19	5.09
A16-smb3_chip1	4	1	14		29.08			46.81		24.11						100	2.47	1.32	1.15	30.30
A16-smb3_chip1	4	2	16		27.59			50.24	22.17							100	1.77	1.42	0.35	10.99
A16-smb3_chip1	4	3	14		21.1			51.24	27.66							100	1.63	1.45	0.18	5.86
A16-smb3_chip1	5	1	28		32.25			50.42	17.33							100	1.85	1.42	0.42	12.97
A16-smb3_chip1	5	2	224		30.34			54.1	15.56							100	1.72	1.53	0.19	5.91
A16-smb3_chip1	5	3	18		33.83			57.68		8.49						100	1.90	1.63	0.27	7.62
A16-smb3_chip1	5	4	12		40.62			59.38								100	1.77	1.67	0.09	2.67
A16-smb3_chip1	6	7	70		34.71			47.13	18.16							100	1.97	1.33	0.64	19.52
A16-smb3_chip1	10	2	13		40.71			57.25		2.04						100	1.87	1.61	0.26	7.39
A16-smb3_chip1	10	3	6		36.09			58.41		5.5						100	1.84	1.65	0.20	5.64
A16-smb3_chip1	12	1			30.21			67.28		2.51						100	1.44	1.90	-0.46	-13.74
A16-smb3_chip1	12	2			39.33			60.67								100	1.71	1.71	0.00	-0.01
A16-smb3_chip1	12	3			39.44			57.76		2.8						100	1.86	1.63	0.23	6.49
A16-smb3_chip1	12	4			16.64			45.03	38.33							100	1.70	1.27	0.43	14.59
A16-smb3_chip1	12	5			28.63			47.75	23.62							100	1.85	1.35	0.50	15.73

Table B 13. EDS results (weight percent) for evaporate mounds hosted D05 samples.

Table B13

EDS results (weight percent) for evaporate mounds hosted by D05 samples.

Sample	Site	Position	Mound size (μm)	F	Na	Mg	Al	S	Cl	K	Ca	Mn	Fe	Cu	Zn	Mo	In	Sn	Pb	Total	∑+	∑-	Σdiff	Σdiff%
D05-0015	1	1			51.64				48.36											100	2.25	1.36	0.88	24.44
D05-0015	1	2		25.21	44.76				26.99		3.04									100	2.10	2.09	0.01	0.25
D05-0015	1	3		33.03	40.93				21.88		4.16									100	1.99	2.36	-0.37	-8.47
D05-0015	2	1		26.19	38.4				28.48		6.92									100	2.02	2.18	-0.17	-3.96
D05-0015	2	2			48.66				51.34											100	2.12	1.45	0.67	18.75
D05-0015	3	1		42.82	35.95				15.66		5.57									100	1.84	2.70	-0.85	-18.82
D05-0015	4	1		22.81	45.26				29.53		2.4									100	2.09	2.03	0.05	1.33
D05-0015	5	2			56.21			4.95	31.32		7.52									100	2.82	1.19	1.63	40.58
D05-0015	5	2			57				43											100	2.48	1.21	1.27	34.30
D05-0015	8	1			43.18			4.14	26.68	12.34	7.49		6.17							100	2.79	1.01	1.78	46.79
D05-smb4	1	2	40	8.6	25.89				40.78		24.73									100	2.36	1.60	0.76	19.11
D05-smb4	2	1	30	14.78	29.25				32.64		23.34									100	2.44	1.70	0.74	17.86
D05-smb4	2	1	14		32.72				47.57		19.71									100	2.41	1.34	1.07	28.41
D05-smb4	2	2	10		34.76				51.63		13.61									100	2.19	1.46	0.73	20.15
D05-smb4	2	3	17		32.25				42.58		22.71								2.47	100	2.58	1.20	1.38	36.51
D05-smb4	3	1	12	23.27	20.92				22.67		33.14									100	2.56	1.86	0.70	15.80
D05-smb4	3	1	3		20.37				47.66	31.98										100	1.70	1.34	0.36	11.80
D05-smb4	3	2	29	30.75	20.41				20.15		28.7									100	2.32	2.19	0.13	2.95
D05-smb4	3	2	3		40.27				54.39	5.34										100	1.89	1.53	0.35	10.35
D05-smb4	3	3	3		18.76				47.03	34.2										100	1.69	1.33	0.36	12.07
D05-smb4	4	1	25		31.87				41.9		26.22									100	2.69	1.18	1.51	39.03
D05-smb4	4	2	16		25.92				42.68		31.4									100	2.69	1.20	1.49	38.24
D05-smb4	5	1	15		32.29				49.46	0.57	17.68									100	2.30	1.40	0.91	24.52
D05-smb4	6	1	24	7.8	25.52				40.8		25.88									100	2.40	1.56	0.84	21.20
D05-smb4	6	1	23		32.33			0.62	45.75		21.3									100	2.47	1.33	1.14	30.02
D05-smb4	6	2	14		32.78				50.75		16.47									100	2.25	1.43	0.82	22.19
D05-smb4	7	1	22		30.61		1.44		51.31	0.75	15.9									100	2.30	1.45	0.86	22.84
D05-smb4	7	1	26	7.89	32.38				47.17		12.57									100	2.04	1.75	0.29	7.67
D05-smb4	7	2	15		32.65				49.06	0.77	17.52									100	2.31	1.38	0.93	25.16
D05-smb4	9	1	23		35.35				50.48		14.16									100	2.24	1.42	0.82	22.37
D05-smb4	10	1	12	11.07	30.99				43.49		14.45									100	2.07	1.81	0.26	6.70
D05-smb4	10	2	20	0	27				45.16		27.84									100	2.56	1.27	1.29	33.61
D05-smb4	11	1	30	10.1	28.23				44.1		17.57									100	2.10	1.78	0.33	8.48
D05-smb4	12	1	17	11.76	28.45		4.03		42.07		13.69									100	2.37	1.81	0.56	13.49
D05-smb4	13	1	20	10.73	32.16			0.99	44.67		11.45									100	1.97	1.89	0.08	2.17
D05-smb4	13	2	24	8.79	32.16				49.03		10.02									100	1.90	1.85	0.05	1.42
D05-smb4	13	3	39	6.08	30.53				49.27		14.13									100	2.03	1.71	0.32	8.64
D05-smb4	14	1	42	4.39	30.84				52.98		11.79									100	1.93	1.73	0.20	5.59
D05-smb4	16	1	24		28.66				57.58	1.18	12.57									100	1.90	1.62	0.28	7.94
D05-smb4	16	2	60		30.9				52.79	1.34	14.98									100	2.13	1.49	0.64	17.62
D05-smb4	17	1	14	12.55	31.38				37.17		18.91									100	2.31	1.71	0.60	14.92
D05-smb4	17	2	32	7.45	27.05				43.82		21.68									100	2.26	1.63	0.63	16.22
D05-smb4	18	1	18	7	36.48				45.13		8.54								2.83	100	2.07	1.64	0.42	11.46
D05-smb4	18	2	20	0	36.32				42.28		21.41									100	2.65	1.19	1.46	37.90

Table B 14. EDS results (weight percent) for evaporate mounds hosted D12 samples.

Table B14

EDS results (weight percent) for evaporate mounds hosted by D12 samples.

Sample	Site	Position	Mound size (μm)	F	Na	Mg	Al	S	Cl	K	Ca	Mn	Fe	Cu	Zn	Mo	In	Sn	Pb	Total	∑+	∑-	Σdiff	Σdiff%
D12-0018	4	1	6		44.91			3.47	20.79	15.68	3.72		11.43							100	2.95	0.80	2.15	57.21
D12-0018	9	1	21		22.71				43.42	2.43	9.12		5.96		5.58	10.78				100	2.11	1.22	0.89	26.63
D12-0018	13	1	40		28.02			8.2	35.38	23.33	5.07									100	2.07	1.51	0.56	15.63
D12-0018	14	1	9		29.97				53.29	0.49	16.25									100	2.13	1.50	0.62	17.19
D12-0018	15	1	9		32.47				47.26		20.27									100	2.42	1.33	1.09	29.04
D12-0018	16	1	10		38.61			6	38.86	4.99	11.54									100	2.38	1.47	0.91	23.69
D12-0018	16	2			39.15				17.3	12.16	31.4									100	3.58	0.49	3.09	76.01
D12-0033	1	1	13		22.16				52.06	13.28	12.49									100	1.93	1.47	0.46	13.49
D12-0033	2	1	14		31.38				59.02	0.44	9.16									100	1.83	1.66	0.17	4.81
D12-0033	3	1	7		41.02				53.44	0.65	4.9									100	2.04	1.51	0.54	15.13
D12-0033	4	1	6		40.69				50.87		8.44									100	2.19	1.43	0.76	20.84
D12-0033	5	1	7		31.89				47.69		20.42									100	2.41	1.35	1.06	28.27
D12-0033	5	2	2		35.97			4.37	36.75		22.91									100	2.71	1.31	1.40	34.81
D12-0033	6	1	10		37.93				53.72		8.35									100	2.07	1.52	0.55	15.38
D12-0033	8	1	12		38.88				54.34		6.79									100	2.03	1.53	0.50	13.94
D12-0033	8	3			39.87				53.48		6.64									100	2.06	1.51	0.56	15.57
D12-0033	9	1			36.79				57.66	0.71	4.84									100	1.86	1.63	0.23	6.68
D12-0042	1	1		63.91	9.36				4.79		21.94									100	1.50	3.50	-2.00	-39.93
D12-0042	2	1		31.9	34.61				20.3		13.19									100	2.16	2.25	-0.09	-1.99
D12-0042	3	1		27.55	38.59				26.86		7.01									100	2.03	2.21	-0.18	-4.23
D12-0042	4	1		47.51	23.39				11.64		17.45									100	1.89	2.83	-0.94	-19.94
D12-0042	5	1		45.36	22.32				12.38		19.93									100	1.97	2.74	-0.77	-16.40
D12-0042	6	1		55.13	17.73				9.08		18.06									100	1.67	3.16	-1.49	-30.75
D12-0042	7	1		56.26	17.09				8.09		18.56									100	1.67	3.19	-1.52	-31.28
D12-0082	3	1	5		35.77				43.37		20.86									100	2.60	1.22	1.37	35.96
D12-0082	3	2	5		41.84				43.13		15.03									100	2.57	1.22	1.35	35.74
D12-0082	4	1	4		44.28				50.7		5.02									100	2.18	1.43	0.75	20.70
D12-0082	4	2	3		44.38				51.62		4									100	2.13	1.46	0.67	18.80
D12-0082	5	2	2		45.62				49.26		5.11									100	2.24	1.39	0.85	23.42
D12-0082	6	1	3		36.56				38.08		25.36									100	2.86	1.07	1.78	45.34
D12-0082	7	1	3		40.51				37.55		21.94									100	2.86	1.06	1.80	45.91
D12-0082	10	1	5		41.63				48.78		9.59									100	2.29	1.38	0.91	24.92
D12-0082	11	2	5		39.38				39.4		21.22									100	2.77	1.11	1.66	42.76
D12-0082	14	1	4		37.81				37.26		24.93									100	2.89	1.05	1.84	46.65
D12-0095	1	1		21.09	33.99				32.22		12.71									100	2.11	2.02	0.09	2.27
D12-0095	2	1		37.42	32				19.85		10.73									100	1.93	2.53	-0.60	-13.51
D12-0095	3	1		34.16	29.79				22.01		14.05									100	2.00	2.42	-0.42	-9.55
D12-0095	4	1			51.59				48.41											100	2.24	1.37	0.88	24.34
D12-0095	5				56.55				43.45											100	2.46	1.23	1.23	33.49
D12-0095	6	1			46.27			4.99	43.66		5.09									100	2.27	1.54	0.72	19.00
D12-0095	7	1		23.75	37.01				29.38		9.86									100	2.10	2.08	0.02	0.55
D12-0095	8	1			49.66			1.7	46		2.64									100	2.29	1.40	0.89	24.04
D12-0095	9	1			52.72				44.3		2.98									100	2.44	1.25	1.19	32.30
D12-0095	10	1			51.25				45.64		3.11									100	2.38	1.29	1.10	29.88
D12-0095	12	1		18.98	45.58				30.21		5.23									100	2.24	1.85	0.39	9.59
D12-0095	13	1		23.48	44.23				27.26		5.03									100	2.17	2.00	0.17	4.07
D12-0095	14	1		24.36	43.71				27.54		4.39									100	2.12	2.06	0.06	1.47
D12-0095	15	1		17.89	41.91				36.35		3.85									100	2.02	1.97	0.05	1.21
D12-2707-3	5	2		34.49	34.4				20.66		9.41		1.04							100	2.00	2.40	-0.39	-8.97
D12-2707-3	8	2			52.92				47.08											100	2.30	1.33	0.97	26.83
D12-2707-3	9	1			50.85			0.35	48.8											100	2.21	1.40	0.81	22.54
D12-2707-3	9	2			54.89				45.11											100	2.39	1.27	1.12	30.47
D12-2707-3	10	1			55.99				44.01											100	2.44	1.24	1.19	32.48
D12-2707-3	11	1		39.06	35.93				17.13		6.88									100	1.91	2.54	-0.63	-14.24
D12-2707-3	12	1		36.32	38.49				19.43		5.76									100	1.96	2.46	-0.50	-11.27
D12-2707-3	12	2			51.95				48.05											100	2.26	1.36	0.90	25.02
D12-2707-3	13	3		33.62	41.21				20.16		5.01									100	2.04	2.34	-0.30	-6.75
D12-2707-3	14	1		24.57	45.29				27.54		2.6									100	2.10	2.07	0.03	0.71
D12-2707-4	2	1		35.59	42.18				19.34		2.89									100	1.98	2.42	-0.44	-10.00
D12-2707-4	3	2			52.69				44.87		2.43									100	2.41	1.27	1.15	31.19
D12-2707-4	4	1		17.73	48.33				32.07	0.45	1.42									100	2.18	1.84	0.35	8.62
D12-2707-4	4	2		16.82	48.03				32.7	0.36	1.7		0.39							100	2.20	1.81	0.39	9.73
D12-2707-4	9	1		17.3	47.4				33.24	0.34	1.73									100	2.16	1.85	0.31	7.71
D12-2707-4	10	1		45.05	24.09				19.56	0.11	10.92	0.27								100	1.61	2.92	-1.32	-29.09
D12-2707-4	11	1		18.89	44.16				34.05	0.19	2.7									100	2.06	1.95	0.11	2.63
D12-2707-6	4	2		17.12	40.22				30.51	0.79	6.4				4.95					100	2.24	1.76	0.48	11.96
D12-2707-6	5	1		11.49	33.92		1.69		38.95		10.18	0.21	1.3		2.26					100	2.29	1.70	0.58	14.63

Table B14 (cont.)

D12-2707-6	5	3		17.27	38.61			31.64	1.38	6.56			4.54			100	2.18	1.80	0.38	9.53
D12-2707-6	6	2		16.09	41.42			32.59	0.75	6.15			3			100	2.22	1.77	0.45	11.37
D12-2707-6	6	3		14.69	43.54			34.2	0.67	3.53			3.38			100	2.19	1.74	0.45	11.52
D12-2707-6	7	1		23.85	41.78			23.71		5.31			5.35			100	2.25	1.92	0.32	7.72
D12-2707-6v	13	1	20		47.21			52.79								100	2.05	1.49	0.56	15.94
D12-3036-2	2	2	5		42.23			50.66		7.11						100	2.19	1.43	0.76	21.05
D12-3036-2	2	3	3		43.87			48.89		7.24						100	2.27	1.38	0.89	24.39
D12-3060	1	1		33.86	35.92		6.3	15.09		8.82						100	2.00	2.60	-0.60	-13.00
D12-3060	2	1		47.61	26.43		6.2	8.8		10.96						100	1.70	3.14	-1.44	-29.86
D12-3060	3	1		48.5	29.67		6.22	6.02		9.59						100	1.77	3.11	-1.34	-27.49
D12-3060	4	1		32.22	35.88		5.83	16.64		9.42						100	2.03	2.53	-0.50	-10.92
D12-3060	5	1		24.82	39.96		3.44	24.61		7.18						100	2.10	2.22	-0.12	-2.75
D12-3060	6	1		23.28	42.09		1.79	27.85		4.99						100	2.08	2.12	-0.04	-1.02
D12-3060	7	1		27.17	34.36		3.37	26.43	0.38	8.29						100	1.92	2.39	-0.47	-10.87
D12-3060	8	1		22.67	45.14			28.18		4						100	2.16	1.99	0.18	4.22
D12-3060	9	1		19.72	43.21		1.31	30.03		5.73						100	2.17	1.97	0.20	4.81
D12-3060	10	1		25.23	41.88			28.07		4.83						100	2.06	2.12	-0.06	-1.36
D12-3060	11	1		40.39	35.55			15.68		8.38						100	1.96	2.57	-0.60	-13.32
D12-3060	13	1		32.1	33.9			26.56		7.45						100	1.85	2.44	-0.59	-13.82
D12-3060	14	1		25.64	38.38			28.47		7.52						100	2.04	2.15	-0.11	-2.57
D12-3060	15	1		30.91	37.33			25.85		5.91						100	1.92	2.36	-0.44	-10.23
D12-3060	16	1		41.69	32.69			17.78		7.83						100	1.81	2.70	-0.88	-19.59
D12-3083	1	1		41.29	30.05			18		8.92				1.74		100	1.79	2.68	-0.89	-19.97
D12-3083	2	1		46.78	25.68	1.84	0.72	14.38	0.22	9.83	0.17	0.39				100	1.84	2.91	-1.07	-22.63
D12-3083	2	1		29.65	44.58			23.01		2.76						100	2.08	2.21	-0.13	-3.10
D12-3083	3	1		46	31.07			13.77		9.16						100	1.81	2.81	-1.00	-21.68
D12-3083	3	1		32.65	37.5		1.17	23.01		5.67						100	1.91	2.44	-0.53	-12.09
D12-3083	7	1		40.99	35.17			16.69		7.16						100	1.89	2.63	-0.74	-16.41
D12-3083	10	1			49.54			41.02		9.44						100	2.63	1.16	1.47	38.83
D12-3083	12	1		41.99	30.08		0.55	18.59		8.79						100	1.75	2.77	-1.02	-22.63
D12-3083	13	1		46.04	26.58		0.61	16.57	0.39	9.53		0.29				100	1.65	2.93	-1.28	-27.87
D12-3083	14	1			50.79			49.21								100	2.21	1.39	0.82	22.83
D12-3083	15	1		21.75	42.58			29.94		4.93		0.8				100	2.13	1.99	0.14	3.34
D12-3083	16	1			52.42			47.58								100	2.28	1.34	0.94	25.90
D12-3136	2	1		27.97	35.46			27.55	1.15	7.35		0.52				100	1.96	2.25	-0.29	-6.94
D12-3136	2	2		41.9	31.95			18.1	0.87	6.47	0.34	0.37				100	1.76	2.72	-0.96	-21.34
D12-3136	4	1		27.13	35.73			28.36	1.59	6.55	0.34	0.29				100	1.94	2.23	-0.28	-6.79
D12-3136	4	2		29.17	37.29			26.21	0.84	6.5						100	1.97	2.27	-0.31	-7.23
D12-3136	4	3		24.43	41.27			27.9	1.05	4.98	0.37					100	2.08	2.07	0.01	0.27
D12-3136	5	1		34.76	30.9			23.41	3.03	6.74	0.54				0.63	100	1.79	2.49	-0.70	-16.33
D12-Tar 5f	1	1			25.32			55.87	0.42	18.4						100	2.03	1.58	0.45	12.60
D12-Tar 5f	7	1			50.2			49.8								100	2.18	1.40	0.78	21.71
D12-Tar 5f	7	2			46.29			53.71								100	2.01	1.51	0.50	14.13
D12-Tar 5f	7	3			47.89			52.11								100	2.08	1.47	0.61	17.26
D12-Tar 5f	7	4			49.51			50.49								100	2.15	1.42	0.73	20.39
D12-Tar 5p	1	1		23.57	39.65			27.09		9.7						100	2.21	2.00	0.20	4.84
D12-Tar 5p	1	2		21.82	35.54	1.86		31.17	0.38	9.23						100	2.22	2.03	0.20	4.60
D12-Tar 5p	1	3		23.56	38.83			27.47	0.37	9.76						100	2.19	2.01	0.17	4.06
D12-Tar 5p	1	4		24.54	42.49			26.51		6.46						100	2.17	2.04	0.13	3.12
D12-Tar 5p	2	2		34.77	37.87			20.61		6.75						100	1.98	2.41	-0.43	-9.72
D12-Tar 5p	2	5		32.44	41.17			18.96		6.8		0.64				100	2.15	2.24	-0.09	-2.03
D12-Tar 5p	4	1			52.4			47.6								100	2.28	1.34	0.94	25.86
D12-Tar 5p	4	2			54.01			45.99								100	2.35	1.30	1.05	28.85
D12-Tar 5p	5	1		17.53	43.05			34.96		4.46						100	2.10	1.91	0.19	4.65
D12-Tar 5p	5	2			53.06			46.94								100	2.31	1.32	0.98	27.09
D12-Tar 5p	5	3		19.75	44.77			30.1	0.41	4.97						100	2.21	1.89	0.32	7.75
D12-Tar 5p	6	1			52.16			47.84								100	2.27	1.35	0.92	25.41
D12-Tar 5p	6	2			53.4			46.6								100	2.32	1.31	1.01	27.73
D12-Tar 5p	6	3			50.56			49.44								100	2.20	1.39	0.80	22.39
D12-Tar 5p	7	1		18.14	47.53			30.2		4.13						100	2.27	1.81	0.47	11.44
D12-Tar 5p	7	2		25.6	43.14			25.97		5.29						100	2.14	2.08	0.06	1.43
D12-Tar 5p	7	3		27.4	39.88			25.23		7.48						100	2.11	2.15	-0.05	-1.08
D12-Tar 5p	7	4		19.69	42.97			32.59		4.75						100	2.11	1.96	0.15	3.71
D12-Tar6 fc	1	1	45		23.03		10.2	29.38	14.76	10.75			11.89			100	2.28	1.46	0.81	21.74
D12-Tar6 fc	3	1	15		39.79		10.53	11.93		18.7		4.15	14.9			100	3.27	0.99	2.27	53.38
D12-Tar6 fc	5	1			36.91			51.53	2.4	3.17		0.67	5.32			100	2.01	1.45	0.56	16.10
D12-Tar6 fc	5	2			35.83			51.57	4.13	4.74			3.72			100	2.01	1.45	0.56	16.12
D12-Tar6 fc	8	1	20		27.96			53.37	5.49	9.27	1.32		2.59			100	1.95	1.51	0.44	12.77
D12-Tar6 fc	8	2	10		29.97			44.73	8.34	12.29			4.67			100	2.27	1.26	1.01	28.60
D12-Tar6 fc	8	3	24		33.32			49.47	5.49	8.22			3.51			100	2.11	1.40	0.71	20.31
D12-Tar6 fc	9	1	9		34.49			46.18	4.51	9.53			5.28			100	2.25	1.30	0.95	26.71

Table B14 (cont.)

D12-Tar6 fc	9	2	12		26.22				45.05	9.96	11.71	1.42	1.84		3.8			100	2.21	1.27	0.94	27.05
D12-Tar6 fc	10	1	18		35.65				51.04	4.71	3.93	1.25	0.91		2.51			100	2.02	1.44	0.58	16.81
D12-Tar6 fc	10	2	5		37.52				53.14		5.81				3.53			100	2.03	1.50	0.53	15.03
D12-Tar6 fc	12	1	5		38.72				49.68		5.86				5.75			100	2.15	1.40	0.75	21.12
D12-Tar6 fc	13	1	20		34.33				51.15	4.46	7.37	1.21	1.48					100	2.07	1.44	0.63	17.89
D12-Tar6 fc	13	2	20		34.28				47.84	5.38	9.43	1.84	1.23					100	2.21	1.35	0.86	24.17
D12-Tar6 fc	14	1	22		38.86				51.96	4.08	5.1							100	2.05	1.47	0.58	16.59
D12-Tar6 fc	15	1	18		39.86				54.81		5.33							100	2.00	1.55	0.45	12.78
D12-Tar6 fc	16	1			44.36				46.27		9.37							100	2.40	1.31	1.09	29.48
D12-Tar6 fc	17	1			35.08				57.26	4.53	3.13							100	1.80	1.62	0.18	5.34
D12-Tar6 fc	19	1			42.03				50.11	3.65	4.2							100	2.13	1.41	0.72	20.23
D12-Tar6 fc	20	1	9		37.87				41.25	2.53	16.07	2.29						100	2.60	1.16	1.43	38.11
D12-Tar6 fc	21	1	15		40.68				47.51	1.89	9.93							100	2.31	1.34	0.97	26.63
D12-Tar6 fc	22	1	16		40.52				52	3.47	4							100	2.05	1.47	0.58	16.59
D12-Tar6 fc	22	2	5		39.23				50.35	1.22	8.05	1.14						100	2.18	1.42	0.76	21.11
D12-Tar6 fc	23	1	20		36.74				55.95	3.15	4.16							100	1.89	1.58	0.31	8.88
D12-Tar6 fc	24	1	2		43.99				56.01									100	1.91	1.58	0.33	9.53
D12-Tar6 fc	25	1	10		43.38				54.46		2.17							100	1.99	1.54	0.46	12.98
D12-Tar7	3	2			48.84				40.24		10.92							100	2.67	1.14	1.53	40.33
D12-Tar7	10	1			51.3				48.38		0.33							100	2.25	1.36	0.88	24.45
D12-Tar7	10	2			56.06				43.94									100	2.44	1.24	1.20	32.60
D12-Tar7	10	3			53.83				46.17									100	2.34	1.30	1.04	28.52
D12-2707-6v	1	1	50		30.99				48.61	0.97	19.43							100	2.34	1.37	0.97	26.16
D12-2707-6v	3	1	36		26.04				49.25	1.09	19.1							100	2.11	1.45	0.67	18.77
D12-2707-6v	4	1	13		28.05				49.73	1.06	21.15							100	2.30	1.40	0.90	24.29
D12-2707-6v	5	1	6		37.16				53.1		9.74							100	2.10	1.50	0.60	16.80
D12-2707-6v	6	1	14		35.71				51.75		12.54							100	2.18	1.46	0.72	19.77
D12-2707-6v	8	1	12		38.5				50.35		11.15							100	2.23	1.42	0.81	22.21
D12-2707-6v	8	2	12		32.88		2.53		49.16		15.43							100	2.48	1.39	1.09	28.31
D12-2707-6v	8	3	12		35.52		1.14		50.75		12.59							100	2.30	1.43	0.87	23.28
D12-2707-6v	8	4	8		40.85				53.82		5.33							100	2.04	1.52	0.52	14.74
D12-2707-6v	9	1	24		30.62				45.86		23.52							100	2.51	1.29	1.21	31.90
D12-2707-6v	9	2	15		31.91				42.6		25.49							100	2.66	1.20	1.46	37.77
D12-2707-6v	9	3	26		39.33				45.76		14.92							100	2.46	1.29	1.16	31.09
D12-2707-6v	10	1	30		29.64			2.03	44.44	20.12	3.77							100	1.99	1.38	0.61	18.15
D12-2707-6v	10	2	10		31.01				46.08	5.66	17.26							100	2.35	1.30	1.06	28.87
D12-2707-6v	10	3	5		38.27				50.15	1.93	9.64							100	2.20	1.41	0.78	21.62
D12-2707-6v	11	1	9		35.45				41.38		23.17							100	2.70	1.17	1.53	39.61
D12-2707-6v	11	2	22		36.81				38.38		24.81							100	2.84	1.08	1.76	44.79
D12-2707-6v	11	3	12		35.62				41.84		22.53							100	2.67	1.18	1.49	38.76
D12-2707-6v	12	1	23		36.66				50.89	0.95	11.51							100	2.19	1.44	0.76	20.89
D12-3037-c	1	1		53.99	22.05			0.73	10.76		12.48							100	1.58	3.19	-1.61	-33.71
D12-3037-c	2	1		48.27	24.93				10.27		14.85		1.67					100	1.89	2.83	-0.95	-20.04
D12-3037-c	4	1		39.79	36.26				15.51		8.45							100	2.00	2.53	-0.53	-11.76
D12-3037-c	5	1		40.65	29.43			0.61	16.31		13							100	1.93	2.64	-0.71	-15.52
D12-3037-c	6	1		56.82	22.12				8.52		12.54							100	1.59	3.23	-1.64	-34.10
D12-3037-c	7	1		42.52	29.19				15.03		13.27							100	1.93	2.66	-0.73	-15.89
D12-3037-c	8	1		43.73	33.11			2.28	13.71		7.16							100	1.80	2.83	-1.03	-22.32
D12-3037-c	9	1		33.78	30.66				18.22		13.78						3.57	100	2.10	2.29	-0.20	-4.47
D12-3037-c	10	1		18.51	44.58				30.97		5.95							100	2.24	1.85	0.39	9.51
D12-3037-c	11	1		19.03	48.01				30.33		2.64							100	2.22	1.86	0.36	8.90
D12-3037-c	12	1			49.63				44.3		6.07							100	2.46	1.25	1.21	32.66
D12-3037-c	13	1		53.4	24				11.58		11.02							100	1.59	3.14	-1.54	-32.62
D12-3037-c	15	1		46.2	31.28				11.68		10.84							100	1.90	2.76	-0.86	-18.44
D12-0050	1	2	9	9.28	39.1				47.75	0.56	3.32							100	1.88	1.84	0.05	1.22
D12-0050	2	1	10	7.52	33.65				46.4	1.02	11.42							100	2.06	1.70	0.36	9.43
D12-0050	5	1	80	8.51	29.12				48.01	2.77	11.21	0.38						100	1.91	1.80	0.11	2.93
D12-0050	5	2	21	7.78	29.35				49.09	3.2	10.59							100	1.89	1.79	0.09	2.52
D12-0050	8	1	25	6.68	30.84				54.24	1.8	6.44							100	1.71	1.88	-0.17	-4.81
D12-0050	8	2	10	9.5	32.72				49.26	2.4	6.12							100	1.79	1.89	-0.10	-2.70
D12-0050	9	1	45	9.46	24.09				42.79		23.66							100	2.23	1.70	0.52	13.31
D12-0050	9	2	18	6.29	33.77		1.26		47.46	0.85	10.37							100	2.15	1.67	0.48	12.53
D12-0050	10	1	12	21.28	34.52				33.39		10.82							100	2.04	2.06	-0.02	-0.50
D12-0050	10	2	5	20.49	34.99				33.72		10.8							100	2.06	2.03	0.03	0.77
D12-006_chip2	3	1	20	13.54	30.59				44.55	0.3	11.03							100	1.89	1.97	-0.08	-2.09
D12-006_chip2	5	1	25		37.28	1.32	1.43	0.52	52.35	0.58	3.3		1.7					100	2.28	1.51	0.77	20.28
D12-006_chip2	7	1	8	15.27	28.23				45.03		11.47							100	1.80	2.07	-0.27	-7.06
D12-006_chip2	8	1	20	24.49	24.84				30.71		19.96							100	2.08	2.16	-0.08	-1.86
D12-006_chip2	11	2	16	7.33	29.4				48.64		14.63							100	2.01	1.76	0.25	6.67
D12-006_chip2	12	1	21	9.62	26.61				47		16.76							100	1.99	1.83	0.16	4.23
D12-006_chip2	14	1	3		4.32				46.67	49.01								100	1.44	1.32	0.13	4.53

Table B14 (cont.)

D12-006_chip2	14	2	5	24.33	26.46			33.62	9	6.59						100	1.71	2.23	-0.52	-13.17
D12-006_chip2	14	3	3	33.59	26.2			24.03	2.54	13.64						100	1.89	2.45	-0.56	-12.94
D12-006_chip2	14	4	2		19.92			46.17	33.92							100	1.73	1.30	0.43	14.22
D12-006_chip2	14	5	2		22.01			43.32	34.66							100	1.84	1.22	0.62	20.29
D12-006_chip2	14	6	5		19.53			43.69	36.78							100	1.79	1.23	0.56	18.46
D12-006_chip2	15	1	10		45.78			54.22								100	1.99	1.53	0.46	13.12
D12-006_chip2	15	2	5		46.58			53.42								100	2.03	1.51	0.52	14.70
D12-006_chip2	15	3	5		46.7			53.3								100	2.03	1.50	0.53	14.94
D12-006_chip2	17	1	15	19.58	23.43			39.41	0.74	16.84						100	1.88	2.14	-0.26	-6.56
D12-2007-4	7	1			48.98			51.02								100	2.13	1.44	0.69	19.37
D12-2007-4	8	1			51.35			48.65								100	2.23	1.37	0.86	23.89
D12-3136	8	2	10	24.78	20.7			31.09	0.83	21.66	0.95					100	2.04	2.18	-0.14	-3.43
D12-3136	8	4	12	17.96	30.21			36.72	4.11	10.99						100	1.97	1.98	-0.01	-0.35
D12-3136	11	3	15	33.72	33.51			23.85	0.17	7.14	0.66	0.19		0.76		100	1.86	2.45	-0.58	-13.53
D12-3136	12	2	11	39.48	29.93			18.96		10.97	0.66					100	1.87	2.61	-0.74	-16.50
D12-3136	12	3	8	27.5	33.76			29.03	0.38	8.85	0.47					100	1.94	2.27	-0.33	-7.85
D12-3136	15	1	8	20.24	39.99			32.92		6.85						100	2.08	1.99	0.09	2.13
D12-3136	16	1	20	35.51	22.11	1.52		25.68		13.68	0.33			0.71	0.47	100	1.85	2.59	-0.75	-16.79
D12-3136	17	1	22	41.2	29.27		0.26	17.17	0.78	10.56	0.77					100	1.85	2.67	-0.82	-18.19
D12-3136	18	1	18	32.28	28.99	2.59		25.47	0.61	9.42	0.64					100	2.06	2.42	-0.36	-8.05
D12-Tar6	1	1			50.69			39.02	10.28							100	2.47	1.10	1.37	38.32
D12-Tar6	1	2			47.37			42.85	6.46	3.32						100	2.39	1.21	1.18	32.85
D12-Tar6	2	2		17.21	45.32		0.7	31.81		4.97						100	2.22	1.85	0.37	9.16
D12-Tar6	3	1			51.15			41.79		7.06						100	2.58	1.18	1.40	37.23
D12-Tar6	3	2		29.33	37.7		1.87	22.78		8.32						100	2.06	2.30	-0.25	-5.69
D12-Tar6	3	3		23.93	43.43			26.66		5.98						100	2.19	2.01	0.18	4.19
D12-Tar6	4	2		16.78	40.67			33.23		9.31						100	2.23	1.82	0.41	10.19
D12-Tar6	5	1		14.82	36.24			36.76		12.19						100	2.18	1.82	0.37	9.19
D12-Tar6	5	1			49.5			45.5		5						100	2.40	1.28	1.12	30.37
D12-Tar6	5	2		16.31	34	2.15		33.13		14.4						100	2.44	1.79	0.64	15.22
D12-Tar6	6	1			49.59			47.86		2.54						100	2.28	1.35	0.93	25.70
D12-Tar6	6	2		16.4	47.46			31.85		4.29						100	2.28	1.76	0.52	12.79
D12-Tar6	7	1			51.74			46.24		2.01						100	2.35	1.30	1.05	28.64
D12-Tar6	7	2			51.53			46.34	2.13							100	2.30	1.31	0.99	27.45
D12-Tar6	7	4			50.49			42.88	2.48	4.16						100	2.47	1.21	1.26	34.21
D12-Tar6	7	5			53.69			46.31								100	2.34	1.31	1.03	28.26
D12-Tar6	7	6			50.87			45.93	3.2							100	2.29	1.30	1.00	27.83
D12-Tar6	8	1		18.89	44.72		0.59	31.56		4.24						100	2.16	1.92	0.24	5.78
D12-Tar6	8	2			51.77			42.92		5.31						100	2.52	1.21	1.31	35.04
D12-Tar6	8	3		27.99	35.47		1.39	22.82		12.33						100	2.16	2.20	-0.05	-1.04
D12-Tar7	1	1		28.72	32.14			27.26		11.87						100	1.99	2.28	-0.29	-6.80
D12-Tar7	1	2		22.97	34.81			30.48	0.52	10.65			0.55			100	2.08	2.07	0.01	0.17
D12-Tar7	2	1		48.7	23.48			14.28		13.54						100	1.70	2.97	-1.27	-27.22
D12-Tar7	2	2		33.32	37.56			21.82		7.3						100	2.00	2.37	-0.37	-8.50
D12-Tar7	2	3		32.41	29.86			25.17		12.56						100	1.93	2.42	-0.49	-11.29
D12-Tar7	3	1		20.54	32.78			33.4		13.27						100	2.09	2.02	0.06	1.58
D12-Tar7	4	1		23.61	42.72			26.98		6.7						100	2.19	2.00	0.19	4.50
D12-Tar7	4	2		33.49	34.74			19.76		12.01						100	2.11	2.32	-0.21	-4.73
D12-Tar7	5	1		32.97	22.68			25.9		18.44						100	1.91	2.47	-0.56	-12.79
D12-Tar7	5	2		42.74	28.92			16.35		11.99						100	1.86	2.71	-0.85	-18.71
D12-Tar7	5	3		32.7	25.94			23.61		17.75						100	2.01	2.39	-0.37	-8.48
D12-Tar7	5	4		32.72	30.22			22.87		14.19						100	2.02	2.37	-0.34	-7.85
D12-Tar7	6	1		32.12	34.25			21.46		12.16						100	2.10	2.30	-0.20	-4.54
D12-Tar7	7	1		28.27	39.97			23.91		7.85						100	2.13	2.16	-0.03	-0.75
D12-Tar7	7	3		32.21	37.16			22.24		8.39						100	2.04	2.32	-0.29	-6.60

Table B 15. EDS results (weight percent) for evaporate mounds hosted D13 samples.

Table B15

EDS results (weight percent) for evaporate mounds hosted by D13 samples.

Sample	Site	Position	Mound size (μm)	F	Na	Mg	Al	S	Cl	K	Ca	Mn	Fe	Cu	Zn	Mo	In	Sn	Pb	Total	∑+	∑-	Σdiff	Σdiff%
D13-smb2	2	1	18		15.41				46.01	38.58										100	1.66	1.30	0.36	12.16
D13-smb2	2	3	16		8.03				44.84	47.12										100	1.55	1.26	0.29	10.28
D13-smb2	7	2	40	22.44	6.2				35.53		35.83									100	2.06	2.18	-0.13	-2.96
D13-smb2	9	1	14	30.4	25.09				23.53		20.98									100	2.14	2.26	-0.13	-2.85
D13-smb2	13	1	10	29.51	24.27				21		25.21									100	2.31	2.15	0.17	3.77
D13-smb2	17	2	45		20.25				44.48	35.27										100	1.78	1.25	0.53	17.39
D13-smb2	20	4	40		36.57				53.59	9.84										100	1.84	1.51	0.33	9.86
D13-Tar 14d	1	1		19.76	27.6			2.03	26.04		24.57									100	2.43	1.90	0.53	12.14
D13-Tar 14d	2	1		17.74	35.54				28.54		15.71					2.47				100	2.38	1.74	0.64	15.60
D13-Tar 14d	6	2			45.51			2.33	37.59		14.56									100	2.71	1.21	1.50	38.36
D13-smb2	1	1	24	7.53	24.69				49.22	0.96	17.6									100	1.98	1.78	0.19	5.11
D13-smb2	1	2	18		41.52				54.32		4.16									100	2.01	1.53	0.48	13.58
D13-smb2	2	1	26	6.56	36.27				50.66	0.54	5.22	0.74								100	1.88	1.77	0.10	2.87
D13-smb2	3	1	23	5.77	35.75			0.76	44.92	1.43	11.36									100	2.16	1.62	0.54	14.31
D13-smb2	3	1	5		26.32				47.67	26.01										100	1.81	1.34	0.47	14.76
D13-smb2	3	2	6		42.75				56.28	0.97										100	1.88	1.59	0.30	8.55
D13-smb2	3	3	6		41.58				56.87	1.55										100	1.85	1.60	0.24	7.07
D13-smb2	5	1	16	8.28	31.23				48.3		12.18									100	1.97	1.80	0.17	4.47
D13-smb2	6	1	7	0	40.92				50.92		8.16									100	2.19	1.44	0.75	20.72
D13-smb2	6	2	10	0	38.99				51.58		9.43									100	2.17	1.45	0.71	19.65
D13-smb2	10	1	8		41.7				55.62											100	1.81	1.57	0.25	7.24

Table B 16. EDS results (weight percent) for evaporate mounds hosted EK samples.

Table B16

EDS results (weight percent) for evaporate mounds hosted by CF samples.

Sample	Site	Position	Mound size (μm)	F	Na	Mg	Al	S	Cl	K	Ca	Mn	Fe	Cu	Zn	Mo	In	Sn	Pb	Total	∑+	∑-	Σdiff	Σdiff%
castle_fred	1	1			12.73			29.56	18.15		39.56									100	1.54	1.43	0.11	3.60
castle_fred	1	2			14.28			22.24	28.27		35.21									100	1.50	1.49	0.01	0.29
castle_fred	1	3			8.72			30.26	19.33		41.69									100	1.42	1.49	-0.07	-2.39
castle_fred	2	1			4.72			38.8	5.82		50.65									100	1.47	1.37	0.09	3.34
castle_fred	2	2			5.4			38.06	6.83		49.71									100	1.48	1.38	0.10	3.35
castle_fred	3	1			6.12			35.28	10.84		47.77									100	1.46	1.41	0.05	1.82
castle_fred	5	1			9.38			28.75	18.45		43.42									100	1.49	1.42	0.07	2.56
castle_fred	7	1			9.64			31.79	16		42.57									100	1.48	1.44	0.04	1.33
castle_fred	10	1			9.77			35.9	11.15		43.18									100	1.50	1.43	0.07	2.33
castle_fred	11	1			3.5			38.74	5.87		51.89									100	1.45	1.37	0.07	2.60
castle_fred	11	1			8.56			35.4	7.84	2.94	45.26									100	1.58	1.33	0.25	8.67
castle_fred	11	2			7			37.36	7.49		48.15									100	1.51	1.38	0.13	4.49
castle_fred	12	1			12.87			32.58	13.35		41.2									100	1.59	1.39	0.20	6.55
castle_fred	13	1			8.6			32.75	13.94		42.69		2.02							100	1.48	1.41	0.06	2.11
castle_fred	14	1			14			25.23	24.52		36.26									100	1.51	1.48	0.04	1.18
castle_fred	14	2			10.59			29.73	19.05		40.62									100	1.47	1.46	0.01	0.33
castle_fred	15	1			9.55			35.18	10.77		44.51									100	1.53	1.40	0.13	4.27
castle_fred	15	3			9.22			35.6	9.2		45.97									100	1.55	1.37	0.18	6.11

Table B 17. EDS results (weight percent) for evaporate mounds hosted CF samples.

Table B17

EDS results (weight percent) for evaporate mounds hosted by EK samples.

Sample	Site	Position	Mound size (μm)	F	Na	Mg	Al	S	Cl	K	Ca	Mn	Fe	Cu	Zn	Mo	In	Sn	Pb	Total	∑+	∑-	Σdiff	Σdiff%
A04-Tar ek	1	1	25		34.72				46.46	4.54		6.79	1.71			11.27				100	2.05	1.31	0.74	22.11
A04-Tar ek	1	2	5		38.3				39.22	5.39		3.39	1.18			4.85				100	2.23	1.11	1.12	33.68
A04-Tar ek	2	1	27		31.87				49.24	4.36		6.95	1.61			7.13				100	1.93	1.39	0.54	16.37
A04-Tar ek	3	1	10		42.61			9.21	41.5	2.35		4.33								100	2.07	1.17	0.90	27.77
A04-Tar ek	4	1	15		36.89				40.56	4.07		3.21								100	2.14	1.14	1.00	30.40
A04-Tar ek	5	2	15		33.23			2.7	42.65	9.57		9.74	2.11			15.59				100	2.12	1.37	0.75	21.44
A04-Tar ek	5	3	15		42.87				36.39	1.75		5.64	2.07			15.27				100	2.42	1.03	1.40	40.49
A04-Tar ek	5	4	5		46.34			5.57	38.29	2.6		4.86	2.33			18.85				100	2.34	1.43	0.91	24.26
A04-Tar ek	6	1	15		34.46				41.16	4.8		6.03	1.26			5.98				100	2.14	1.16	0.98	29.71
A04-Tar ek	7	1	18		40.13				35.05	4.36		3.98	0.89							100	2.36	0.99	1.37	40.92
A04-Tar ek	8	1	10		34.97				48.87	1.93		5.82	0.73		0.68					100	1.97	1.38	0.60	17.79
A04-Tar ek	9	1	6		36.67				48.02	5.51		3.02	1.94			12.52				100	2.02	1.35	0.66	19.63
A04-Tar ek	10	1	12		35.3			5.94	44.44	6.14		6.3	1.89			12.3				100	1.99	1.62	0.37	10.10
A04-Tar ek	12	1	17		40.24				37.68	2.18		2.67	0.93							100	2.28	1.06	1.21	36.33
A04-Tar ek	13	1	9		46.67			9.18	39.72			2.22	2.21			16.3				100	2.19	1.69	0.50	12.78
A04-Tar ek	14	1	12		35.59				46.29	5.5		3.03	1.23		1.23	5.77				100	2.03	1.31	0.72	21.69
A04-Tar ek	15	1	15		43.52			13.25	30.43	5.94		6.86								100	2.29	1.68	0.61	15.31
A04-Tar ek	15	2	25		36.76				39.69	1.51		3.19								100	2.15	1.12	1.03	31.44
A04-Tar ek	16	1	22		38.54			6.47	42.8	6.88		2.01	1.56		1.74	7.01				100	2.03	1.61	0.42	11.61